



**ARISTOTLE UNIVERSITY OF THESSALONIKI**  
**FACULTY OF SCIENCES**  
**PHYSICS DEPARTMENT**

**DOCTORAL THESIS**

**BETSOU CHRYSOULA**

**DETERMINATION OF THE  
BIOACCUMULATION OF RADIONUCLIDES  
AND TRACE ELEMENTS IN MOSSES USING  
NUCLEAR METHODS**

**THESSALONIKI, MAY 2020**



**ΑΡΙΣΤΟΤΕΛΕΙΟ ΠΑΝΕΠΙΣΤΗΜΙΟ ΘΕΣΣΑΛΟΝΙΚΗΣ**  
**ΣΧΟΛΗ ΘΕΤΙΚΩΝ ΕΠΙΣΤΗΜΩΝ**  
**ΤΜΗΜΑ ΦΥΣΙΚΗΣ**

**ΔΙΔΑΚΤΟΡΙΚΗ ΔΙΑΤΡΙΒΗ**

**ΜΠΕΤΣΟΥ ΧΡΥΣΟΥΛΑ**

**ΠΡΟΣΔΙΟΡΙΣΜΟΣ ΜΕ ΠΥΡΗΝΙΚΕΣ ΜΕΘΟΔΟΥΣ**  
**ΤΗΣ ΒΙΟΣΥΣΣΩΡΕΥΣΗΣ ΡΑΔΙΟΝΟΥΚΛΙΔΙΩΝ**  
**ΚΑΙ ΙΧΝΟΣΤΟΙΧΕΙΩΝ ΣΕ ΒΡΥΑ**

**ΘΕΣΣΑΛΟΝΙΚΗ, ΜΑΪΟΣ 2020**



## PhD committee

Ioannidou A. (supervisor), Associate Professor, Department of Physics, AUTH

Stoulos S., Associate Professor, Department of Physics, AUTH

Krmar M., Professor, Department of Physics, University of Novi Sad, Serbia

Kitis G., Professor, Department of Physics, AUTH

Liolios A., Professor, Department of Physics, AUTH

Tsabaris C., Research Director of HCMR, Athens

Klouvas A., Professor, School of Electrical and Computer Engineering, AUTH

Day of Defense:

28 May 2020

This research has been financially supported by General Secretariat for Research and Technology (GSRT) and the Hellenic Foundation for Research and Innovation (HFRI) (Scholarship Code: 569).

## Abstract

Mosses are ideal biomonitors as they do not have roots and all the nutrients and the water they need are taken through wet and dry deposition. They are a useful tool for monitoring the air quality, without requiring any special instrumentation. Due to their unique morphological and physiological characteristics, mosses are able to accumulate airborne pollutants such as trace elements, organic compounds and radionuclides.

Since the 80's, different surveys have been conducted using mosses as biological indicators of trace elements and radionuclides. Ever since, and in a five years' interval a European moss survey is conducted under the framework of the ICP Vegetation, providing data on the elemental concentrations in naturally growing mosses. The latest moss survey was conducted in 2015/2016, coordinated by the Joint Institute of Nuclear Research, under the auspice of the ICP Vegetation Programme. Greece participated in this European moss survey with our team consisted by Professor Dr Alexandra Ioannidou and Dr Evdoxia Tsakiri. It's the first time that the levels of trace elements deposited in mosses in the Greek territory are included in the European moss data base.

In the middle of 2016 summer, ninety-five (95) samples of *Hypnum cupressiforme* Hedw. moss species were collected from the vicinity of Northern Greece. They were cleaned manually and were prepared for Epithermal Neutron Activation Analysis (ENAA) and gamma ray measurements for the determination of trace elements and radionuclides concentrations respectively.

The elemental concentrations of forty-four (44) trace elements (Al, As, Ni, V, Cr, Zn, Fe, Br, Cl, I, Mg, Na, K, Sc, Ti, Mn, Co, Se, Rb, Sb, Au, Th, U, Si, Sr, Ca, Zr, Cs, Ba, La, Ce, Nd, Sm, Gd, Tb, Dy, Tm, Yb, Lu, Hf, Ta, In, Mo, Ag) were defined. The concentrations of Al, As, Ni, V, Cr, Zn and Fe range between 1350-46100  $\mu\text{g g}^{-1}$ , 0.52-17.90  $\mu\text{g g}^{-1}$ , 1.72-90.20  $\mu\text{g g}^{-1}$ , 2.61- 33.4  $\mu\text{g g}^{-1}$ , 2.04- 222  $\mu\text{g g}^{-1}$ , 14.60-282  $\mu\text{g g}^{-1}$  and 1010-28700  $\mu\text{g g}^{-1}$  respectively. Additional to these 95 moss samples, ten more moss samples from the region of Skouries were studied, close to active mining activities. The same trace elements were defined and the concentrations of most of them are higher than the rest moss samples of Northern Greece, highlighting the impact of the mining activities on the surrounding environment.

The PMF 5 model was run for the determination of the sources of the trace elements. Five sources are identified: *The Soil Dust, the Aged Sea Salt, the Road Dust, the Lignite Power Plant and the Mn-rich source*. The areas of W. Macedonia and Skouries are distinguished and characterized by the lignite power plant source, the Mn-rich source and the road dust source respectively. The soil dust source contributes more than 50% to the majority of the moss samples, indicating that the majority of trace elements are transferred to mosses, through the resuspended soil.

The elemental concentrations in soil samples collected from the same sampling sites were also determined. The elements Al, K, Si and Ti have similar concentrations in almost all sites, proving the negligible impact of anthropogenic activities on them. The areas that present high concentrations of Ni, Mn, Fe, Mg and Cr in mosses correspond to those in soil, indicating the same sources.

The activity concentrations of  $^7\text{Be}$ ,  $^{210}\text{Pb}_{\text{uns}}$ ,  $^{40}\text{K}$ ,  $^{232}\text{Th}$ ,  $^{226}\text{Ra}$  and  $^{137}\text{Cs}$  in mosses are also studied.  $^7\text{Be}$  ranges from 69 to 1280  $\text{Bq kg}^{-1}$ , while  $^{210}\text{Pb}_{\text{uns}}$  ranges from between 147 to 2049  $\text{Bq kg}^{-1}$ . The terrestrial nuclides  $^{40}\text{K}$ ,  $^{232}\text{Th}$  and  $^{226}\text{Ra}$  range between 120 to 1060  $\text{Bq kg}^{-1}$ , 0 to 66  $\text{Bq kg}^{-1}$  and 0 to 126  $\text{Bq kg}^{-1}$  respectively. The artificial nuclide  $^{137}\text{Cs}$  is found between 0 to 590  $\text{Bq kg}^{-1}$ . There is no correlation between the radionuclides and the altitude, temperature and precipitation.

The cosmogenic  $^7\text{Be}$  ends up in mosses through wet and dry deposition of aerosols to which it was attached right after its formation in the troposphere.  $^{210}\text{Pb}_{\text{uns}}$  comes from the decay of  $^{222}\text{Rn}$  in the atmosphere.  $^{232}\text{Th}$  and  $^{226}\text{Ra}$  are transferred to mosses both through soil particles and aerosol deposition. The terrestrial nuclide  $^{40}\text{K}$ , is placed on mosses via the soil dust particles that are dispersed in the atmosphere through the wind. The same pattern is followed by the artificial nuclide  $^{137}\text{Cs}$ , which is deposited on mosses through the resuspended soil particles.

Mosses were collected from different substrate types (rocks, branches, surface soil and near roots). Slight differences are observed in the radionuclides concentrations based on the substrate surface.  $^7\text{Be}$  presents higher activities in mosses collected from the ground surface, than those that were collected near roots. The nuclides  $^{210}\text{Pb}$ ,  $^{226}\text{Ra}$ ,  $^{232}\text{Th}$  do not present any significant difference between those collected from surface and near roots. There is a homogeneity for the concentrations of the artificial radionuclide  $^{137}\text{Cs}$ , while  $^{40}\text{K}$  is found in higher concentrations in those mosses that were picked up mostly near roots.

Radionuclides were also measured in soil samples. The concentrations of  $^{137}\text{Cs}$  range between 0.34 to 2569  $\text{Bq kg}^{-1}$ , of  $^{40}\text{K}$  between 52.79 to 1148  $\text{Bq kg}^{-1}$ , and of  $^{210}\text{Pb}$  from 11.46 to 1381  $\text{Bq kg}^{-1}$ . No special fit is identified between the concentrations of  $^{40}\text{K}$  and  $^{210}\text{Pb}$  in mosses and the corresponding soil samples. On the other hand, there is a match between the areas that present high concentrations of  $^{137}\text{Cs}$  in soil and in mosses, with those areas that were characterized as the most influenced after the Chernobyl accident. Finally, the resuspended soil is the main source of almost all the trace elements and radionuclides in mosses.

## Περίληψη

Τα βρύα αποτελούν ιδανικούς βιοϊχνηθέτες. Δε διαθέτουν ριζικό σύστημα, οπότε όλα τα θρεπτικά συστατικά καθώς και το νερό που χρειάζονται τα παίρνουν κατευθείαν από την υγρή και ξηρή εναπόθεση. Αποτελούν ένα χρήσιμο εργαλείο για τη μέτρηση της ποιότητας του αέρα, χωρίς να απαιτείται κάποιος ειδικός εξοπλισμός. Χάρη στη μορφολογία και φυσιολογία τους, έχουν τη δυνατότητα να συσσωρεύουν τους αέριους ρύπους όπως ιχνοστοιχεία, οργανικές ενώσεις και ραδιονουκλίδια.

Από το 1980 τα βρύα έχουν χρησιμοποιηθεί σε διάφορες έρευνες για τον προσδιορισμό των ιχνοστοιχείων και των ραδιονουκλιδίων. Από τότε, και κάθε 5 χρόνια διεξάγεται μια Ευρωπαϊκή έρευνα στο πλαίσιο του ICP Vegetation Programme σε σχέση με τις συγκεντρώσεις των ιχνοστοιχείων σε φυσικά αναπτυσσόμενα βρύα. Η τελευταία έρευνα πραγματοποιήθηκε το 2015/2016. Η Ελλάδα συμμετείχε για πρώτη φορά με την ομάδα μας, που αποτελείται από τις Καθηγήτριες Δρ. Αλεξάνδρα Ιωαννίδου και Δρ. Ευδοξία Τσακίρη. Είναι η πρώτη φορά που οι συγκεντρώσεις των ιχνοστοιχείων στα βρύα στην Ελλάδα καταγράφονται στην Ευρωπαϊκή βάση δεδομένων.

Στα μέσα του καλοκαιριού του 2016, ενενήντα πέντε (95) δείγματα βρύων *Hypnum cupressiforme* Hedw. συλλέχθηκαν από την περιοχή της Βορείου Ελλάδος. Αφού καθαρίστηκαν, προετοιμάστηκαν για τη μέτρησή τους με τη μέθοδο της Νετρονικής Ενεργοποίησης και της γαμμα-φασματοσκοπίας, για τον προσδιορισμό των συγκεντρώσεων των ιχνοστοιχείων και των ραδιονουκλιδίων αντίστοιχα.

Μετρήθηκαν οι συγκεντρώσεις 44 ιχνοστοιχείων (Al, As, Ni, V, Cr, Zn, Fe, Br, Cl, I, Mg, Na, K, Sc, Ti, Mn, Co, Se, Rb, Sb, Au, Th, U, Si, Sr, Ca, Zr, Cs, Ba, La, Ce, Nd, Sm, Gd, Tb, Dy, Tm, Yb, Lu, Hf, Ta, In, Mo, Ag). Οι συγκεντρώσεις των Al, As, Ni, V, Cr, Zn και Fe κυμαίνονται μεταξύ των 1350-46100  $\mu\text{g g}^{-1}$ , 0.52-17.90  $\mu\text{g g}^{-1}$ , 1.72-90.20  $\mu\text{g g}^{-1}$ , 2.61- 33.4  $\mu\text{g g}^{-1}$ , 2.04- 222  $\mu\text{g g}^{-1}$ , 14.60-282  $\mu\text{g g}^{-1}$  και 1010-28700  $\mu\text{g g}^{-1}$  αντίστοιχα. Εκτός από αυτά τα 95 δείγματα βρύων, συλλέχθηκαν ακόμη 10 δείγματα από την περιοχή των Σκουριών, κοντά στα μεταλλεία. Προσδιορίστηκαν οι συγκεντρώσεις των ίδιων ιχνοστοιχείων, οι οποίες είναι μεγαλύτερες από αυτών της υπόλοιπης Βορείου Ελλάδας, υπογραμμίζοντας έτσι τον αντίκτυπο που έχουν οι εργασίες εξόρυξης στο περιβάλλον.

Για τον προσδιορισμό των πηγών των ιχνοστοιχείων, εφαρμόστηκε το μοντέλο PMF5, σύμφωνα με το οποίο αναγνωρίστηκαν 5 πηγές: η σκόνη από το χώμα, το παλαιωμένο θαλασσινό αλάτι, η σκόνη από τον δρόμο, τα εργοστάσια καύσης λιγνίτη και τέλος η πλούσια σε Mn πηγή. Οι περιοχές της Δυτ. Μακεδονίας και των Σκουριών είναι αυτές που ξεχωρίζουν και συνδέονται με τα εργοστάσια καύσης λιγνίτη, την πλούσια σε Mn πηγή και τη σκόνη από τον δρόμο αντίστοιχα. Η σκόνη από το χώμα συνεισφέρει στα περισσότερα δείγματα των βρύων σε ποσοστό πάνω από 50%, υποδεικνύοντας ότι η πλειοψηφία των ιχνοστοιχείων μεταφέρεται στα βρύα μέσω της επαναιώρησης του χώματος.

Μελετήθηκαν ακόμη οι συγκεντρώσεις των ιχνοστοιχείων στο χώμα. Τα στοιχεία Al, K, Si και Ti βρίσκονται σε παρόμοια επίπεδα σε όλα τα δείγματα, δείχνοντας έτσι ότι δεν οφείλονται σε ανθρωπογενείς πηγές. Οι περιοχές που παρουσιάζουν υψηλές

συγκεντρώσεις των Ni, Mn, Fe, Mg και Cr στα βρύα, αντιστοιχούν με αυτές του εδάφους, υποδεικνύοντας επομένως την ύπαρξη των κοινών πηγών τους.

Μελετήθηκαν ακόμη οι συγκεντρώσεις των εξής ραδιονουκλιδίων:  ${}^7\text{Be}$ ,  ${}^{210}\text{Pb}_{\text{uns}}$ ,  ${}^{40}\text{K}$ ,  ${}^{232}\text{Th}$ ,  ${}^{226}\text{Ra}$  και  ${}^{137}\text{Cs}$  οι οποίες κυμαίνονται ως εξής: 69- 1280 Bq kg<sup>-1</sup>, 147 - 2049 Bq kg<sup>-1</sup>, 120- 1060 Bq kg<sup>-1</sup>, 0- 66 Bq kg<sup>-1</sup>, 0- 126 Bq kg<sup>-1</sup> και τέλος 0- 590 Bq kg<sup>-1</sup> αντίστοιχα. Δεν βρέθηκε κάποια συσχέτιση μεταξύ των συγκεντρώσεων των ραδιονουκλιδίων και του ύψους, της θερμοκρασίας και των υγρών κατακρημνίσεων.

Το  ${}^7\text{Be}$  αφού δημιουργηθεί στην τροπόσφαιρα, προσκολλάται στα διάφορα αεροζόλ, οπότε καταλήγει στα βρύα μέσω της εναπόθεσής (υγρή, ξηρή) τους. Ο  ${}^{210}\text{Pb}_{\text{uns}}$  προέρχεται από την αποδιέγερση του  ${}^{222}\text{Rn}$  στην ατμόσφαιρα, την προσκόλληση του στα αεροζόλ και τέλος την εναπόθεση τους μέσω της υγρής και ξηρής εναπόθεσης στα βρύα. Τα ραδιονουκλίδια  ${}^{232}\text{Th}$  και  ${}^{226}\text{Ra}$  τοποθετούνται στα βρύα τόσο μέσω της εναπόθεσης αεροζόλ όσο και σωματιδίων χόματος. Το  ${}^{40}\text{K}$  προέρχεται από τα σωματίδια χόματος που αιωρούνται στην ατμόσφαιρα. Το ίδιο μοτίβο ακολουθεί και το τεχνητό ραδιονουκλίδιο  ${}^{137}\text{Cs}$ , το οποίο καταλήγει στα βρύα μέσω της επαναιώρησης των σωματιδίων του εδάφους.

Τα βρύα συλλέχθηκαν από διάφορες επιφάνειες (πάνω από πέτρες, στο έδαφος, σε κλαδιά και κοντά στις ρίζες). Παρατηρούνται μικρές διαφορές στις συγκεντρώσεις τους, ανάλογα με την επιφάνεια συλλογής τους. Το  ${}^7\text{Be}$  παρουσιάζει μεγαλύτερες συγκεντρώσεις στα δείγματα που συλλέχθηκαν από το έδαφος από ότι κοντά στις ρίζες. Τα νουκλίδια  ${}^{210}\text{Pb}$ ,  ${}^{226}\text{Ra}$  και  ${}^{232}\text{Th}$  δεν παρουσιάζουν καμιά ιδιαίτερη διαφορά. Παρουσιάζεται μια ομοιογένεια στις συγκεντρώσεις του  ${}^{137}\text{Cs}$ , ενώ το  ${}^{40}\text{K}$ , εμφανίζει μεγαλύτερες συγκεντρώσεις στα βρύα που βρίσκονταν κοντά στις ρίζες.

Οι συγκεντρώσεις των ραδιονουκλιδίων μελετήθηκαν επιπλέον στα αντίστοιχα δείγματα χόματος και κυμαίνονται ως εξής: για το  ${}^{137}\text{Cs}$  από 0.34 μέχρι 2569 Bq kg<sup>-1</sup>, για το  ${}^{40}\text{K}$  από 52.79 μέχρι 1148 Bq kg<sup>-1</sup>, και για τον  ${}^{210}\text{Pb}$  από 11.46 μέχρι 1381 Bq kg<sup>-1</sup>. Δεν παρατηρείται καμιά συσχέτιση μεταξύ των συγκεντρώσεων των  ${}^{40}\text{K}$  και  ${}^{210}\text{Pb}$  στα βρύα και στα χόματα. Αντίθετα, υπάρχει μια ταύτιση μεταξύ των περιοχών που παρουσιάζουν υψηλές συγκεντρώσεις  ${}^{137}\text{Cs}$  στα βρύα, στα χόματα και αυτών που είχαν χαρακτηριστεί ως οι πιο επιβαρυνμένες ακριβώς μετά το ατύχημα στο Τσέρνομπιλ. Τελος, η επαναιώρηση του χόματος είναι η κύρια πηγή της πλειοψηφίας των ιχνοστοιχείων και των ραδιονουκλιδίων στα βρύα.

*To my father,  
my sister and our angel  
my mother*

## **Acknowledgements**

First of all, I would like to express my deepest gratitude to my supervisor, Associate Professor Alexandra Ioannidou for her continuous academic and moral support during my studies and in every minute of my life since I have met her. I am really thankful for her aspiring guidance, motivation and patience during this PhD, for suggesting the subject and for introducing me to the world of Environmental Radioactivity. Moreover, I appreciate the most her eternal effort for my financial support, the achievement of being accepted for ELIDEK Scholarship during my PhD studies and for her encouragement in participating in a lot of conferences and workshops. I attribute the level of PhD to her encouragement and effort and without her, this thesis would not have been completed and written. A friendly and perspicacious supervisor- my mentor in PhD and life simultaneously. Thank you so much!

Additionally, I would like to thank the members of my three-member committee, Professor Miodrag Krmar and Associate Professor Stylianos Stoulos for their academic support, advice, guidance and training in gamma ray measurements. I am indebted to Associate Professor Stylianos Stoulos for his enlightenment, counseling, help and the humorous moments during my PhD. A special thanks to Professor Miodrag Krmar for suggesting our participation in the European Moss Survey by ICP Vegetation, for introducing me to gamma ray measurements of mosses and their analysis, for measuring our samples in their laboratory, in the University of Novi Sad, Serbia and for his assistance during my whole accommodation in Novi Sad. I would like also to thank Dr. Jan Hansman for his contribution to gamma measurements of our moss samples.

I am pretty thankful to our open-heart mentor from the Frank Laboratory of Neutron Physics Joint Institute for Nuclear Research (JIRN) in Dubna and coleader of the ICP Vegetation - Dr. Marina Frontasyeva, for measuring in their laboratory our mosses via ENAA technique, her consultation, her academic and moral support during my PhD and especially during my stay in Dubna. I am also grateful to my friend, Omar Chaligava, researcher of JINR, for his assistance and advice on ENAA results.

I would like to attribute my greatest gratitude to Dr. Evdoxia Tsakiri, for her enormous assistance in mosses, as without her this research could not be conducted. Moreover, I would like to thank Dr. Costas Kalfas for providing the gamma ray analysis software as well to Drs. Nerantzis Kazakis, Lambrini Papadopoulou and Evagelia Diapouli for their assistance, XRF measurements and Source Apportionment Analysis.

I would like to extend my warm thanks to my first professor during my master studies, Professor Athina Pakou, University of Ioannina, for her support, enlightenment and taking care of my first steps in the world of experimental nuclear physics.

Furthermore, I would like to acknowledge all the members of the review committee for dedicating time in this thesis and for their valuable comments.

Last but not least, I would like to warmly thank my family and more specifically my father, my sister and our angel-my mother who is no longer with us, for their love, support and patience during my PhD studies. A special thanks to my Paschalis for coming into my life and making it prettier and more cheerful.

## Table of Contents

<b>Abstract</b> .....	6
<b>Περίληψη</b> .....	8
<b>Acknowledgments</b> .....	11
<b>Chapter 1 Introduction</b> .....	15
<b>Chapter 2 Theoretical Background</b> .....	20
2.1 Gamma ray emission.....	20
2.2 Radioactivity.....	20
2.2.1 The Radioactive Decay Law.....	22
2.2.2 The Radioactive Decay Chains.....	23
2.3 Gamma ray detection.....	24
2.3.1 The Photoelectric Effect.....	24
2.3.2 The Compton Scattering.....	25
2.3.3 The Pair Production.....	25
2.3.4 Principles of Detectors: HPGe Detector.....	27
2.4 X-ray emission.....	29
2.5 X-ray detection.....	30
2.6 Trace Elements.....	31
2.6.1 Definition of the term Trace Elements.....	31
2.6.2 Sources of Trace Elements.....	31
2.7 Bryophytes.....	32
2.7.1 General information.....	32
2.7.2 Bryophytes growth and nutrients requirements.....	34
2.7.3 <i>Hypnum cupressiforme</i> Hedw. moss species used as bioindicator in this study.....	35
<b>Chapter 3 Experimental Details</b> .....	37
3.1 Study area.....	37
3.1.1 Sampling methodology.....	37
3.2 Sample preparation.....	39
3.2.1 Moss sample preparation for gamma-spectrometry.....	39
3.2.2 Moss sample preparation for ENAA.....	39

3.2.3 Soil sample preparation.....	40
3.3 Gamma ray measurements.....	41
3.3.1 Detector set-up for $\gamma$ -ray measurements.....	41
3.3.2 Energy calibration.....	44
3.3.3 Efficiency calibration of gamma detectors.....	45
3.3.4 Soil samples efficiency calibration.....	46
3.3.5 Moss samples efficiency calibration.....	51
3.4 Epithermal Neutron Activation Analysis (ENAA) Measurements.....	55
3.5 X-ray fluorescence spectrometry measurements.....	66
<b>Chapter 4</b> <b>Trace Elements</b> .....	<b>68</b>
4.1 Trace Elements concentrations in mosses.....	68
4.1.1 Spatial distributions of trace elements in mosses.....	70
4.1.2 Correlation analysis between the trace elements in moss samples.....	80
4.1.3 The influence of the surface type on elemental concentrations.....	82
4.2. Case Study – Mosses collected near a gold mine in Skouries (Chalkidiki Prefecture, Central Macedonia Region).....	83
4.2.1 History of the gold mining in Skouries.....	83
4.2.2 Sampling and Analysis.....	84
4.2.3 Distributions of the elemental concentrations of the different moss species.....	86
4.2.4 Correlation between the trace elements concentrations determined in the moss samples.....	88
4.2.5 “Skouries” elemental concentrations vs the rest Northern Greece concentrations.....	90
4.2.6 Other studies related with the area of “Skouries”.....	91
4.3 Comparison with data in literature.....	91
4.3.1 Other studies in Greece.....	92
4.3.2 Other international studies.....	95
4.4 Source apportionment analysis.....	99
4.4.1 Positive Matrix Factorization (PMF) model.....	99
4.4.2 PMF Analysis Results.....	102

4.5 Trace elements concentrations in soil.....	108
4.5.1 Distribution of elements in soil samples.....	108
4.5.2 Comparison of the elemental concentrations in soil and moss samples.....	112
4.5.3 Transfer of resuspended soil to mosses.....	113
4.5.3.1 Transfer of resuspended soil to mosses and different substrate type of mosses.....	114
4.5.4 Comparison with data from other studies in Greece.....	116
4.5.5 Comparison with data from other studies around the world.....	118
<b>Chapter 5 Radionuclides.....</b>	<b>121</b>
5.1 Radionuclides concentrations in mosses.....	121
5.1.1 Spatial distributions of radionuclides in mosses.....	122
5.1.2 General statistic of the radionuclides activities.....	130
5.1.3 The role of substrate surfaces in radionuclides concentrations.....	136
5.1.4 Results from other Greek studies.....	137
5.1.5 Results from other studies around the world.....	138
5.2 Radionuclides concentrations in soil samples.....	141
5.2.1 Spatial distributions of radionuclides in soil.....	141
5.2.2 Transfer of resuspended soil to mosses.....	145
5.2.3 Comparison with other data in the literature.....	147
<b>Chapter 6 Conclusions.....</b>	<b>149</b>
<b>References.....</b>	<b>154</b>
<b>Appendix.....</b>	<b>183</b>

## Chapter 1

## Introduction

Air pollution is one of the most serious problems nowadays. Since industrial revolution and due to the increasing human activities and urbanization, the chemical composition of the atmosphere has changed over time and the air quality has deteriorated (Seinfeld & Pandis, 2006; Gerdol et al.; 2014; González Ortiz et al., 2019). The increase of atmospheric pollutants in urban and industrial areas consists one of the main European scientific concerns since the 1970's and currently is considered to be the most important environmental risk to human health and ecosystems (Gerdol et al., 2014; Di Palma et al., 2016).

Some of the most important pollutants of the atmosphere are the particulate matter (PM), the trace elements and the persistent organic compounds. Trace elements are those pollutants of the atmosphere which are going to be studied in the current survey. They can enter in all ecosystems while they are emitted to the atmosphere in different forms, gas or even in particulate matter (Herpin et al., 1996; Cucu-Man, 2004). There are different sources of the atmospheric emitted trace elements, such as housing and commercial properties, industrial processes and oil combustion (Cr, Ni, V, Cu), metallurgy (Mn, Zn, Pb, Cd), sea spray (Cl, Na, Mg), soil and road dust (Fe, Ca, Al, Si), traffic emissions (such as brake abrasion: Cu, Ba, Sb, combustion of lubricating oil: Zn, Ca) and agriculture (atmospheric ammonia) (Pio et al., 1989; Marengo et al., 2006; Almeida et al., 2005; Yin et al., 2005; Shauer et al., 2006; Zabalza et al., 2006; Viana et al., 2008; Harmens et al., 2008; 2011).

Trace elements can be transported over long distances and can be deposited many kilometers away from their emitting sources, impacting on human health and the environment (Meyer et al., 2015). The exposure to elevated concentrations of trace elements have significant impacts on human health, particularly in urban areas (González Ortiz et al., 2019). They have been associated with different health problems such as respiratory, cardiovascular and immunological problems (Metzger et al., 2004; Meng et al., 2007; Bell et al., 2008; Vuković, 2015; Mirabelli et al., 2020). They can influence all the ecosystems. They have several environmental impacts, and can affect the vegetation, fauna and the quality of water and soil (González Ortiz et al., 2019).

It is crucial for humans to deal with this global thread by recognizing all the pollutants, understanding how they are transformed in the atmosphere and how they can affect human health and ecosystems. As a result, monitoring the air quality is considered necessary. During the last 20 years, different instructions (1999/30/ EC, 2002/3/EC, 2004/107/EC and 2008/50/EC) have been officially followed by the European Community for air quality assessments related to trace elements, nitrogen and sulphur dioxides, and ozone concentrations in the atmosphere (Di Palma et al., 2016). The international cooperation for controlling and reducing the air pollution during this period, has significantly contributed to the decrease of trace elements emissions in Europe (Meyer et al., 2015; Ilyin et al., 2013). For example, during the period 1990 to 2012, there was a decline in the total deposition of the elements Pb, Cd, and Hg of the order of 78%, 53% and 23% respectively (De Wit et al., 2015).

For monitoring the quality of air, different complementary modelling techniques have been used and they are mostly based on physico-chemical measurements of different

air pollutants (2008/50/EC; Adamo et al., 2011). Monitoring the quality of ambient air is a complex procedure, as it requires expensive analytic instrumentations which need power supply and permanent maintenance, large number of potentially dangerous substances and finally temporal and spatial variations in the input rates of different pollutants (Boubel et al., 1994; Adamo et al., 2011; Tørseth et al., 2012; Gerdol et al., 2014). Due to these difficulties, different alternatives were examined and finally the idea of biomonitoring became a reality in the late 1960's by Rühling and Tyler (1968).

Biomonitoring is a technique that gives the possibility to detect spatial and temporal variations in the atmospheric deposition of different pollutants and to define their possible sources (Pott & Turpin, 1998; Bargagli, 1998; Markert et al., 2003; Lehto et al., 2008; Schröder et al., 2008; 2010; Holy et al., 2009; Harmens et al., 2010; Adamo et al., 2011; Gerdol et al., 2014). This technique uses living organisms as biomonitors either passively or actively, based on their sensitivity to air pollution or their capacity of accumulating pollutants in their tissues (Falla et al., 2000; Wolterbeek, 2002; Gerdol et al., 2014).

During the recent decades and among the different living organisms (vascular plants, mosses and lichens) that can be used as bioaccumulators of airborne pollutants (Paatero et al., 1998; Conti et al., 2001; Onianwa, 2001; Malizia et al., 2012; Gerdol et al., 2014), mosses and lichens have been systematically chosen for environmental monitoring. Mosses are special living organisms- one of the earliest land plants in evolutionary terms (Decker et al., 2006), and they have reasonably attracted the interest of the researchers as they present very unique characteristics that have not been noticed in other plants (Czarnowska et al., 1974).

The idea of using mosses as biomonitors in order to measure the atmospheric depositions of metals was originally established in 1980 as a Swedish initiative under the leadership of Åke Rühling in Sweden (Harmens et al., 2015). Using mosses as bioindicators of atmospheric fallout, is based on the fact that elemental concentrations in mosses are closely related to atmospheric deposition (Rühling & Tyler, 1968; Little & Martin, 1974; Gjengedal & Steinnes, 1990; Steinnes et al., 1992). Mosses are able to accumulate airborne pollutants such as trace elements (Rühling & Tyler, 1968; Little & Martin, 1974; Herrmann, 1976; Tomassini et al., 1976; Thomas, 1986; Tyler, 1990; Bargagli et al., 1995; Schröder et al., 2008) and organic compounds (Harmens et al., 2013) due to their morphological and physiological characteristics (Gerdol et al., 2014).

Mosses are non-vascular plants and they have no roots; they develop only rhizoids for anchoring on the substrate and all the nutrients and water are obtained mainly from wet and dry deposition (Schwartzenberg, 2006; Glime, 2017). The uptake of trace elements from the ground is not significant (Harmens et al., 2010). Due to the fact that they do not grow very fast, they are able to accumulate trace elements over a large time period. The elemental concentrations accumulated every year in mosses can be revealed by studying each annual growth segment of mosses (Chakraborty & Paratkar, 2006). Some moss species are appropriate for assessing the quality of air on large geographic scale due to the fact that they compose extensive populations (Gerdol et al., 2014; Harmens et al., 2012). The elemental concentrations in mosses which cover a large geographic scale may vary. This is due to the fact that the accumulation of elements in

moss tissues can be seriously influenced by local pollution sources and different environmental factors (Schröder et al., 2008; Tørseth et al., 2012; Gerdol et al., 2014).

The moss analysis technique is an easy and less expensive method than the conventional deposition analysis as no special deposition collectors are required and a high sampling density can be carried out (Berg et al., 1995; Gusev et al., 2009; Harmens et al., 2010). Information about trace elements deposition can be obtained even in remote places, covering a big spatial grid during the same period. Mosses do not provide direct quantitative measurements of elements deposition. However, relating the information from different moss surveys to deposition monitoring data for each country, information about elemental concentrations can be extracted and the areas that are at risk from air pollution can be identified at a high spatial resolution (Berg & Steinnes, 1997; Berg et al., 2003; Harmens et al., 2010; Schröder et al., 2010).

The first European moss survey on trace elements was conducted in 1990 and since then it has been repeated every five years (Harmens et al., 2013). The first two moss surveys (1990 and 1995) were coordinated by the Nordic Working Group on Monitoring and Data, Nordic Council of Ministers (Harmens et al., 2015). Since 2000, the International Cooperative Programme on Effects of Air Pollution on Natural Vegetation and Crops (ICP Vegetation) handed over the coordination of moss biomonitoring at the Centre for Ecology & Hydrology (CEH) in Bangor, UK. The European moss survey provides data on concentrations of As, Al, Sb, Cd, Cr, Cu, Fe, Hg, Ni, Pb, V, Zn elements in naturally growing mosses (Harmens et al., 2015).

According to the latest ICP Vegetation results, the lowest elemental concentrations in mosses have been found in Scandinavia, in the Baltic states and in northern parts of the UK, while the highest ones are found in Belgium and south-eastern Europe, resulting in a more or less declining gradient from south-east to north-west. There is a general decline in emission and deposition of metals across Europe which has also resulted in a decrease in the elemental concentrations in mosses for the majority of metals. Since 1990, the median concentration in mosses across Europe has declined the most for lead (77%), followed by vanadium (55%), cadmium (51%), chromium (43%), zinc (34%), nickel (33%), iron (27%), arsenic (21%, since 1995), mercury (14%, since 1995) and copper (11%). The decline of the concentrations of Cd, Pb and Hg in mosses are also positively correlated and verified by the declines in atmospheric deposition modelled by the European Monitoring and Evaluation Programme across Europe (EMEP: Co-operative Programme for monitoring and evaluation of the long-range transmission of air pollutants in Europe) (Harmens et al., 2015).

The latest moss survey was conducted in 2015/2016, coordinated by the Joint Institute of Nuclear Research (JINR; Dubna, Russian Federation), under the auspice of the ICP Vegetation Programme (United Nations Economic Commission for Europe Convention on Long-Range Transboundary Air Pollution. Monitoring of Atmospheric Deposition of Heavy Metals, Nitrogen and POPs in Europe using Bryophytes) (Frontasyeva et al., 2015). Greece participated in this European moss survey with our group consisted by Professor Dr. Alexandra Ioannidou and Dr. Evdoxia Tsakiri. It's the first time that the levels of trace elements deposited in mosses in the Greek territory are included in the European moss data base. For Greece there is only one previous related report available;

an attempt that aimed to monitor cross-border mapping of metals and toxic elements accumulated in mosses reflecting wet and dry deposition, covering a small area in Northeastern Greece and the adjacent area of Southern Bulgaria (Yurukova et al., 2009).

Mosses except of being great bioindicators of trace elements can also be a very good tool for the detection of different radionuclides. During the last thirty years, they have been successfully used as monitors of different radionuclides such as  $^{210}\text{Pb}$ ,  $^{210}\text{Po}$ ,  $^{137}\text{Cs}$ ,  $^7\text{Be}$  and  $^{40}\text{K}$  (Papastefanou et al., 1989; Papastefanou & Manolopoulou, 1992; Godoy et al., 1998; Delfanti et al., 1999; Uğur et al., 2003; Krmar et al., 2007, 2009, 2016; Cevik & Celik, 2009; Sert et al., 2011; Ziembic et al., 2013; Boryło et al., 2017). Mosses accumulate and retain radionuclides through passive processes and thus their spatial and temporal deposition patterns can be recorded (Loppi et al., 2003; Sawidis et al., 2009). More specifically, mosses due to their widespread occurrence, slow growth, morphology and their continuous exposure to radionuclides deposition, they are able to preserve all the previous deposited activity providing the history of the radionuclide supply in the environment (Sawidis et al., 2009; Krmar et al., 2009, 2016). These characteristics of mosses favor the study of different atmospheric processes which are correlated with the airborne radionuclides, such as  $^7\text{Be}$  and  $^{210}\text{Pb}$ . The study for example of the cosmogenic radionuclide beryllium, which is accumulated in mosses, helps understanding and tracking the aerosols in the atmosphere. This is due to the fact that beryllium, after its formation, is attached to aerosols particles and the fate of Be becomes the fate of the carrier aerosols (Papastefanou & Ioannidou, 1995a). Additionally, useful information about any local processes and depositional characteristics concerning the  $^{137}\text{Cs}$  and  $^{40}\text{K}$  nuclides can be provided by the mosses analysis (Krmar et al., 2007).

The main aim of the current survey is to study the bioaccumulation of trace elements and radionuclides in mosses from Northern Greece. Until now, in Greece no other research has used mosses as bioindicators in order to describe simultaneously the elemental and radionuclides concentrations coming from the atmospheric deposition in such a big scale, covering the whole region of Northern Greece.

For this purpose, at the end of summer till middle of autumn of 2016, moss samples of *Hypnum cupressiforme* Hedw. were collected from the Regions of West, Central and East Macedonia & Thrace. The fact that *Hypnum cupressiforme* Hedw. is a species that could be found and collected in all the phytogeographical areas of Greece (Tsakiri, 2009), gave the possibility of performing an overall overview of the atmospheric deposition of trace elements and radionuclides in mosses during a five years' period, according to the ICP Vegetation 'Moss Survey Protocol'. Furthermore, by investigating the spatial distribution of trace elements in mosses, including the areas that are closer to the borders, leads to track and understand any transboundary transport of them and identify any possible source not located in the Greek territory but may be associated to the neighboring countries activities.

For the purposes of this research, the 'Epithermal Neutron Activation Analysis' technique (ENAA), in combination with gamma spectrometry analysis are the tools that were used for the determination of trace elements and radionuclides concentrations in

mosses, while the 'Source Apportionment' technique is the statistical tool that was used for the identification of their sources.

This thesis consists of five more chapters. The theoretical background and the methodology for the moss survey are described in Chapter 2 and 3 respectively, followed by a summary of spatial distributions of different trace elements presented in maps (Chapter 4). In Chapter 5, the radioactive nuclides accumulated in mosses are discussed and finally the conclusions are drawn in Chapter 6.

## Chapter 2

## Theoretical Background

This chapter provides the basic concepts of  $\gamma$ -ray spectroscopy. The modes of radioactive decay, mechanisms of gamma-ray photon interaction with matter and how these relate to  $\gamma$ -ray spectrometry are discussed. A brief summary is provided about X-ray fluorescence (XRF) spectroscopy. In the end, a short description about trace elements, mosses and their use as biomonitors is provided.

### 2.1 Gamma ray emission

The nucleus is characterized by discrete energy levels (Leo et al., 1994). The stability of the nucleus depends on the neutron-proton ratio ( $N/Z$ ). An unstable nucleus may undergo several decay processes in order to reach stability. If there is a slight imbalance of the neutron-proton ratio, the radionuclide will undergo beta ( $\beta$ ) decay, whereas if there is a large imbalance, alpha ( $\alpha$ ) decay will occur. Both the  $\alpha$  and  $\beta$  decay modes may produce a daughter nucleus in an excited state (Gilmore, 2008; Kaniu, 2017).

The excited nucleus will go from the excited state to another state of lower energy (ground state) instantly ( $\sim 10^{-12}$  s), via internal conversion or  $\gamma$  emission processes. Concerning the  $\gamma$  emission process, the energy difference between these two states is released in the form of a photon (Leo et al., 1994; Gilmore, 2008; Kaniu, 2017). In internal conversion process, the nucleus de-excites by transferring its nuclear excitation energy directly to an atomic electron, rather than emitting a photon. The electron is ejected with a kinetic energy equal to the excitation energy minus its atomic binding energy (Leo et al., 1994). The internal conversion process is not going to be studied in the present work.

The gamma decay is described in equation 2.1:



where,

${}^A_ZX^*$  indicates the excited nucleus which de-excites to a lower energy state nucleus  ${}^A_ZX$ , accompanied by the emission of  $\gamma$ - ray (Tsoulfanidis & Landsberger, 2010). The half-lives of gamma emissions are usually between  $10^{-9}$  s till hours or days.

### 2.2 Radioactivity

Radioactivity is a spontaneous process during which an unstable nucleus (parent) emits a particle and it is transformed into another nucleus (daughter) that may or may not be stable. During the transition, the nucleus (parent) loses energy. This energy (decay energy) is emitted in the form of electromagnetic radiation or kinetic energy of the reaction products. Radioactivity is traditionally measured in units *Curies* (Ci), which is defined as the activity of 1 g of pure radium-226. For laboratory-scale radioisotope sources, its submultiples are more suitable (mCi and  $\mu$ Ci), as well as the unit of

Becquerel (Bq), which means one disintegration per sec. One Curie is equivalent to  $3.7 \times 10^{10}$  Bq (Leo et al., 1994; Gilmore, 2008).

Radioactivity is divided into two types, natural and artificial radioactivity, depending on the anthropogenic or not origin of it. The radioactive nuclides (natural or artificial), which have atomic number  $Z > 82$  (the elements that are above  $^{208}\text{Pb}$ ), tend to gradually decay via alpha, beta and gamma emission. The radioactive nuclides have been created during different processes such as the Big Bang, different cosmic processes (e.g. supernova) and nuclear reactions that occur on Earth (Gilmore, 2008; Papa, 2018).

Natural radioactive nuclides can be found in a lot of materials in the surrounding, such as in the terrestrial environment (rocks and minerals), but also in the atmosphere due to nuclear reactions that occur there such as  $^3\text{H}$ ,  $^7\text{Be}$ ,  $^{14}\text{C}$ . Natural radioactivity of the terrestrial environment originates from long-lived primordial radionuclides, namely potassium ( $^{40}\text{K}$ ), actinium ( $^{235}\text{U}$  and its daughters), uranium ( $^{238}\text{U}$  and its daughters) and thorium ( $^{232}\text{Th}$  and its daughters). Terrestrial materials i.e. soil, rocks, minerals that contain these radionuclides are referred to as naturally occurring radioactive materials (NORM) (Gilmore, 2008). The three natural radioactive series of  $^{238}\text{U}$ ,  $^{235}\text{U}$  and  $^{232}\text{Th}$  are presented in Figure 2.1 (Mermier & Seldon, 1969).

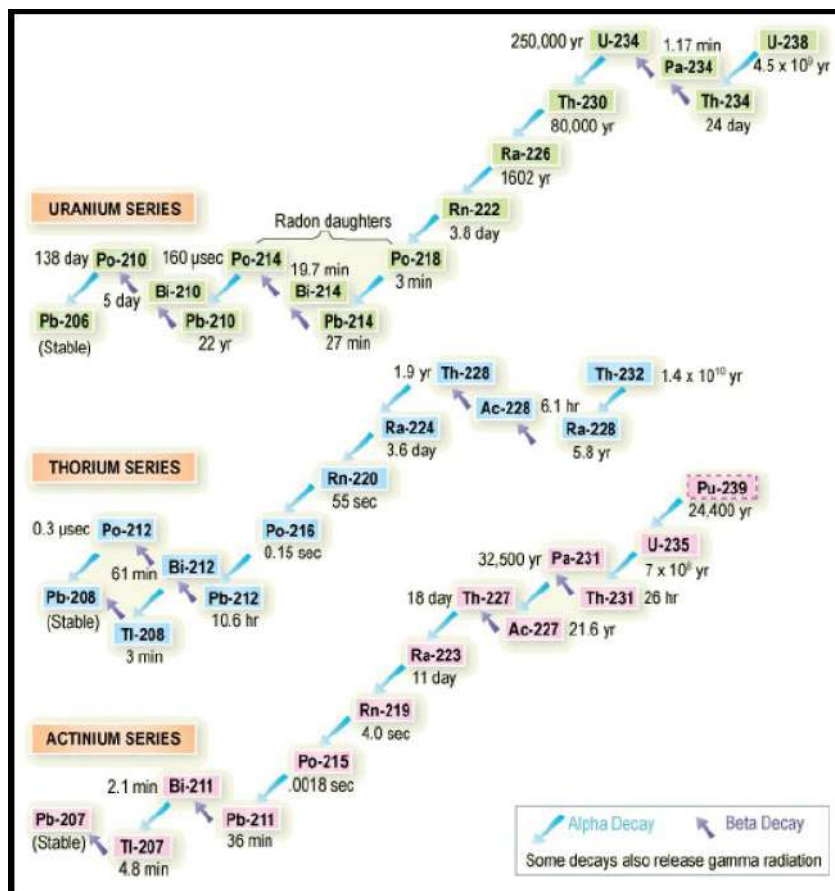


Figure 2.1. The three natural radioactive series of  $^{238}\text{U}$ ,  $^{235}\text{U}$  and  $^{232}\text{Th}$  (Ferreira et al., 2015).

### 2.2.1 The Radioactive Decay Law

The radioactive decay law was firstly established experimentally by Rutherford and Soddy. It states out that the activity of a radioactive sample decays exponentially in time (Leo et al., 1994). According to the decay law, each nuclear decay process is characterized by a transition probability per unit time  $\lambda$ . The decay rate  $\left(\frac{dN}{dt}\right)$  is proportional to the present number of atoms (N) of radionuclide in the sample (equation 2.2), assuming that no new nuclei are introduced into the sample (Gilmore, 2008).

$$A = -\frac{dN}{dt} = \lambda N \quad (2.2)$$

where,

A is the activity of the radionuclide in Bq and  $\lambda$  is the decay constant in  $s^{-1}$ .

The number of radionuclides N(t) follows the exponential behavior:

$$N(t) = N_0 e^{-\lambda t} \quad (2.3)$$

where,

$N_0$  is the number of radionuclides at  $t=0$  s. Thus the exponential decrease in the activity of a radioactive sample is governed by the decay constant  $\lambda$  (Leo et al., 1994). The decay equation describes also the radioactivity A(t), as it is proportional to the number of radionuclides.

The probability that a nucleus *will not decay* in time  $t$ - is given by the ratio of

$$\frac{\text{atoms not decaying in time } t}{\text{atoms at } t=0} = \frac{N(0)e^{-\lambda t}}{N(0)} = e^{-\lambda t} \quad (2.4)$$

The probability that a nucleus will decay between  $t$  and  $t+dt$  is  $p(t) dt = \lambda e^{-\lambda t} dt$ . The mean lifetime ( $\bar{t}$ ) which represents the needed time for a sample of radionuclides to decay to 1/e of its initial activity is defined as:

$$\bar{t} = \lambda \int_0^{\infty} t p(t) dt = \lambda \int_0^{\infty} t e^{-\lambda t} dt = \frac{1}{\lambda} \quad (2.5)$$

The half-life  $t_{1/2}$  is defined as the time it takes for the sample to decay to one half of its original activity (Leo et al., 1994; Tsoufanidis & Landsberger, 2010).

$$\frac{N(t_{1/2})}{N_0} = \frac{1}{2} \Rightarrow e^{-\lambda t_{1/2}} = \frac{1}{2} \Rightarrow \lambda = \frac{\ln 2}{t_{1/2}} \quad (2.6)$$

Finally, in the case of samples with big volumes, in order to describe the activity of a radionuclide per unit mass of the sample ( $Bq \text{ kg}^{-1}$ ), it should be assumed that the activity is distributed in the whole sample in a uniform and homogeneous way (Tsoufanidis & Landsberger, 2010; Pappa, 2018).

## 2.2.2 The Radioactive Decay Chains

It is very often for a nuclide to decay to a daughter nucleus, which will also decay to another unstable nucleus and so on. As a result, a radioactive decay chain is generated. The first nucleus is called “parent” nuclide, while the produced radioactive products are referred as “daughters” or “progenies” of the parent nuclide. The decay chains can be very complex especially when the granddaughter and several of its progenies are also radioactive (Gilmore, 2008; Kaniu, 2017).

The decay kinetics can be described in equation 2.7. The radioactive parent nuclide  $P$ , decays with a decay constant  $\lambda_P$  into a daughter nuclide  $D$ , that in turn will decay into a stable granddaughter nuclide  $G$ , with a decay constant  $\lambda_D$ .



After applying the radioactive decay law, the following equations come up:

$$\frac{dN_P}{dt} = -\lambda_P N_P \quad (2.8)$$

$$\frac{dN_D}{dt} = -\lambda_D N_D \quad (2.9)$$

$$\frac{dN_G}{dt} = -\lambda_G N_G \quad (2.10)$$

Then, the number of P atoms at time t and the number of daughter nuclei D present at time t are given by equations (2.11) to (2.13).

$$N_P(t) = N_P(0)e^{-\lambda_P t} \quad (2.11)$$

$$N_D(t) = N_P(0) \frac{\lambda_P}{\lambda_D - \lambda_P} [e^{-\lambda_P t} - e^{-\lambda_D t}] \quad (2.12)$$

$$N_G(t) = N_P(0) \left\{ 1 + \frac{1}{\lambda_D - \lambda_P} [\lambda_P e^{-\lambda_D t} - \lambda_D e^{-\lambda_P t}] \right\} \quad (2.13)$$

where  $N_P(0)$  is the number of P atoms at time  $t=0$ .

Then the activity of D at time t ( $A_D(t)$ ) is given by equation (2.14).

$$A_D(t) = \lambda_D N_D(t) = A_P(t) \frac{\lambda_P}{\lambda_D - \lambda_P} [1 - e^{-(\lambda_D - \lambda_P)t}] \quad (2.14)$$

where  $A_P(t) = \lambda_P N_P(t)$  and it's the activity of P at time t (Leo et al., 1994; Gilmore, 2008; Kaniu, 2017).

Using the Bateman equation (equation 2.15), the general chain of decaying nuclei can be described. More specifically, the Bateman's equation describes the number of atoms of the  $i^{\text{th}}$  isotope  $N_i(t)$  of the series ( $N_i(0)$ ) at time  $t=0$  and  $N_i(0)=0$  for  $i > 1$ .

$$N_i(t) = \lambda_1 \lambda_2 \cdots \lambda_{i-1} N_1(0) \sum_{j=1}^i \frac{e^{-\lambda_i t}}{\prod_{k \neq j} (\lambda_k - \lambda_j)} \quad (2.15)$$

There are three types of equilibrium:

a) secular equilibrium ( $\lambda_i \ll \lambda_{i+1}$ ) - the daughter nuclide is decaying in the same rate at which it is produced)

b) transient equilibrium ( $\lambda_i < \lambda_{i+1}$ )- the daughter nuclide decays with the characteristic decay constant of its parent)

c) non equilibrium ( $\lambda_i > \lambda_{i+1}$ ) the parent nuclide decays quickly and the daughter activity rises to a maximum and then decays with its characteristic decay constant) (Tsoulfanidis & Landsberger, 2010).

In the natural decay series, radioactive decay and emissions from the daughter products of  $^{238}\text{U}$  and  $^{232}\text{Th}$  are used to estimate their ( $^{238}\text{U}$  and  $^{232}\text{Th}$ ) activity concentrations with the assumption that secular equilibrium exists (Kaniu, 2017). However, disequilibrium especially in the uranium decay series occurs due to escape of radon gas ( $^{222}\text{Rn}$ ) and removal or addition of members of the series by processes such as dissolution or precipitation e.g. leaching of  $^{230}\text{Th}$  and  $^{226}\text{Ra}$  (IAEA, 2003).

## 2.3 Gamma ray detection

Gamma-ray photons interact with matter either with the nuclei or orbital electrons of the absorbing medium (Knoll, 2000). The photon-orbital electron interactions are between the photon and either (i) loosely bound electron in Thomson and Compton scattering processes or (ii) tightly bound electron via photoelectric absorption and Rayleigh scattering processes. Interactions between the photon and electrostatic field of the nucleus occur via the pair production process. The three primary and most relevant interactions described in this section are the photo-electric absorption, the Compton scattering and the pair-production (Kaniu, 2017).

### 2.3.1 The Photoelectric Effect

During the photoelectric effect (Figure 2.2) a photon (gamma ray) interacts with a bound atomic electron, resulting in the disappearance of the photon and the ejection of the atomic electron from the atom. The free electron is called *photoelectron* and its kinetic energy is given by equation (2.16).

$$E_e = E_\gamma - E_b \quad (2.16)$$

where,

$E_e$  is the kinetic energy of the photoelectron,  $E_\gamma$  is the photon energy and  $E_b$  is the binding energy of the electron to the atomic orbit.

The photoelectric effect always occurs on bound electrons, in order the momentum to be conserved. As a result, the nucleus absorbs the recoil momentum (Knoll, 2000; Gilmore, 2008; Pappa, 2018).

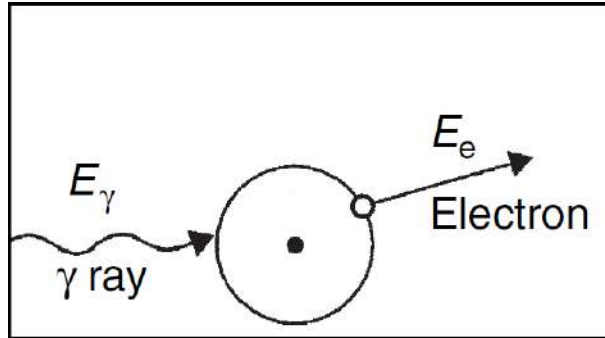


**Figure 2.2.** The photoelectric effect (Gilmore, 2008).

### 2.3.2 The Compton scattering

In the Compton scattering (Figure 2.3) process, a photon scatters from a free or nearly free atomic electron, resulting in a less energetic photon and a scattered electron carrying the energy lost by the photon. The kinetic energy of the scattered electron is given by equation 2.17.

$$E_e = E_\gamma - E_{\gamma'} \tag{2.17}$$

where,  $E_e$  is the kinetic energy of the scattered electron,  $E_\gamma$  is the photon energy and  $E_{\gamma'}$  is the energy of the scattered photon.

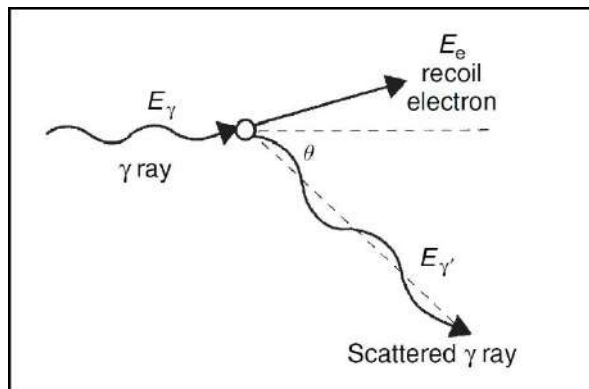


**Figure 2.3.** The Compton Scattering (Gilmore, 2008).

### 2.3.3 The Pair Production

Unlike the photoelectric absorption and Compton scattering, the pair production is a result of the interaction of the gamma-ray with the atom as a whole. The process takes place within the Coulomb field of the nucleus, resulting in the conversion of a gamma-ray into an electron–positron pair. In order this process to take place, the gamma-ray must carry an energy at least equivalent to the combined rest mass of the two particles

– 511 keV each, making 1022 keV in all (Gilmore, 2008). Thus, according to the conservation of energy, the kinetic energy of the electron and the positron is given by equation 2.18.

$$E_{e^-} + E_{e^+} = E_\gamma - (mc^2)_{e^-} - (mc^2)_{e^+} = E_\gamma - 1.022\text{MeV} \quad (2.18)$$

where,

$E_{e^-}$  is the kinetic energy of the electron,  $E_{e^+}$  is the kinetic energy of the positron,  $E_\gamma$  is the photon energy and  $mc^2$  is the rest mass of electron or positron (Pappa, 2018). During pair production the original photon is eliminated, however two photons are created when the positron is annihilated (Figure 2.4).

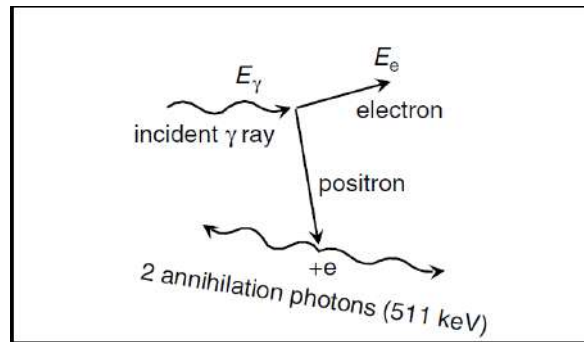


**Figure 2.4.** The mechanism of pair production (Gilmore, 2008).

The dependence of the above gamma ray interaction processes, with  $E_\gamma$  and  $Z$  is described in Figure 2.5. The line at the left represents the energy at which photoelectric absorption and Compton scattering are equally probable as a function of the absorber atomic number. The line at the right represents the energy at which Compton scattering and pair production are equally probable. Three areas are thus defined on the plot within which photoelectric absorption, Compton scattering, and pair production each predominate (Knoll, 2000).

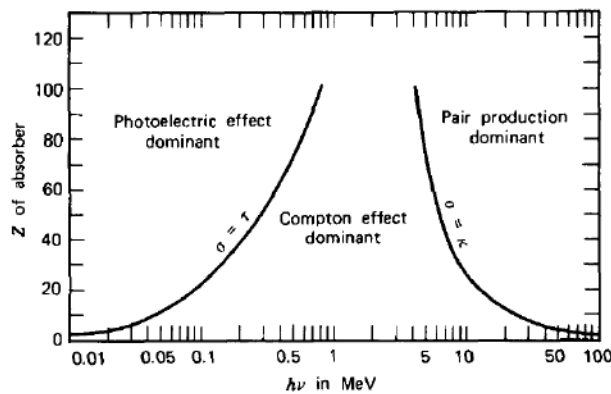


**Figure 2.5.** The dependence of the photoelectric absorption, Compton scattering and pair production with  $E_\gamma$  and  $Z$  (Knoll, 2000).

### 2.3.4 Principles of Detectors: HPGe Detector

After describing the interactions of gamma ray photons with matter the basic principles of semiconductor detectors and specifically of Ge and HPGe detector follow.

Semiconductors are crystalline materials which can be considered as a sum of interacting atoms. When the atoms approach each other close enough to form a solid, the valence electrons interact with each other and their atomic levels are broadened into wider regions, the energy bands. This energy band structure is consisted of three regions: the valence band, the "forbidden" energy gap and the conduction band (Figure 2.6).

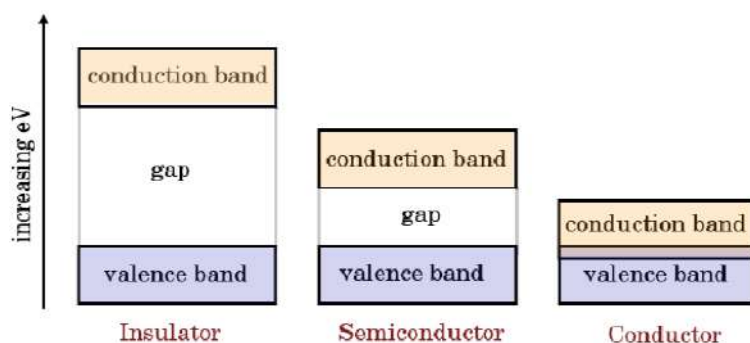


**Figure 2.6.** The energy band of an insulator, semiconductor and conductor (Betsou, 2015).

The valence band corresponds to the outer-shell electrons which are tightly bound to specific lattice sites in the crystal and it is totally occupied by electrons. In the "forbidden" energy gap there are no available energy levels and its size determines whether the material is classified as a conductor, an insulator or a semiconductor. The conductivity band is the region where the electrons are detached from their parent atoms and they are free to traverse the entire crystal (Leo, 1994; Knoll, 2000).

In the semiconductors the energy gap between the valence and conduction bands is a small one (0.67 eV in Ge). At low temperatures, most electrons are fixed in the valence band of the crystal. Electrons are able to move since they gain energy (e.g. via interaction with ionizing radiation). That additive energy moves electron from the valence band to the conduction band and they can move freely in the crystal. An equal number of holes (positively charged ions) is created in the valence band, so as the gap of the missing electrons to be filled. Under the influence of the electric field the electrons-hole pairs travel to the electrodes (to the positive and negative contact, respectively). By collecting the electron-hole pairs, the detection signal is formed and it is sent to the Multi-Channel Analyzer (MCA) (Vagena, 2016).

The semiconductor detectors are divided into two types: a) the *intrinsic* detectors and b) the impurity or *extrinsic* detectors. In a pure semiconductor (*intrinsic semiconductor*), the number of electrons in the conduction band is equal to the number of holes in the valence band. This balance can be destroyed by the introduction (doping) of a small amount of impurity atoms, which have one more or one less valence electron in their atomic shell. For example, for the silicon semiconductor, which is tetravalent, the dopant may be pentavalent or trivalent (Leo, 1994; Knoll, 2000).

In case of extrinsic semiconductors, the detectors are doped with other materials to increase the number of charge carrier and thus the possibility of conduction. When the doping process leads to an increment of the number of electrons, an *n-type* (negative type) semiconductor is formed. In case the doping process leads to an excess of the holes in the valence band, a *p-type* semiconductor is formed. For example, doping a silicon detector with small amounts of antimony (Sb) constructs an n-type detector (donor), while doping boron (B) creates a p-type detector (acceptor) (Vagena, 2016).

The semiconductor detectors are based on the formation of a junction between the *n-type* and the *p-type* semiconductors. Due to the different concentrations of the electrons and the holes in the two regions of the junction, there is a diffusion of holes to the *n-region*, as well as a diffusion of conduction electrons towards the *p-region* (Figure 2.7). Thus, the p-region has a negative charge, while the n-region becomes positive. This effect creates an electric field across the junction which finally stops the further diffusion and an immobile charge distribution is presented. The region over which the charge imbalance exists is called as *depletion region* and is presented in both the p and the n sides of the junction (Leo, 1994; Knoll, 2000). This region corresponds to the active volume and it is sensitive to detect X-rays and gamma rays. This depletion region can get larger depending on the voltage that creates the electric field. This voltage is called “reverse bias”. On the available semiconductor materials, silicon (Si) detectors are mostly used for charged particle detectors, whereas germanium (Ge) detectors are used for gamma spectrometry (Vagena, 2016).

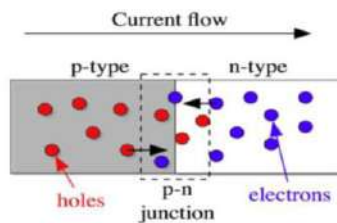


**Figure 2.7.** The p-n junction. The electrons from the n-region are diffused to the p-region while the holes from the p-region are diffused to the n-region (Betsou, 2015).

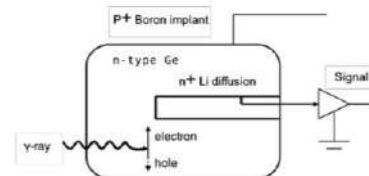


**Figure 2.8.** The n-type intrinsic germanium closed end co-axial detector (Vagena, 2016).

High density of the semiconducting germanium (Ge) in combination with the good intrinsic energy resolution and the possibility of large active volumes make HPGe the most preferred material for  $\gamma$ -ray spectrometry.

There are two main types of HPGe detectors: a) the coaxial and b) the well type. For the purpose of decay counting, a coaxial dipstick detector is used. The dipstick system (Figure 2.8) includes a rod made of copper that results to the cooling of the Ge detector. These types of detector present a more uniform, efficient cross section of the active detector volume to samples that are counted at a short distance from the detector. When a  $\gamma$ -ray interacts in the active volume, it creates electrons which are collected on the n+ contact, while the holes are collected on the p+ contact, and the current that occurs as

the electrons and holes move toward the electrodes, once integrated, constitutes the  $\gamma$ -ray energy signal. Due to the narrow bandgap, the main characteristic of the semiconductor materials, Ge detectors need to be cooled so as to reduce the electrical noise that is caused by the charge carriers due to temperature. The width of the bandgap is reduced when the temperature is increased. The detector is mounted in a vacuum chamber, which is attached to or inserted into a LN2 Dewar. For the cooling, liquid nitrogen is used and the system is cooled to a temperature of 77 K (-196°C). Finally, for the reduction of the background radiation, lead (Pb) shielding is needed in Ge gamma spectroscopy systems (Figure 2.9) (Vagena, 2016).

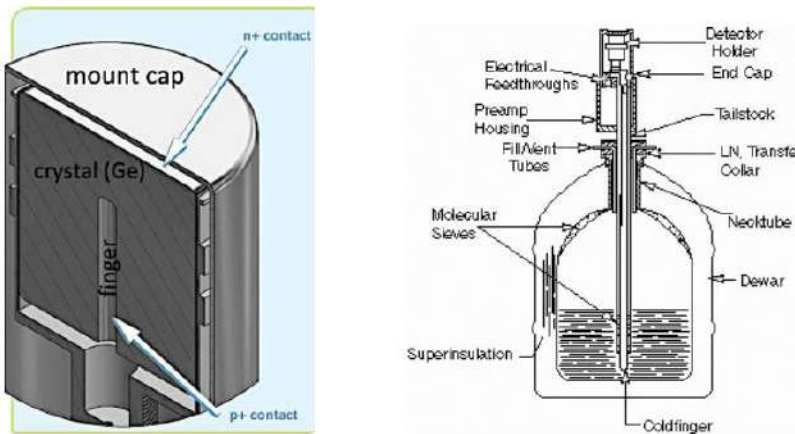


**Figure 2.9.** A p-type Ge detector followed by representation of the cryostat and the liquid nitrogen reservoir (Canberra, 2003; Vagena, 2016)

## 2.4 X-ray emission

The X-ray emission is the result of the atomic electron rearrangement, after the electron capture and internal conversion. The electron during e.g. the excitation process, is ejected from the bound state having a kinetic energy equal to the excitation energy minus the electron's atomic binding energy. The excited atom or an electron from another state will move preferentially to the lowest possible energy state so as to fill the vacant spot ( $E_i$ ), emitting X-rays. The electron transitions are characterized by the letters K, L, M, etc. which represent the final energy state ( $E_f$ ). Therefore, transitions to the L state, from other initial state, are called L X-rays. These discrete characteristics X-rays, can be used as atom's fingerprints (Gilmore, 2008; Pappa, 2018). The emitted electromagnetic radiation (X-ray) during an electron transition is characterized by the frequency described in equation 2.19.

$$\nu = \frac{E_i - E_f}{h} \quad (2.19)$$

where,

$E_i$  is the energy of the initial orbit (state),  $E_f$  is the energy of the final orbit (state) and  $h$  is Planck's constant.

According to Moseley's law the energy of the X-ray depends on the atomic number (equation 2.20) and it may range from a few eV (light elements) to few hundreds of keV (heaviest elements).

$$E_x = h\nu = E_i - E_f = k(Z - a)^2 \quad (2.20)$$

where,

$Z$  is the atomic number,  $k$  is a constant for a particular spectral series and  $a$  is a screening constant for the repulsion correction due to other electrons in the atoms (Van Grieken & Markowicz, 2002; Pappa, 2018).

## 2.5 X-ray detection

The X-rays are photons of lower energy than gamma rays. They can interact with matter through the main processes of photoelectric effect and Compton scattering. As it was already mentioned the emission of the characteristic X-rays comes before the ionization of the inner atomic shells as a result of the photoelectric effect and Compton scattering. The K shell electrons, as the most tightly bound to the atom orbit, are the most important for the photoelectric effect in the energy region considered in X-Ray spectrometry. However, the photoelectric effect cannot occur in the case of photon energy below the binding energy of a given shell.

Another mechanism with which X-rays interact with matter is the elastic or coherent scattering called Rayleigh. During the Rayleigh scattering the incident X-ray photon interacts with the whole atom and the electrons oscillate in the X-ray photon frequency, while the photon scatters without changing its energy and no energy is transferred to the atom (Gilmore, 2008; Pappa, 2018).

Finally, by detecting and measuring the X-rays, information about the elements which are involved in a matrix can be obtained and makes the XRF analysis a useful tool for the determination of the elemental concentrations of different matrices.

## 2.6 Trace Elements

### 2.6.1 Definition of the term “trace elements”

Until now, there is no precise definition for the description of the term “trace elements” by any authoritative institution such as the International Union of Pure and Applied Chemistry (IUPAC). Generally speaking, the word “trace” is usually related to elements that are present in a matrix in very low concentrations, ppm or less (Bargagli, 1998; Duffus, 2002; Vuković, 2015). It is a fact that some elements can be characterized like trace elements when it's about biological materials, but they cannot be characterized like that when it's about environmental mediums such as water, soil and air (Vuković, 2015).

Although the term “trace elements” is often replaced by the term “heavy metals”. This misuse of the term “heavy metals” instead of the term “trace elements”, is a very often mistake in the literature. It is known that heavy metals consist a large group of chemical elements (more than 40) with atomic mass higher than 50 carbon units. Most of them are important nutrients for all the living organisms (human, animals, plants) when they occur in small amounts (Zn, Cu, Mn, Cr, Ni, V), whereas some others cause toxic effects when they occur excessively (Pb, Cd, Hg) (Spiegel, 2002; Duffus, 2002; Hoodaji et al., 2012). The degree of the toxicity of the elements varies, depending on the element and on the organism which is involved (Vuković, 2015).

Based on the chemical characteristics that they present, such as their specific density, the term “heavy metals” include those metals or metalloids (semi-metals) that have a density greater than  $4.5 \text{ g cm}^{-3}$ . In addition, some “lighter” metals such as Al ( $2.7 \text{ g cm}^{-3}$ ) and Be ( $1.85 \text{ g cm}^{-3}$ ), along with the metalloids As ( $5.72 \text{ g cm}^{-3}$ ) and Sb ( $6.68 \text{ g cm}^{-3}$ ) and the non-metal Se ( $4.8 \text{ g cm}^{-3}$ ), can be characterized as “heavy metals” due to their high toxicity (Markert, 1993; Vuković, 2015). The term “heavy metals” is additionally based on the relative atomic mass, the atomic number, as well as other chemical properties (Duffus, 2002; Vuković, 2015). Additionally, there is another term, the “major elements”, which is related to Al, Ca, Fe, K, Na, Mg, and Zn elements.

It should be also mentioned that in the literature, there are some other terms that are used instead of the term “trace elements”, such as the terms “micronutrients” or “essential elements” or “toxic elements”. Although, in this dissertation, only the term “trace elements” is going to be used. It indicates all these elements whose concentrations in the analyzed moss samples are lower than  $1000 \mu\text{g g}^{-1}$  (Bargagli, 1998; Vuković, 2015), irrespective of how essential or toxic these elements might be to the specific organisms.

### 2.6.2 Sources of trace elements

There are two different sources of trace elements in the environment, the natural and the anthropogenic ones. The natural source of the trace elements is from crustal material that is either dissolved or eroded from the Earth's surface or is injected into the atmosphere due to volcanic activities. For example, some trace elements that have

natural origin are the elements Mg, Al, Ti, Si, Ca, Th, Ba, La, K, Fe, Cl, Br, Na. The different particles that are present in the atmosphere are released not only through the windblown dust, but also by vegetation too (Hoodaji et al., 2012).

Except of the natural source of trace elements, there are also the anthropogenic ones. There are multiple anthropogenic emissions of trace elements in the environment. They can enter into the environment mainly via three routes:

1)the deposition of the atmospheric particulates (road transport, industrial and mining activities, metallurgical processes, fossil fuel combustion, cement production)

2)the disposal of sewage sludge and effluents, fertilizers and animal waste, which are enriched with trace elements

3)the by-products created during different metal mining processes (Shrivastav, 2001; Hoodaji et al., 2012).

For example, some trace elements (such as Ni, V, Cr, Co, As, Sb, Hg, Pb, Cd) that come from anthropogenic activities, are released into the atmosphere mainly through the deposition of particulates.

A general characteristic of all the trace elements is that they do not remain only near the source of emission but they can spread over long distances due to the wind and the local meteorological circumstances that are present in each area. After their possible spread (even through borders) they are deposited to the environment through wet or dry deposition (Hoodaji et al., 2012).

The exposure to trace elements may have a serious health impact on humans, and it emphasizes the importance of monitoring them in terms of air pollution. For this purpose, different approaches can be used. The technique of biomonitoring is among them, and it's the one that is being studied in this dissertation. More specifically the use of mosses as biomonitors of trace elements is the approach that is being discussed in this study.

## **2.7 Bryophytes**

### **2.7.1 General information**

Bryophytes are generally considered to be the first plants that invaded land 450 million years ago consisting the second largest group of plants. Bryophytes are plants that produce chlorophyll a and b (like flowering plants), but they lack of lignin and do not have true roots and leaves nor true conducting tissues (Glime, 2017a b). Despite their small size (the majority are only a few centimeters tall) they can be found all over the world, in a variety of habitats, from the sea level to high altitudes, with only exception being the sea water. The great variety of microhabitats where they can grow is due to their ability to exploit even small differences in the ecological conditions of the substrate and the environment (water and light availability, nutrients, etc.). They can

grow in almost all the substrates, on the ground, on rocks as epiphytes, on tree logs and branches, in streams, lakes and even on different man-made constructions such as roofs, etc. They have a major impact on the ecosystem as they could affect the nutrient cycling, water retention and water availability, especially in water related habitats such as peatlands, etc. (Smith, 1982; Shaw & Goffinet, 2000; Glime, 2017a).

Bryophytes consist of three Phyla (Divisions):

1. Anthocerotophyta (hornworts) with a limited number of only 100 species (or ca 200 species according to other authors),
2. Marchantiophyta (liverworts), which are estimated 6000 to 8000 thallose and leafy liverwort species, and
3. Bryophyta (mosses), being the biggest and most common Division including more than 10.000 species; they are distinguished into acrocarp and pleurocarp mosses (Figures 2.10 & 2.11) based upon the orientation and branching of the stems and the position of gametangia (Shaw & Goffinet, 2000).

The life cycle of a typical moss (Division Bryophyta) begins with the spore germination that leads to the growth of a green, leafy gametophyte that represents the dominant generation of the moss (i.e. the part of the plant that is the most conspicuous and the most long-lived during the life cycle). The gametophyte is what we recognize as a moss species; it has a stem with small green-colored leaves (but not typical) and rhizoids (also not typical) which serves only for anchoring to different substrates, without being able to absorb water from it (Figure 2.10). On the gametophyte, after fertilization, the sporophyte is being formed which is totally depended for its growth on the gametophyte (Figure 2.11). For the completion of the life cycle, water presence is essential in order the sperm to be able to reach the egg for the fertilization (Glime, 2017c).

The main sources of water for bryophytes are through wet deposition (rainfall, dew, mist, snowmelt), but not groundwater (due to lack of true roots). Since bryophytes lack the cuticle (in contrast with flowering plants) they can absorb water by their whole surface (stem and leaves). The majority are relying on external transport of water (ectohydric mosses), although there are species that also have the ability of internal water movement (via a central cylinder; endohydric mosses). (Glime, 2017b; d). There are extreme bryophyte examples, like *Sphagnum* species known to be able to absorb up to 22 times their mass (water capacity equals 2.200% of their dry mass); a property for which they were used as bandages during the World War I, as they could absorb 5-6 times more than the cotton pads, in addition of also having antibacterial activity (Glime, 2017e). Bryophytes ability to act like sponges, in order to cover their own water needs, affects also specific aquatic, bryophytes dominated, habitats (such as peatlands where *Sphagnum* species are the dominant plants of the habitat) and generally the **ecosystem**.

**Bryophyte species** are also poikilohydric, i.e. they depend on the external environmental conditions to regulate their water content; thus they dry out when temperature is increasing and there is no water available and they are re-hydrated and slowly gain physiological activity when water is available again. How much tolerant can a bryophyte species be to desiccation depends on the species, but its microhabitat's and habitat's structure are also important for providing adequate hydration state. For

example, aquatic mosses seem to be less tolerant to dehydration comparing to dry habitat mosses which can withstand more extended periods of desiccation and resume photosynthesis easier. There are species that seems to avoid drought by using special structural adaptations and others that complete their life cycle in a way to avoid the vegetative plant getting dehydrated. When they are dry, bryophytes can survive months to even some years depending on the species (Glime, 2017b, e).

### **2.7.2 Bryophytes growth and nutrients requirements**

For the growth of bryophytes, a number of factors play an important role (water, nutrients, light, temperature), with the availability of water being the most important. After covering the water requirements, moderate temperatures are also required for the growth of bryophytes (usually less than 25°C), thus during summer, especially in dry climates their growth is being reduced. In temperate climates, as is the situation in the sampling area of Northern Greece, growth generally seems to occur during spring and autumn but it slows down and even stops in summer (depending on the area where the moss species grow), while during winter they remain relatively dormant. Many moss species survive winter and are ready for photosynthesis when the snow disappears, using the snowmelt water to rehydrate their tissues. There are also bryophyte species in warmer climates that grow best during winter when moisture is available, whereas in Polar regions summer growth is observed (Glime, 2017f).

Bryophytes seem to require the same nutrients (macro-nutrients and trace elements) as do the angiosperms (flowering plants) but in lower concentrations and are used almost for the same purposes. The major nutrient sources that bryophytes use are the soil, the stream water, the atmospheric dust, the precipitation (including throughfall) and the leaf litter, depending on both the species and its growth habitat. Bryophytes receive all the necessary elements through wet and dry deposition. All the elements are absorbed by bryophytes through their entire surface; they are either dissolved first in rainwater (or stream water) or they are accumulated as dust on the mosses or the leaf litter and then dissolved by rainfall and absorbed by the moss plants. The absorbed nutrients (elements) are used for different purposes and this is why they are located in different parts in the moss body and in the cells, in order to cover structural needs (as compounds of membranes and cell walls) or they are stored in the cells and used when they are needed (e.g. as defense compounds). Also, based on the fact that the needs in nutrients of the younger shoots are greater than those of the older shoots, the elements can be moved from the older to younger tissues in the moss plant (Glime, 2017f).

Bryophytes have seasonal differences in their nutrient needs, with the elements uptake and movement also to differ seasonally. Younger shoots have greater needs for elements than older shoots; thus N, P, and K are found in younger shoots in their highest concentrations. Also, not all of the elements are absorbed in the same rate by all mosses. Each species presents a different rate of absorption with the most important factors influencing the uptake of elements being the season, the moisture, the pH and the habitat where they grow.

Elements (such as Fe, Ca, Mg, Cu, Mo, N, P, S, B, Cl) are essential for mosses and play an important role concerning the species composition and diversity. For example, nitrogen (N) and phosphorus (P) are essential in making proteins and in DNA, while P is also needed to maintain energy. Magnesium (Mg) is vital for chlorophyll, though calcium (Ca) acts as a messenger and is needed to maintain the integrity of the mosses cell walls and membranes. Iron (Fe) is collected by bryophytes by the dust fall, but may also be taken in from water that goes into the moss or can be obtained from the rock substrata and is important in moss plants as consists part of many enzymes and of chlorophyll.

Elements and particularly heavy metals, in bigger concentrations than trace amounts, are probable to have toxic effects on bryophytes, but many species counteract in ways that heavy metals won't be toxic for their survival (Glime, 2017f). Bryophytes ability to absorb considerable large quantities of heavy metals made them suitable for use as biomonitors, for monitoring heavy metal pollution.

### **2.7.3 *Hypnum cupressiforme* Hedw. moss species used as bioindicator in this study**

*Hypnum cupressiforme* Hedw. is a pleurocarpous moss species (Figure 2.10 and 2.11) that belongs to the largest Class of the 'Division Bryophyta' which includes ca 98% of the moss species; Class: Bryopsida, Family: Hypnaceae. (Glime, 2017c).

In the current survey, *Hypnum cupressiforme* Hedw. moss species was used as bioindicator of trace elements and radionuclides and moss samples were collected in the Regions of West, Central and East Macedonia & Thrace.

As already mentioned, bryophytes can receive the necessary elements from the substrate, precipitation and dust. The bryophyte species that form thick, horizontal mats are more likely to depend mainly on precipitation (Glime, 2017f). *Hypnum cupressiforme* Hedw., is a pleurocarpous moss which is most often found living in forests, forming thick mats on the forest floor. Is considered to receive the necessary elements for its growth mainly from the atmosphere (dust and precipitation), as it can easily get wet due to the fact that it grows horizontally on the substrate. This is one of the characteristics that led *Hypnum cupressiforme* to be used as biomonitor in the current study. In addition, the moss species is widespread in Northern Greece (Tsakiri, 2009) and is also the most studied and analyzed moss species in the ICP Vegetation Programme (United Nations Economic Commission for Europe Convention on Long-Range Transboundary Air Pollution. Monitoring of Atmospheric Deposition of Heavy Metals, Nitrogen and POPs in Europe using Bryophytes) (Frontasyeva et al., 2015).



**Figure 2.10.** *Hypnum cupressiforme* Hedw. pleurocarpous moss species. Photo by Dr. Evdoxia Tsakiri, with permission.



**Figure 2.11.** *Hypnum cupressiforme* Hedw. pleurocarpous moss species, with sporophytes. The arrows indicate the abundant spore capsules of the sporophytes. Photo by Dr. Evdoxia Tsakiri, with permission.

## Chapter 3

## Experimental Details

### 3.1 Study area

Greece is located in the Southern and Southeast Europe (Figure 3.1), situated on the southern tip of the Balkan Peninsula. It shares land borders with Albania to the northwest, North Macedonia and Bulgaria to the North, and Turkey to the Northeast. The Aegean Sea lies to the east of the mainland, the Ionian Sea to the west, the Cretan Sea and the Mediterranean Sea to the south. Almost 80% of Greece is mountainous. The climate in Greece is predominately Mediterranean, but due to the country's unique geography, it has a remarkable range of micro-climates (Figure 3.2). The area under study is the North part of Greece, and, more specifically, the prefectures of West, Central, East Macedonia and Thrace. The climate of these regions are mostly Mediterranean and in the mountainous regions almost continental.



**Figure 3.1.** The map of Europe and the location of Greece (dark green).

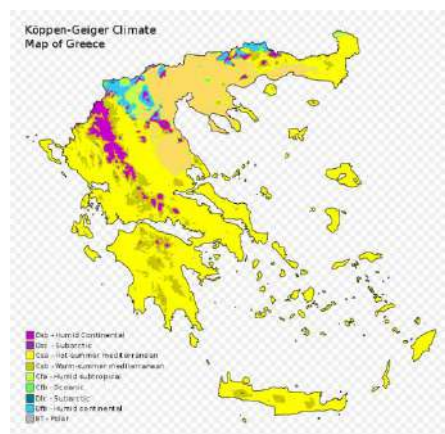


**Figure 3.2.** Map of Greece and the different micro-climates that can be found.

#### 3.1.1 Sampling methodology

During the end of the summer 2016, ninety-five (95) samples of *Hypnum Cupressiforme* Hedw. and *Pseudoscleropodium purum* mosses were collected from the vicinity of Northern Greece in compliance with the UNECE ICP Vegetation Moss Manual (Frontasyeva and Harmens, 2020). The distribution of the sampling sites from where the samples were collected, were located from 39.97° North to 41.65° North and from 20.97° East to 26.26° East covering a grid of 30 m x 30 m (Figure 3.3). The elevations where mosses were found, ranged between 30 m to 1450 m above the mean sea level.

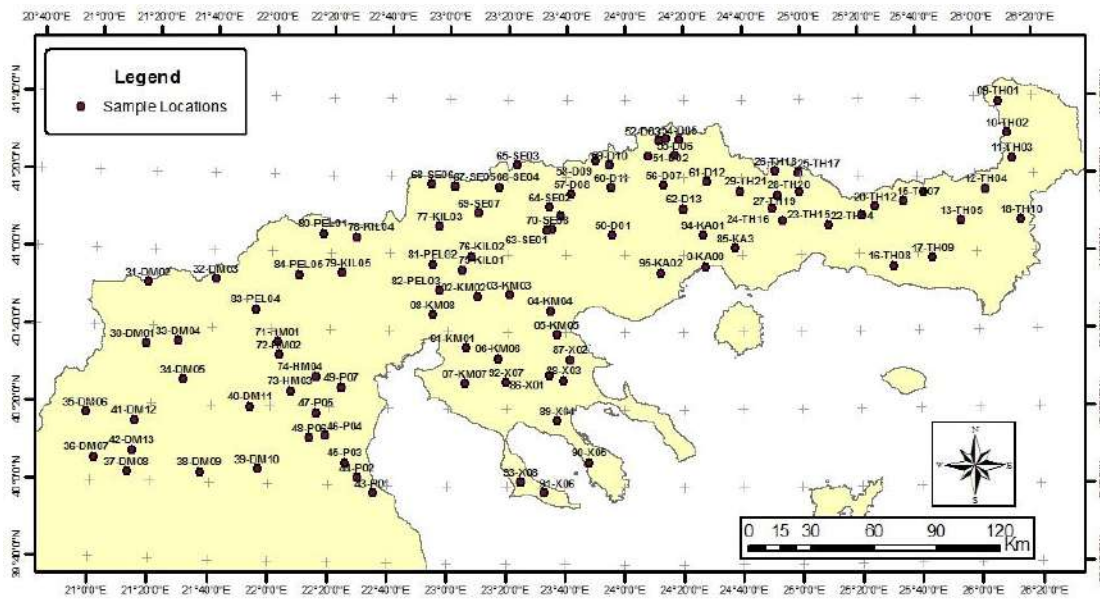


**Figure 3.3.** The sampling sites from which moss and soil samples were collected during the summer of 2016, from the area of Northern Greece.

Samples were collected from different surface types: from rocks, from branches, from soil surface and near roots. All fresh plant material was collected according to the guidelines of the standardized Protocol of the European Survey ICP Vegetation (Frontasyeva and Harmens, 2020). There was no rain during the sampling. Therefore, there was no exposure to additional precipitation. The accumulation of the extra airborne radionuclides originating from the rain washing of the atmosphere was limited (Krmár et al., 2013). Each sampling site was located at least 300 m from main roads and populated areas, and at least 100 m from any road or single house. In forests, most of the samples were gathered in small open regions, avoiding contact with surface water and the canopy drip. Each sample was a composite of three sub-samples. Extraneous materials and litter were removed from the samples, and only the last three years' growth segments (the green part) were used for the analysis. Samples were frozen and stored under those conditions until further preparation and analysis. The further preparation procedure of the moss samples, is described in the following paragraphs in details.

Except of moss samples, soil samples were also collected simultaneously with mosses from the same sampling sites. All the samples were surface soil samples, taken from maximum 5 cm depth and from a square surface of 100 cm x 100 cm. Gamma spectrometry of soil samples allowed determination of radionuclides content and the content of trace elements was determined by means of XRF. More details are given in the next paragraphs.

## 3.2 Sample preparation

After sampling and identification of the moss species, mosses were cleaned manually from extraneous material very carefully, and they were put into plastic bags and transferred at the Aristotle University of Thessaloniki. Then they were put into refrigerator and frozen until further treatment. The preparation of the samples differed depending on the kind of measurements that they were going to have. So one part of each moss sample was prepared for the gamma measurements, while the rest of the moss sample was prepared for ENAA in Dubna, Russia.

### 3.2.1 Moss sample preparation for gamma-spectrometry

For those mosses that were chosen for gamma spectrometry, the following procedure was performed. It should be mentioned that no chemical treatment was performed, and mosses were not washed at all. Before analysis mosses were air-dried at 105 C° for 2 hours to a constant weight. After the preparation of the samples, mosses were put into two cylindrical plastic containers (Figure 3.4), diameter 7.2 cm and height 6.4 cm. The average mass of the dry mosses was around 27 g. All moss samples from the 2016 sampling, were subjected to gamma spectrometry in the Nuclear Lab of the Physics Department, Faculty of Sciences, University of Novi Sad, in Serbia.



**Figure 3.4.** The moss sample placed in plastic cylindrical container for measurement of gamma spectra.

### 3.2.2 Moss sample preparation for ENAA

The rest of mosses that were collected during the 2016 sampling, were prepared in a slightly different way before they subjected to ENAA. Again, no chemical treatment was performed after the sampling. Mosses were air-dried at 40 C° for 3 to 5 hours till to reach a constant weight. After that, a quantity of 5 gr has been selected and well homogenized in a ball mill (agate mortar) (Figure 3.5). From the homogenized material samples were weighted using balance (Figure 3.6) (weight of 0.3 g) and pelletized by means of a pneumatic press and ceramic matrices. The pills were then packed in two separate ways: in plastic bags for short irradiation and in aluminum foil cups for long-term irradiation (Figure 3.7 and 3.8). Epithermal Neutron Activation Analysis (ENAA)

was performed in the radio-analytical complex REGATA of the Frank Laboratory of Neutron Physics, Joint Institute for Nuclear Research (JINR) in Dubna, Russia (Frontasyeva, 2008).



**Figure 3.5.** The chemical laboratory of Frank Laboratory in Dubna. The ball mill (agate mortar) which was used for homogenization of the moss samples.



**Figure 3.6.** The balance where the pills of mosses were weighted. Only 0.3 g of moss material is required for the ENAA.



**Figure 3.7.** Preparing the aluminum foil cups for long-term irradiation.



**Figure 3.8.** The plastic bags where the pills were put for short-term irradiation and the aluminum foil cups for long-term irradiation.

### 3.2.3. Soil sample preparation

For the soil samples, a preparation procedure was different: both for gamma and XRF measurements. There was no need in chemical treatment of the samples both for gamma spectrometry and XRF measurements.

After sampling, soil samples were put into plastic bags, and they were transferred to the Aristotle University. Then they were dried at 80 °C, sieved with an 800 µm plastic sieve in order to remove pebbles and organic material. After the sieving, the soil samples were stored into plastic cylindrical containers with dimensions of 1.8 cm height and

diameter 5.8 cm for gamma ray measurements. The average mass of the dry soil was around 65 g.

For the XRF measurements, a small portion of the sieved dried soil powder (around 16 g) was used. The soil powder, after sieving, was mixed with a binding additive (2 wax powder pills of 0.6 g total weight) and it was pressed using a manual hydraulic press system (Figure 3.9 and 3.10). Pressure of 15 tons was performed for each soil sample. The pressed pellets that were prepared, they were of ~ 4 cm diameter and ~ 0.6 cm width. (Figure 3.11). The pellet's surface was free from cracks and wrinkles. This smooth surface and the stability of the pellets provided accurate XRF measurements and finally the determination of the concentrations of trace elements in soil samples.



**Figure 3.9.** The sieved soil with the wax, before the homogenization and the creation of the pressed pellet.



**Figure 3.10.** The manual pneumatic press system that was used for the creation of the pellets. Pressure of 15 tons was performed for each soil sample.



**Figure 3.11** The pressed pellet that was used for the XRF measurements.

### 3.3 Gamma ray measurements

#### 3.3.1 Detector set-up for $\gamma$ -ray measurements

The moss samples were measured for radioactive nuclides by gamma spectrometry at the Nuclear Lab of the Physics Department, Faculty of Sciences, University of Novi Sad in Serbia, immediately after the sampling. Two HPGe detectors were used for the measurements of gamma spectra from the moss samples for the determination of the concentrations of the radioactive nuclides.

The first one (Figure 3.12) was a low-background extended range HPGe detector equipped with a Be window. The Be window was used in order to determine the concentrations of  $^{210}\text{Pb}$ . The relative efficiency of the detector was 32%. The background count was reduced using a passive shield (18 cm of lead, 1 mm of tin and 1.5 mm of copper) which did not interfere with gamma photons that were emitted from

samples. For each gamma spectrum, the statistical uncertainty of the 477.6 keV  $^7\text{Be}$  line was up to 5%, the same as the statistical uncertainty of 46.5 keV  $^{210}\text{Pb}$  line. The detection efficiency was established using the following reference materials prepared by IAEA: Irish Sea Sediment –IAEA 385, Moss-Soil (IAEA-447), Thorium Ore (IAEA-RGTh-1) and Uranium Ore (IAEA-RGU-1). All the reference materials were packed in the same geometry as the samples. The source self-attenuation due to different chemical composition and density of sample was corrected using a computer program based on Moens et al. (1981). The accuracy of the efficiency calibration was tested using IAEA source made from dry grass (Krmár et al., 2013).

The second detector that was used (Figure 3.13) was an HPGe detector (GX10021) equipped with a carbon window, suitable also for low energy measurements. The relative efficiency of this detector was 100%. The diameter and the length of the detector were 80 mm and 77.5 mm respectively, while the resolution was 2.1 MeV at 1.33 MeV of  $^{60}\text{Co}$  and 1.2 MeV at 122 keV of  $^{57}\text{Co}$ .



**Figure 3.12.** The low-background extended range HPGe detector equipped with a Be window.



**Figure 3.13.** The HPGe detector with 100% relative efficiency.

The rest of the gamma measurements took place in the Nuclear Lab of the Aristotle University of Thessaloniki. Three different detector systems were used. A high purity germanium detector (HPGe) of 42% relative efficiency (Canberra GC4018), an HPGe detector of 20% relative efficiency (Canberra GC2018) and a Ge planar detector (GL 2020R) (Figure 3.14 and 3.15). Details about the detectors are presented in Table 3.1. All of them were used for the determination of the activities of soil and moss samples collected during the present study. All the samples were measured for  $2 \cdot 10^5$  seconds, for minimizing the statistical uncertainties. Before the analysis of the samples, energy and efficiency calibration of the detectors were performed in order to enable the identification and the quantification of the radionuclides in each sample.

**Table 3.1.** Characteristics of the three different gamma detectors that are used in the AUPh Nuclear Physics Lab.

characteristics	HPGe (42%)	HPGe (20%)	Ge planar
Diameter	61 mm	61 mm	50.5 mm
Length	61 mm	31 mm	20 mm
Relative efficiency	42%	20%	-
Resolution at 1.33 MeV of $^{60}\text{Co}$	1.8 keV	1.8 keV	-
Resolution at 122 keV of $^{57}\text{Co}$	0.875 keV	0.850 keV	700 eV
Peak/Compton	63:1	51:1	-
Shielding	4" Pb	Steel	4" Pb



**Figure 3.14.** The HPGe 20% relative efficiency detector.



**Figure 3.15.** The HPGe 42% relative efficiency detector.

The detector set-up of each gamma spectroscopy system can be seen in Figure 3.16. Each detector system comprises a Germanium detector which was coupled to a preamplifier, an amplifier, a high voltage supply (HV), a multichannel analyzer (MCA) and an analog to digital converter (ADC).

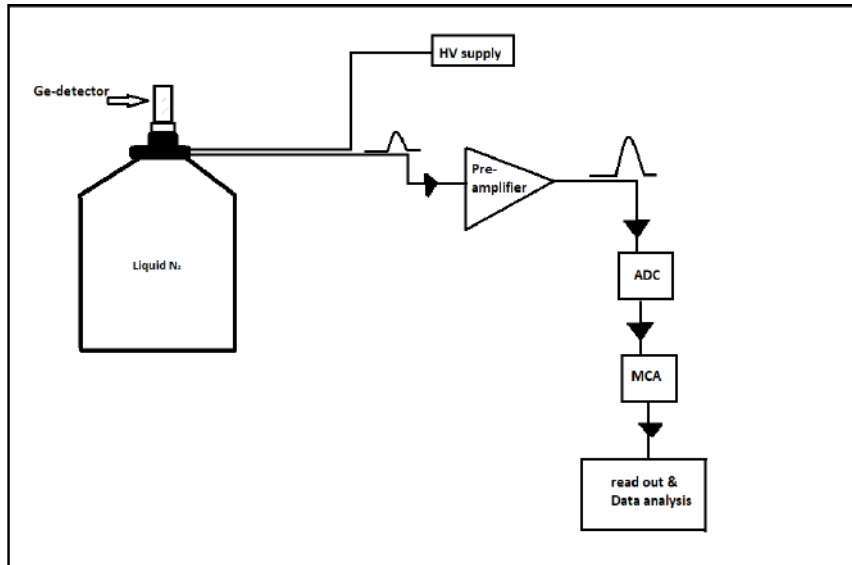


**Figure 3.16.** Schematic diagram of the detector set-up in  $\gamma$ -ray spectrometer.

After the detection of photons, a pulse output was created, with an amplitude proportional to the energy of the incident photon. The pulse output was integrated by a charge sensitive preamplifier, producing a slow decaying exponential pulse, which was digitized by the Analog to Digital Converter (ADC) and processed by the Multichannel Analyzer (MCA). All the pulses that were measured are recorded into a gamma ray spectrum. Finally, the analysis of the data is the last step of the gamma ray measurement.

### 3.3.2 Energy calibration

In order the gamma-ray spectrum to be interpreted in terms of energy and not in terms of channel or voltage, and amount of radionuclides rather than number of pulses, the calibration of the detector should have been performed. The main calibration tasks that were performed, were the energy calibration and the efficiency calibration.

The object of the energy calibration is to extract a relationship between peak position in the spectrum and the corresponding gamma-ray energy. It is normally performed before measurements in a preliminary manner, but it can be performed later by spectrum analysis programs.

The energy calibration can be accomplished by taking the spectrum of a measured source emitting gamma-rays of precisely known energy and comparing each measured peak position with energy. The measurement lasts long enough in order to achieve a good statistical precision of the peaks. The identification of the peaks can be done manually or automatically. The computer searches first for the peaks, measures the peak position to a fraction of a channel and deduce the energy/channel relationship like below:

$$E(\text{keV}) = a * \text{Channel} + b(\text{keV}) \quad (3.1)$$

where  $a$  is the gradient of the calibration line,  $b$  is the intercept and  $channel$  is the channel position (Gilmore, 2008).

In this study all the spectra of mosses and soil samples were calibrated peak to peak automatically, one by one, using the GENIE2000 software and the SPECTRW software (Kalfas et al, 2016), respectively, according to the formula 3.1.

### 3.3.3 Efficiency calibration of gamma detectors

There are different definitions that characterize the detector's efficiency: the *relative efficiency*, the *absolute full peak energy peak efficiency*, the *absolute total efficiency*, the *intrinsic efficiency* and the *geometric efficiency*.

The *relative efficiency* is a general performance measure relating the efficiency of detection of the  $^{60}\text{Co}$  gamma-ray at 1332 keV of the detector to that of a standard sodium iodide scintillation detector.

The *absolute full energy peak efficiency* is used to relate the peak area in the spectrum to the amount of radioactivity that it represents.

The *absolute total efficiency* is used to relate the number of gamma-rays that are emitted by the source to the number of counts that are detected in the spectrum. It is factored into two parts: the intrinsic efficiency  $\varepsilon_{int}$  and the geometrical efficiency  $\varepsilon_{geom}$ . (equation 3.2).

$$\varepsilon_{tot} = \varepsilon_{int} * \varepsilon_{geom} \quad (3.2)$$

The *intrinsic efficiency* relates the counts in the spectrum to the number of gamma-rays that are incident on the detector. It is a function of the type of radiation, its energy and the detector material.

The *geometric efficiency* is that fraction of the source radiation which is geometrically intercepted by the detector. It depends on the geometrical configuration of the detector and source (Leo, 1994; Gilmore, 2008).

The most significant parameter in gamma spectrometry is the *full energy peak efficiency*. It can be defined as the probability that a photon which strikes the detector, will produce a pulse in the full energy peak of the spectrum (Gilmore, 2008; Challan, 2013).

The efficiency  $\varepsilon$  is the ratio between the corrected number of pulses that were registered in the full absorbed energy peak versus the number of photons that were emitted by the sample. The efficiency values can be easily calculated by a fitted curve when the intensity of the peak  $P_\gamma$  and activity  $A$  are well known, as well as the  $N$  (net counts) are well determined by the gamma measurement.

More specifically, the efficiency can be calculated by the formula (3.3).

$$\varepsilon = \frac{N/t}{A \cdot P_\gamma} \quad (3.3)$$

where

$\varepsilon$ : counting system efficiency at the energy E for the specific geometry

N: peak net counts corresponding to the Energy E

t: counting time of the gamma-measurement in seconds

$P_\gamma$ : intensity of the gamma-ray peak

A: activity of the radionuclide in Bq

The error of the efficiency can be calculated according to uncertainty propagation as it can be seen in the below equations (3.4 to 3.6):

$$\sigma_\varepsilon = \sqrt{\left(\frac{\partial \varepsilon}{\partial A} \sigma_A\right)^2 + \left(\frac{\partial \varepsilon}{\partial R} \sigma_R\right)^2 + \left(\frac{\partial \varepsilon}{\partial P_\gamma} \sigma_{P_\gamma}\right)^2} \Rightarrow$$

$$\sigma_\varepsilon = \sqrt{\left(\frac{R}{A^2 P_\gamma} \sigma_A\right)^2 + \left(\frac{1}{A P_\gamma} \sigma_R\right)^2 + \left(\frac{R}{A P_\gamma^2} \sigma_{P_\gamma}\right)^2} \quad (3.4)$$

where R is the number of counts per second after they are corrected with the half-life of each isotope. More precisely:

$$R = \frac{N}{t} e^{+\lambda t} \quad (3.5)$$

and  $\lambda$  is the decay constant and is expressed as follows:

$$\lambda = \frac{\ln 2}{t_{1/2}} \quad (3.6)$$

In the Nuclear Lab, the efficiency calibration was performed for each detector system including soil and moss matrices.

### 3.3.4 Soil samples efficiency calibration

All the gamma detectors of the AUTH laboratory were calibrated for soil matrices using multinuclide reference standard materials that were supplied by the IAEA. More specifically three different standard materials were used for the efficiency calibration of soil samples: the IAEA-444 spiked soil sample (2007), the IAEA CU-2006-03 Soil Sample-01 (2006) and the IAEA TEL 2015-3 Proficiency Test Syrian Soil. The first two reference materials contained four radionuclides with five well resolved peak energies while the last one reference material contained only one radionuclide ( $^{137}\text{Cs}$ )

with one well defined peak of 661.65 keV. Also the first two reference materials contained some radionuclides that are not referred below. This is due to the fact that a long period had passed since the creation of these materials by IAEA, and as a result these radionuclides were already totally disintegrated, so they could not be identified during the current measurements. Details about the activities of each reference material and the radionuclides that were used in the efficiency calibration are given in Table 3.2.

**Table 3.2.** Details about the standard materials that were used for the efficiency calibration (the IAEA-444 spiked soil sample (2007), the IAEA CU-2006-03 Soil Sample-01 (2006) and the IAEA TEL 2015-3 Proficiency Test Syrian Soil). The Activities and their uncertainties are given in Bq kg<sup>-1</sup> as they were defined by IAEA.

isotope	IAEA CU-2006-03 Soil Sample			IAEA-444 spiked soil sample			IAEA TEL 2015-3 Proficiency Test		
	A	$\sigma A$	Ref. date	A	$\sigma A$	Ref. date	A	$\sigma A$	Ref. date
<sup>241</sup> Am	96.6	2.78	01/06/2006	55.6	1.6	15/10/2007	-	-	-
<sup>210</sup> Pb	259.5	12.53	01/06/2006	55.6	1.6	15/10/2007	-	-	-
<sup>137</sup> Cs	52.6	1.08	01/06/2006	48.0	1.5	15/10/2007	715	30	01/01/2015
<sup>60</sup> Co	56.1	1.37	01/06/2006	68.5	1.4	15/10/2007	-	-	-

Two different geometries were used for the soil samples. The first one was a plastic cylindrical container (small box) with dimensions 1.8 cm height and diameter 5.8 cm (Figure 3.17), while the second one was a cylindrical container (big box) with dimensions 4 cm height and diameter 5.9 cm (Figure 3.18). So, for each detector, different efficiency values were calculated, for each different container.



**Figure 3.17.** The *small* box that was used for gamma measurements.



**Figure 3.18.** The *big* box that was used for gamma measurements.

### The 42% efficiency HPGe detector

The soil samples of IAEA-444 spiked soil sample (2007), IAEA CU-2006-03 Soil Sample-01 (2006) and of IAEA TEL 2015-3 Proficiency Test Syrian Soil were used for the calculation of the efficiency values for the *small* box geometry. The efficiencies of the energies 604.7 keV ( $^{134}\text{Cs}$ ), 661.6 keV ( $^{137}\text{Cs}$ ), 1173.24 ( $^{60}\text{Co}$ ) and 1332.5 ( $^{60}\text{Co}$ ) were calculated according to the equation 3.3 and the error of each efficiency was based on the uncertainty propagation (equation 3.4). The final efficiency of each energy was calculated as the weighted mean value of the efficiencies of the above three reference materials. The calculation of the weighted mean and its error was based on the equations 3.7 and 3.8 and the results are presented in Table 3.3.

$$\bar{\varepsilon} = \frac{\sum_{i=1}^N \left( \frac{\varepsilon_i}{\sigma_i^2} \right)}{\sum_{i=1}^N \left( \frac{1}{\sigma_i^2} \right)} \quad (3.7)$$

$$\sigma_{\bar{\varepsilon}} = \frac{1}{\sum_{i=1}^N \left( \frac{1}{\sigma_i^2} \right)} \quad (3.8)$$

**Table 3.3.** The calculated weighted mean values of the efficiencies for the energies of 604.7 keV, 661.6 keV, 1173.24 keV and 1332.5 keV for soil samples using the *small* box geometry at the 42% relative efficiency HPGe detector. In parenthesis the corresponding uncertainties (%) are presented.

isotope	E (keV)	$\varepsilon$ (%)
$^{134}\text{Cs}$	604.70	0.0247(4)
$^{137}\text{Cs}$	661.60	0.0238(2)
$^{60}\text{Co}$	1173.24	0.0139(3)
$^{60}\text{Co}$	1332.50	0.0127(2)

The same reference materials were used for the calculation of the efficiencies concerning the *big* box geometry of the same detector. The efficiencies of the energies 604.7 keV ( $^{134}\text{Cs}$ ), 661.6 keV ( $^{137}\text{Cs}$ ), 1173.24 ( $^{60}\text{Co}$ ) and 1332.5 ( $^{60}\text{Co}$ ) were found. The final efficiency of each energy was calculated as the weighted mean value of the efficiencies of the above three reference materials (Table 3.4).

**Table 3.4.** The calculated weighted mean values of the efficiencies for the energies of 604.7 keV, 661.6 keV, 1173.24 keV and 1332.5 keV for soil samples using the *big* box geometry at the 42% relative efficiency of HPGe detector. In parenthesis the corresponding uncertainties (%) are presented.

isotope	E (keV)	$\varepsilon$ (%)
$^{134}\text{Cs}$	604.70	0.0175(2)
$^{137}\text{Cs}$	661.60	0.0170(2)
$^{60}\text{Co}$	1173.24	0.0106(3)
$^{60}\text{Co}$	1332.50	0.0098(3)

### The 20% efficiency HPGe detector

For the calculation of the efficiencies of the *small* box geometry, the same reference soil samples were used. The weighted mean values of the efficiencies accompanied by their uncertainties are presented in Table 3.5.

**Table 3.5.** The calculated weighted mean values of the efficiencies for the energies of 604.7 keV, 661.6 keV, 1173.24 keV and 1332.5 keV for soil samples using the *small* box geometry at the 20% relative efficiency HPGe detector. In parenthesis the corresponding uncertainties (%) are presented.

isotope	E (keV)	$\varepsilon$ (%)
$^{134}\text{Cs}$	604.70	0.0227(9)
$^{137}\text{Cs}$	661.60	0.0205(3)
$^{60}\text{Co}$	1173.24	0.0117(3)
$^{60}\text{Co}$	1332.50	0.0098(3)

The weighted mean efficiency values with the uncertainties concerning the *big* box geometry of the same detector based on the aforementioned reference materials are presented in Table 3.6.

**Table 3.6.** The calculated weighted mean values of the efficiencies for the energies of 604.7 keV, 661.6 keV, 1173.24 keV and 1332.5 keV for soil samples using the *big* box geometry at the 20% relative efficiency HPGe detector. In parenthesis the corresponding uncertainties (%) are presented.

isotope	E (keV)	$\varepsilon$ (%)
$^{134}\text{Cs}$	604.70	0.0145(13)
$^{137}\text{Cs}$	661.60	0.0144(5)
$^{60}\text{Co}$	1173.24	0.0080(4)
$^{60}\text{Co}$	1332.50	0.0072(3)

### The Ge planar detector

For the determination of the efficiencies of the *small* geometry only the soil samples of IAEA-444 spiked soil sample (2007) and IAEA CU-2006-03 Soil Sample-01 (2006) were used. The weighted mean values of the efficiencies were calculated and are presented in Table 3.7. In Figure 3.19, a gamma spectrum of the reference material IAEA-CU-2006-03 Soil sample is presented, and the peaks of 26.34 keV ( $^{241}\text{Am}$ ), 59.54 keV ( $^{241}\text{Am}$ ) and 46.5 keV ( $^{210}\text{Pb}$ ) can be identified.

**Table 3.7.** The calculated weighted mean values of the efficiencies for the energies of 26.34 keV, 59.54 keV and 46.5 keV for soil samples using the *small* box geometry for the Ge planar detector. In parenthesis the corresponding uncertainties (%) are presented.

isotope	E (keV)	$\varepsilon$ (%)
$^{241}\text{Am}$	26.34	0.0322(60)
$^{210}\text{Pb}$	46.50	0.0659(47)
$^{241}\text{Am}$	59.54	0.0760(63)



**Figure 3.19.** Gamma spectrum of IAEA-CU-2006 reference material. The peaks of 26.34 keV ( $^{241}\text{Am}$ ), 59.54 keV ( $^{241}\text{Am}$ ) and 46.5 keV ( $^{210}\text{Pb}$ ) are presented.

For the *big* box geometry, the same reference materials were used and the weighted mean values of the efficiencies with their uncertainties are presented in Table 3.8.

**Table 3.8.** The calculated weighted mean values of the efficiencies for the energies of 26.34 keV, 59.54 keV and 46.5 keV for soil samples using the *big* box geometry for the Ge planar detector. In parenthesis the corresponding uncertainties (%) are presented.

isotope	E (keV)	$\varepsilon$ (%)
$^{241}\text{Am}$	26.34	0.0200(60)
$^{210}\text{Pb}$	46.50	0.0478(47)
$^{241}\text{Am}$	59.54	0.0525(6)

The efficiency calibration of soil samples was also performed in the Nuclear Lab of the University of Novi Sad, for two detector systems: one for the low background Germanium detector with Be window and 32% relative efficiency and the second one for the Germanium detector of 100% efficiency with carbon window.

The geometry that was used for both the detectors included two identical plastic cylindrical containers packed together with dimensions 6.4 cm height and 7.2 cm diameter in total (Figure 3.21). For quality control the Irish Sea Sediment –IAEA 385, Moss-Soil (IAEA-447), Thorium Ore (IAEA-RGTh-1), and Uranium Ore (IAEA-RGU-1) were used as reference materials. For those gamma lines that did not exist in the reference materials, but they were necessary for the current measurements, the interpolation method using the efficiency curve was performed. The software ANGLE (Advanced Gamma Spectroscopy Efficiency Calibration) by Ortec was also used to get efficiency for some arbitrary geometry. Just by having some experimental data for one sample size and shape, the software could recalculate the efficiencies for different sample geometries and matrices.

The measured efficiencies with the uncertainties for both the detectors are presented in Table 3.9.

**Table 3.9.** The efficiencies of the energies of 46.5 keV, 477.6 keV, 661.6 keV and 1460.8 keV for soil samples measured at the 32% and 100% efficiency detectors in the University of Novi Sad. In parenthesis the corresponding uncertainties (%) are presented.

Radionuclide/energy	Detector (32%)	Detector (100%)
	$\varepsilon$ (%)	$\varepsilon$
Pb-210 (46.5 keV)	0.0235(7)	0.0258(10)
Be-7 (477.6 keV)	0.0143(3)* (calculated)	0.029(7)* (fitted value)
Cs-137 (661.6 keV)	0.0097(2)	0.0248(3)
K-40 (1460.8 keV)	0.0049(2)	0.0143(3)

### 3.3.5 Moss samples efficiency calibration

The first efficiency calibration for moss samples was performed at the Nuclear Lab of the University of Novi Sad. Two detector systems were used, the same ones that were used for the soil measurements. The first one was the low background Ge detector with Be window and 32% relative efficiency and the second one was the Germanium detector of 100% efficiency with carbon window. The efficiencies for both the detectors were obtained using reference materials produced by IAEA such as IAEA-372 (grass), IAEA-330 (spinach) and IAEA-447 (soil). The measured efficiencies with their uncertainties for both the detectors are presented in Table 3.10.

**Table 3.10.** The efficiencies of the energies of 46.5 keV, 477.6 keV, 661.6 keV and 1460.8 keV for moss samples measured at the 32% and 100% efficiency detectors in the University of Novi Sad. In parenthesis the corresponding uncertainties (%) are presented.

Radionuclide/energy	Detector (32%)	Detector (100%)
	$\varepsilon$ (%)	$\varepsilon$ (%)
Pb-210 (46.5 keV)	0.0301(6)	0.0565(5)
Be-7 (477.6 keV)	0.0118(3)	0.0293(7)
Cs-137 (661.6 keV)	0.0110(2)	0.0278(3)
K-40 (1460.8 keV)	0.0040(2)	0.0164(3)

Based on the measurements of moss samples at the University of Novi Sad, an efficiency calibration of the Ge detectors of the AUPh lab was carried out. More specifically, moss samples whose activities were determined at the University of Novi Sad, were used as reference materials at the AUPh Nuclear Lab. The efficiency curve was built using the four well resolved peaks of  $^7\text{Be}$ ,  $^{210}\text{Pb}$ ,  $^{137}\text{Cs}$  and  $^{40}\text{K}$  radionuclides, and more specifically the peaks of the energies of 477.6 keV, 46.5 keV, 661.6 keV and 1460.8 keV respectively.

For the moss samples measurements, two different geometries were used. The first one was a plastic cylindrical container with dimensions 3.2 cm height and 7.2 cm diameter (Figure 3.20), while the second geometry included 2 containers of the above geometry (6.4 cm height and 7.2 cm diameter) (Figure 3.21).



**Figure 3.20.** The one box geometry for the moss measurements.



**Figure 3.21.** The two boxes geometry for the moss measurements.

### The 42% efficiency HPGe detector

For the 42% relative efficiency HPGe detector, two different efficiency curves were built, one for each geometry separately. For the geometry of *one* box, three peaks were analyzed: the 477.6 keV, 661.6 keV and 1460.8 keV peaks. The efficiency for each

energy and its uncertainty were calculated according equations 3.3 and 3.4. The weighted mean values of the efficiency for each energy were calculated and are presented in Table 3.11.

**Table 3.11.** The measured efficiencies of the energies of 477.6 keV, 661.6 keV and 1460.8 keV for mosses using the *one* box geometry at the 42% efficiency detector. In parenthesis the corresponding uncertainties (%) are presented.

isotope	E (keV)	$\varepsilon$ (%)
<sup>7</sup> Be	477.6	0.0275(32)
<sup>137</sup> Cs	661.6	0.0235(18)
<sup>40</sup> K	1460.8	0.0122(21)

For the *two boxes* geometry, the counts of three peaks were analyzed (477.6 keV, 661.6 keV, and 1460.8 keV peaks). The efficiency for each energy and its uncertainty were calculated according to the equations 3.3 and 3.4. The weighted mean values of the efficiencies for each energy were calculated and presented in Table 3.12.

**Table 3.12.** The measured efficiencies of the energies of 477.6 keV, 661.6 keV and 1460.8 keV for mosses using the two boxes geometry at the 42% efficiency detector. In parenthesis the corresponding uncertainties (%) are presented.

isotope	E (keV)	$\varepsilon$ (%)
<sup>7</sup> Be	477.6	0.0159(19)
<sup>137</sup> Cs	661.6	0.0146(11)
<sup>40</sup> K	1460.8	0.0053(21)

#### The 20% relative efficiency HPGe detector

For the geometry of *one* box, the same peaks were analyzed and the calculated are presented in Table 3.13.

**Table 3.13.** The measured efficiencies of the energies of 477.6 keV, 661.6 keV and 1460.8 keV for mosses using the one box geometry at the 20% efficiency detector. In parenthesis the corresponding uncertainties (%) are presented.

isotope	E (keV)	$\varepsilon$ (%)
<sup>7</sup> Be	477.6	0.0311(26)
<sup>137</sup> Cs	661.6	0.0197(13)
<sup>40</sup> K	1460.8	0.0034(20)

The efficiency values for the *two boxes* geometry follows. The 661.6 keV and 1460.8 keV peaks were analyzed. The peak of 477.6 keV was not analyzed for this geometry in this detector, due to the long period that had passed after the decay of  $^7\text{Be}$ . The efficiency for each energy and its uncertainty were calculated according to equations 3.3 and 3.4. The weighted mean values of the efficiencies are shown in Table 3.14.

**Table 3.14.** The measured efficiencies of the energies of 661.6 keV and 1460.8 keV for mosses using the two boxes geometry at the 20% efficiency detector. In parenthesis the corresponding uncertainties (%) are presented.

isotope	E (keV)	$\varepsilon$ (%)
$^{137}\text{Cs}$	661.6	0.0131(11)
$^{40}\text{K}$	1460.8	0.0005(22)

So the most convenient geometry that is also suggested to be used for moss samples for the 20% relative efficiency detector, is the *one box* geometry.

#### The Ge planar detector

The peak of 46.5 keV was analyzed for the geometry of *one box* and *two boxes* geometry for the planar detector. The weighted mean values of the efficiency are presented in Table 3.15 and 3.16.

**Table 3.15.** The measured efficiencies of the energies of 46.5 keV for mosses using the one box geometry at the Ge-planar detector. In parenthesis the corresponding uncertainty (%) is presented.

isotope	E (keV)	$\varepsilon$ (%)
$^{210}\text{Pb}$	46.5	0.0572(48)

**Table 3.16.** The measured efficiencies of the energies of 46.5 keV for mosses using the two boxes geometry at the Ge-planar detector. In parenthesis the corresponding uncertainty (%) is presented.

isotope	E (keV)	$\varepsilon$ (%)
$^{210}\text{Pb}$	46.5	0.0370(48)

For the planar detector, the geometry that is suggested for moss samples measurements is the *one box* geometry again.

After the determination of the efficiencies of the detectors and the energy calibration of the gamma spectra, samples (moss and soil) were subjected to gamma spectrometry to determine the content of radionuclides using the already mentioned detectors in the Nuclear Lab of the University of Novi Sad and the Aristotle University of Thessaloniki. Details about the measurements are presented later in the Chapter 5.

### 3.4 Epithermal Neutron Activation Analysis (ENAA) Measurements

As it was already described, ninety-five moss samples were collected from Northern Greece. After the sampling and the preparation of samples, mosses were subjected to ENAA, which is the most sensitive method for the multi-element analysis. ENAA was performed at the Pulsed Fast Reactor IBR-2 in the radio-analytical complex REGATA of the Frank Laboratory of Neutron Physics, at the Joint Institute for Nuclear Research (JINR) in Dubna, in Russia during 2017. Details about the technique and the analysis are given below.

More specifically, the dried material of mosses was firstly homogenized and a small quantity (0.3 g for each pill) was taken and formed into pills using simple press forms. Then half of these moss pills were packed into polyethylene foil bags for short term irradiation in order to determine the short lived isotopes. The rest ones were put into aluminum foil cups for long term irradiation, in order to determine the long lived isotopes. After the preparation of the moss pills, samples were sent through a pneumatic rabbit system, for irradiation to the Pulsed Fast Reactor IBR-2 of the JINR (Frontasyeva, 2011).

The Pulsed Fast Reactor IBR-2 is one of the best modern facilities in this class (Figure 3.22) (Frontasyeva and Steinnes, 1997; Frontasyeva, 2008). It's a fast neutron pulsed reactor with narrow neutron pulse (240  $\mu\text{s}$ ) and small repetition rate of pulses (5 Hz) (Pavlov et al., 2016). The average heat power was 2 MW and its peak pulse power was 1500 MW. The average density of the thermal neutron flux at the moderator surface was  $10^{13}$  neutrons  $\text{cm}^2 \text{s}^{-1}$ , and its pulse density was  $10^{16}$  neutrons  $\text{cm}^2 \text{s}^{-1}$  (Frontasyeva, 2011).

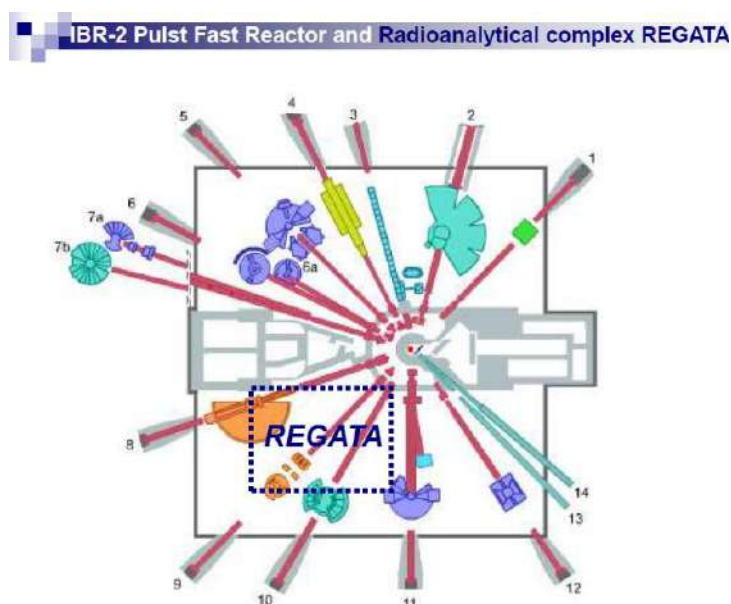


Figure 3.22. The IBR-2 Pulsed Fast Reactor and the Radioanalytical complex REGATA.

More specifically, the Pulsed Fast Reactor IBR-2, was equipped with the pneumatic system REGATA for NAA (Figure 3.23), which provided activation with thermal, epithermal and fast neutrons (Peresedov, 1996). It consisted of four channels for

irradiation (Ch1-Ch4), the pneumatic transport system (PTS) and three gamma-spectrometers which were located at three special rooms on the ground floor of the reactor IBR-2. Channel Ch1, which was intended for ENAA, was equipped with a cylinder shaped 0.7 mm thick cadmium shield. The main parameters of all the irradiation channels are presented in Table 3.17 (Frontasyeva and Pavlov, 2000; Frontasyeva, 2011).

**Table 3.17.** The main characteristics of the irradiation channels at 1.5 MW.

Irradiation site	Neutron flux density ( $n/cm^2 s$ ) $\times 10^{12}$			T ( $^{\circ}C$ )	Channel, diam., (mm)	Channel, length, (mm)
	Thermal	Resonance	Fast			
Ch1	Cd-coated	3.31	4.32	70	28	260
Ch2	1.23	2.96	4.10	60	28	260
Ch3	Gd-coated	7.50	7.70	30-40	30	400
Ch4	4.2	7.60	7.70	30-40	30	400

There was a unique three-loop cooling system that ensured the appropriate conditions for irradiation of biological and environmental samples at the temperature of 60–70 $^{\circ}C$ . The channels Ch3, Ch4 were cooled by water, and the channels Ch1, Ch2, were cooled by air. That was the reason why the temperature in channels Ch3 and Ch4 was lower than the temperature in channels Ch1 and Ch2 in spite of the greater neutron flux density (Frontasyeva, 2011).

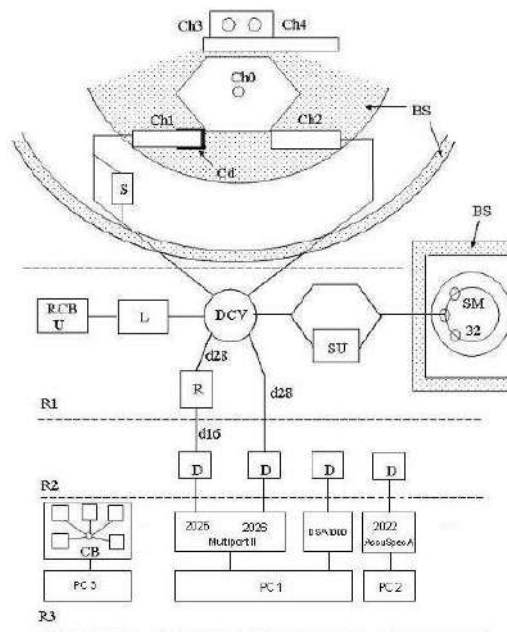


**Figure 3.23.** The REGATA experimental set-up at the IBR-2 Pulse Fast Reactor. Ch1-Ch4 –irradiation channels, S- intermediate storage, DCV- directional control valves, L- Loading unit, RCB- radiochemical glove-cell, U- unloading unit, SU- separate unit, SM- storage magazine, R- repacking unit, D- HPGe detector, AA- amplitude analyzer, CB- control board, CCCAMAC controller, R1 -R3- the rooms where the system is located.

The channels Ch1, Ch2 were air tightly connected with the REGATA pneumatic transport system (PTS) through tubes of ~50–60 m long and the delivery time was 3 to 20 s. The transport containers (Figure 3.24 and Figure 3.25) of polyethylene, teflon and aluminum were used to deliver samples to the irradiation position and back. In special cases containers of fluoro-plastic or pure carbon were also used. Up to seven containers could be loaded simultaneously into each channel for long-term irradiation. The neutron flux density was controlled by monitors (Au, Zr, etc.). The reduction of the neutron flux density along the channel length, could be 30 to 50%, so it was taken into consideration during the data analysis. The pneumatic system (PTS) transported the containers by compressed air (at 3-6 atm. pressure). All its units were located far away from the reactor core (50-60 m). The polyethylene containers were transported to irradiation site for 7-20 s, while the aluminum containers were transported much faster (3-7 s).

Acoustic detectors were placed on the «flight pipe», which was used for the transportation of the samples at the irradiation channels, behind the first ring of the biological shield. They provided the time of the container arrival and the departure time accurately. There were a lot of noise pulses during the flight of the container in the «flight pipe». Each noise pulse cleared the irradiation timer. The knock of the capsule at the bottom of the channel formed the last clearing pulse. After this last clearing pulse, the timer started counting, and the irradiation of the container began. Such positioning of acoustic detectors protected the containers from radiation damage and therefore extended their lifetime.

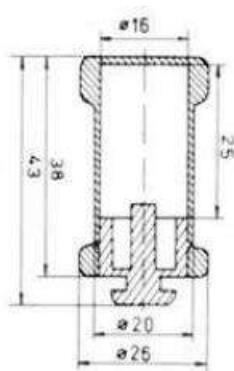


**Figure 3.24.** Polyethylene transport container and inner capsule for a sample.



**Figure 3.25.** Transport capsules for irradiation.

The irradiation time of the polyethylene containers depended on the temperature resistance of the polyethylene and could be equal to 30 minutes, both for channels Ch1 and Ch2. The irradiation channels Ch1 and Ch2 were the same, with the difference that Ch1 was Cd-coated, as already said. The teflon containers could be used for irradiation up to 5 hours. The aluminum containers were used for longer irradiation, due to the fact that the polythelene material (tubes, containers) had low resistance to radiation especially in the IBR-2 reactor, where the flux of gamma-rays and fast neutrons was very high. That was the reason why 80–90 samples could be irradiated simultaneously during 3–4 days in the aluminum transport containers After the irradiation, the activity of the aluminum containers was very high and it requested long cooling time before

manual repacking of the samples into clean polyethylene containers for measurements (Pavlov et al., 2016). The internal volume of the polyethylene container was equal to approximately 4 cm<sup>3</sup>, and the volume of the aluminum container was 1.5 times larger. The time of sample irradiation in channels Ch3, Ch4 depended on the operation cycle duration of the reactor and it was equal to 10-12 days (Frontasyeva and Pavlov, 2000; Frontasyeva, 2011).

The cadmium-screened irradiation channel Ch1 was used for the determination of the long lived isotopes. The aluminum packed samples were irradiated for 4-5 days with a neutron flux density of  $3.6 \times 10^{11} \text{ n (cm}^2 \times \text{s)}^{-1}$ . The long term irradiated samples were measured twice, once 3 days after the irradiation for 5 hours, and then a second time, 20 days after the irradiation for 20 hours respectively.

The polyethylene foil packed samples were irradiated for 180 seconds through the conventional irradiation channel Ch2, in order to activate short lived isotopes (Mg, Al, Cl, Ca, V, Mn, I). Samples were irradiated for 3 min and measured two times for 5–8 min after three to five delays and for 15 min after 20 min delay (Frontasyeva and Pavlov, 1999). The elements with a short half-life (seconds) were determined by cyclic ENAA with the possibility of automatic transportation of the irradiated sample to the detector through a pneumatic transport system.

More specifically, when short-lived isotopes were studied, a small polyethylene capsule was placed into the transport container. There was a special unit (R) to extract a small capsule from the transport container. PTS had loading (L) and unloading (U) units to load and to extract containers from the system. All the mechanical operations, including the removal of the capsules with the samples from the transport containers, were performed automatically by the control system signals. For radiation safety reasons, the unloading unit was placed into a glove-cell. All devices of the pneumatic system were equipped with photo sensors and end-switches for indicating the container's position in the system and for the correct operation of all mechanisms.

An intermediate storage (S), which could fit up to 15 containers, was used for the reduction of the activity of the aluminum containers after the long term irradiation. It was located between the two rings of the biological shield of the reactor. For the storage of highly activated samples, a magazine with 32 cells (SM) was used. It was surrounded by a biological shield which was made of lead and concrete blocks. There were three hot cells for material sciences studies equipped with a set of instruments and devices to measure the mechanical characteristics of samples. One of these three hot chambers was connected through the lock with the unloading unit of extracting the irradiated samples from the system (Frontasyeva and Pavlov, 1999).

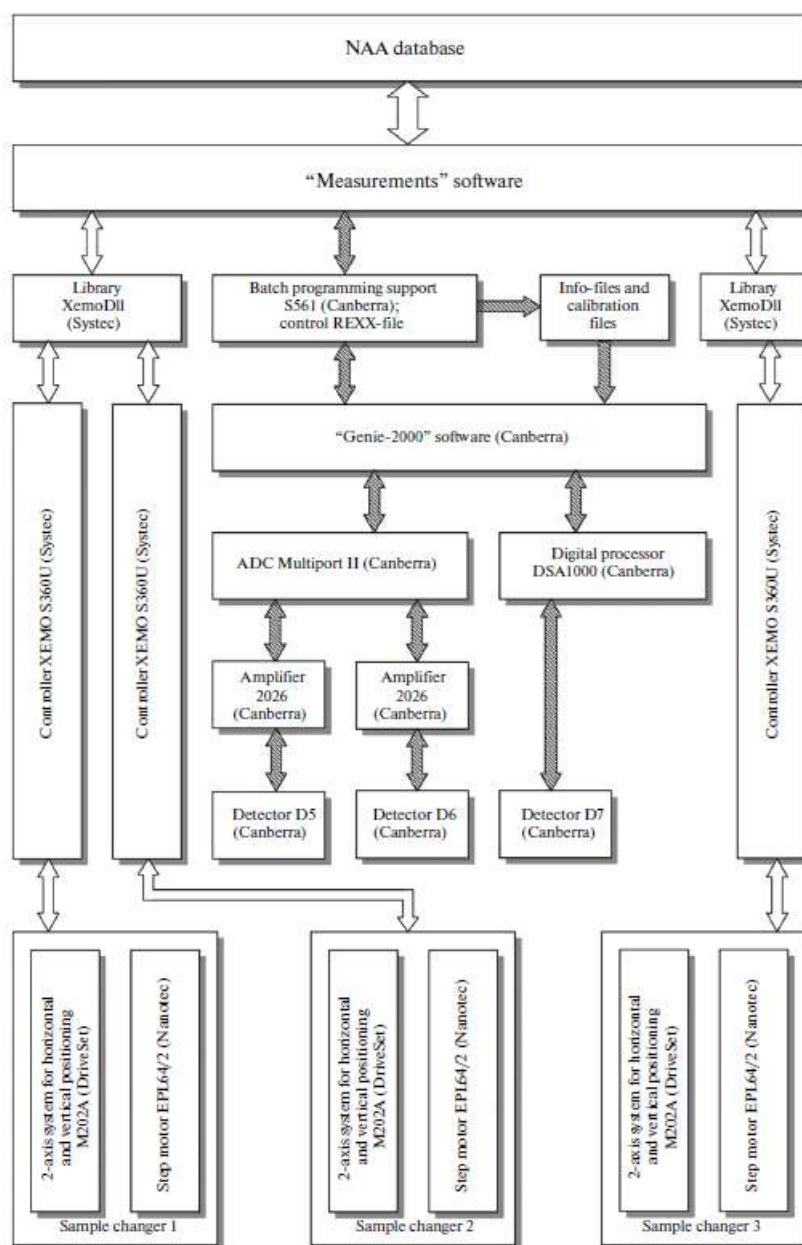


**Figure 3.26.** The diagram of the automation system for gamma-spectrum measurements.

Personal computer controlled the pneumatic transport system and amplitude spectrometers. After the unloading of the transport containers, samples were repacked from there and gamma-radiation measurements were performed. All the units of gamma-spectrometers and counting electronics were made in CAMAC at JINR. More details about the automation system for measurement of  $\gamma$ -ray spectra of induced activity are given below.

REGATA had four spectrometric circuits for gamma measurements. Three of them were equipped with sample changers and each of them used their own controller. All controllers were connected to the same PC via USB ports. Each sampler (Figure 3.27) consists of one disk with 45 slots (Figure 3.28) for containers with samples that were prepared at the JINR lab. The movement of the containers from the disk to the detectors

(Figure 3.28) and back, was carried out by a device M202A which was manufactured by the DriveSet company. This device comprised horizontal and vertical linear positioning modules and was controlled individually for each sampler.

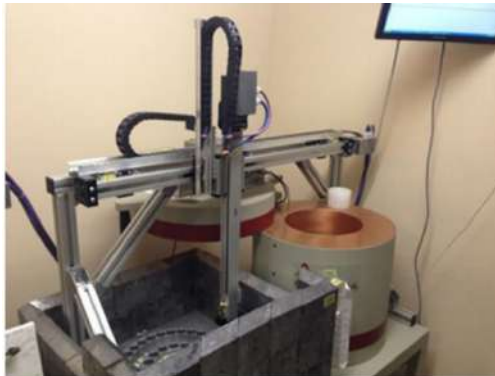


**Figure 3.27.** View of the sample changer.



**Figure 3.28.** The disk with the slots for containers.

Each container which was selected from the disk, was transferred to the detector and was held above it, in one of the three fixed height positions for measurement. The control of the container position during the measurement of the spectra was performed by incremental encoders. After the measurement was completed, the container was returned to the same location on the disk, which then rotated and selected the next sample (Pavlov et al., 2016). The detectors that were used were three HPGc superconductor detectors with a resolution of 1.74 keV for the  $^{60}\text{Co}$  1332.4 keV  $\gamma$ -line and the detection efficiency 40% in comparison to the efficiency of a 3" x 3" NaI detector for the same line.



**Figure 3.29.** The grab of container.

For processing the amplitude spectra (peak search, peak fitting and nuclide identification routines and calculation of the concentrations of the elements), a software package which was developed at FLNP JINR was used (Frontasyeva and Pavlov, 2000; Frontasyeva, 2011; Dmitriev et al., 2013; Pavlov et al., 2014; Pavlov, 2016). It was the program *Measurements* that was developed in order to automate the measurements of gamma-spectra of induced activity by Genie-2000, to control the sample changers of the spectrometers during the measurements simultaneously and to exchange the information with the ENAA database both in automatic and semi-automatic modes

(Figure 3.26). This program was written in Visual Basic. The Genie-2000 software by Canberra, as already mentioned, was used for the analysis of the gamma spectra (Figure 3.30-3.32). Also the Genie-2000 software, before the measurement, it processed a test measurement of the spectra for each detector during a period of 10 s, in order to determine the dead time. If the dead time was more than 20 %, the program changed the position of the samples in the detectors. In Table 3.18-3.20, information (half life, energy) about the gamma lines that were analyzed are provided. Spectrum for each separate element produced after irradiation are presented in Appendix A<sub>a</sub>.

Each sample changer was equipped with an Ethernet video camera, which allowed controlling the operation of the system in a remote mode, making a picture of the sample during the measurement and saving this picture in the database. So possible human mistakes during the installation of the samples to the discs were avoided. Simultaneous measurements were conducted at the three detectors as required by the mass analysis of the samples.

The placement of the samples on the disc and the spectra measurement was carried out according to the list of the measured samples that were received automatically from the database. During the whole process, there was a permanent exchange of information with the ENAA database, and the last ones could be seen in the spectrum. Some initial settings were necessary every time before the program started. After the beginning of the spectra all the necessary data for the calculation of the concentrations were taken from the database, according to the name of each sample. These included: the batch code and code of the sample to be measured, the measurement type, the date and time of the beginning of irradiation, the date and time of the end of irradiation, the weight of the sample, the sample height above the detector and the name of the experimenter. Depending on the number-code of the detector which was used in the measurements, the program automatically found the necessary energy and efficiency calibration files for the selected position of the sample above the detector and recorded the calibrations in the spectra.

Every time when the spectra measurements ended, the program stored the spectra to the hard disc of PC and the file names of the measured spectra were transferred to the ENAA database. Then the measured samples were returned to the same cells on the disc and the samples from the next cells were moved to the detectors. The maximum number of the spectrometers and the sample changers that were controlled by this program was four.

For the visualization of the obtained information, the program automatically found each specific file with the areas of interest and displayed them in a Genie-2000 window. While the spectrum was processed, the areas of interest were automatically found by the program which performed graphical peak intervals. The Genie-2000 program with an additional interactive peak fitting module S506 was used for processing the obtained spectra. These treatment results were stored into a file with the values of the activities of the identified isotopes in the sample and the minimal detectable activity of these isotopes (Frontasyeva and Pavlov, 2000; Frontasyeva, 2011; Dmitriev et al., 2013; Pavlov et al., 2014; Pavlov, 2016). This file was going afterwards to be used by the “*Concentration*” program for the determination of the elements in the samples.

More specifically, the calculation of elemental concentrations in the samples was performed by a relative method using the program “*Concentration*” (Pavlov et al., 2014; Pavlov et al., 2016). The “*Concentration*” program was based on the fact that the moss samples were irradiated and measured under the same exactly conditions with high quality standards materials of identical weight with well-known elemental concentrations and calculated activities. The element contents were calculated by the relative method using different certified reference materials (Frontasyeva, 2011).

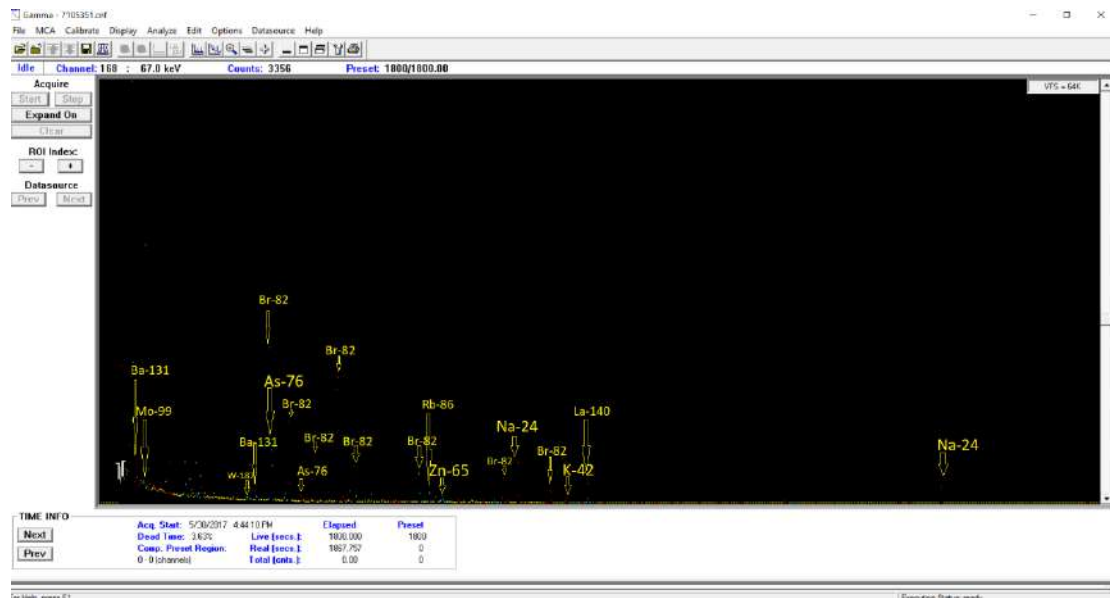


Figure 3.30. A gamma spectrum for the determination of the long lived isotopes.

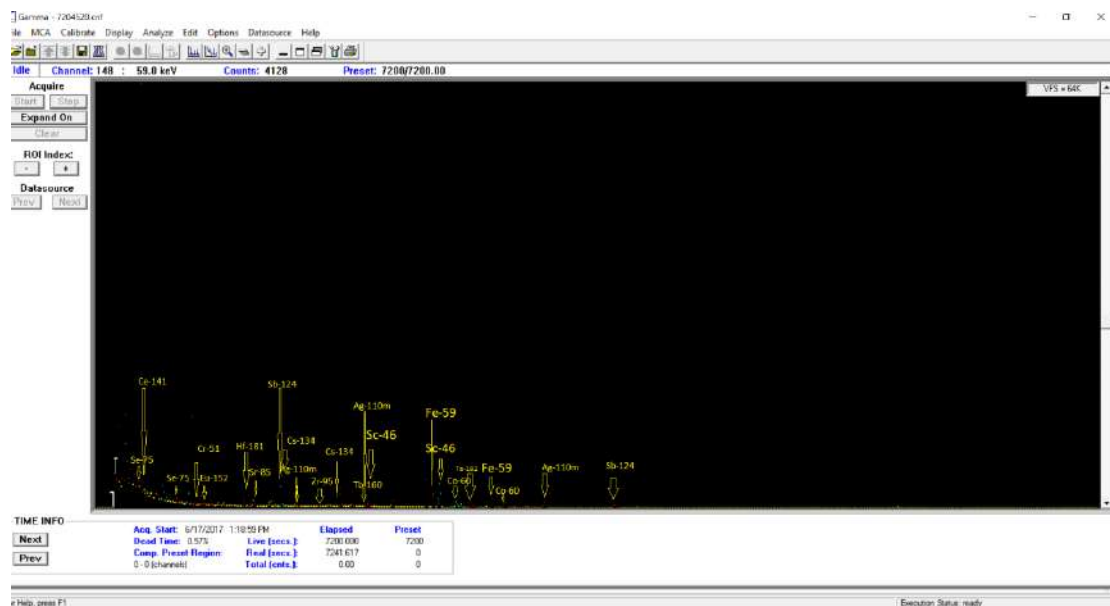
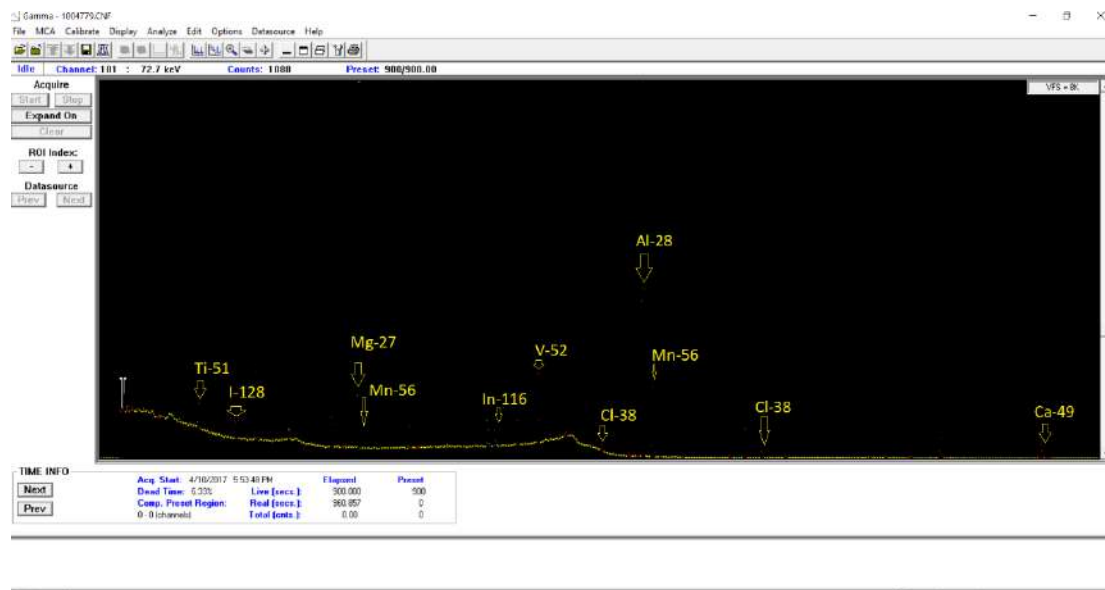


Figure 3.31. Another gamma spectrum for the determination of the long lives nuclides, after a long term irradiation of the samples.



**Figure 3.32.** A gamma spectrum from the analysis with the Genie-2000 software for the determination of the short lived isotopes.

More specifically, high quality certified reference materials (SRM) were used for the quality control of the ENAA results, such as peach leaves-1547, coal fly ash-1633b and 1633c, coal-1632c, Montana soil-2710, San Joaquin Soil-2709 and Calcareous soil-ERM-CC690. All the reference materials were provided by the National Institute of Standards & Technology (NIST) and the Institute for Reference Materials and Measurements (ERM). The SRMs were packed and irradiated together with the moss samples under the same conditions in each transport container. The results that were obtained were compared with the certified values (Table 3.21). The reference material that presented the least deviation between the measured and the certified values of each elemental concentration was chosen.

Thereby, the concentrations of the analyzed elements were defined by the simple formula 3.9:

$$C_{sample} = C_{stand} * \frac{A_{sample}}{A_{stand}} \quad (3.9)$$

Where the  $C_{sample}$  is the elemental concentration of the moss sample,  $C_{stand}$  is the well-known elemental concentration of the standard material,  $A_{sample}$  is the calculated activity of the moss sample, and  $A_{stand}$  is the calculated activity of the standard materials. So, the program “*Concentration*” used the values of the radionuclide activities that were recorded in the output files of the Genie-2000 analysis of the spectra of the samples and of standards, and calculated the values of the elemental concentrations in the samples. Finally, the values of the calculated concentrations of the elements with uncertainties of calculations and minimal detectable concentrations for the given experimental conditions were stored into the ENAA database (Frontasyeva, 2011; Pavlov et al., 2014; Pavlov et al., 2016). The elemental concentrations of the moss samples and their uncertainties were afterwards extracted from the database. Details about the elemental content of the moss samples and their analysis are presented in Chapter 4.

**Table 3.18.** Information about the measured short lived isotopes after 180 sec irradiation. In parenthesis the intensity of each peak is presented.

Isotope	Half life	Energy (keV)	Energy (keV)
Ti-51	5.76 min	320.08 (93.1%)	
I-128	24 min	442.9 (18.1%)	
Mg-27	9.46 min	843.76 (71.8%)	1014.4 (28.0%)
Mn-56	2.58 h	846.76 (98.9%)	1810 (27.2%)
I-116m	54 min	1293.54 (84.4%)	
V-52	3.74 min	1434.06 (100%)	
Cl-38	37.24 min	1642.71 (31.9%)	2167.41 (42.4%)
Al-28	2.2 min	1778.85 (100%)	
Ca-49	8.72 min	3084.4 (92.1%)	

**Table 3.19.** Information about the measures long-lived isotopes after 4 days irradiation. In parenthesis the intensity of each peak is presented.

Isotope	Half life	Energy (keV)	Energy (keV)
Se-75	119.79 d	136.0 (58.3%)	264.66 (58.9%)
Ce-141	32.50 d	145.44 (48.2%)	
Cr-51	27.7 d	320.08 (9.92%)	
Hf-181	42.39 d	345.93 (15.12%)	
Sr-85	64.84 d	514.0 (96.0%)	
Sb-124	60.20 d	602.73 (98.3%)	1690.98 (47.79%)
Cs-134	2.0 y	604.7 (97.62%)	795.86 (85.53%)
Ag110m	249.79 d	884.68 (73.19%)	937.49 (34.60%)
Zr-95	64.02 d	724.19 (44.17%)	756.73 (54.56%)
Sc-46	83.79 d	889.27 (99.98%)	1120.54 (99.99%)
Tb-160	72.3 d	879.38 (30.1%)	
Fe-59	44.5 d	1099.25 (56.5%)	1291.59 (43.2%)
Co-60	5.27 y	1173.2 (99.97%)	1332.5 (99.99%)
Ta-182	114.43 d	1121.3 (34.9%)	

**Table 3.20.** The measured long lived isotopes after their irradiation for 4 days. In parenthesis the intensity of each peak is presented.

Isotope	Half-life	Energy (keV)	Energy (keV)
Na-24	(14.8 h)	1368 (100%)	2754 (99.9%)
K-42	(12 h)	1524 (18.08%)	
Zn-65	(244 d)	1115 (50.6%)	
As-76	(1.07 d)	559 (45%)	
Br-82	(35 h)	776 (83.5%)	554 (70.8%)
Rb-86	(18 d)	1077 (8.64%)	
Mo-99	(65 h)	739 (12%)	
Ba-131	(11.5 d)	496 (46.8%)	123 (28.9%)
La-140	(1.6 d)	1596 (95.4%)	
W-187	(23 h)	685 (100%)	

**Table 3.21.** The measured and certified values for different elements in ( $\mu\text{g g}^{-1}$ ) and their uncertainties (%) that were used for quality control purposes of the ENAA results. The subscription of each element shows the standard reference material that was used for the calculation of the elements: <sup>1</sup> SRM 2709, <sup>2</sup> SRM 1547, <sup>3</sup> SRM 1633c, <sup>4</sup> SRM 1632c, <sup>5</sup> SRM 2710, <sup>6</sup> SRM 1633b, <sup>7</sup> ERM CC690.

Elements	Certified value	Determined Value	Elements	Certified value	Determined Value
Na <sup>1</sup>	11600.0 (2.6)	11599.9 (3.1)	Mn <sup>5</sup>	10100.0 (4.0)	10096.4 (6.1)
Mg <sup>2</sup>	4320.0 (3.5)	4306.1 (2.3)	Fe <sup>6</sup>	77800.0 (3.0)	76890.7 (5.4)
Al <sup>3</sup>	132800.0 (6.1)	132820.3 (4.9)	Cu <sup>5</sup>	2950.6 (4.4)	2951.2 (29.1)
S <sup>3</sup>	1100.0 (19.0)	1100.7 (36.1)	As <sup>6</sup>	136.2 (1.9)	135.9 (6.8)
Cl <sup>4</sup>	1139.0 (4.1)	1140.9 (9.0)	Sb <sup>1</sup>	7.9 (7.6)	7.91 (7.80)
K <sup>1</sup>	20300.0 (3.0)	20300.5 (8.3)	Ba <sup>1</sup>	968.0 (4.1)	967.7 (13.6)
Ca <sup>2</sup>	15590.0 (1.02)	15577.9 (7.9)	La <sup>7</sup>	24.4 (7.0)	24.4 (7.1)
Tl <sup>3</sup>	7240.0 (3.0)	7237.4 (5.7)	Sm <sup>7</sup>	3.5 (11.4)	3.49 (11.60)
V <sup>3</sup>	286.2 (2.8)	286.0 (4)	Dy <sup>3</sup>	18.7 (1.6)	18.73 (16.40)

### 3.5 X-ray fluorescence spectrometry measurements

X-ray fluorescence (XRF) spectrometry can be applied for qualitative analysis as it can recognize a majority of elements between beryllium and uranium. The XRF analysis is based on the fact that the irradiated surface using primary X-rays, represents the whole sample. As a result, the preparation of both of the samples and the standards should be performed very carefully. The XRF technique is a very sensitive technique and requests clean samples, e.g. fingerprints on a sample can affect the result of the analysis.

Ninety-five soil samples were prepared into pellets, as it was described earlier, for trace elements measurements via the X-ray fluorescence analysis. The X-ray Spectrometry S4-Pioneer (Bruker-AMS, Deutschland) in the Geology Department of the Aristotle University was used (Figure 3.33 and 3.34).

The samples were irradiated by an intense X-ray beam, known as incident beam. Some of the energy was scattered, but some was also absorbed within the sample in a manner that depended on its chemistry. The incident X-ray beam was produced from a Rh target, with a system of 5 crystals (LIF200, LIF220, LIF420, XS-55 and PET) and two detectors: one gas proportional counter and one scintillation counter for the detection of the emitted X-rays.

More specifically, when the incident X-ray beam irradiated the sample, the sample was excited. Then, the excited sample emitted X-rays along a spectrum of wavelengths characteristic of the types of the atoms that were present in the sample. The atoms in the sample absorbed the X-ray energy by ionizing, ejecting electrons from the lower (usually K and L) energy levels. The ejected electrons were replaced by electrons from an outer, higher energy orbital. When this happened, energy was released due to the decreased binding energy of the inner electron orbital compared with an outer one. This energy that was released and detected, was in the form of emission of characteristic X-rays indicating the type of atom present.

The intensity of the energy that was measured by the detectors was proportional to the abundance of the element in the sample. The exact value of this proportionality for each element was derived by comparison to the reference materials of GSN (granite), MAN (granite), JG-2 (granitoidete), RGM-1 (rhyolite), JR-1 (rhyolite), JG-3 (granitoidete), ACE (granite), G2 (granite) that were used for the calibration of the spectrometry.



**Figure 3.33.** The X-ray Spectrometry S4-Pioneer (Bruker-AMS, Deutschland) was used for the determination of trace elements content in 95 soil samples.

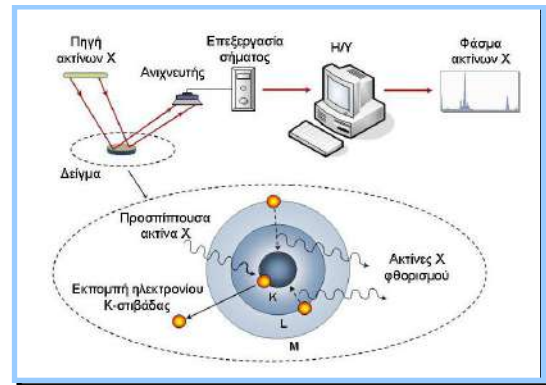


**Figure 3.34.** The X-ray Spectrometry.

Each detector could measure specific intensity of the emitted beams. The gas proportional counter, which used a P10 gas (a mixture of 90% Ar and 10% CH<sub>4</sub> gases), could measure long wavelength (>0.15 nm) X-rays that were typical of K spectra of elements lighter than Zn. The scintillation counter was used to analyze shorter wavelengths in the X-ray spectrum (K spectra of element from Nb to I; L spectra of Th and U). X-rays of intermediate wavelength (K spectra produced from Zn to Zr and L spectra from Ba and the rare earth elements) were generally measured by using both detectors in tandem. Finally, the oxides of the elements Si, Ti, Al, Fe Mn, Mg, Ca, K, Na, P were analyzed during the measurements, while voltage of 60 kV and bias of 45 mA, was applied. More details about the results that came up after the measurements are given in the fourth chapter.

## Chapter 4 Trace Elements

### 4.1 Trace elements concentrations in mosses

Ninety-five moss samples were collected from the region of Northern Greece (Figure 4.1). The moss sampling was followed by the preparation of the samples in the laboratory according to the instructions of the ICP Vegetation Protocol, and then mosses were analyzed by means of Neutron Activation Analysis as described in details in section 3.2.

The elemental concentrations of forty-four (44) trace elements (Al, As, Ni, V, Cr, Zn, Fe, Br, Cl, I, Mg, Na, K, Sc, Ti, Mn, Co, Se, Rb, Sb, Au, Th, U, Si, Sr, Ca, Zr, Cs, Ba, La, Ce, Nd, Sm, Gd, Tb, Dy, Tm, Yb, Lu, Hf, Ta, In, Mo, Ag) were measured and are presented with details in Tables A1 and A2 in the Appendix. The descriptive analysis (mean, median, min, max, standard deviation, kurtosis and skewness) of the above elemental concentrations was also performed. In Table 4.1 the descriptive analysis of the first twenty-three (23) elements, the most frequently analyzed and published elements in studies, is presented, while in Table 4.2 the descriptive analysis of the rest twenty-one (21) elements is also presented.

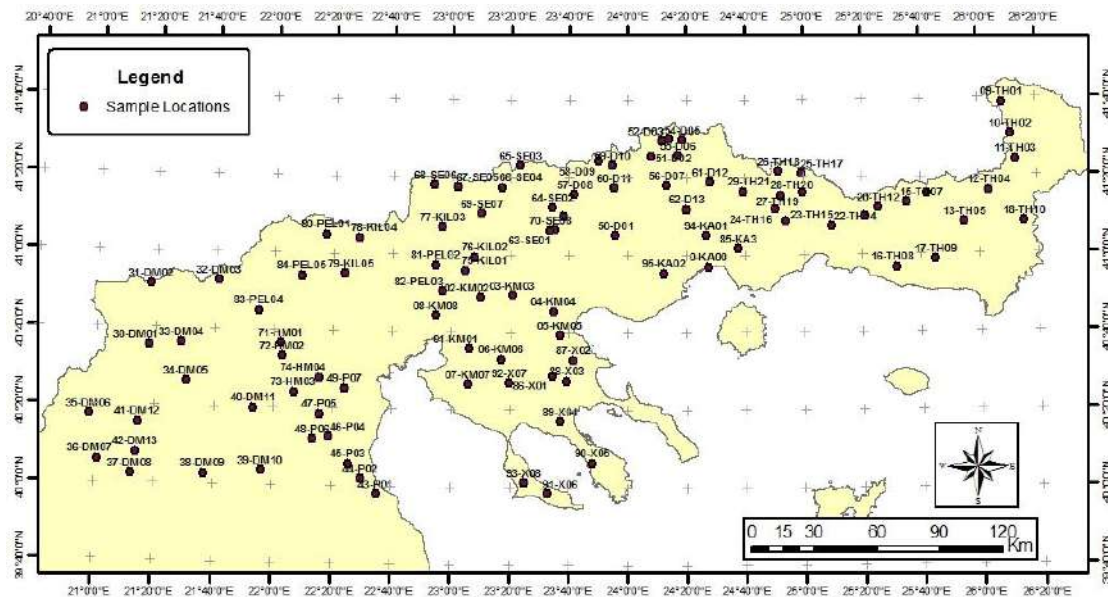


Figure 4.1. The sampling sites of mosses in the region of Northern Greece.

**Table 4.1.** The descriptive analysis of the 23 most frequently analyzed and published in studies elements that were determined in the moss samples, by means of Neutron Activation Analysis (NAA).

	Na	Mg	Al	Cl	K	Sc	Ti	V	Cr	Mn	Fe	Co	Ni	Zn	As	Se	Br	Rb	Sb	I	Au	Th	U
Mean	1730	4432	7886	145	6360	2.12	440	10.08	24.04	269	5974	3.02	12.83	56.56	2.45	0.23	6.48	21.59	0.27	2.64	0.00123	2.07	0.55
Median	751	3600	5840	130	5670	1.44	327	8.17	11.50	219	3770	1.69	7.26	37.60	1.44	0.23	5.85	15.50	0.20	2.30	0.00073	0.99	0.3
Min	184	705	1350	47	2160	0.30	97	2.61	2.04	34	1010	0.43	1.72	14.60	0.52	0.02	1.69	5.11	0.02	1.03	0.00004	0.28	0.07
Max	9210	17800	46100	380	17200	8.92	1760	33.4	222	1090	28700	20.30	90.20	282	17.90	0.48	15.00	82.90	3.23	7.36	0.0172	13.6	3.38
Range	9026	17095	44750	333	15040	8.63	1663	30.79	219.96	1056	27690	19.87	88.48	267.4	17.38	0.45	13.31	77.79	3.21	6.33	0.01716	13.32	3.31
St. Dev.	2266	2813	6812	68	2956	1.90	327	6.12	35.60	200	5182	3.25	12.77	52.74	2.99	0.08	2.90	17.20	0.39	1.20	0.00216	2.44	0.6
Kurt.	3.6	5.8	10.8	2.2	4.0	3.30	3.8	2.3	17.02	4.8	4.6	10.47	13.66	5.98	11.53	0.16	0.90	3.20	42.18	2.78	33.41952	6.03	6.31
Skew.	2.1	2.1	2.8	1.4	1.9	1.90	1.9	1.5	3.90	1.9	2.0	2.90	2.90	2.40	3.20	0.30	1.10	1.80	6.15	1.58	5.26292	2.34	2.31

**Table 4.2.** The descriptive analysis of the rest 21 elements that were determined in the moss samples, by means of Neutron Activation Analysis (NAA).

	Si	Sr	Ca	Zr	Cs	Ba	La	Ce	Nd	Sm	Gd	Tb	Dy	Tm	Yb	Lu	Hf	Ta	In	Mo	Ag
Mean	78458	52.13	8900	35.18	0.88	104.71	5.42	11.07	4.68	0.237	0.441	0.126	0.62	0.06	0.34	0.097	0.903	0.196	0.06	0.28	0.06
Median	62200	38.20	8170	21.50	0.68	65.90	3.22	9.11	3.19	0.009	0.318	0.076	0.44	0.03	0.20	0.062	0.552	0.115	0.04	0.23	0.06
Min	11500	12.70	3960	3.29	0.17	15.90	0.50	1.87	0.59	0.003	0.068	0.022	0.06	0.01	0.02	0.001	0.129	0.03	0.01	0.02	0.02
Max	340000	197.0	23400	219	5.08	519.0	35.2	46.10	28.90	3.680	3.23	0.567	3.93	0.38	2.83	0.474	4.700	1.09	0.23	2.31	0.16
Range	328500	184.3	19440	215.7	4.91	503.1	34.7	44.23	28.32	3.677	3.162	0.546	3.87	0.38	2.81	0.473	4.571	1.06	0.22	2.29	0.14
St. Dev.	64318	38.10	3236	38.91	0.79	94.16	5.40	7.86	4.61	0.495	0.424	0.120	0.54	0.06	0.41	0.091	0.938	0.209	0.05	0.25	0.02
Kurt.	7.2	4.05	3.1	6.95	8.09	5.52	9.77	4.98	8.07	25.582	20.181	3.550	14.86	10.6	15.86	3.588	4.776	6.664	2.80	46.48	2.62
Skew.	2.5	2.00	1.4	2.39	2.42	2.18	2.63	1.73	2.48	4.347	3.741	2.000	3.18	3.02	3.51	1.832	2.127	2.476	1.98	5.90	1.33

### 4.1.1 Spatial distributions of trace elements in mosses

The elemental concentrations of moss samples are visualized using the ArcGIS software. Only the spatial distributions of the twenty-three (23) most frequently analyzed elements (Al, As, Ni, V, Cr, Zn, Fe, Br, Cl, I, Mg, Na, K, Sc, Ti, Mn, Co, Se, Rb, Sb, Au, Th and U) are presented in Figures 4.2-4.24.

#### *Aluminum*

Aluminum (Al) is a natural component of the Earth's crust and can be easily transferred through the windblown soil dust (Berg and Steinnes, 1997; Zechmeister, et al., 2003, Harmens et al., 2008).

The distribution of the Al concentrations in mosses is presented in Figure 4.2. The areas which present high values of Al are the ones on the east direction of Kozani, on the south-east direction of Thessaloniki, and close to Bulgarian borders. The lowest concentration of Al has been measured close to the borders with Republic of North Macedonia and Bulgaria.

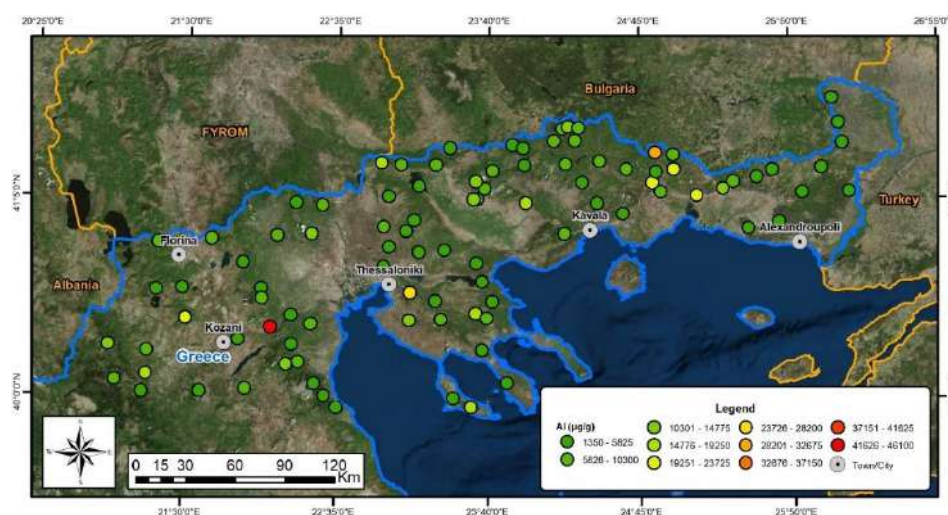


**Figure 4.2.** The concentrations of Al ( $\mu\text{g g}^{-1}$ ) in the 95 moss samples collected in the region of Northern Greece.

#### *Arsenic*

Arsenic (As) is a natural occurring element and occurs in many minerals (Eliopoulos et al., 2012). It is often related to copper and gold mines, to coal combustion and to “non-ferrous metals industries” and other manufacturing industries and constructions (Harmens et al., 2008; Marinova et al., 2010).

In Figure 4.3 the concentrations of As are presented. High concentrations of As are measured mostly on the southeast direction of the city of Thessaloniki, close to the borders with Bulgaria and the Republic of North Macedonia, and on the north-west

direction of the city of Alexandroupoli, in Thrace Region. Lower concentrations of As were found around the city of Kozani, in the Region of West Macedonia.

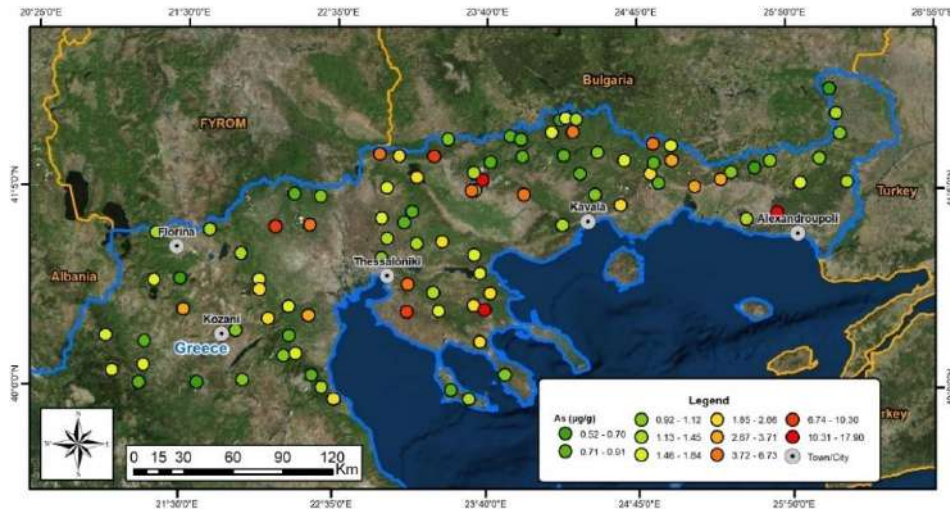


**Figure 4.3.** The concentrations of As ( $\mu\text{g g}^{-1}$ ) in the 95 moss samples collected in the region of Northern Greece.

### Nickel

Nickel (Ni) is an element that can be found mixed with a lot of metals in nature. It is associated with anthropogenic activities such as coal and lignite burning, petroleum refining, public electricity, heat production, manufacturing industries and construction (Foscolos et al., 1989; Filipidis et al., 1996; Harmens et al., 2008).

The concentrations of Ni element are displayed in Figure-4.4. High values of Ni are found mainly in the Region of West Macedonia, north of the city of Thessaloniki, and close to borders with the Republic of North Macedonia and Bulgaria.

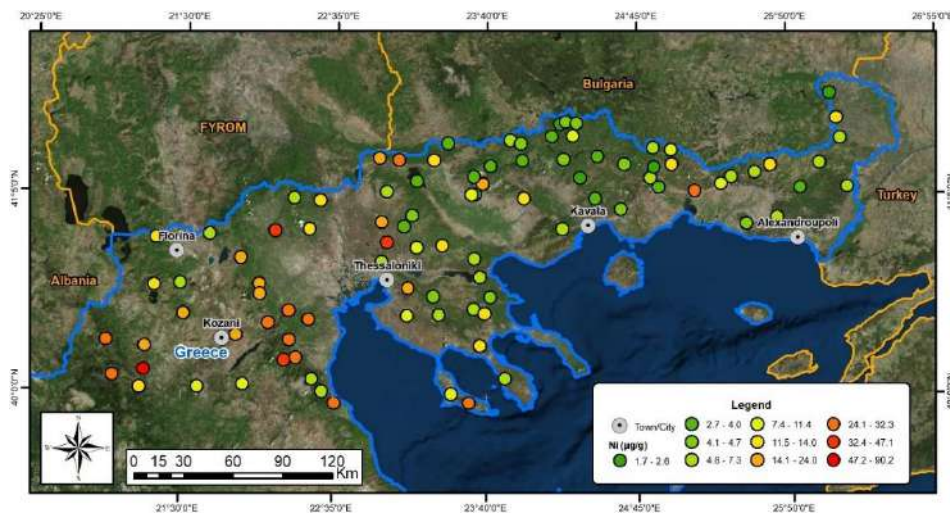


**Figure 4.4.** The concentrations of Ni ( $\mu\text{g g}^{-1}$ ) in the 95 moss samples collected in the region of Northern Greece.

## Vanadium

Vanadium (V) is an element found combined in various minerals (carnotite, vanadinite, patronite), in phosphate rocks, coal and petroleum. It is usually connected with anthropogenic activities such as the combustion of fuel oils (Harmens et al., 2008).

The spatial distribution of V is presented in Figure 4.5. As presented in the map, high concentrations of V have been found in the Region of West Macedonia-around the city of Kozani and Florina, on the southeast from the city of Thessaloniki, and close to the borders with the Republic of North Macedonia and Bulgaria.

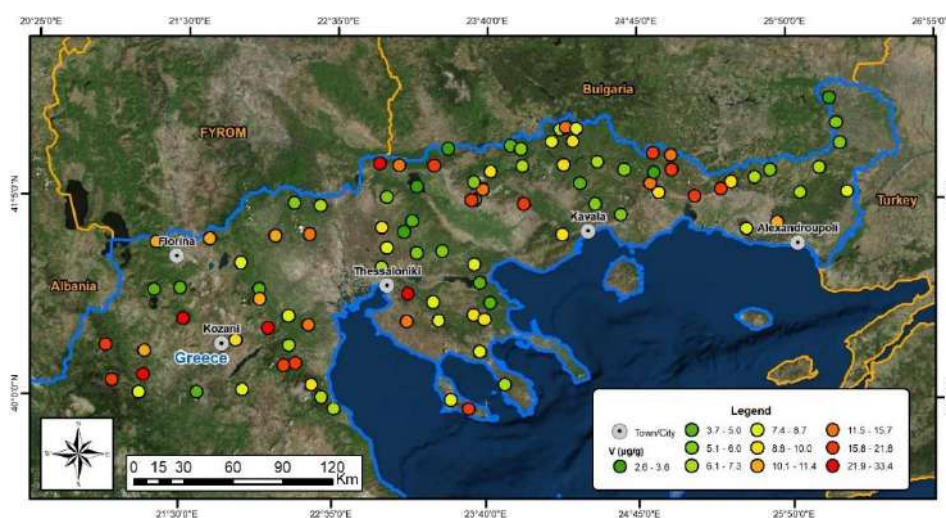


**Figure 4.5.** The concentrations of V ( $\mu\text{g g}^{-1}$ ) in the 95 moss samples collected in the region of Northern Greece.

## Chromium

Chromium (Cr) is an element that is usually connected with anthropogenic activities such as the fossil fuel burning, iron and steel mills (Harmens et al., 2008). The distribution of Cr in Northern Greece is presented in Figure 4.6. According to this distribution, Cr shows elevated concentrations both in the Regions of West and Central Macedonia, and specifically close to Kozani Prefecture, east of the city of Thessaloniki, and close to the borders with the Republic of North Macedonia.

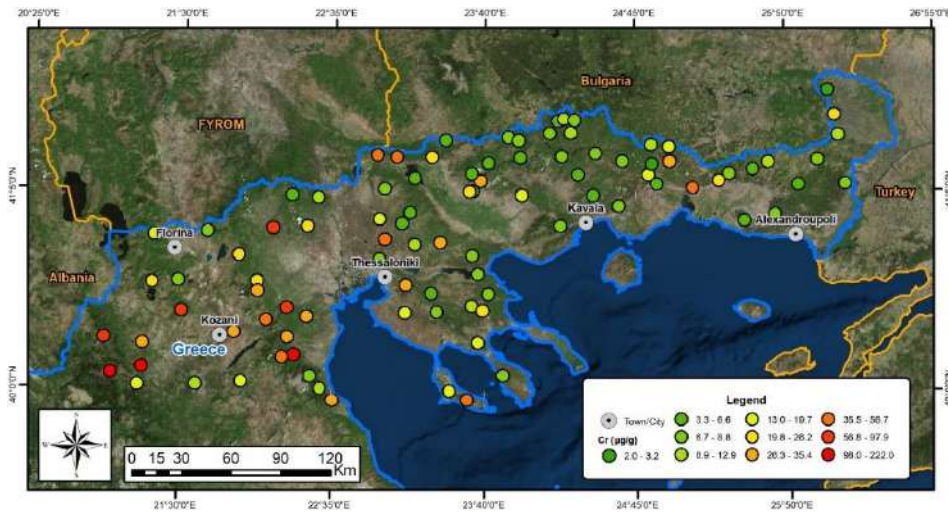
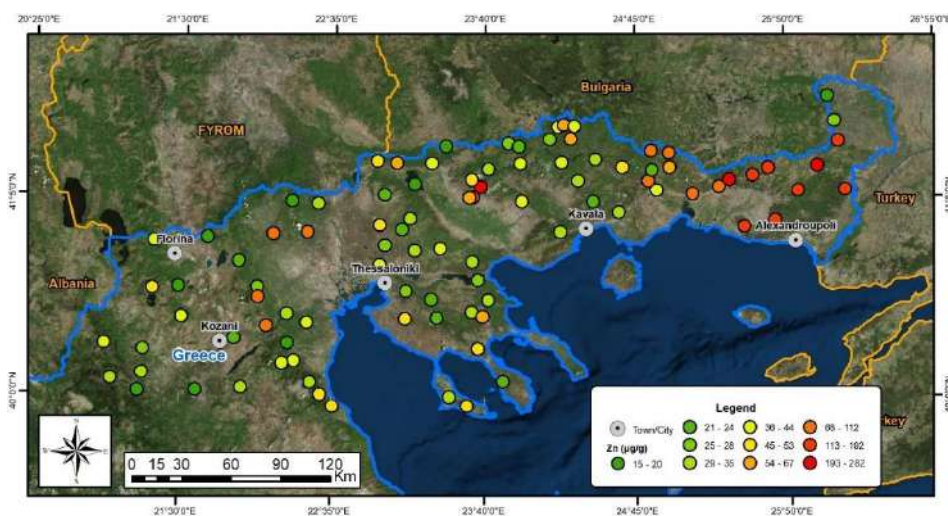


**Figure 4.6.** The concentrations of Cr ( $\mu\text{g g}^{-1}$ ) in the 95 moss samples collected in the region of Northern Greece.

### Zinc

Zinc (Zn) is an essential element to all organisms as a constituent of many metalloenzymes and of several other proteins. It can be affected by different anthropogenic emissions such as from the road transportation (tires), the metal production, steelworks, metal smelters and the coal mining areas (Harmens et al., 2008).

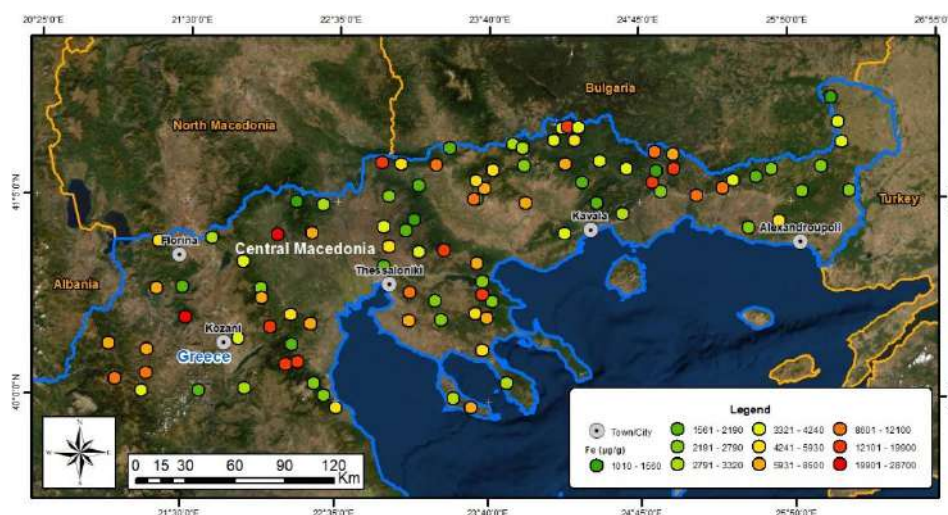
The highest concentrations of Zn that were measured during this survey are on the Eastern part of Northern Greece, in the Region of Thrace. According to the spatial distribution of Zn in Figure 4.7, around the city of Alexandroupoli till the borders with Turkey and especially towards the borders with Bulgaria the majority of the sampling sites have the most elevated concentrations of Zn.



**Figure 4.7.** The concentrations of Zn ( $\mu\text{g g}^{-1}$ ) in the 95 moss samples collected in the region of Northern Greece.

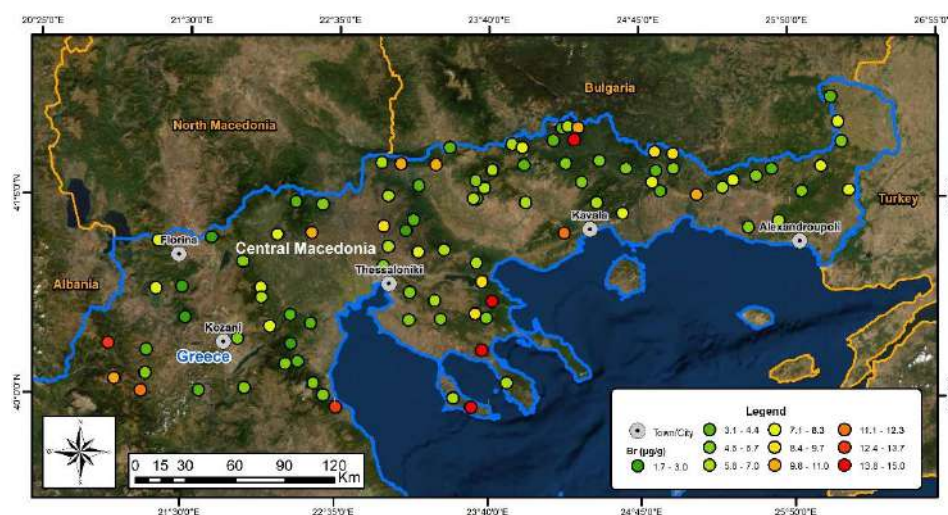
## Iron

Iron (Fe) is found in great abundance in the Earth's crust. It is usually connected with the windblown soil dust and the iron and steel industry. Iron concentrations are displayed in Figure 4.8. The sites which present high concentrations are those around the cities of Kozani and Thessaloniki and close to the Bulgarian borders.

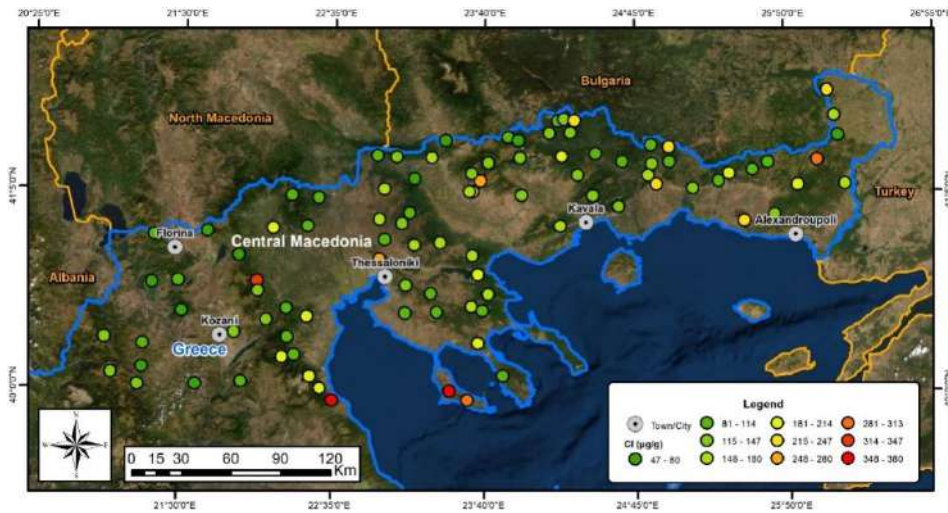


**Figure 4.8.** The concentrations of Fe ( $\mu\text{g g}^{-1}$ ) in the 95 moss samples collected in the region of Northern Greece.

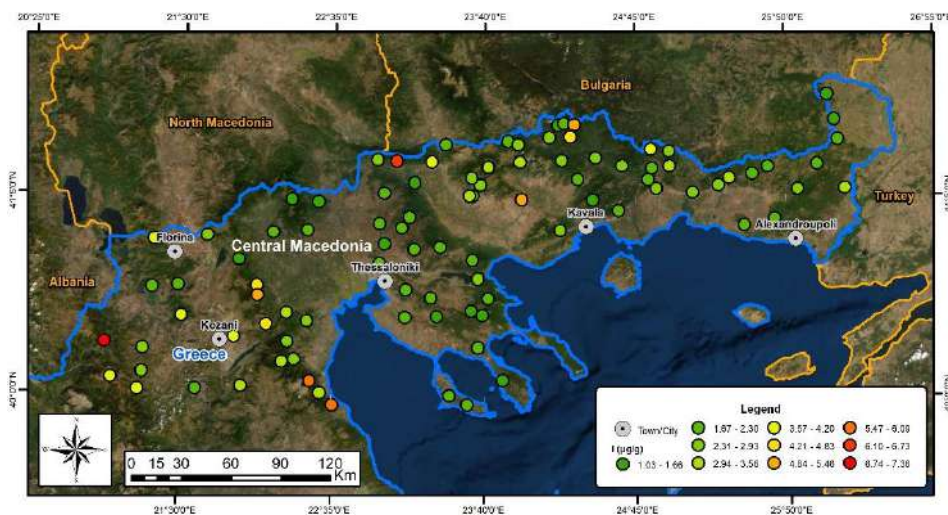
Additional elemental distributions are presented in Figures 4.9-4.24. More specifically, the elemental concentrations of Br, Cl, I, Mg, Na, K, Sc, Ti, Mn, Co, Se, Rb, Sb, Au, Th and U are presented, with no special remarks provided.



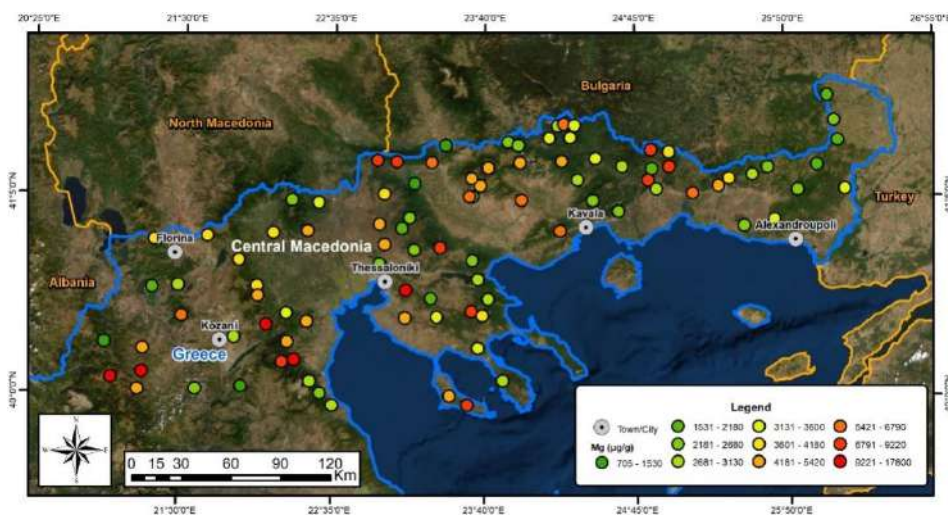
**Figure 4.9.** The concentrations of Br ( $\mu\text{g g}^{-1}$ ) in the 95 moss samples collected in the region of Northern Greece.



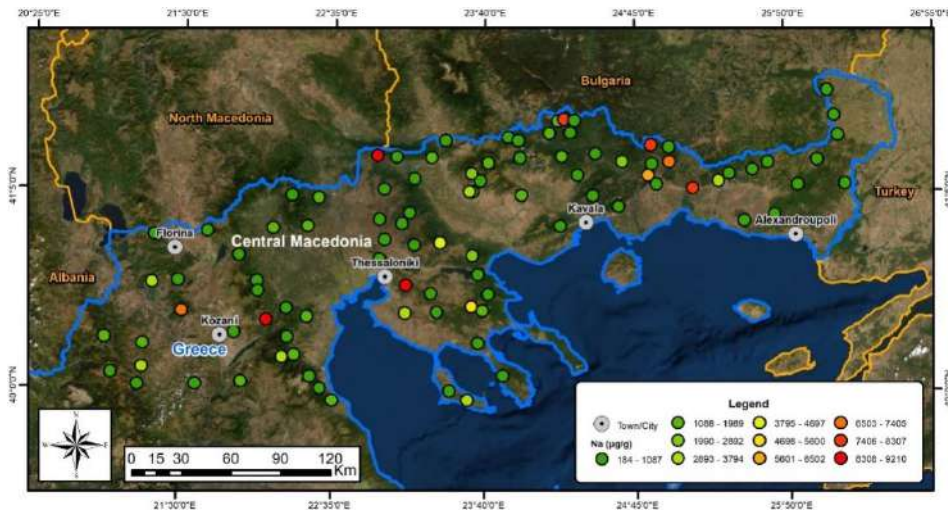
**Figure 4.10.** The concentrations of Cl ( $\mu\text{g g}^{-1}$ ) in the 95 moss samples collected in the region of Northern Greece.



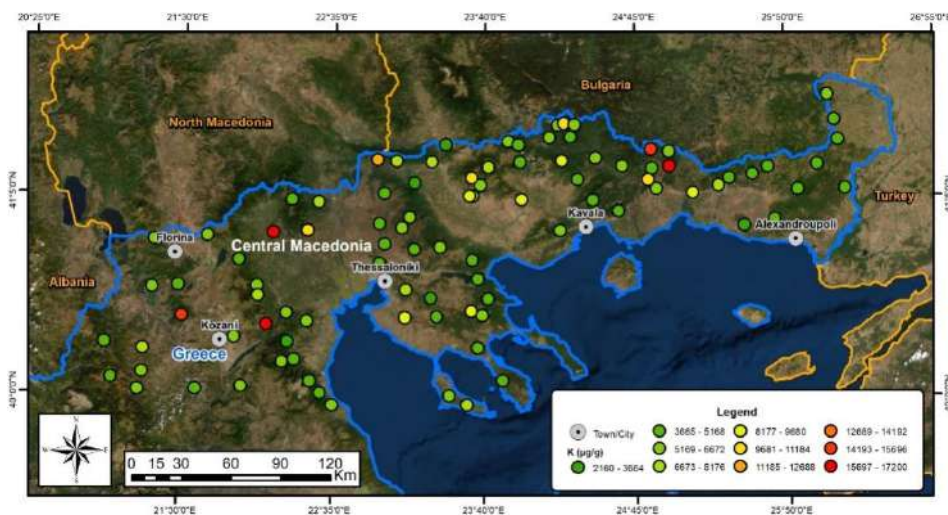
**Figure 4.11.** The concentrations of I ( $\mu\text{g g}^{-1}$ ) in the 95 moss samples collected in the region of Northern Greece.



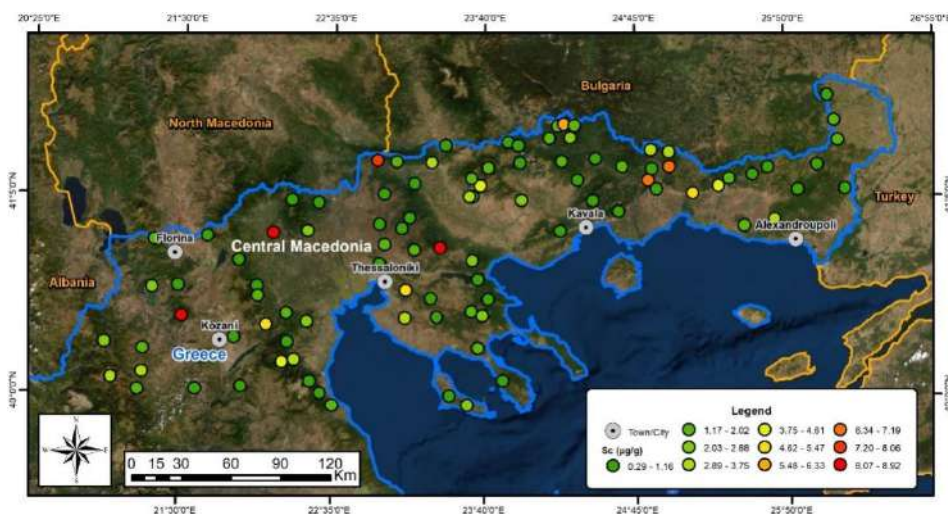
**Figure 4.12.** The concentrations of Mg ( $\mu\text{g g}^{-1}$ ) in the 95 moss samples collected in the region of Northern Greece.



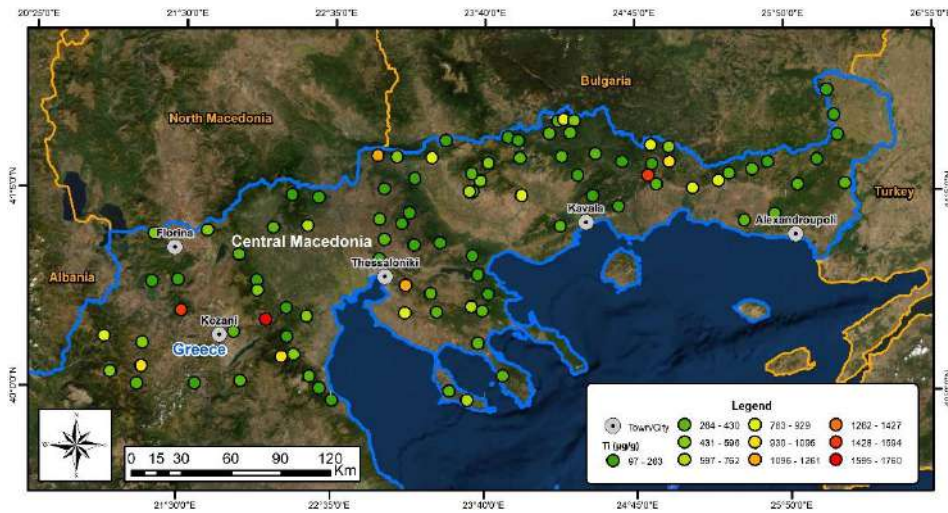
**Figure 4.13.** The concentrations of Na ( $\mu\text{g g}^{-1}$ ) in the 95 moss samples collected in the region of Northern Greece.



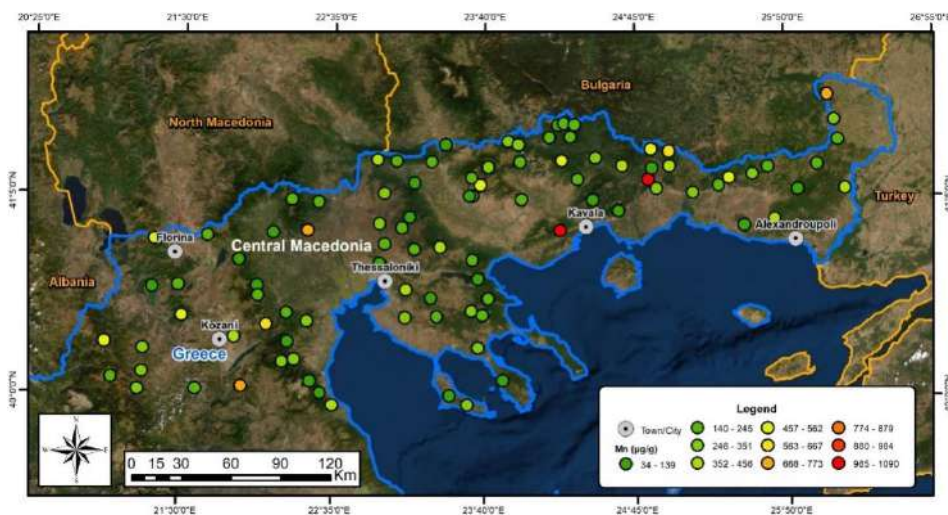
**Figure 4.14.** The concentrations of K ( $\mu\text{g g}^{-1}$ ) in the 95 moss samples collected in the region of Northern Greece.



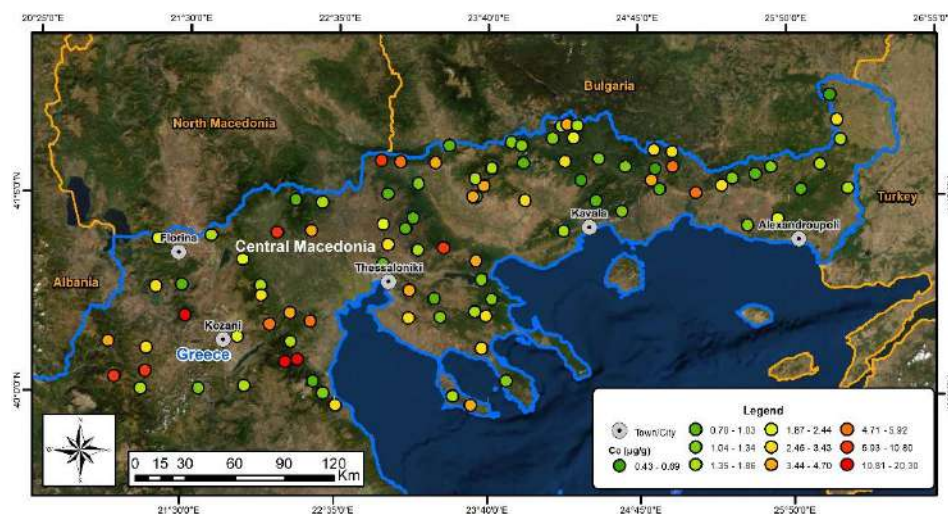
**Figure 4.15.** The concentrations of Sc ( $\mu\text{g g}^{-1}$ ) in the 95 moss samples collected in the region of Northern Greece.



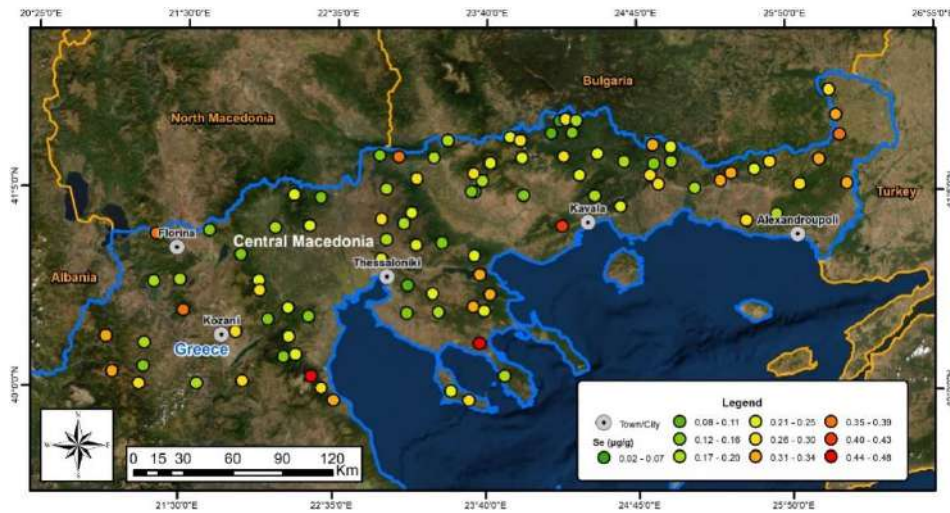
**Figure 4.16.** The concentrations of Ti ( $\mu\text{g g}^{-1}$ ) in the 95 moss samples collected in the region of Northern Greece.



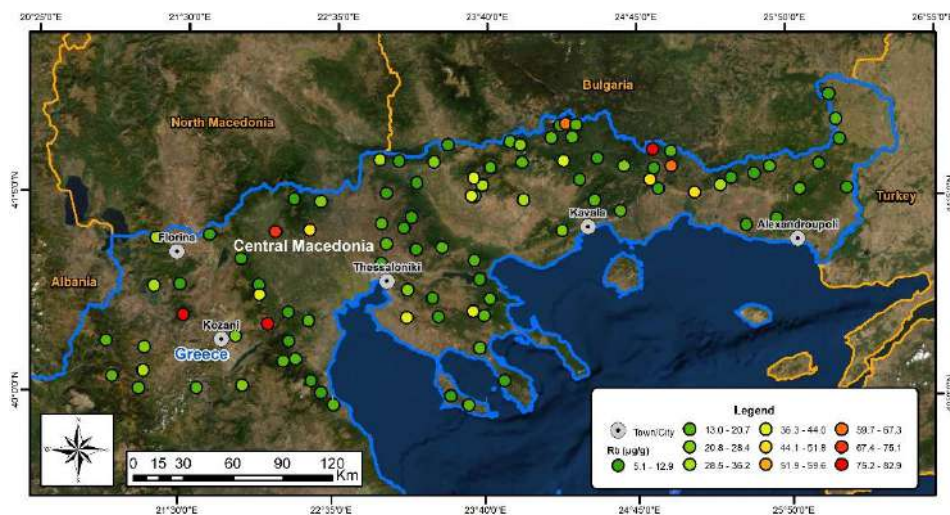
**Figure 4.17.** The concentrations of Mn ( $\mu\text{g g}^{-1}$ ) in the 95 moss samples collected in the region of Northern Greece.



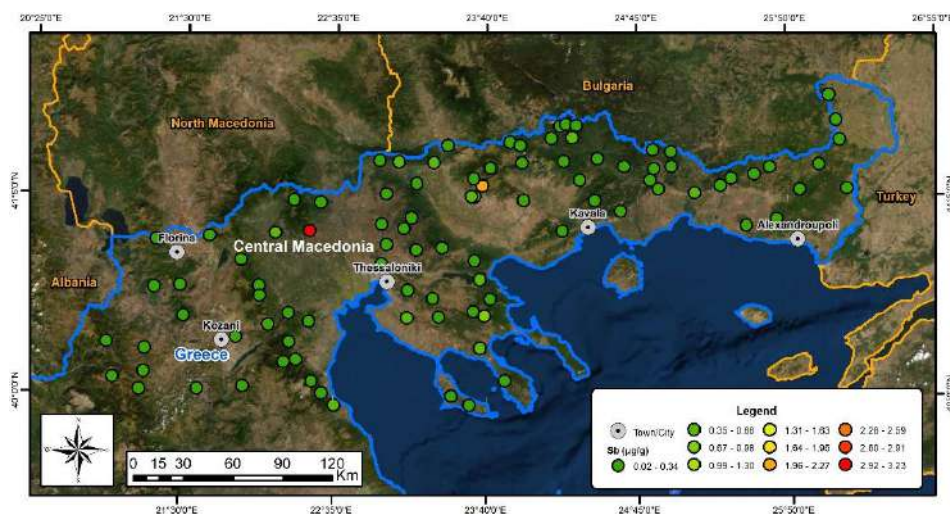
**Figure 4.18.** The concentrations of Co ( $\mu\text{g g}^{-1}$ ) in the 95 moss samples collected in the region of Northern Greece.



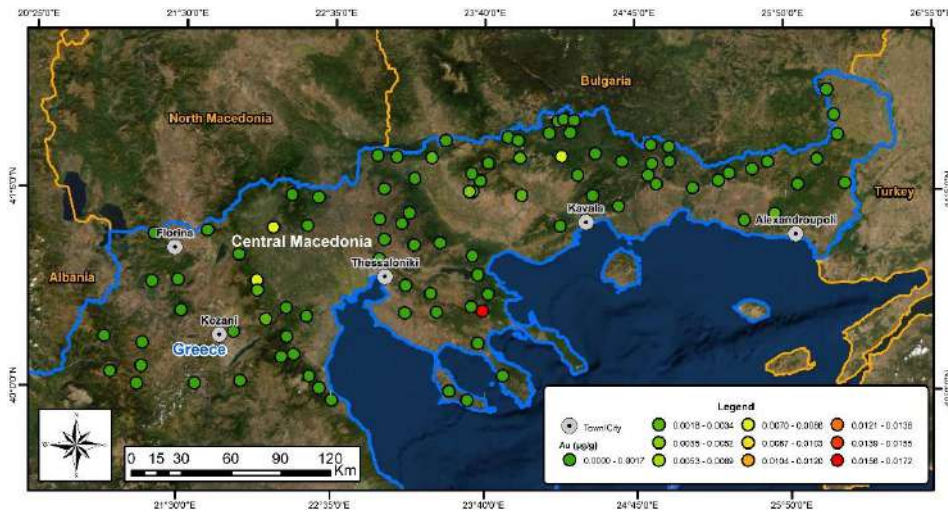
**Figure 4.19.** The concentrations of Se ( $\mu\text{g g}^{-1}$ ) in the 95 moss samples collected in the region of Northern Greece.



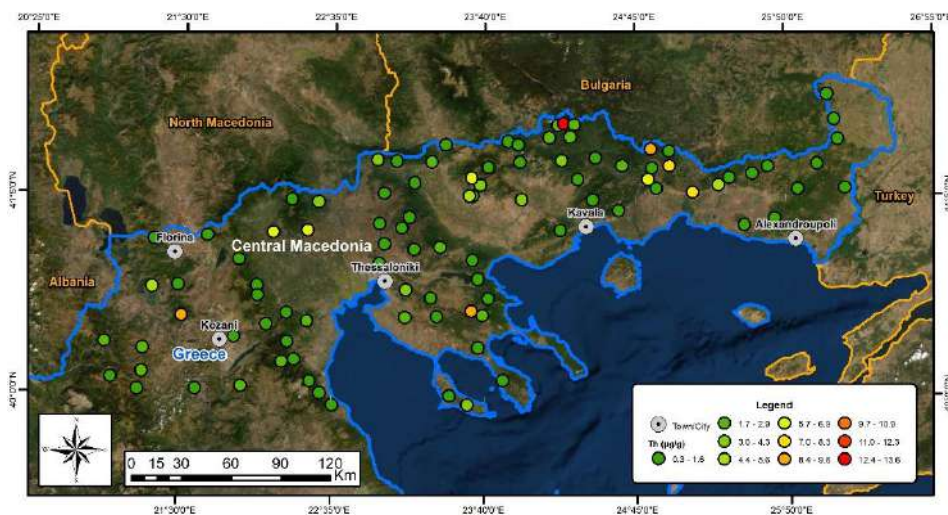
**Figure 4.20.** The concentrations of Rb ( $\mu\text{g g}^{-1}$ ) in the 95 moss samples collected in the region of Northern Greece.



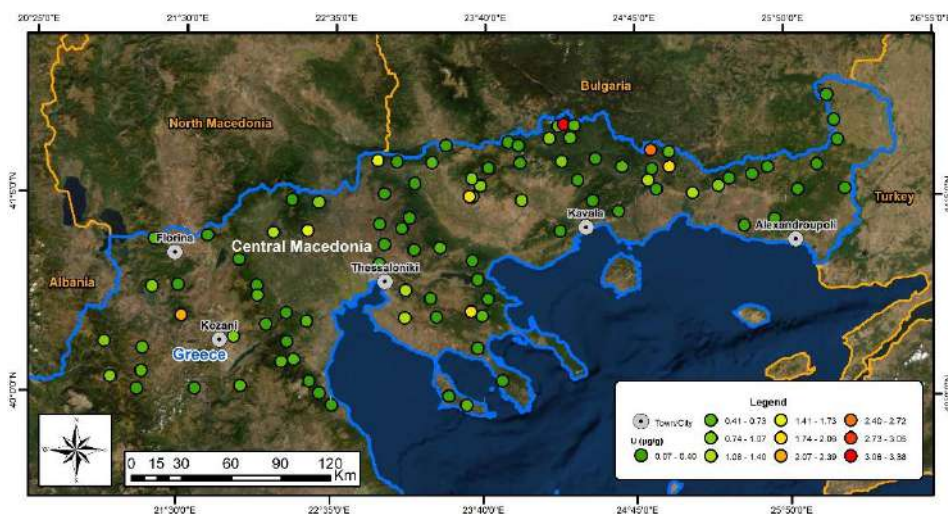
**Figure 4.21.** The concentrations of Sb ( $\mu\text{g g}^{-1}$ ) in the 95 moss samples collected in the region of Northern Greece.



**Figure 4.22.** The concentrations of Au ( $\mu\text{g g}^{-1}$ ) in the 95 moss samples collected in the region of Northern Greece.



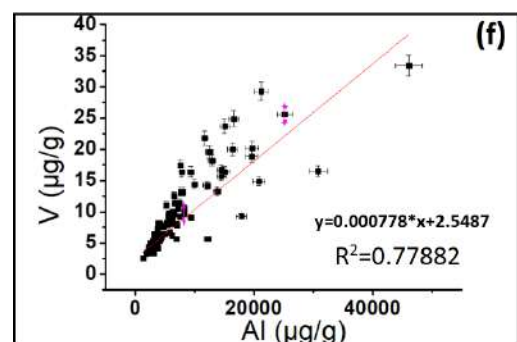
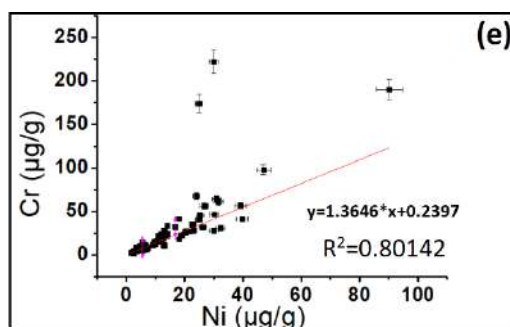
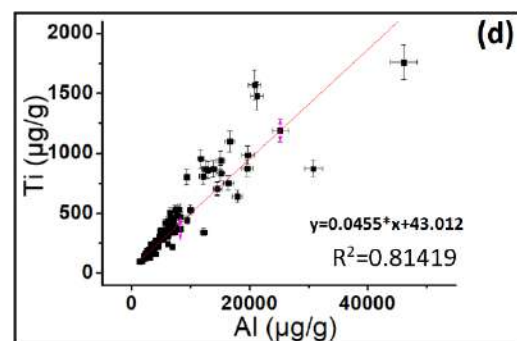
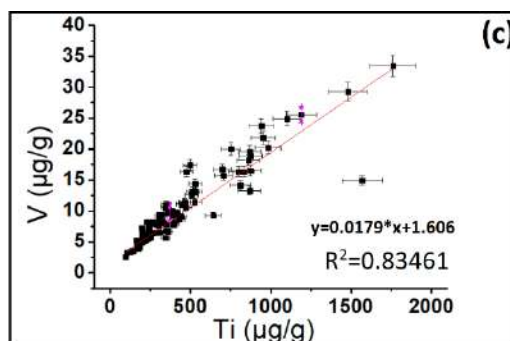
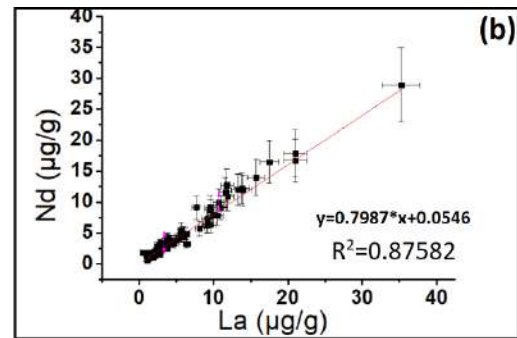
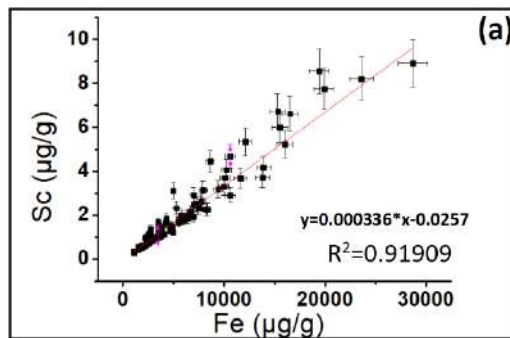
**Figure 4.23.** The concentrations of Th ( $\mu\text{g g}^{-1}$ ) in the 95 moss samples collected in the region of Northern Greece.



**Figure 4.24.** The concentrations of U ( $\mu\text{g g}^{-1}$ ) in the 95 moss samples collected in the region of Northern Greece.

#### 4.1.2 Correlation analysis between the trace elements in moss samples

After performing the spatial distributions of the most frequently analyzed trace elements, the next step is to examine any correlation between different trace elements and determine their natural or anthropogenic origins (Qarri et al., 2015). Correlation between different trace elements (Sc-Fe, Nd-La, V-Ti, Ti-Al, Cr-Ni, Al-V, Co-Fe, Th-U, K-Rb and Ba-La) are given in Figures 4.25 (a)-(j).



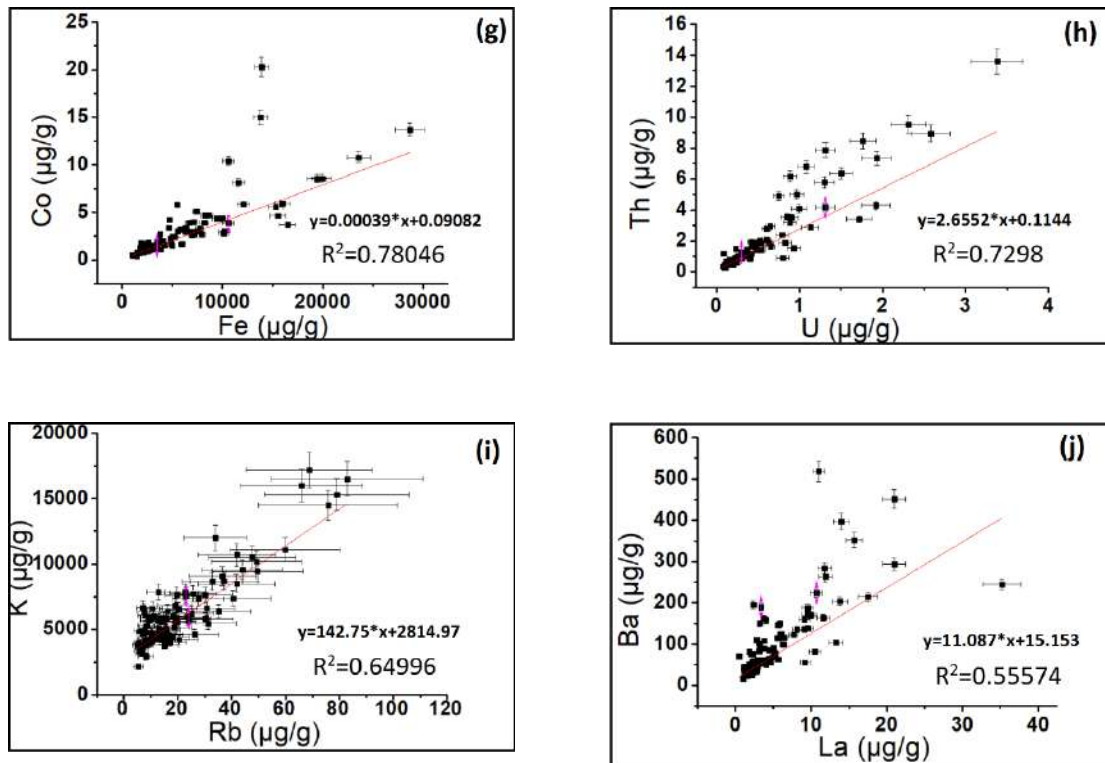


**Figure 4.25.** The correlations between the different trace elements measured in moss samples.

The strong positive correlation between the above elements verifies the quality of the measurements and points out the common origin of the elements (either naturally existing or due to human activities such as industry, transportation, heating, mining activities, smelters etc.).

For example, the strong positive correlation between the elements Sc-Fe, Nd-La, V-Ti, Ti-Al, Al-V, Th-U, K-Rb and Ba-La, reveals one common source, the windblown soil dust source. On the other hand, the relative high correlation between Cr and Ni is an indicator of industrial activities (Saitanis et al., 2012; Qarri et al., 2015).

The positive correlation between Co-Fe, is an indication of common source. They can be connected either with the soil dust or with the industrial activities. When the concentration of Co is higher than Fe this means that Co comes mostly from industrial use, while Fe can be characterized as an earth component (personal conversation with Professor Krmar). One characteristic example is the area of West Macedonia, where a lot of industrial activities take place, such as the coal fired power plants. In this area, the Co concentrations were found to be higher than Fe (Table A1).

### 4.1.3 The influence of the surface type on elemental concentrations

Moss samples were collected from different surface types (on rocks, surface, branches and near roots). Differences can be observed in the elemental concentrations depending on the surface type from where mosses were collected and some representative box plots of them (Al, As, Cr, Fe, Mg, Ni) are presented (Figures 4.26 (a)-(f)). The ratio of the elemental concentrations between mosses collected from the surface and those collected near roots  $\left(\frac{C_{surface}}{C_{roots}}\right)$  for almost all the elements are above 1, indicating that the majority of the elements were deposited on mosses through the soil resuspension, which is favored by the arid climate of Greece.

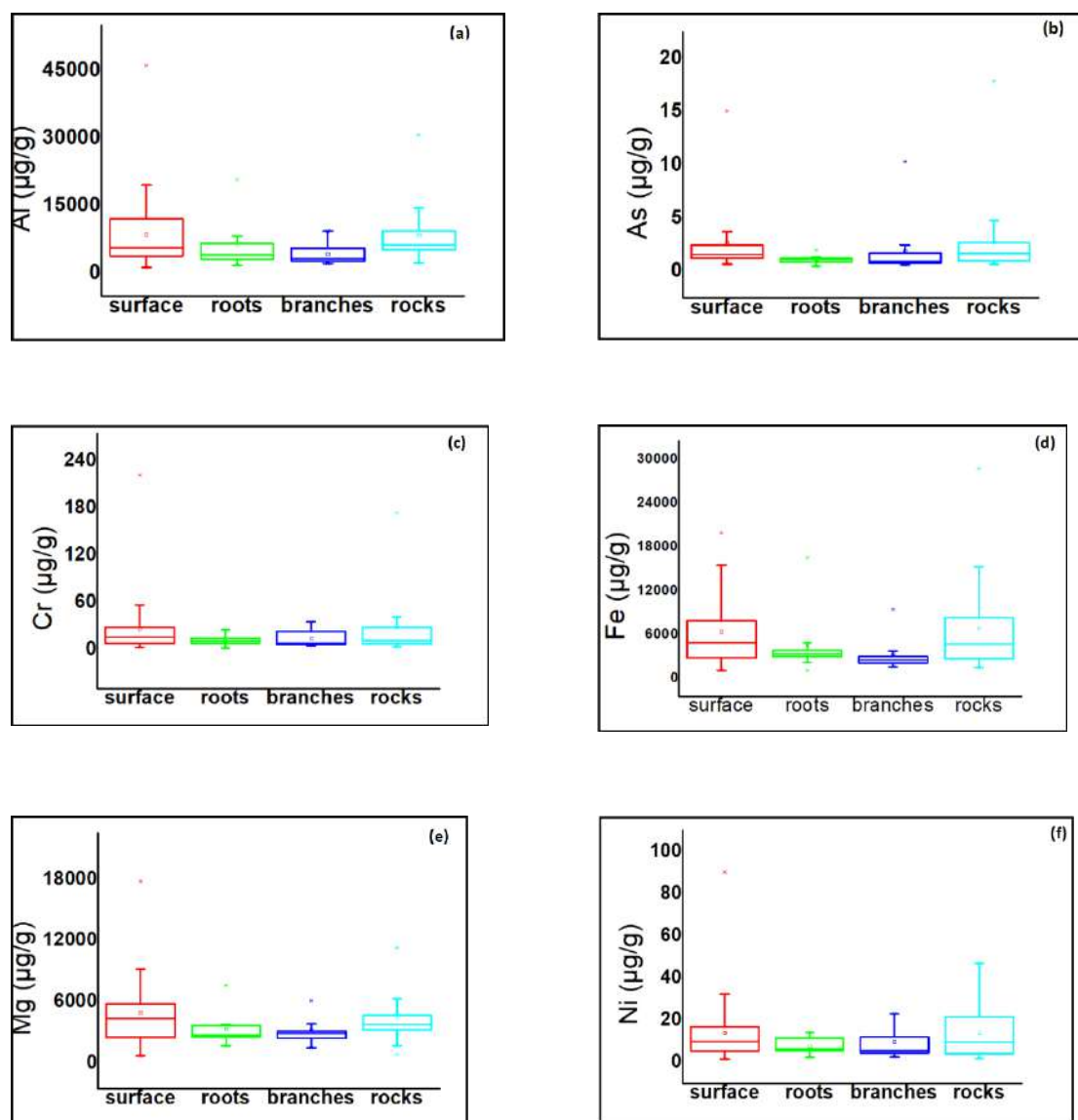


**Figure 4.26 (a)-(f).** “Box/whisker” plots of the elemental concentrations of Al, As, Cr, Fe, Mg and Ni based on the different surface types from where mosses were collected.

## 4.2. Case Study – Mosses collected near a gold mine in Skouries (Chalkidiki Prefecture, Central Macedonia Region)

### 4.2.1 History of the gold mining in Skouries

Skouries gold mine is an interesting to study area in the North part of Greece (Figure 4.27). It is located in the Northeastern Chalkidiki peninsula (Lon.: 23,698 and Lat.: 40,479) and has a long mining history since ancient times; some brief details about the historical path of the gold mining are given below.

The earliest mining activities in Chalkidiki date back to the 6<sup>th</sup> century B.C. However, the mines flourished during the time of Philip II (Macedonian Kingdom), and they continued their operation during the Roman, Byzantine and Ottoman Empire. After the era of Ottoman Empire, the interest in mining investment was increased rapidly, especially in the late 19<sup>th</sup> century. Since then, the mining ores that are located in Skouries region, are being exploited intensively by different companies. More specifically, after the Ottoman Empire, the Greek State took ownership of the Cassandra Mines in 1913, and leased them to the Anonymous Greek Company of Chemical Products and Fertilizers until 1992 (Hovardas, 2017; Tsavdaroglou et al., 2017; <https://www.miningreece.com/mining-greece/mining-projects/kassandras-mines/>).

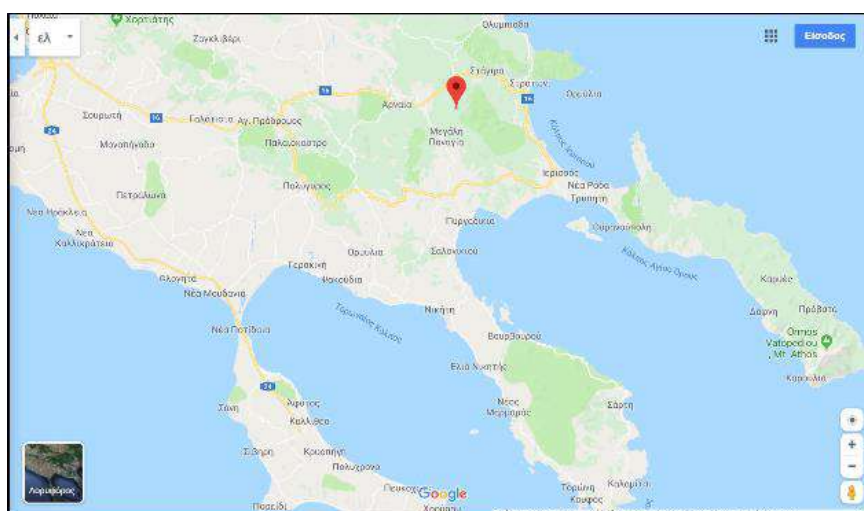


**Figure 4.27.** The location of the Skouries in Northern Greece (Prefecture Chalkidiki).

Three years later (1995), mining was taken over by the Canadian ‘TVX Gold’ and its Daughter Company ‘TVX Hellas’ till 2003. In 2004, the ‘Hellas Gold Company’ bought all the mining rights and facilities from the Greek State and started exploiting the mining ores (Tsavdaroglou et al., 2017). In 2011, a new mining project was approved for the Skouries area, which involved open-pit mining and on-site ore processing. The project which was firstly taken over by ‘Hellas Gold’, has been controlled by ‘Eldorado Gold’ since 2012 (Hovardas, 2019).

The mining activities and especially the open-pit mining cause a series of landscape alterations of a considerable climax, involving tree-felling to create the open-pit mine,

removal and processing of soil to extract the ore, and change in drainage basins for the creation of tailings ponds. The open-pit mining is also accompanied by other environmental side effects, like the soil dust from the extractions, which contains different trace elements and can be easily transferred, deposited in the surrounding area and being absorbed by the biota (Hovardas, 2017).

Based on all the previous mentioned data, a lot of public concerns and movements have been arisen about the impact of the current mining activities on the local environment and the potential hazard for the public health. For these reasons, during the last years, different studies have been performed, investigating the environmental pollution of the area due to the mining activities (Lazaridou-Dimitriadou et al., 2004; Papa et al., 2016; Chantzi et al., 2016; Argyraki et al., 2017). In this study, it is the first time that moss samples are used as indicators of trace elements originated to the mining activities.

The metal mining activities that are being expanded even more during the last years motivated us to perform a *special case study* including moss samples collected from the area of Skouries. More specifically, different species of moss samples were collected in the surroundings of the mining facilities and were analyzed for trace elements concentrations, in order to check the impact of the mining activities in the area.

#### **4.2.2 Sampling and Analysis**

Ten samples of different moss species were collected from the area of Skouries, next to the mining facilities. More specifically the moss species of *Antitrichia curtipendula*, *Dicranum scoparium*, *Hypnum cupressiforme*, *Homalothecium sericeum*, *Isothecium alopecuroides*, *Plagiochilla porelloides* and *Pterogonium gracile* were collected, all species that were found growing in abundance in the area. Sampling of different moss species allows to study and understand any difference in the accumulative efficiency of trace elements of each different moss species of the different moss species.

Moss samples were cleaned manually from impurities in the field. Then, they were prepared for NAA measurements, analyzed using NAA technique, following the same procedures and conditions as described earlier for the other moss samples of this survey and finally, the elemental concentrations of 44 trace elements were determined (the same elements as described earlier for the rest of the moss samples in this study). The elemental concentrations are presented in Table C1 and C2 in the Appendix and the descriptive analysis is presented in Tables 4.3 and 4.4.

**Table 4.3.** The descriptive analysis of the 23 most frequently analyzed and published in studies elements that were determined in the moss samples from the Skouries area, by means of Neutron Activation Analysis (NAA).

	Na	Mg	Al	Cl	K	Sc	Ti	V	Cr	Mn	Fe	Co	Ni	Zn	As	Se	Br	Rb	Sb	I	Au	Th	U
Mean	1079	10094	11595	599	7078	2.73	670	21	118	652	9866	6.8	86	48	11.4	0.50	18	26	0.69	6.9	0.0097	1.91	0.41
Median	901	11350	12050	353	6195	2.48	636	20	102	538	8955	6.4	77	47	10.7	0.48	14	26	0.65	7.0	0.0069	1.76	0.40
Min	668	1880	7170	271	4910	1.74	352	14	66	338	6350	4.5	52	35	7.5	0.38	5	19	0.32	3.8	0.0043	1.27	0.16
Max	1710	16400	17300	2070	14800	4.12	1230	30	200	1760	14300	10.6	138	72	15.4	0.72	59	34	1.03	9.8	0.0319	2.92	0.67
Range	1042	14520	10130	1799	9890	2.38	878	16	134	1422	7950	6.1	86	37	7.9	0.34	54	15	0.71	6.0	0.0276	1.65	0.52
St. Dev.	401	4353	3449	549	2827	0.94	268	6	46	408	3256	2.4	30	12	3.1	0.10	16	5	0.24	2.4	0.0083	0.59	0.16
Kurt.	-1.7	-0.14	-1.12	7.04	7.92	-1.9	1	-1	-1	8	-2	-1.6	-1	1	-1.8	0.88	7	-1	-1.28	-2.2	6.9600	-1.3	-0.83
Skew.	0.5	-0.54	0.18	2.55	2.71	0.33	1	0	1	3	0	0.4	1	1	0.1	1.08	2	0	-0.10	-0.1	2.5700	0.5	0.15

**Table 4.4.** The descriptive analysis of the rest 21 elements that were measured in the moss samples from the Skouries area, by means of Neutron Activation Analysis (NAA).

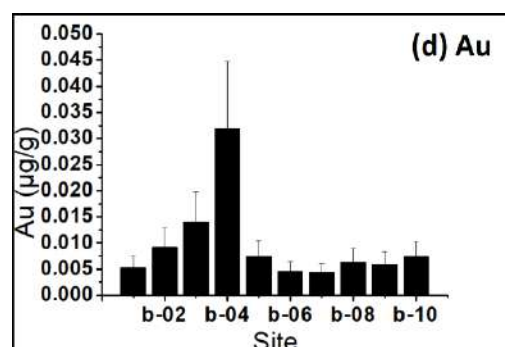
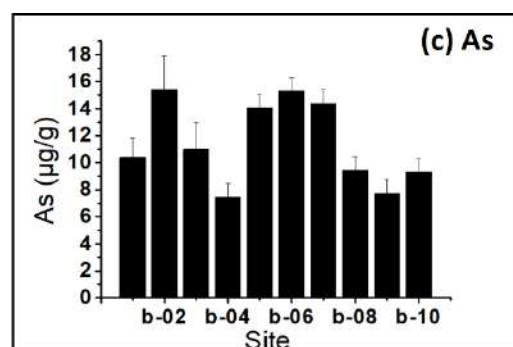
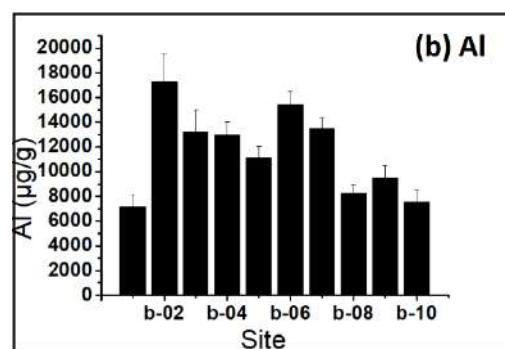
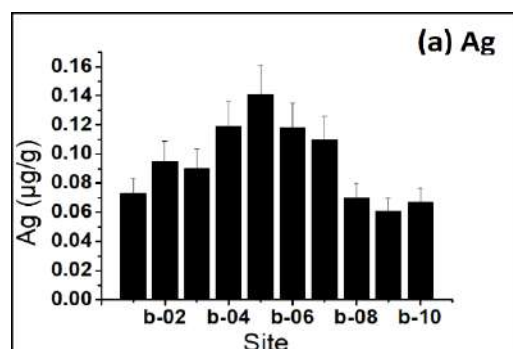
	Si	Sr	Ca	Zr	Cs	Ba	La	Ce	Nd	Sm	Gd	Tb	Dy	Tm	Yb	Lu	Hf	Ta	In	Mo	Ag
Mean	65120	57	10088	28.88	1.01	151	5.53	11.14	4.43	0.80	0.53	0.13	0.72	0.09	0.14	0.100	0.91	0.14	0.15	0.22	0.09
Median	56050	49	9270	25.05	1.04	123	5.19	10.34	4.36	0.88	0.52	0.13	0.67	0.09	0.14	0.108	0.82	0.14	0.18	0.24	0.09
Min	40400	35	6090	16.60	0.74	75	3.65	7.39	1.59	0.01	0.45	0.08	0.46	0.04	0.07	0.001	0.54	0.08	0.04	0.05	0.06
Max	168000	104	16800	50.70	1.28	367	8.78	17.50	7.08	1.42	0.64	0.18	1.15	0.13	0.20	0.156	1.71	0.27	0.30	0.33	0.14
Range	127600	69	10710	34.10	0.54	292	5.13	10.11	5.49	1.41	0.19	0.11	0.69	0.08	0.13	0.155	1.17	0.19	0.26	0.27	0.08
St. Dev.	37186	24	3064	11.70	0.18	87	1.80	3.65	1.69	0.49	0.07	0.04	0.23	0.02	0.05	0.050	0.38	0.06	0.10	0.08	0.03
Kurt.	9	1	2	-0.71	-1.44	4	-1.05	-1.30	-0.67	-0.60	-0.78	-1.84	-0.52	0.24	-2.04	-0.113	0.56	2.37	-1.30	0.96	-1.09
Skew.	3	1	1	0.69	-0.10	2	0.54	0.45	-0.12	-0.69	0.54	0.11	0.73	0.04	0.01	-0.739	1.01	1.36	0.12	-0.72	0.36

### 4.2.3 Distributions of the elemental concentrations of the different moss species

In Table 4.5 the moss species collected from the ore mining area in Skouries are given. In Figures 4.28 (a)-(l), the distributions of the elements Ag, As, Al, Au, Co, Cr, Fe, Mg, Mn, Ni, Sb and V are presented. The *Hypnum cupressiforme* species is the one that is the most frequently found in Greece and the most studied by the ICP Vegetation ‘Moss Survey Protocol’. However, based on the above figures it is noticed that the moss species *Isothecium alopecuroides* (Figure 4.29) and *Dicranum scoparium* (Figure 4.30) present the highest elemental concentrations of As, Al, Co, Fe, V and Cr, Mg, Ni, Sb respectively.

**Table 4.5.** The moss species samples that were collected from the area of Skouries.

Sample	Moss species
b-01	<i>Hypnum cupressiforme</i>
b-02	<i>Isothecium alopecuroides</i>
b-03	<i>Isothecium alopecuroides</i>
b-04	<i>Pterogonium gracile</i>
b-05	<i>Plagiochilla poreloides</i>
b-06	<i>Dicranum scoparium</i>
b-07	<i>Dicranum scoparium</i>
b-08	<i>Homalothecium sericeum</i>
b-09	<i>Antitrichia curtispindula</i>
b-10	<i>Antitrichia curtispindula</i>



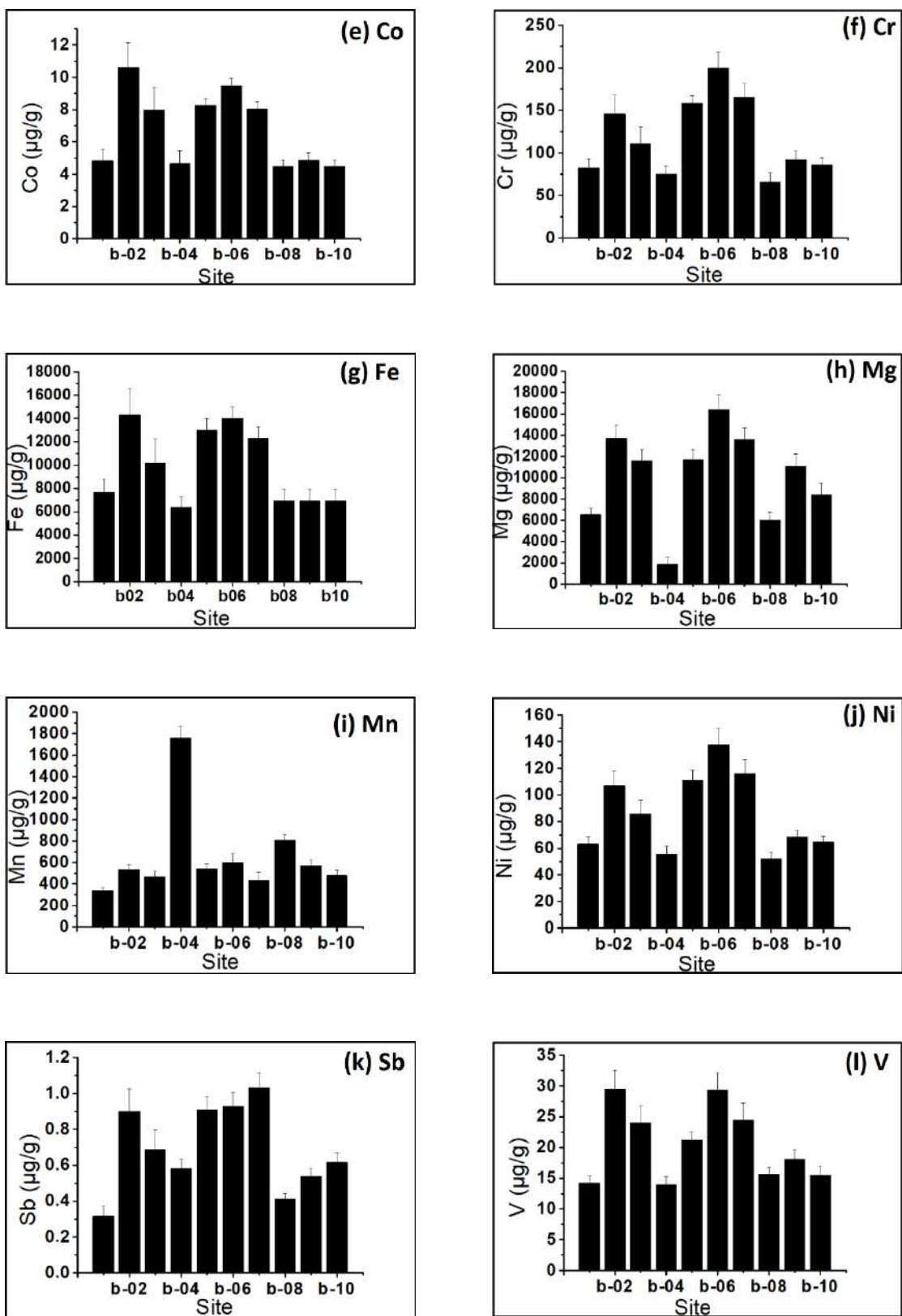


**Figure 4.28.** The distributions of trace elements in-moss species collected in the area of Skouries (a) Ag, (b) Al, (c) As, (d) Au, (e) Co, (f) Cr, (g) Fe, (h) Mg, (i) Mn, (j) Ni, (k) Sb and (l) V.



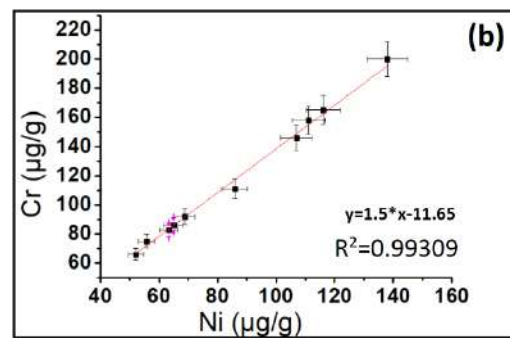
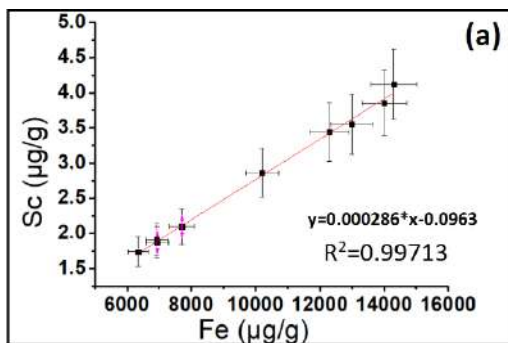
**Figure 4.29.** The *Isoetecium alopecuroides* moss species.



**Figure 4.30.** The *Dicranum scoparium* moss species.

#### 4.2.4 Correlation between the trace elements concentrations determined in the moss samples

The correlation between different pairs of elements has been examined (Figures 4.31 (a)-(h)). According to the correlation figures, linear correlations between the elements Sc and Fe, Cr and Ni, Ce and La, Fe and Ce, Co and Fe, U and Th, Ni and Fe, Sc and V were observed. The plots of the less strongly correlated elements (Ni-V, Ti-Al, Al-V, Nd-La, Si-Ti, Si-Fe, Fe-Ti, Zn-Fe, Ti-V, Cl-Br) are presented in the Appendix D.



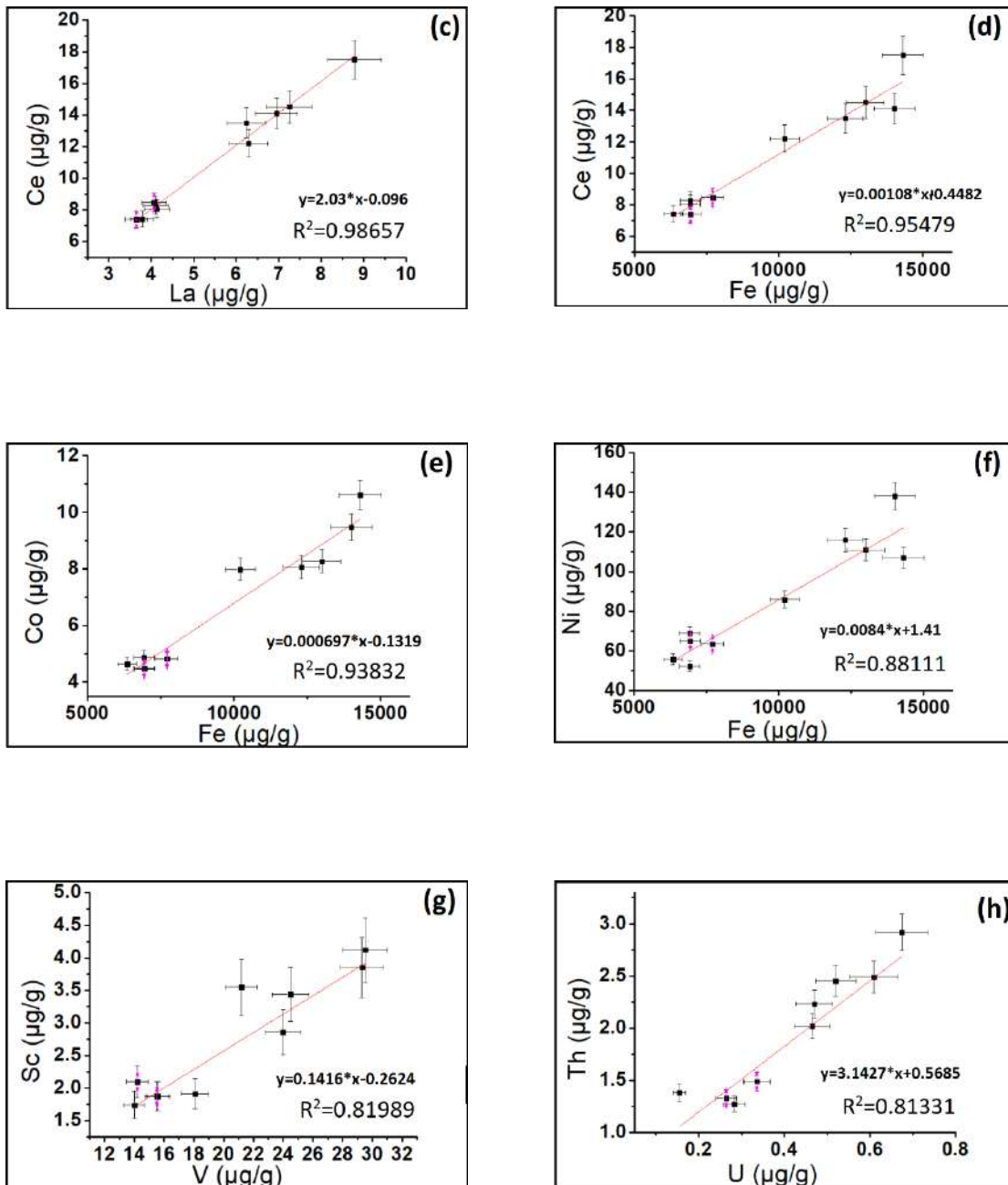


**Figure 4.31.** The correlation between the different trace elements determined in the moss samples collected in the area of Skouries.

The strong positive correlation that exists between the pairs of elements (Sc-Fe, Cr-Ni, Ce-La, Fe-Ce, Co-Fe, U-Th, Ni-Fe, Sc-V) verifies the quality of the measurements and points out the common origin of the specific elements (natural or anthropogenic such as industry, transportation, heating, mining activities, smelters etc.) (Qarri et al., 2015).

The strong correlations between Sc and Fe, Ce and La, Ce and Fe, Th and U, Sc and V, as well as the correlations between Ti and Al, Al and V, Nd and La, Ti and V, Ti and Fe, Ti and Si, Si and Fe, are indicators of the windblown soil dust source (Saitanis et al., 2012).

The positive correlations between Cr and Ni, as well as Ni and V elements are indicators of the anthropogenic activities (Qarri et al., 2015) in the mining facilities.

The positive correlation between Co and Fe, as well as Ni and Fe, is an indication of the anthropogenic activities that take place in the mining facilities.

The positive correlation between Zn and Fe is an indication of the resuspended soil dust from the mining activities.

The Source apportionment analysis that follows, reveals the exact origins of the elements (section 4.4).

#### **4.2.5 “Skouries” elemental concentrations vs the rest Northern Greece concentrations**

The ten (10) moss samples collected from the Skouries area, were collected very close to the ore mine. Among the ninety-five (95) samples collected in this survey in Northern Greece, the one closest to the area of Skouries is the sample “ID: x-88”. However, the moss sample x-88 has been collected a few kilometers away from the gold mining facilities. This distance between the two sampling sites (‘Skouries site’ and ‘x-88’) explains the higher observed values of the elemental concentrations in the moss samples that were collected very close to the mine (Tables C1, C2, 4.3, 4.4). The concentrations from ‘Skouries site’ are two to ten times higher than the concentrations of the moss sample x-88. More specifically, the concentrations of the elements Au, Fe, Sb and Sc are two times higher, while the concentrations of V, Al and Co are three times higher than in the sample x-88. Also, the elements Cr and Mn are seven times higher, while the concentration of Ni is almost ten times higher in the “Skouries” samples. Finally, for the elements As and Zn were determined concentrations more than 10% higher in “Skouries” moss samples than in the sample x-88.

Most of the times, the element As is related to copper and gold mines (Marinova et al., 2010) which can explain the higher observed concentration in Skouries.

The elements Au, Fe and Mn are found in higher concentrations due to the metal ore mining activities in the area.

The elements Ni, V, Cr and Co which are usually connected with anthropogenic activities (Harmens et al., 2008), have higher concentrations due to anthropogenic activities held in the mine.

The high observed values of the elements Al, Zn and Sc can be explained as a result of the windblown soil dust that is more intense and dispersed close to the mining facilities.

Finally, the elemental concentrations of Au, Mn, and Ni determined in these ten (10) moss samples in Skouries, are much higher than the concentrations of all ninety-five (95) samples collected from Northern Greece (Tables A1, A2, 4.1, 4.2). More specifically, the concentrations of the elements Au, Mn and Ni exceed those of the rest of Northern Greece, since Au in “Skouries” mosses ranges between 0.0043 to 0.039  $\mu\text{g g}^{-1}$ , Mn ranges between 338 to 1760  $\mu\text{g g}^{-1}$  and Ni ranges between 52 to 138  $\mu\text{g g}^{-1}$ . All these elements are clearly associated with the activities that occur in the gold mine of Skouries. Detailed analysis follows in the 4.4 section.

#### 4.2.6 Other studies related with the area of “Skouries”

Several studies concerning the elemental concentrations in different matrices (water, seaweeds, fish, sediments, soil) have been conducted in the area of Skouries (Prefecture Chalkidiki).

For example, sediment samples were collected close to the coastal mining facilities (Ierissos Gulf) and showed that As concentrations ranged between 320 to 4100  $\mu\text{g g}^{-1}$ , Zn ranged between 940–4100  $\mu\text{g g}^{-1}$  and Mn ranged from 3840 to 26000  $\mu\text{g g}^{-1}$  (Pappa et al., 2016). The concentrations of Cu, Pb and Zn in surface sediments samples from the Ierissos Gulf were also studied and their highest values were measured in the area near the load-out facility of the mining operations in Stratoni Bay. Chromium and Ni had been also measured and were considered as results of the weathering action of the rivers that flew into the Gulf (Stamatis et al., 2001; 2019).

The chemistry of water samples was also studied in Ierissos Gulf and the main conclusion that extracted was that the surface water samples exceeded the limit of WHO especially for the elements As, Sb, Cr, Ni, Cd, Pb, Mn and Fe (Chantzi et al., 2016).

In another research, different kind of samples from water streams (surface water, sediments, edible fish) from the area of Skouries and Olympias were collected, and it was determined that the bioaccumulation of trace elements affected a lot the higher trophic levels and mostly fish (Lazaridou-Dimitriadou et al., 2004). High Pb, Zn and Cu concentrations were also determined in limpet samples from Stratoni area, while the concentrations of Mn, Ni and Cr were comparable to those reported for other non-polluted geographical regions of the Mediterranean area (Kelepertsis, 2013).

In the Stratoni area, soil samples were collected and the average concentration of Zn was found 712  $\mu\text{g g}^{-1}$ , of Mn 2900  $\mu\text{g g}^{-1}$  and of As 296  $\mu\text{g g}^{-1}$  (Argyraki et al., 2017). Finally, in another study concerning the area of Stratoni (Kelepertsis et al., 2006), soil samples were also collected and studied for Pb, Zn, Cu, As, Cd, Mn, Fe, Ni, Co and Cr concentrations. All these elemental concentrations were above the global soil mean values, and especially As and Ni concentrations exceeded the tentative guidelines set by the UK and the Netherlands regulations (Alloway, 1995).

In addition to the above studies, this moss survey will add useful data in the literature concerning the elemental concentrations in the area of Skouries using a different matrix. Finally, it could also be the basis for future moss bioindicator studies in the area.

#### 4.3 Comparison with data in literature

As already mentioned, the moss sampling and analysis of the samples of this study was performed under the framework of the ICP Vegetation Programme (United Nations Economic Commission for Europe Convention on Long-Range Transboundary Air Pollution. Monitoring of Atmospheric Deposition of Heavy Metals, Nitrogen and POPs in Europe using Bryophytes) (Frontasyeva et al., 2015). During the last decades, more and more countries from Europe and recently from Asia (almost 40 countries in the last

survey report) took part in this ‘Moss survey’ providing data for the levels of trace elements in their territories. The general trend of some elements in Europe during the last years is also provided through the reports of the ICP Vegetation Task Force Meetings (Harmens et al., 2008). The comparison of the current elemental concentrations observed in Northern Greece with results from previous studies in Greece, as well as with the data from other European countries is given below.

#### **4.3.1 Other studies in Greece**

In Greece, only a limited number of studies exist that use mosses for the determination of trace element concentrations. This survey is the first attempt of studying the atmospheric deposition of trace elements by using mosses collected in such a big territory in Greece, during a five years’ period.

A previous study has been conducted close to Athens, in a limited area close to a highly polluted area, where moss bags were used for investigating the elemental atmospheric deposition (Saitanis et al., 2012). According to this study, the concentrations of the elements Al, Zn, Fe, Cr, Ni and V were higher in the sites that were closer to the industrial zone, but there was not clear association between the anthropogenic activities and the observed elements. Another interesting outcome of this study was that the main source of Mn element was not an anthropogenic one, but it was supported that Mn was originally present in the moss as an essential element and that it could be easily replaced by other elements during the exposure and through leaching. These results do not agree to the estimations of the current study, where Mn is probably connected with mining activities in the regions enriched with Mn.

A more detailed, relevant, biomonitoring study, was conducted in Northern Greece, covering the area of east Central Macedonia Region and the Region of East Macedonia and Thrace. The study concerned the transboundary transport of trace elements between Bulgaria and the Northeastern part of Greece (Yurukova et al., 2009). According to this study, in the Greek territory, the relative high concentrations of the elements As, Cr, Fe, Ni and V were due to old mines, soil contamination by windblown dust and road transportation. The same study showed that, the Pb-Zn complex close to Kardzhali town in Bulgaria was responsible for the rise of the concentrations of Cr, Fe, Ni and As in the territory of Bulgaria.

The present study verifies the results of the previously mentioned investigation (Figures 4.32-4.37) regarding the pollutants’ chemical composition in the region of Northeastern part of Greece, next to the Bulgarian borders. Areas that are characterized by high concentrations of Al, As, Fe and V are observed in both of the studies, with some differences concerning the concentration levels of each element. For example, the concentration of As close to ‘Kerkini Lake’, presents a reduction of almost 30% from the previous study, while Al remains in similar levels. In specific areas close to the Bulgarian borders, the concentrations of Zn, Cr, Fe, Ni and V are two to three times higher than the previous observed concentrations. The reasons of this rise, ten years after the previous study, can be partially clarified. It might be due to the windblown

dust coming from manufacturing and metals industries, motorway constructions (Fe and Zn) or from coal mining activities and even from the ophiolitic rocks (Cr and Ni) that are present in the Greek territory (Betsou et al., 2019). However, it might be due to transboundary transport from sources in Bulgarian borders and further investigation needs to be done especially after the publication of the Bulgarian data of the current moss survey 2015/2016.

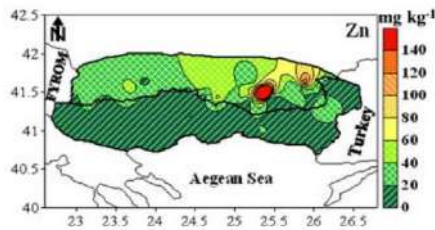


**Figure 4.32.** The concentrations of Zn according to Yurukova et al. (2009).

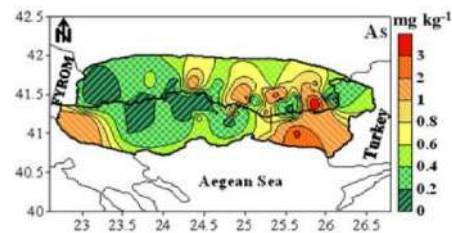


**Figure 4.33.** The concentrations of As according to Yurukova et al. (2009).

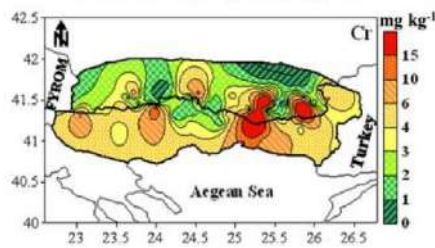


**Figure 4.34.** The concentrations of Cr according to Yurukova et al. (2009).

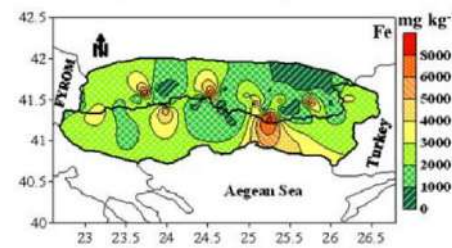


**Figure 4.35.** The concentrations of Fe according to Yurukova et al. (2009).

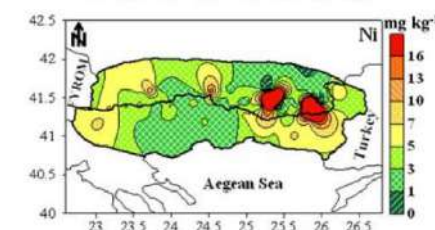


**Figure 4.36.** The concentrations of Ni according to Yurukova et al. (2009).

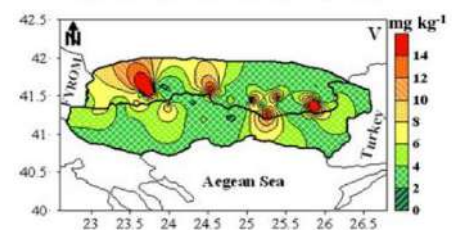


**Figure 4.37.** The concentrations of V according to Yurukova et al. (2009).

Another study that was performed in the framework of Tsikritzis thesis (2002), was about the concentrations of trace elements and radionuclides in vegetation (moss, lichens, leaves of trees) and soil in West Macedonia. According to this study, the concentrations of the trace elements in mosses are higher than in lichens, and they followed the order Fe>Mn>Cr>Ni>Pb>Cu>Cd. Moreover, the values of Cr ranged

between  $26.3 \mu\text{g g}^{-1}$  and  $147.4 \mu\text{g g}^{-1}$ , of Mn between  $203.3 \mu\text{g g}^{-1}$  and  $496.3 \mu\text{g g}^{-1}$ , of Fe from  $4565 \mu\text{g g}^{-1}$  to  $30492 \mu\text{g g}^{-1}$  and of Ni from  $7.7 \mu\text{g g}^{-1}$  to  $74.1 \mu\text{g g}^{-1}$ .

Looking at the minimum and maximum values of the current survey for the whole part of Northern Greece, someone can observe that the maximum values of Cr, Mn and Ni are higher in this present study than in the previous one. But by looking specifically at the concentrations of the above elements only in the region of West Macedonia and close to the coal power plants (Agios Dimitrios and Kardia) where the samples of Tsikritzis were collected, the conclusion that may be conducted is that the concentrations in the present study are eventually lower than the previous one.

The reason for this decline (more than 30%) might be that after 2002 some regulations about the reduction of the air pollutants have been taken into account both from the lignite power plants and the lignite mining ores, thus the region from where the samples were collected might be not so affected anymore. Also the distance between the current sampling sites and the coal power plants is higher than the previous study. So, as the farther someone moves from the source, the less elemental concentrations are detected and it is reasonable in this case to have decreased elemental concentrations. Finally, the different species of mosses that were used in these two studies might play a role in the accumulation of the above elements.

In the framework of another doctoral thesis (Tsigaridas, 2014), different vegetation species, water and microorganisms were used as biomonitors of heavy metals. Samples were taken around the coal power plants of Agios Dimitrios, Kardia and Ptolemaida and in the directions of North, South and East. The highest mean values of Cr and Ni were found in the south direction of the Agios Dimitrios coal power plant ( $56.3 \mu\text{g g}^{-1}$  for Cr and  $33.4 \mu\text{g g}^{-1}$  for Ni), while the general mean values of all the directions were measured at  $95.43 \mu\text{g g}^{-1}$  for Cr and  $60.99 \mu\text{g g}^{-1}$  for Ni. Comparing the results of the current thesis with the previous data, a reduction of more than 50% can be observed.

In Northern Greece, there are no other surveys that used mosses as biomonitors for the accumulation of trace elements or radionuclides for such a large region like in the present survey. There are some studies that used lichens samples for the determination of the radionuclides concentrations or trace elements in specific only areas like the previous ones and like the surveys of Chettri et al., 1997a,b; Chettri and Sawidis, 1997; Chettri et al., 1998; Riga-Karandinos and Karandinos, 1998; Sawidis et al., 2009; Sawidis et al., 2010. Although, the data they provide cannot be compared with the current elemental concentrations due to the different kind of bioindicators that were used (different ability of accumulation and absorption of the elements) and due to the different under study areas.

### 4.3.2 Other international studies

According to Table 4.6, differences can be observed between the concentrations of trace elements in the present study in Northern Greece and the data from the other countries that participated in the 2005/2006 and 2010/2011 moss surveys (Harmens et al., 2008; 2013). More specifically, data from countries that are close to the vicinity of Greece, as well as far from Greece (either in Central or North Europe) were chosen to be compared with the data of the present study.

Greece presents lower maximum concentrations of Zn, Mn, Co than Norway, in contrast to the max elemental concentrations of Bulgaria and Switzerland. Maximum concentrations of Ni are almost in the same levels like in Bulgaria, but lower than in Norway, Poland and Albania. The Greek median value of As is similar to the Serbian one, but higher than Republic of North Macedonia and Albania. Chromium median value in Greece is higher than almost all the countries, but the maximum Cr value in Poland is 30% higher than in the Greek territory. Vanadium and Zinc are in the same levels in the Greek, Serbian and Croatian territory according to the 2005/2006 moss survey results.

On the other hand, the minimum concentrations of Ni and Zn that were measured in Greece were lower than the minimum concentrations that were detected in Belgium and Republic of North Macedonia. Moreover, Greek Cr minimum concentration is almost similar with that one that was measured in Republic of North Macedonia, in contrast to Al and Sb concentrations (which were measured 5% and 50% times higher than in Greece respectively).

An additional interesting notice about the elemental concentrations close to the Greek-Republic of North Macedonian borders is the following one. In these areas, the elements Fe, V, Zn, As, Co, Ni and Cr show lower concentrations than in the Kavadarci region (Baradonovski et al., 2008; Bačeva et al., 2012) in Republic of North Macedonia. The Kavadarci region is a region known for the ferronickel mining and other metallurgical activities. These elemental concentrations in mosses verify the correlation of the above elements with the ferronickel mining, and maybe indicate a possible transboundary transfer of elements from the Republic of North Macedonia to the Greek territory.

Another possible transboundary transfer of elements (especially of Zn) is noticeable in the region between Bulgarian and Greek borders. In Bulgaria there are active zinc mines and two big smelters in the region of Rhodope Mountains (in the cities of Kardzhali, Madan, Madjarovo and Ada Tepe). These regions are known for the non-ferrous metallurgy and specialize in the production of Pb and Zn. The open way of ore mining, combined with the former mines and the ongoing mines are directly connected with the high concentrations of Pb and Zn concentrations in Bulgaria but also in Greek sites. Thus, they are possible indicators of the transboundary transfer of zinc particles through the air to the Greek territory (Yurukova, 2007; Harmens et al., 2008; Thöni et al., 2011; Tsirampides and Filippidis, 2016).

Except of the previous comparisons including mosses collected directly from nature, comparisons might be performed with the results of other surveys where moss bags were used as biomonitors. In different countries like, in Italy, Romania, Russia, Serbia

several studies specializing in moss bags technique, have been performed through the last decade (Culicov et al., 2005; Aničić et al, 2007; Aničić et al, 2009b, Giordano et al., 2009; 2013; Lazić et al., 2016, Goryainova et al., 2016; Capozzi et al., 2016a,b; Aničić et al, 2017; Di Palma et al., 2017).

For instance, moss bags were placed in the city of Naples, in Italy and they were exposed for at least 6 weeks. The conclusions that were derived were that even during their min exposure, all the elemental concentrations were elevated more than 30% than before the placement of the moss bags (Giordano et al., 2009).

Finally, another survey, where moss bags were used was conducted in Belgrade (Aničić et al, 2009a). The concentrations of the elements As, Al, Ni, V, and Zn of the current survey are at least 20% lower than the corresponding concentrations measured in the moss bags in Belgrade.

**Table 4.6** The concentrations of seven trace elements (As, Cr, Fe, Ni, V, Zn, Al) in moss samples (mg kg<sup>1</sup>) from the current survey and from other European countries derived from the 2005/2006 and 2010/2011 moss survey.

<b>As</b> Median ( <i>min-max</i> )	<b>Cr</b> Median ( <i>min-max</i> )	<b>Fe</b> Median ( <i>min-max</i> )	<b>Ni</b> Median ( <i>min-max</i> )	<b>V</b> Median ( <i>min-max</i> )	<b>Zn</b> Median ( <i>min-max</i> )	<b>Al</b> Median ( <i>min-max</i> )	<b>Sb</b> Median ( <i>min-max</i> )	
1.44 (0.52-17.9)	11.5 (2.04-222)	3770 (1010-28700)	7.26 (1.72-90.2)	8.17 (2.61-33.4)	37.6 (14.6-282)	5840 (1350-46100)	0.20 (0.02-3.23)	<b>Current study</b>
- -	2.43 (0.79-57.8)	1399 (186-9493)	2.99 (0.92-90)	3.88 (0.77-24.3)	27.9 (9.38-366)	1495 (426-10394)	- -	<b>Bulgaria, 2005</b> (Thöni et al., 2011)
0.63 (0.15-10.8)	2.06 (0.72-38.1)	1101 (307-8546)	2.61 (0.84-82.1)	3.07 (0.96-22.4)	22.2 (8.22-286)	1245 (402-8886)	- -	<b>Bulgaria, 2010</b> (Harmens et al., 2013)
0.68 (0.18-4.32)	6.79 (2.09-82)	2239 (999-8130)	5.82 (1.8-43.1)	6.38 (2.5-31.9)	35.6 (16.4-91.3)	3600 (1466-25860)	0.15 (0.044-0.92)	<b>F.Y.R. Macedonia, 2005</b> (Barandovski et al., 2012)
0.48 (0.23-1.9)	6.46 (2.46-35)	1900 (890-5400)	4.3 (1-55)	3.8 (1.5-14)	29 (13-94)	2400 (1100-6800)	- -	<b>F.Y.R. Macedonia, 2010</b> (Baradonovski et al., 2015)
0.12 (0.004-4.61)	0.58 (0.099-65.5)	273 (50.4-9972)	1.24 (0.055-1016)	1.40 (0.25-22.1)	31.4 (8.04-694)	255 (58.3-12121)	0.070 (0.015-0.94)	<b>Norway, 2005</b> (Steinnes et al., 2007)
0.13 (0.02-4.84)	0.59 (0.16-47.9)	278 (27-24684)	1.16 (0.15-857)	1.41 (0.29-25.9)	30.7 (7.4-368)	283 (46-4581)	- -	<b>Norway, 2010</b> (Steinnes et al., 2011)
1.41 (0.22-21.6)	6.44 (2-78.8)	2267 (670-16100)	4.43 (1.7-23.8)	5.76 (1.94-32.7)	29.0 (13.2-259)	3946 (117-31180)	0.24 (0.059-1.37)	<b>Serbia, 2005</b> (Frontasyeva et al., 2004)
0.305 (0.05-2.86)	4.75 (1.62-31.8)	1618 (469-5488)	5.85 (1.56-131)	3.51 (1.15-16.9)	13.8 (1-68.1)	1638 (535-6974)	- -	<b>Albania, 2010</b> (Qari et al., 2014; Bekteshi et al., 2015)
0.37 (0.1-6)	2.8 (0.76-33)	1000 (320-12140)	2.7 (0.66-18)	3.1 (0.91-32)	29 (12-283)	1350 (398-21460)	0.15 (0.046-1.39)	<b>Croatia, 2005</b> (Špirić et al., 2012)
0.36 (0.05-1)	1.94 (0.41-8.55)	789 (85-4028)	3.16 (1.04-14.66)	2.55 (0.23-37.3)	24.8 (11.6-77.1)	878 (112-4493)	- -	<b>Croatia, 2010</b> (Špirić et al., 2013)
0.15 (0.053-1.07)	1.2 (0.33-7.96)	261 (95.4-2380)	1.59 (0.5-7.77)	0.67 (0.21-3.55)	31.4 (10.1-179)	- -	- -	<b>Switzerland, 2005</b> (Thöni et al., 2011)

0.22 (0.065-1.78)	1.0 (1.62-31.8)	320 (97-2800)	1.0 (0.31-4.50)	1.30 (0.34-17.0)	24 (13-81)	347 (81.9-3024)	0.16 (0.04-1.60)	<b>Austria, 2010</b> (Harmens et al., 2013)
0.12 (0.006-0.34)	3.21 (0.66-5.23)	416 (194-1030)	0.23 (0.086-1.21)	1.19 (0.59-1.68)	34.1 (21.5-94.7)	557 (267-1650)	0.096 (0.026-0.34)	<b>Belarus, 2010</b> (Harmens et al., 2013)
0.15 (0.052-0.49)	1.20 (0.18-11.60)	394 (167-2243)	1.25 (0.55-5.65)	1.33 (0.40-9.57)	31.3 (17.6-65.1)	758 (194-9200)	0.11 (0.039-0.23)	<b>Belarus, 2005</b> (Harmens et al., 2008)
0.16 (0.052-0.89)	0.92 (0.54-3.89)	365 (171-1109)	1.41 (0.72-22.7)	1.14 (0.41-2.76)	44.2 (16.6-132)	242 (114-696)	- -	<b>Belgium, 2010</b> (Harmens et al., 2013)
0.68 (0.21-2.34)	4.47 (1.44-18.5)	967 (290-4172)	3.97 (2.04-7.23)	4.52 (2.31-15.30)	77.4 (35.1-151)	- -	- -	<b>Belgium, 2005</b> (Harmens et al., 2008)
0.26 (0.068-1.08)	1.01 (0.46-4.35)	348 (150-2072)	1.15 (0.37-4.47)	1.18 (0.44-6.10)	33.9 (20.1-105)	435 (184-3227)	0.096 (0.001-0.82)	<b>Czech Rep., 2010</b> (Harmens et al., 2013)
0.29 (0.10-1.82)	1.15 (0.51-4.54)	409 (187-2570)	1.42 (0.52-4.94)	1.47 (0.68-7.18)	33.3 (20.9-98.8)	477 (208-2862)	0.16 (0.041-1.73)	<b>Czech Rep., 2005</b> (Harmens et al., 2008)
- -	0.68 (0.36-2.40)	180 (93-617)	0.82 (0.43-2.10)	1.07 (1.05-2.85)	30.9 (19.3-55.6)	188 (79-492)	- -	<b>Estonia, 2010</b> (Harmens et al., 2013)
0.10 (<0.1-0.38)	0.80 (0.34-14)	209 (53-2230)	1.24 (0.42-88.2)	1.00 (<1-14.2)	29.5 (11.5-102)	187 (44-958)		<b>Finland, 2010</b> (Harmens et al., 2013)
0.18 (<0.05-2.46)	1.43 (0.52-5.91)	343 (86-3540)	1.75 (0.55-10.2)	1.24 (0.42-6.35)	30.7 (14.1-97.3)	286 (62-2020)	0.11 (0.03-0.58)	<b>France, 2010</b> (Harmens et al., 2013)
0.22 (0.14-0.95)	1.59 (0.78-3.37)	431 (232-646)	1.69 (0.89-3.36)	1.37 (0.91-1.90)	37.1 (17.7-68.4)	- -	- -	<b>Italy, 2010</b> (Harmens et al., 2013)
0.29 (0.086-2.69)	1.46 (0.43-4.77)	520 (171-1449)	1.44 (0.58-3.94)	1.21 (0.55-4.2)	31.5 (12.7-156)	511 (173-1459)	0.069 (0.04-0.15)	<b>Spain, 2010</b> (Harmens et al., 2013)
0.26 (0.13-0.83)	1.56 (0.72-13.7)	548 (243-1391)	2.12 (0.85-8.16)	2.30 (1.0-7.0)	29.0 (14.7-66.7)	- -	0.12 (0.06-0.76)	<b>Slovenia, 2010</b> (Harmens et al., 2013)
- -	1.27 (0.2-293)	344 (110-2618)	1.15 (0.14-108)	0.65 (0.11-4.69)	47.5 (7.46-211)	- -	- -	<b>Poland, 2010</b> (Harmens et al., 2013)



characterized as a variant of Factor Analysis with no-negative factor elements, as it does not implement any negative constraints (hence the use of the term “positive” can be explained) and only physically valid results are obtained (Vaccaro et al., 2007).

The fundamental principle of the PMF model is that a mass conservation between the emission source and the study site can be assumed and a mass balance analysis can be used to identify and apportion the sources of the atmospheric pollutants (Belis et al., 2014; Olivier et al., 2019). So, the identification of the sources is performed through the mass balance equation (equation 4.1).

$$c_{ij} = \sum_{k=1}^p g_{ik} * f_{kj} + e_{ij} \quad (4.1)$$

where

$c_{ij}$  is the concentration of a chemical species  $j$  measured during a time period in the sample that can be expressed as the sum of the contributions of its different emission sources. It is a matrix having a dimension of  $n$  rows and  $m$  columns, where  $n$  and  $m$  are the number of samples and species.

$p$  is the number of factors (sources) that contribute to the samples

$g_{ik}$  is the relative contribution of the source  $k$  to the  $i$  sample

$f_{kj}$  is the concentration of the  $j$  species in the  $k$  source (the mass fraction of species  $j$  in the chemical profile of source  $k$ )

$e_{ij}$  is the residual (the difference between the measured and the fitted value)- actually it is the error of the PMF model for the  $j$  species measured on the  $i$  sample

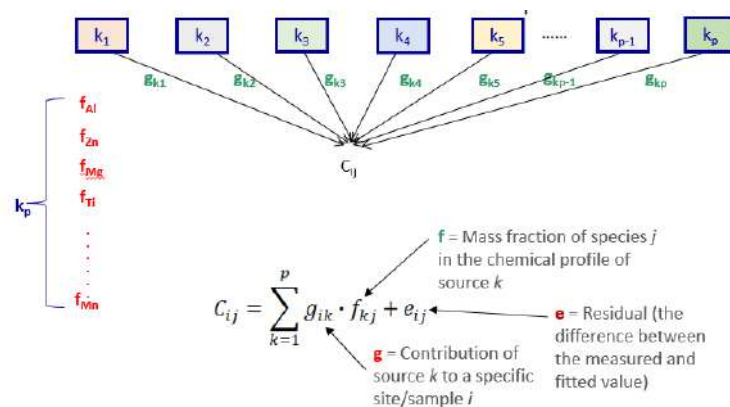


**Figure 4.39** The schematic representation of the mass balance equation for the identification of the sources. Source “ $k$ ” contribute by “ $g$ ” to the final concentration. Each source “ $k$ ” has a specific fraction “ $f$ ” of a chemical species.

In other words, the concentration  $c_{ij}$  of a chemical species  $j$  that was measured during a time period in an  $i$  sample can be expressed as the sum of the contributions of its

different emission sources (Manousakas et al., 2017a; Olivier et al., 2019). More specifically, each source  $k$  is constituted of different chemical species, in different fractions (e.g.  $f_{Al}$ ,  $f_{Zn}$ ,  $f_{Mg}$ , etc). When a chemical species is detected in an  $i$  sample, this means that each source contributes to the concentration of the specific species a  $g_{ik}$  factor (Figure 4.39). So, by summing up all the contributions of the sources for the specific chemical species  $g_{ik}$ , multiplying them with the concentrations of the species in each source  $f_{kj}$  and taking into account the residual, the concentration of this specific element comes up.

The source types can be identified by comparing them to already measured profiles. No data on specific emission compositions are required. Each source contributes to each sample in a specific proportion. This relative contribution is given by the  $g_{ik}$  value as already mentioned.

In order to find the sources, a dataset with a large amount of data (elemental concentrations) gathered from a number of samples is required. The larger the data matrix, the higher the chances that the model will identify distinct factors that can be identified as sources (Raman et al., 2010; Olivier et al., 2019). In the data matrix, except of the observed values (concentrations), the uncertainties of each individual concentration are also included.

In addition, the PMF model takes into account the errors of the data points, by using them as point-by-point weights in order to obtain the most physically explainable factors (Comero et al., 2009; Dutton et al., 2010; Manousakas et al., 2017b). It also permits individual weighting, which increases the model's ability to handle outliers, missing values, and below detection limit values (Lu et al., 2008).

The most important feature of the PMF model is that the number of factors or sources is chosen initially, before it runs. The choice of factors- sources is always a compromise as the PMF model is a descriptive model and there is no objective criterion to choose the ideal solution. If only few factors are used in the model, the sources which have different nature might be combined together, whereas if too many factors are used, there is a possibility of a real factor to be separated into two or more unreal sources (Manousakas et al., 2015).

After the model runs, two products- matrices are obtained. One that gives the contribution of each of the source factors to each measurement and another one that gives the contribution of each independent measurement (elemental concentration) to each of the sources.

The aim is to find the appropriate  $g_{ik}$ ,  $f_{kj}$  and  $p$  values that best reproduce the  $c_{ij}$  concentration. For the achievement of this goal different tools are used. First of all, the values of  $g_{ik}$  and  $f_{kj}$  are adjusted until a minimum value of  $Q$  for a given  $p$ -factor is found.  $Q$  value is defined as follows (equation 4.2):

$$Q = \sum_{j=1}^m \sum_{i=1}^n \frac{e_{ij}^2}{s_{ij}^2} \quad (4.2)$$

where

$s_{ij}$  is the uncertainty of the  $j$  species concentration in the sample  $i$

$n$  is the number of samples

$m$  is the number of species

$e_{ij}$  is the residual (the difference between the measured and the fitted value) (Manousakas et al., 2017a)

Usually, different  $Q$  values for different solutions resulting from a range of  $p$  number of sources are examined. If  $p$  approximates the number of underlying factors in the data, then  $Q$  should be approximately equal to the number of data points in the matrix. If this solution lacks physical validity, then other solutions are examined until the most physically valid solution is found (Manousakas et al., 2015).

Except of the  $Q$  value interpretation for the choice of the best solution, there is the problem of the rotation of the matrices. This rotational ambiguity of matrices is solved through the Fpeak tool of the model. The Fpeak tool investigates the possibility that the solution is a rotation. The uniqueness of the solution is examined through the parameter “Fpeak”, assigning both positive and negative values. Positive Fpeak values mainly impact the factor profiles and negative values impact the factor contributions (Manousakas et al., 2017a).

Finally, in the choice of the most appropriate solution the GPlots are involved. GPlots of the sources are the plots of the contributions of each source  $g_{ik}$  against one another, and they are an additional measure to determine the existence of rotations. The G space plots illustrates the so-called edges, such as the well-defined straight borders between regions densely occupied by points and regions where no points occur. If there are unrealistic rotations in the solution, then some of the edges are oblique. The oblique edges may act as an indication that the rotations should be modified (Manousakas et al., 2015).

#### 4.4.2 PMF Analysis Results

In the current study, the Positive Matrix Factorization (PMF) analysis was performed by means of the PMF 5.0 model (the newest version of USEPAPMF model). The number of the samples that were included in the dataset used for the PMF source apportionment were 105. The number of the chemical species that were inserted in the model were 30 (Na, Mg, Al, Si, Cl, K, Ca, Cd, Ti, V, Cr, Mn, Fe, Co, Ni, As, Br, Rb, Sr, Mo, Sc, Sb, Cs, Ba, La, Ce, Tb, Hf, Ta and Th).

Based on the Signal-to-Noise ratio (S/N), for each chemical species over all samples, some species were defined as “weak” species such as Mg, Al, Cd, Th, while some others species were defined as the strong ones such as Na, Si, Cl, K, Ca, Sc, Ti, V, Cr, Mn, Fe, Co, Ni, As, Br, Rb, Sr, Mo, Sb, Cs, Ba, La, Ce, Tb, Hf, Ta. The weak species (when S/N ratio is between 0.2 and 2) were not fit well by the model, giving higher uncertainty-3 times their original one, while their impact on the final PMF solution was extremely low (Diapouli et al., 2017). The rest of the chemical species that were

detected in mosses and whose S/N ratio was lower than 0.2 were excluded from the analysis.

The uncertainties of the concentrations of all chemical species were calculated based on the sampling and analytical uncertainties and depending on the method of analysis. The PMF5 model was run on the robust mode, where the uncertainties were dynamically readjusted through an iterative reweighting. The robust mode was used to reduce the influence of extreme points (defined as these point that exceed four times the error estimate in the process of model irritations) by suitably down-weighting them. For example, a measured concentration value was processed as an outlier if the residual exceeded 4 times the data point uncertainty. In that case the uncertainty was increased in order to decrease the influence of this data point (Diapouli et al., 2017). Extra modelling uncertainty was put in the model to account for modelling errors. It was typically set at 10%.

In order to determine the number of factors, the model run 100 times for each possible number of sources. The model run multiple times in order to ensure that the solution which was achieved was based on a universal minimum and not a local minimum. The minimum referred to the fact that the aim of the PMF model was the minimization of the residual. So only the solution with the minimum residuals would be accepted.

Solutions with different number of factors (ranging from 4 to 10) were examined. The basic criteria for choosing the best solution of the model were the distributions of the residuals, the G-space plots and the Q values. Additionally, the rotational ambiguity of the solutions was assessed through the use of different Fpeak values, which ranged between -1.0 to 1.5.

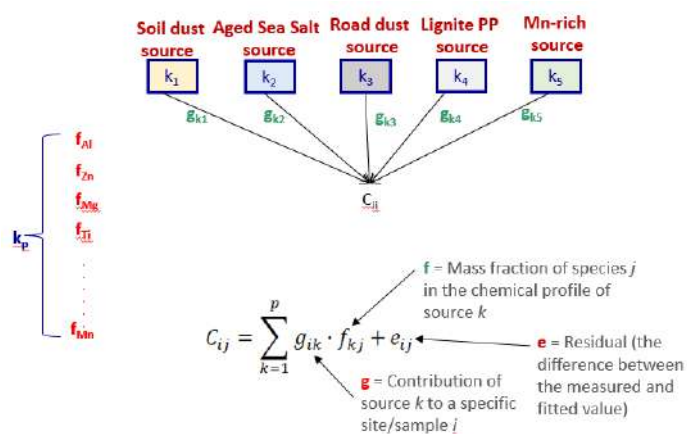


**Figure 4.40.** The schematic representation of the contribution of the five factors in each chemical species measured in mosses.

After taking into account all the above criteria, the model resolved five factors presenting a physical meaning. The uniqueness of this solution was also verified by the Fpeak value, which was equal to -0.5. Only in this case the minimum correlation between the contributions of the different sources was performed. Thus, this solution

included the following five sources: *The Soil Dust, the Aged Sea Salt, the Road Dust, the Lignite Power Plant and the Mn-rich source* (Figure 4.40).

The source profiles obtained for Northern Greece, as well as the species' relative mass (%) apportioned to each factor/source are presented simultaneously in Figures 4.41.-4.45. In each of these figures, the blue bars, which correspond to the left axis, represent the concentrations as mass fractions of  $\left(\frac{\mu\text{g of the specific chemical species}}{\text{total } \mu\text{g of the source}}\right)$ . The red dots, which correspond to the right axis, represent the percentage of each species' mass that is assigned to this source. In other words, the identification of each source is also based on the percentage of the species' mass assigned to each source (red dots).

The first source profile is attributed to soil dust (Figure 4.41). Mainly elements that are abundant in the Earth's crust and soil (crustal components) contribute to this source, such as the elements Mg, Al, Ti, Si, Ca, Th, Ba, La, K and Fe. More than 40% of the mass of Si, Ca, Cl, K, and Mg is assigned to the Soil dust source. All these elements were transferred to mosses through the resuspension of the soil from fields by local winds. It should be mentioned that the dry climate of Greece favors the soil resuspension even in long distances (Manousakas et al., 2017b). Although, the mass fractions of the crust components (blue bars) are high in all the source profiles figures. This happens due to the fact that these elements contribute a lot to the total elemental concentrations that were measured in moss samples.

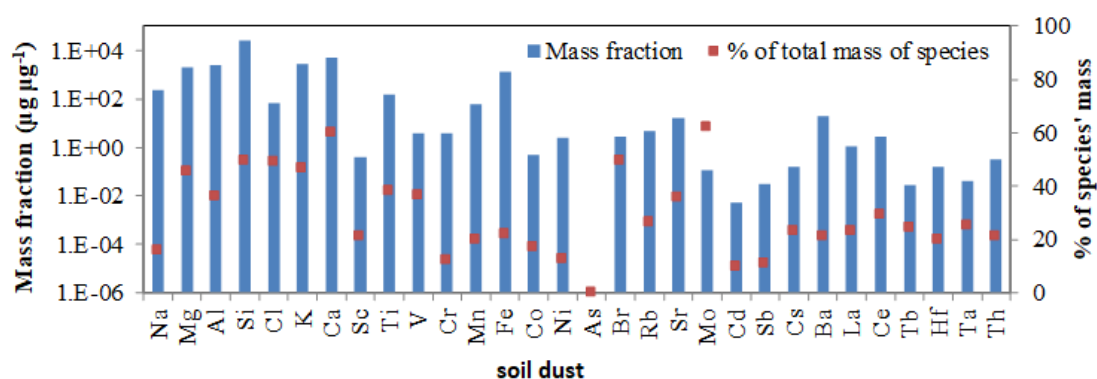


**Figure 4.41.** The chemical profile of the soil dust source.

The Aged sea salt factor is presented in Figure 4.42. It is represented by the elements Na, Rb, Sr, Hf and Ta. Sodium is the element that contributes the most in this source. Chlorine is present in the factor but in much lower concentration than expected for sea salt by stoichiometry. That is an indicator of the depletion of Cl. This Cl depletion in the factor points out that the sea salt cannot be characterized as fresh but rather as aged. The ratio Cl/Na is much lower than 1.8 which is the value of the fresh sea salt. Fresh sea salt is mainly found on fresh particles and has no seasonal trend (Eleftheriadis et al., 2014; Manousakas et al., 2017b). In this case, the sea salt particles that were deposited in mosses are not fresh and probably they had previously interacted with other chemical species such as crustal minerals and other urban pollutants (Diapouli et al., 2017).

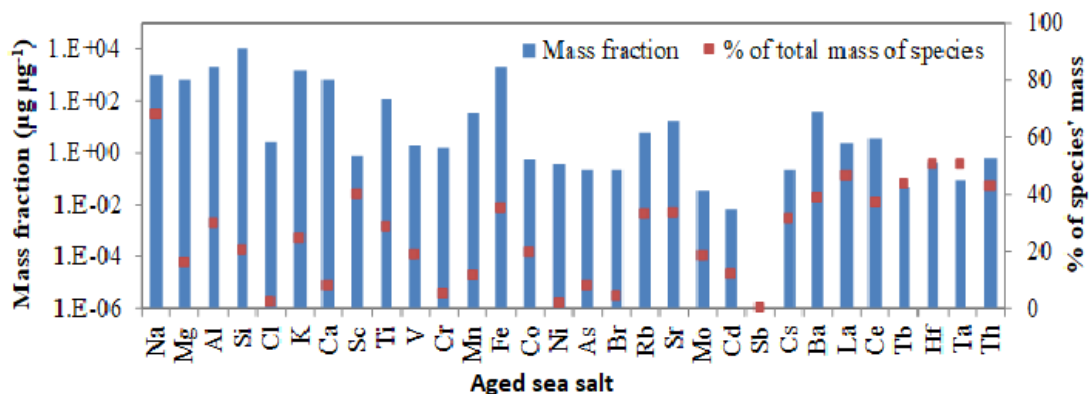


Figure 4.42. The chemical profile of the Aged sea salt source.

The third factor contains high loadings of Sb and As. It could be characterized as the dispersed Road dust (Figure 4.43). This source is related to vehicular traffic and can be identified by common traffic tracers such as Sb and Fe. More than 70% of the mass of Sb is assigned to the dust from the traffic network. It should be mentioned that most of the times, the atmospheric Sb's main source are the brake pads in cars, so it is connected with the dispersed road dust (Harmens et al., 2008).

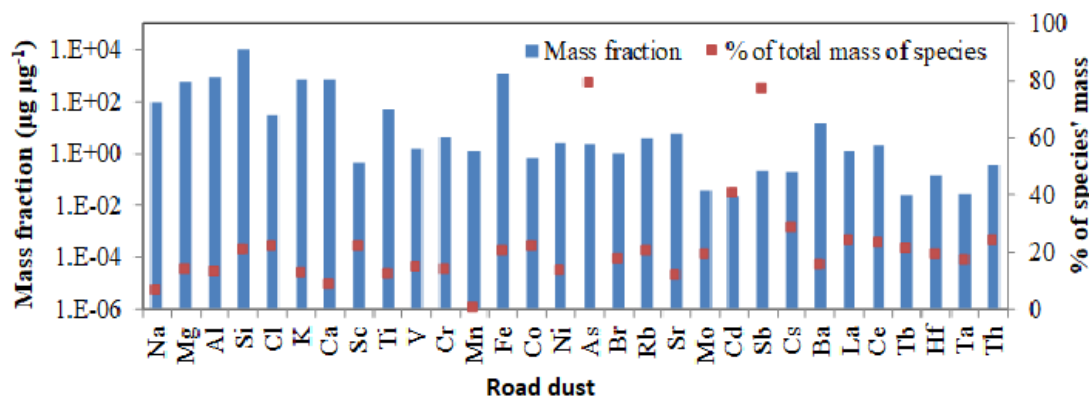


Figure 4.43. The chemical profile of the Road dust source.

The fourth factor is identified as the Lignite power plant source (Figure 4.44). There is high contribution of Ni, Cr and Co. More than 60% of the masses of Ni and Cr are assigned to the Lignite power plant factor. This factor could also be related to heavy oil combustion emissions. Ni is a good tracer of this source as well. Heavy duty vehicles used in the mining processes of the lignite power plants and for the lignite transfer are highly likely to contribute to this source by enhancing the dust resuspension.

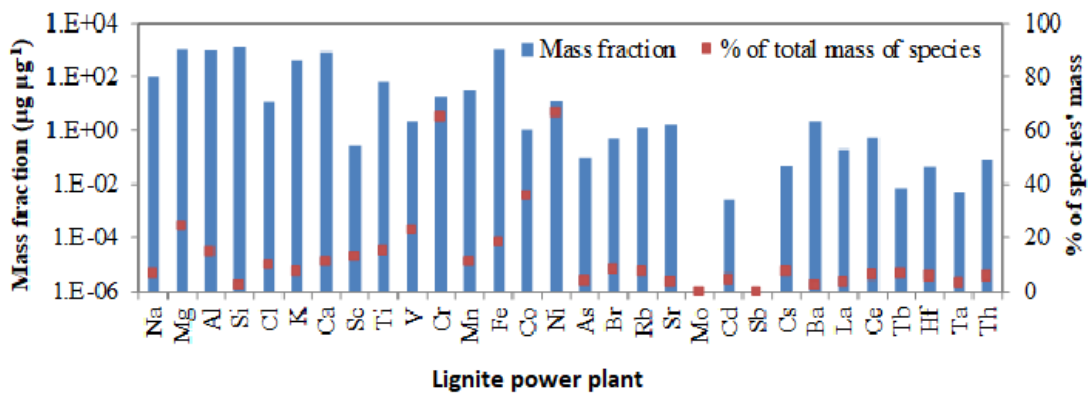


Figure 4.44. The chemical profile of the Lignite power plant.

In addition, Cr originates among other sources from fossil fuel burning. Vanadium and Magnesium are also present in this factor but in lower concentrations. Both of them are usually included in the fly ash produced by the burning process. The fly ash might escape the filters of the power plants and thus is emitted in the air (Diapouli et al., 2017). Cobalt is also connected with the heavy oil combustion source and has similar behavior like Ni element. High contribution of this source is found in samples named b-01 to b-10, which were collected from areas close to mining activities. Additionally, it is linked with the prefecture of Western Macedonia, where the complex of the lignite power plant Ptolemaida-Amyntaio is located,

The last factor that was produced by the model, is characterized as the Mn-rich source. It is not an artifact of the program. It is possibly connected with mining activities. Around 60% of the mass of Mn is correlated to this source according to the chemical profile in Figure 4.45. This source is strongly associated with the samples named as b-01 to b-10 which were collected from areas close to mining activities in Chalkidiki.

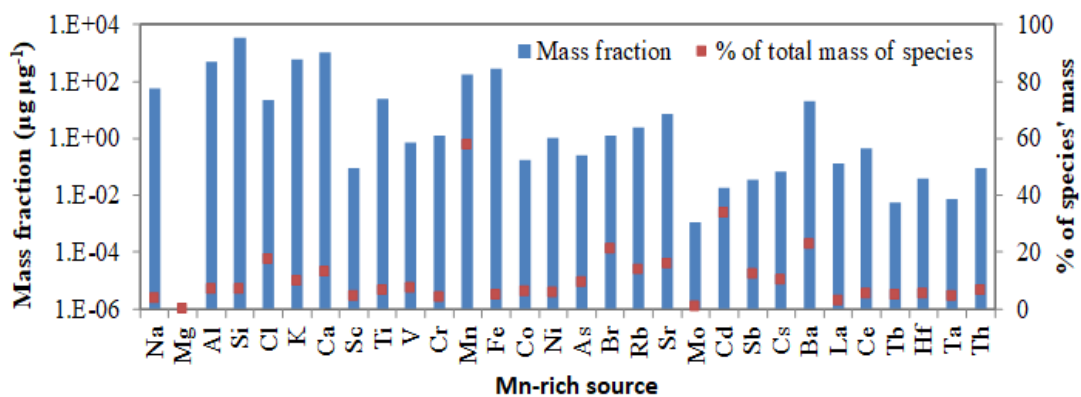
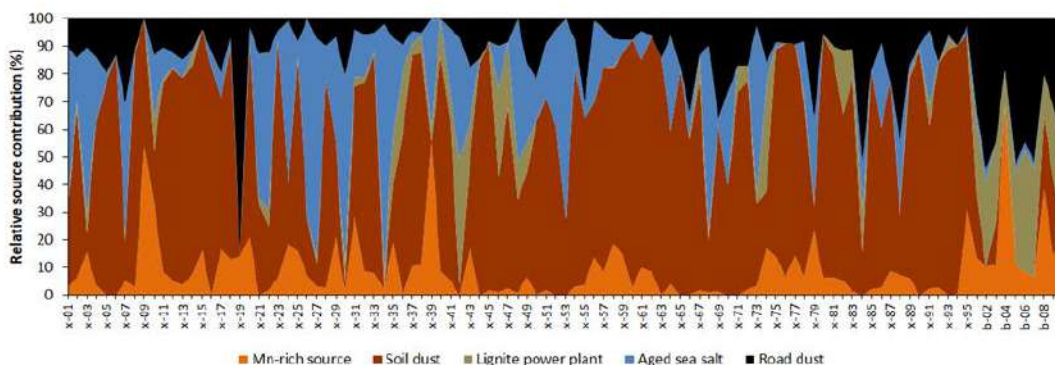


Figure 4.45. The chemical profile of the Mn-rich source.

Except of the chemical profiles of each source, it is useful to display how much each source contributes to each moss sample. In Figure 4.46 the relative source contributions for each sample are presented. The soil dust and the sea salt sources contribute more than 60% to many of the moss samples. Similar relative contributions of the road dust source occur to almost all mosses.



**Figure 4.46.** The relative source contribution for each sampling site.

Two regions can be distinguished according to Figure 4.46. The first one is the Region of Western Macedonia (sites x-30 to x-42). It is an area characterized mostly by the Lignite power plant factor. In this region, as already mentioned, the Ptolemaida-Amyntaio complex Lignite power plants are located. In these mosses, the elements Ni, V, Cr and Co were found in high concentrations and could be directly linked with the Lignite power plant source (Lignite mining and burning in the power plants).

The second area that is distinguished is the one with ID b-01 to b-10. This area corresponds to the area of Skouries (described in Section 4.2) which is characterized by the mining activities. In this area there are high contributions of the Mn-rich source, the lignite power plant source as well as the road dust source. These sources contain the elements Mn, Ni, V, Co, Sb and Cr which were found in elevated concentrations, and could be linked directly to the mining procedure and the dust that is dispersed in the surroundings through the traffic network. These contributions can also be seen from the diagram with the average source contributions (Figure 4.47). The road dust source along with the Mn-rich and Lignite power plant sources are the ones that contribute the most in the elemental concentrations of the Skouries samples.

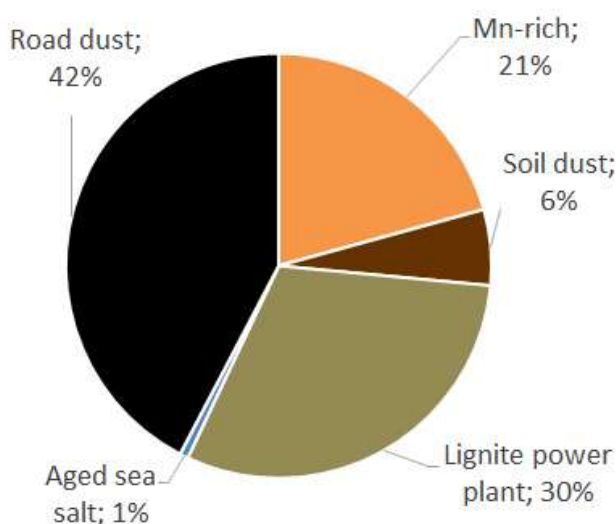


**Figure 4.47.** The average source contribution for the region of Skouries. The Road dust along with the Lignite power plant and the Mn-rich sources have the biggest influence in the elemental concentrations.

Except of the average source contribution for the Skouries area, the average contribution of sources for the whole vicinity of Greece is displayed in Figure 4.48. According to this diagram, the soil dust source contributes the most in mosses (52%), with the Aged sea salt and the road dust being the next ones that influence the elemental concentrations in mosses. It should be mentioned that one of the main reasons that could explain the high contribution of the soil dust source in Northern Greece, is the dry climate of Greece. The arid climates, favor the resuspension of the dust and in combination with the aid of the local winds, the soil particles can easily travel in even further distances, increasing the different elemental concentrations in mosses.

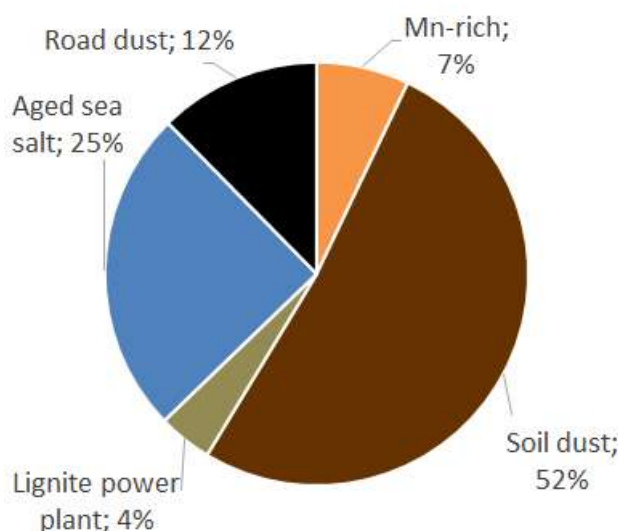


**Figure 4.48.** The average source contribution for Northern Greece. The soil dust source is the most prominent enrichment source of elements in mosses.

In conclusion, after applying the PMF model in the elemental concentrations of mosses, five factors were identified: The Soil dust source, the Aged sea salt, the Road dust source, the Lignite power plant source and finally the Mn-rich source. Among them, the soil dust source is the one that has the highest contribution in all the moss samples of Northern Greece. Therefore, the majority of the elements are deposited on mosses through the resuspended soil.

## 4.5 Trace elements concentrations in soil

### 4.5.1 Distribution of elements in soil samples

Ninety-five surface soil samples were collected from the same sampling sites where moss samples were collected from. Soil samples were prepared appropriately and they were measured through XRF analysis technique. The concentrations of 19 elements were determined and are presented with details in Tables E1 and E2 in the Appendix E. The descriptive analysis (mean, median, min, max, standard deviation, kurtosis and skewness) of the above elemental concentrations in soil samples was also performed and is presented in Tables 4.7 and 4.8. The elemental distributions of As, Cr, Fe, Mg,

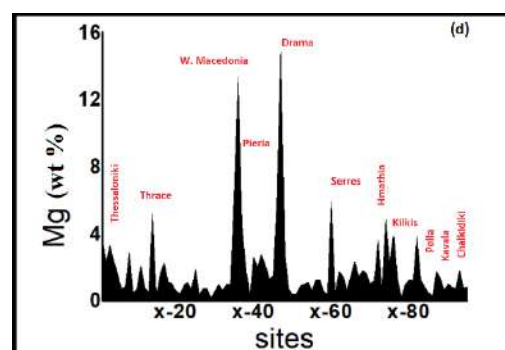
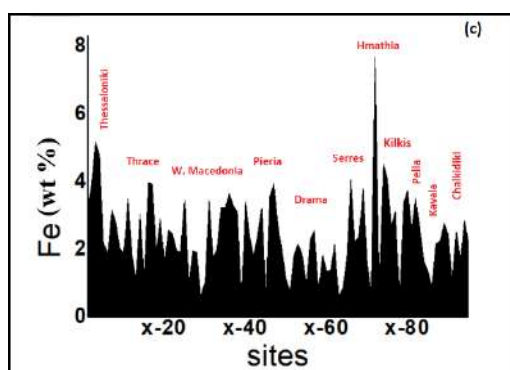
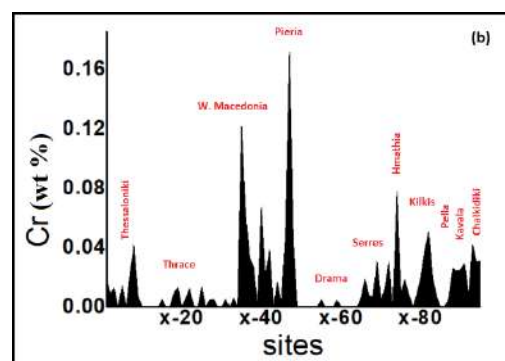
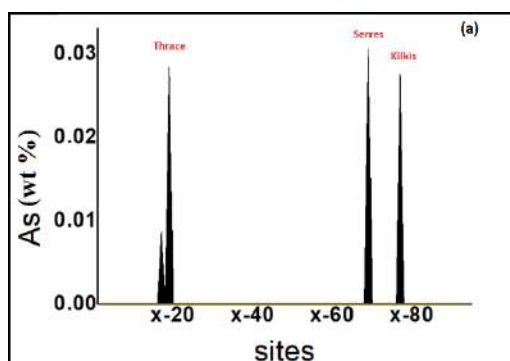
Mn and Ni (the most frequently studied elements) are presented in Figures 4.49 (a)- (f) while the distributions of the rest 13 elements are presented in Appendix E.

**Table 4.7.** The descriptive analysis of the first 10 elements that were measured in soil samples using the XRF analysis technique. The concentrations are given in wt %.

	Si	Al	Fe	Ca	Mg	Na	Ti	K	Mn	Sr
Mean	24.12	4.53	2.40	4.84	1.88	0.51	0.47	1.16	0.12	0.03
Median	24.67	4.70	2.21	1.86	1.15	0.46	0.46	1.11	0.11	0.01
Min	5.53	0.97	0.59	0.13	0.23	0.03	0.11	0.21	0.01	0.00
Max	34.86	8.45	7.70	50.30	14.91	1.51	1.00	2.85	0.65	0.10
Range	0.61	0.13	0.12	0.88	0.23	0.04	0.02	0.05	0.01	0.002
St.Dev.	29.32	7.47	7.10	50.17	14.68	1.48	0.89	2.64	0.64	0.10
Kurt.	5.94	1.28	1.20	8.58	2.25	0.36	0.19	0.53	0.09	0.02
Skew.	1.03	0.70	2.87	13.73	17.84	0.02	0.09	0.23	15.86	4.32

**Table 4.8.** The descriptive analysis of the rest 9 elements that were measured in soil samples using the XRF analysis technique. The concentrations are given in wt %.

	S	Cr	Zr	Zn	Ni	Cu	As	Cl	Co
Mean	0.05	0.02	0.02	0.01	0.01	0.003	0.001	0.002	0.001
Median	0.03	0.01	0.02	0.01	0.00	0.000	0.000	0.000	0.000
Min	0.00	0.00	0.00	0.00	0.00	0.000	0.000	0.000	0.000
Max	0.34	0.17	0.05	0.03	0.20	0.041	0.031	0.104	0.011
Range	0.01	0.002	0.001	0.001	0.003	0.001	0.001	0.001	0.0002
St.Dev.	0.34	0.17	0.05	0.03	0.20	0.041	0.031	0.104	0.011
Kurt.	0.06	0.03	0.01	0.01	0.03	0.006	0.005	0.013	0.002
Skew.	10.37	16.02	1.37	1.14	15.18	18.55	26.663	47.664	6.397



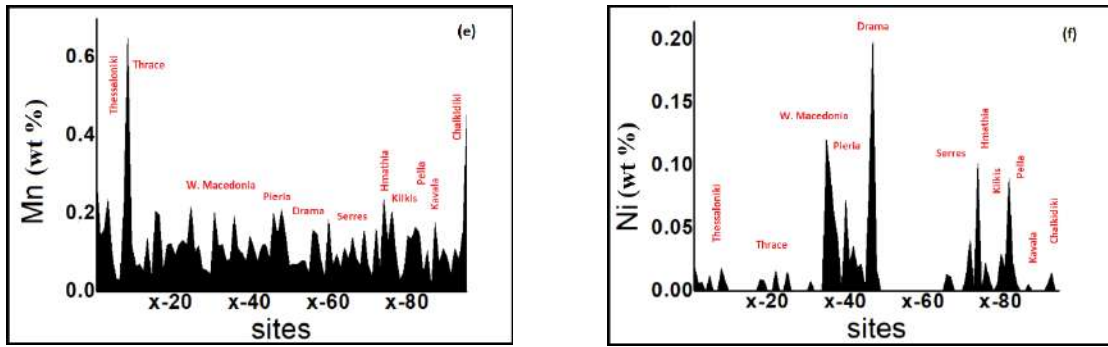


**Figure 4.49 (a) - (f).** The distributions of the elements As, Cr, Fe, Mg, Mn and Ni in soil samples collected from Northern Greece.

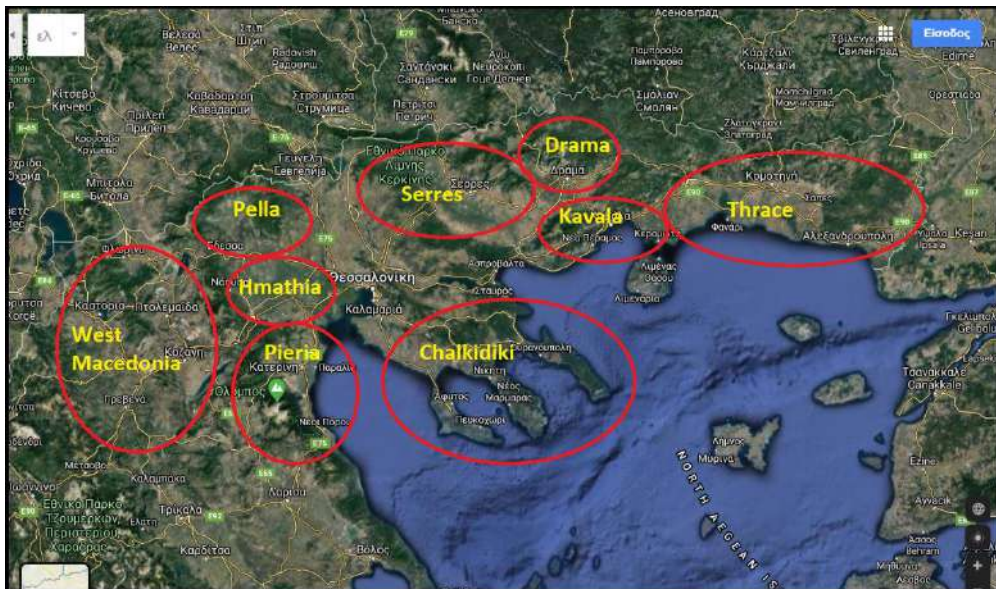


**Figure 4.50.** The areas of Northern Greece from where soil samples were collected. The names of the regions in which some elements were found in high concentrations are presented in the red circles.

According to the distribution diagrams (Figure E in Appendix), the elements Al, K, Si and Ti have similar concentrations in almost all sites, proving that there is no impact of anthropogenic activities on them and the majority are just typical components of the soil.

On the other hand, the concentrations of some elements (Cr, As, Cl, Mn, Zn, Ni, Mg) in soil samples do not present any homogeneity, but they vary across Northern Greece (Figure 4.50), indicating that these elements are not exclusive constituents of the soil but they might be connected with some other anthropogenic sources (e.g. lignite power plants, transportation, mining activities, fuel burning, industrial activities.).

For instance, some samples from the Region of Thrace present high concentrations of As, Cl and Mn, while some other sites in the Region of West Macedonia have elevated concentrations of Cl, Cr, Mg and Ni. The area of Serres in the Region of Central

Macedonia include some samples with elevated concentrations of As, Ca, Cl, S and Zn elements. Pieria and Hmathia are two other areas of Northern Greece which include samples characterized by higher levels of Ca, Cl, Co, Cr, Fe, Ni, S than the rest ones, whereas in Chalkidiki the levels of Mn in some sites are also elevated.

The first step for the identification of the origins of these elements is to normalize their concentrations to the concentrations of Al. The normalization to the Al concentrations was chosen based on the fact that Al, as a component of the Earth’s crust, can be used as a marker of the soil source (Bargagli et al., 1995a,b; Sardans & Peñuelas., 2005). Then, comparing the normalized elemental concentrations of the samples with the chemical composition of a reference soil sample (in this case the “Mason-Zucc” soil is used), the elements that are associated to the soil can be distinguished. The profile of this soil reference material describes a general soil composition, not a specific Greek soil composition, that’s why there is not a total match between them.

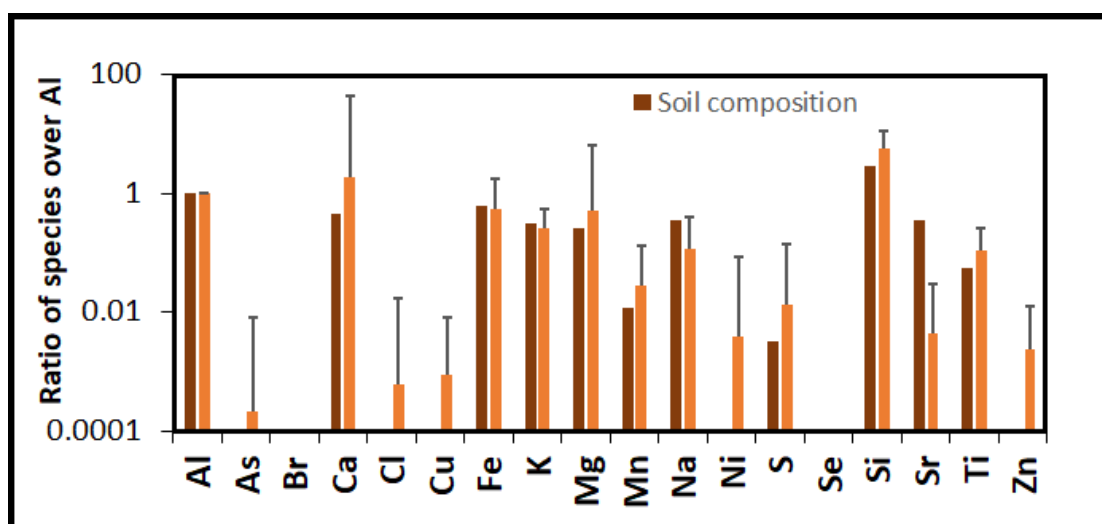


**Figure 4.51.** The diagram where the mean ratios of the different elements over Al are presented both for the current study’s samples and the reference soil sample “Mason- Zucc”.

According to Figure 4.51, in most of the cases, the chemical composition of the soil samples is similar to the reference’s chemical composition, indicating that the role of anthropogenic activities is not so big in the majority of them. Although, there are some samples in which particular elements (As, Cu, Ni, Zn and Cl), are measured in high concentrations and might be connected with “anthropogenic factors”. In addition, attention should be given to the concentrations of the elements Fe, Mn and Mg, which are in some cases higher than the majority of the samples. In order to have a clearer view and recognize the possible anthropogenic sources of the aforementioned elements, the elemental concentrations in soil are compared with the corresponding concentrations in mosses.

#### 4.5.2 Comparison of the elemental concentrations in soil and moss samples

The elemental concentrations in soil samples are compared with the elemental concentrations in the corresponding moss samples. Taking into advantage the source apportionment results of mosses, the origin of the elements As, Ni, Zn, Cl, Cr, Fe, Mg and Mn in soil samples can be estimated.

To begin with, comparing the distributions of Ni in mosses and soil, there is a match between the sites where the concentrations of Ni are high. The source of Ni in mosses according to the source apportionment analysis are the heavy combustion oil and the Lignite Power Plants. This fit between the concentrations of Ni both in soil and mosses could indicate the above anthropogenic activities as their common sources.

Arsenic and zinc are two other elements that were found in high concentrations in moss and soil matrices in the same areas. According to the PMF model, both of them are associated to the road dust source, which could also be the same reason of their elevated concentrations in soil samples. Arsenic in the area of Thrace could also be connected with the presence of arsenopyrites in the area, and might be deposited on mosses through the windblown road dust source.

Chromium in mosses comes from the fossil fuel burning (Diapouli et al, 2017) and it has traveled to mosses through the fly ash that was produced during the burning process in the lignite power plants. The sites where Cr levels are elevated in mosses suit with the sites characterized by elevated Cr in soil. This fit declares that Cr in the soil comes from the same source as in mosses (the fly ash from the fuel burning).

Checking the concentrations of Fe in soil and moss samples, the conclusion that could be made is that, Fe, which is an Earth's component, is definitely coming from the soil dust in mosses. But in some cases, soil dust is not the only factor that is responsible for its high concentration in mosses. This is verified by the enrichment in Fe of some soil samples, which could only be explained through the road dust that is dispersed from the traffic. So, elevated Fe concentrations in both matrices are also due to the dispersion of the road dust through the wind, but the resuspension of soil remains its main source.

Magnesium high concentrations in moss samples match with those of the soil samples. Soil dust is the main source for both of them, but in some cases the Mg enrichment of both matrices might be due to the lignite burning in the power plants that is scattered in the surroundings.

The high concentrations of Cl in soil do not match exactly with the corresponding high concentrations in mosses. Cl according to the source apportionment results is associated with the Aged sea salt. Indeed, the sea salt particles that were deposited in mosses could also have been deposited in soil but due to the fact that some possible interactions with other chemical species and other pollutants had occurred (Diapouli et al., 2017), its concentration in soil could be affected.

Finally, the elevated concentrations of Mn in soil samples match with the corresponding concentrations in mosses. The Mn-rich source is the one that is responsible for these elevated concentrations including anthropogenic activities such as the mining ones.

### 4.5.3 Transfer of resuspended soil to mosses

Another tool to understand the level of the influence of the soil on plants is the efficiency called “transfer factor”. In general, the soil to plant transfer factor is a factor that shows the uptake of the elements from the soil to plants (Puschenreiter and Horak, 2000; Kabata-Pendias, 2004; Bitterli et al., 2010; Laço et al., 2012; Chackraborty et al., 2013; Ogoko, 2015; Mirecki et al., 2015; Papaioannou et al., 2018; Antoniadis et al., 2019). The term transfer factor is used in the radioecology too (Freytang, 1986; Puschenreiter and Horak, 2000; Uchida et al., 2007; Dragović et al., 2010; Kadovic et al., 2011) and will be used in the fifth chapter of this study too.

In the case of mosses, the transfer of resuspended soil to mosses reveals the transfer of the elements from the resuspended soil to mosses, not through the uptake from roots (as mosses do not have roots), but through the soil dust that is carried by the wind and is placed on mosses, especially in arid climates. The transfer of trace elements from soil to mosses is defined as the ratio of the elemental concentration in moss to the elemental concentration in soil equation (4.3).

$$\frac{\text{Concentration of trace element in moss}}{\text{Concentration of trace element in soil}} \quad (4.3)$$

The transfer of resuspended soil to mosses for fifteen (15) elements (Al, Si, Fe, Ca, Mg, Na, Ti, K, Mn, Sr, Cr, Zr, Zn, Ni, Co) were calculated and are presented in Table F1 in the Appendix. The elemental concentrations units of both matrices were expressed in  $\mu\text{g g}^{-1}$ .

The highest values are determined in the cases of Ca (6.23), Zn (2.95), Mn (2.96), K (2.95) and Mg (3.06), while the lowest in the cases of Mg (0.01), Ti (0.01) and K (0.01). However, the transfer of resuspended soil to mosses for some elements (Sr, Cr, Zr, Zn, Ni and Co) could not be calculated for all samples, due to the negligible elemental concentrations detected in some of them.

The mean value of transfer varies between 0.1 and 0.7 for all the elements (Figure 4.52). More specifically, the mean value of Ti and Cr is 0.1, while the mean of Al and Zr is 0.2. The elements Fe, Si, Mn and Sr have a mean transfer value around 0.3, while the elements Mg, Na and Zr around 0.4. Finally, the average transfer value of Ca and K is 0.7. Only the elements Ni and Co have very low transfer values ( $< 0.1$ ) and this is due to their very low concentrations in soil samples.

The fact that the mean values of the transfer of resuspended soil to mosses of Ca and K are the highest ones, verifies that these two elements come entirely from the windblown soil dust according to the source apportionment results of mosses. The same conclusion about the rest elements (except of Ni, Co, Cr) can be extracted, verifying also the fact that the soil dust source is the source that contributes the most to many of the moss samples.

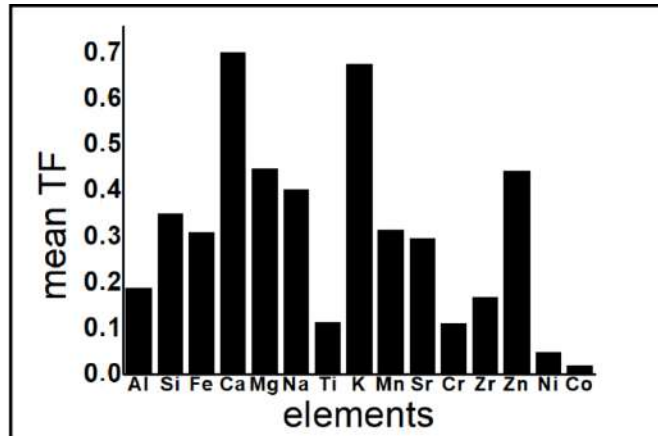


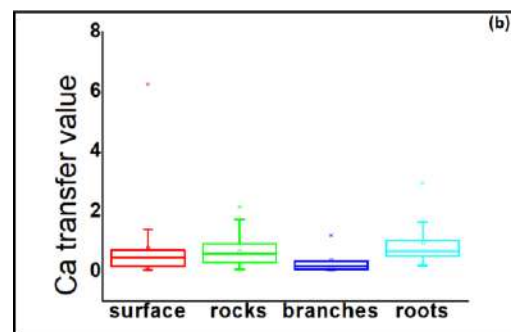
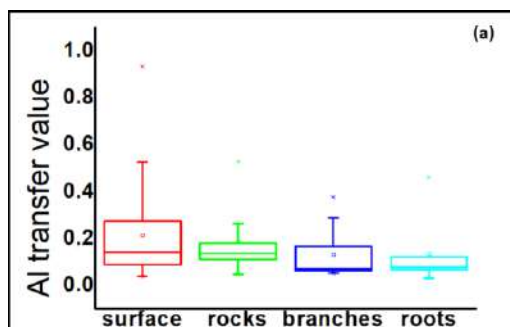
**Figure 4.52.** The mean transfer factors for the elements Al, Si, Fe, Ca, Mg, Na, Ti, K, Mn, Sr, Cr, Zr, Zn, Ni and Co.

#### 4.5.3.1 Transfer of resuspended soil to mosses and different substrate type of mosses

There are different parameters that may influence the transfer factor of elements from soil to plants such as the climate, the plant species, the part of the plants (leaves and other organs), the soil characteristics and the physico-chemical form in the soil (Uchida et al., 2007; Bitterli et al., 2010; Mbong et al., 2014).

In this study only the influence of the substrate where the mosses were collected from is studied. This is the only parameter that was chosen based on the fact that mosses do not take any element from the roots, but only from the atmospheric deposition. Thus, the percentage of exposure to soil dust deposition is the one that might play a role in the accumulation of metals in mosses.

Mosses, as it is already said, were collected from different substrate types (surface, rocks, branches and near roots). The relationship between the transfer of resuspended soil to mosses and the types of the substrate from where they were collected is presented in Figures 4.53 (a)-(h). In the Appendix F, the transfer relationships with the elements Mn, Na, Sr and Zn are also presented.



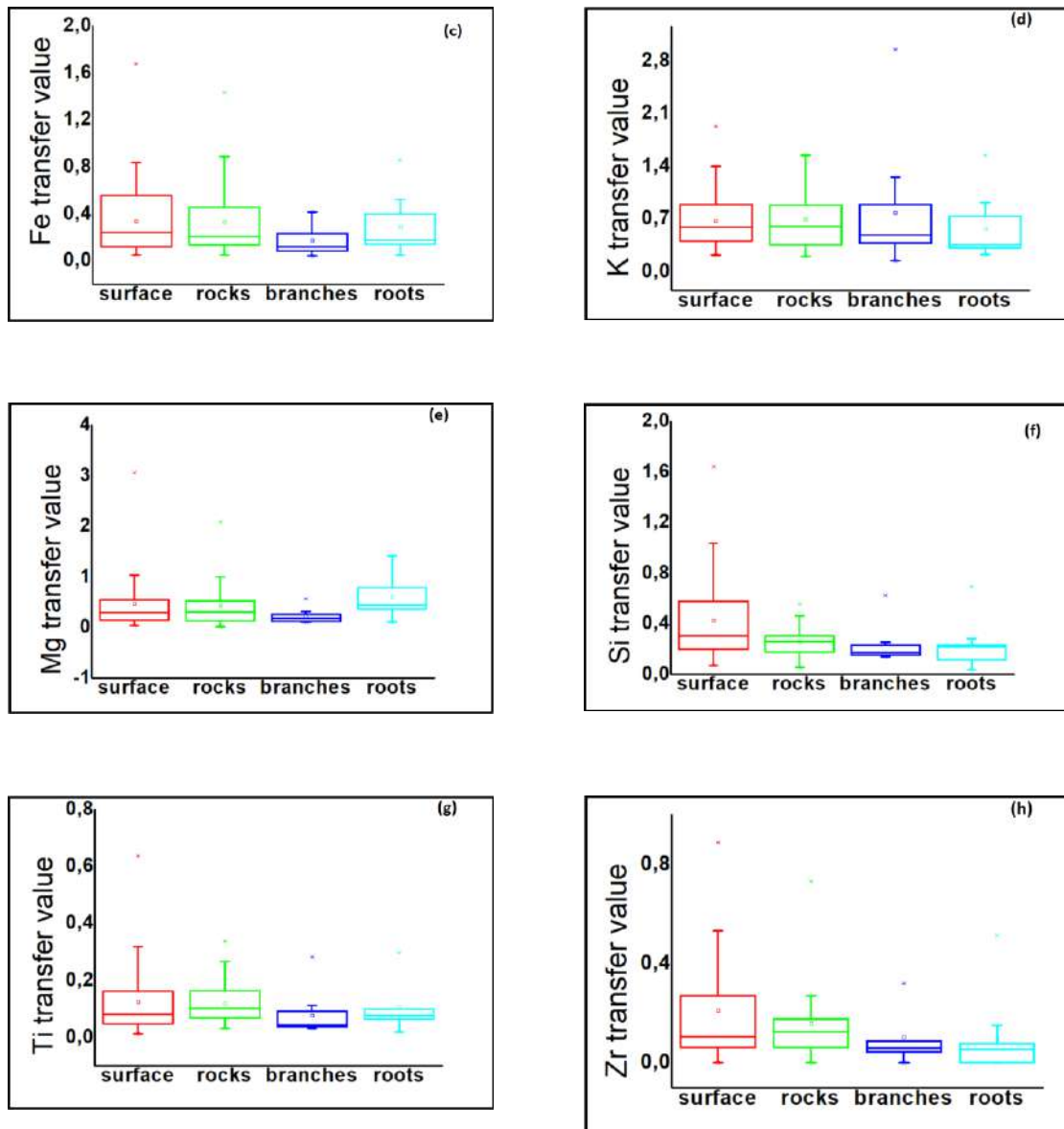


**Figure 4.53.** The relationships between the transfer of resuspended soil to mosses for the elements Al, Ca, Fe, K, Mg, Si, Ti, Zr and the type of substrate from where mosses were collected (surface, rocks, branches, roots).

The higher the transfer of resuspended soil to mosses is, the higher amount of soil dust is deposited on mosses through the air and the higher the accumulation of the elements in mosses is. This means that mosses that were entirely exposed to the atmospheric deposition in open areas (Figure 4.54) have the privilege of receiving and accumulating higher amounts of elements that are associated to the soil dust source. So, concerning the “soil-dust source” elements, mosses collected from surface and rocks should have higher transfer coefficients than those collected from branches and roots (the last ones might have been influenced by the canopy tree effect-where it was not possible to be avoided during the sampling).

Indeed, the transfer of Al, Ca, Fe, Mg, Si, Ti, K, Zn and Zr elements reveal the strong relationship between the surface and rocks with the high percentage of the soil dust that was received by mosses and verify the source apportionment results concerning the “soil dust source” elements.

No plots about the Co, Cr and Ni elements are presented due to the fact that their concentrations in soil were so low that could not give representative transfer factors plots. Concerning the plots of Mn and Sr (Appendix F), there are no big differences in the transfer values based on the type of substrate. Finally, Na plot shows that there is a strong correlation between Na and soil dust, although according to the source apportionment analysis, Na is connected with the Aged Sea Salt factor. Probably, Na particles react with other particles in the atmosphere and are deposited on mosses like the “soil dust” elements.

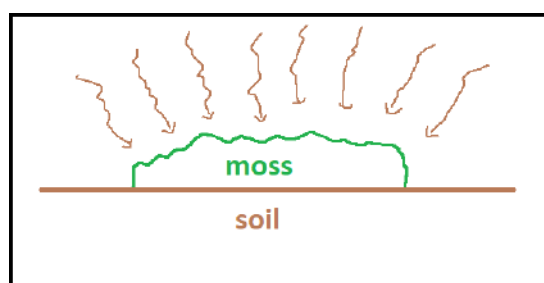


**Figure 4.54.** The atmospheric deposition of the soil dust on mosses. There is no uptake from the roots, so the only way the elements that are associated with the soil dust source to be placed on mosses is through the atmospheric deposition.

To conclude, the transfer of resuspended soil to mosses is a useful tool for the identification of the “soil dust” elements, verifying simultaneously the PMF model that was run for the elemental concentrations in mosses.

#### **4.5.4 Comparisons with data from other studies in Greece**

There are data from various studies (Pentari et al., 2006; Papastergios et al., 2011; Skordas et al., 2013; Nikolaidis et al., 2013; Argyraki-Kelepertzis, 2014; Sofianska and Michailidis, 2015; Botsou et al., 2016; Noli and Tsamos, 2016; Argyraki et al., 2017; Topalidis et al., 2017; Kelepertzis et al., 2018; Antoniadis et al., 2019) occurred in different areas of Greece concerning the levels of trace elements in soil of rural and urban areas during the last two decades. The samples that were collected in most of the cases were soil samples from urban areas (through the city, close to roadsides and highways, abandoned mines and industrial areas), as well as from agricultural areas (apple, cotton and wheat cultivated areas, vineyards). The results of the above studies are presented in Table 4.9. Differences can be observed between the concentrations of trace elements determined in the present and the previous studies.

More specifically, the current data present lower min concentrations of all the elements compared to the data provided by almost all the previous studies. The mean values of the elements Fe and K of the current study are similar to those of Argyraki-Kelepertzis results (2014), in contrast to Ca which is three times lower. In addition, Na mean value is found in 50 % lower concentration than in Noli and Tsamos (2016) research (in Filotas area), whereas Mn and Sr mean concentrations are 50 % higher than in the studies of Argyraki-Kelepertzis, 2014 and Pentari et al. (2006) respectively.

On the contrary, the majority of the max concentrations of all the elements (except of Zn, Cu and As) of the current study are higher than the max values determined in all the other studies. Zinc max values of this research are three to sixty times lower than the researches of Argyraki-Kelepertzis (2014) and Nikolaidis et al. (2013). In addition, As max concentrations are two times to two order of magnitude lower than the corresponding max concentrations measured in the studies of Nikolaidis et al. (2013) and Antoniadis et al. (2019). Finally, the max levels of Cu of the current study are in a good agreement with the results of the previous studies performed in the Greek territory. According to all the previous studies, the majority of the measured elements derive from anthropogenic activities such as industry, traffic, fertilizers, fossil fuel burning and agricultural activities, but also from natural processes such as the weathering of parent rocks like (Mn, Cu, Al, Fe) in Papastergios et al. study (2011).

Extra comparisons can be performed based on common regions where the samples were collected from. For example, the concentrations of Mn and Zn of the current study in the area of Stratoni are two and eight times lower than it was reported by Argyraki-Kelepertzis (2014), highlighting the impact of the mining activities on the area. The levels of Zn close to Thessaloniki city are similar to those described by Topalidis et al. (2017), while they are almost two times higher compared to those mentioned in Drama area by Sofianska and Michailidis (2015). Moreover, Mn and Zn concentrations in the industrial area of Kavala are two times higher than those reported by Papastergios et al. (2011). The human activities occurred in the above areas are those that influence the most the elemental concentrations.

In the area of Kirki, the levels of Zn and As are found in much lower concentrations (around two and one orders of magnitude respectively) than those cited by Nikolaidis et al. (2013). The main reason of these high concentrations is the influence of the old zinc mine that operated in the area. Finally, in the basin of Ptolemaida and close to Lehovio area, the concentrations of Fe are similar to those described by Noli and Tsamos (2016), of Na, Co, Cr are two and nine times lower, whereas Zn is one order of magnitude higher, indicating that the anthropogenic activities of the area (lignite power plants and road dust) are the main sources of them.

#### 4.5.5 Comparison with data from other studies around the world

The elemental concentrations reported by different studies worldwide during the last two decades are presented in Table 4.10. The mean concentrations of the elements Mn, Cr, Zn, As and Ni are higher than the worldwide average soil concentrations (Kabata-Pendias; 2011). More specifically, Zn and As are 1.5 times higher, Mn and Cr are 2.5 times higher, while Ni is almost 5 times higher than the values reported by Kabata-Pendias (2011). In contrast, the levels of Sr, Cu and Co are similar to the global ones.

Kabata-Pendias (2011) give also the European mean values of trace elements in topsoils, which are slightly different than the international ones. Still there are some differences between the data of the current survey and the European ones. For example, Mn and Cu of the current survey are more than 2 times higher, while Sr, Zn and Cr are approximately 1.5 higher than the European mean levels. Cobalt is found in similar concentrations whereas As is 14% lower than in Europe. These differences can be explained due to the different soil properties and anthropogenic activities that occur in each country.

The max concentrations of almost all the elements of the current study are higher than those reported in Table 4.10. For instance, the max concentrations of Al, Fe and Ca are 2 to 13 times higher than the rest studies, while the max levels of Mg, K and Na overcome these differences (more than 4 times at least higher). Moreover, the max concentrations of Zn and Cu are two order of magnitudes lower than those recorded in the industrial area of Berlin, while of As and Ni are two times higher (Birke and Raugh; 2000). These differences are based on the industrial activities that take place in the area. Finally, comparing the max concentration of Zn with this of the Oslo city (Tijhuis et al., 2002), it seems that Zn concentration in Greece is 70% lower than in Oslo city, indicating the high impact of the road traffic factor in Oslo.

In conclusion, there are differences between the elemental concentrations in soil around the world, and it is reasonable if someone thinks about the natural processes from where most of the elements come (so as the soil properties), as well as the anthropogenic activities which have a great impact on their concentrations depending on the development of each country.

The most important conclusion of this chapter that could be made, is that by combining and measuring the elemental concentrations in soil and mosses, it's easier to identify and understand their sources and take the appropriate measures for their control.

**Table 4.9.** Data from studies occurred in Greece. The range, the mean values (in parenthesis) and the median values [in brackets] of the elemental concentrations in soil ( $\mu\text{g g}^{-1}$ ) are presented.

study	Area of study	Al	Fe	Ca	Mg	Na	K	Mn	Sr	Cr	Zn	Ni	Cu	As	Co
This study	(Northern Greece) (near abandoned coal mine-Mavropigi)	9175-84454 (241223)	5936-76966 (23956)	1307-503000 (48435)	2262-149100 (18761)	338-15147 (5134)	2070-28478 (11644)	101-6473 (1214)	0-989 (184)	0-1721 (156)	0-339 (98)	0-1982 (140)	0-414 (39)	0-306 (10)	0-112 (10)
Pentari et al., 2006	(abandoned coal mine-Mavrodendri)	-	-	-	-	-	-	-	(63.3)	(169)	(79)	(125)	(47.1)	(6.9)	(41.8)
Pentari et al., 2006	(industrial area in Kavala)	-	-	-	-	-	-	-	(86.4)	(876)	(110)	(655)	(44.4)	(11.7)	(80)
Papastergios et al., 2011	(apple cultivated area-Central Greece)	(4500)	(6350)	(27980)	(2830)	(1880)	(1380)	(524.2)	(35.59)	(16.08)	(147.7)	(14.9)	(22.3)	(55.06)	(6.83)
Skordas et al., 2013	(abandoned mine in Kirki)	-	-	-	-	-	-	-	-	-	..-190 [94.6]	..-480 [165.3]	..-430 [94]	..-242 [17.1]	-
Nikolaidis et al., 2013	(Athens city areas)	10000-82000 (45000)	6000-48000 (24000)	12000-380000 (135000)	-	-	3000-19000 (11000)	168-2731 (587)	-	43-1586 (163)	18-1089 (122)	27-727 (111)	11-410 (48)	6-204 (29)	-
Argyrazi & Kelepertzis, 2014	(plain in Drama)	-	-	-	-	-	-	-	-	-	..-207 [90.6]	-	..-77 [33]	..-65 [18.8]	-
Sofianska & Michailidis, 2005	(roadside Athens)	-	-	-	-	-	-	-	-	-	51.3-169 (81.6)	90.6-620 (247)	23.3-48 (30.8)	-	-
Botsou et al., 2016	(off roadside-)	-	-	-	-	-	-	-	-	-	29.2-166 (71)	106-656 (246)	14.5-41.3 (26.8)	-	-
Botsou et al., 2016	(Filotas-W.Macedonia)	-	32940-38830 (36968)	-	-	11120-12150 (11683)	12100-15870 (13990)	-	210-302 (259)	328-836 (521)	82.9-150 (117)	-	-	1.8-5.6 (4.5)	16.4-23.2 (20.7)
Noli & Tsamos, 2016	(sulfide ore mining village Stratoni)	-	-	-	-	-	-	(2900)	-	-	(712)	-	-	(296)	-
Argyrazi et al., 2017	(close to highway Thessaloniki)	-	-	-	-	-	-	-	-	-	..-103	-	..-62	-	-
Topalidis et al., 2017	(urban area of Athens)	-	[22600]	-	-	-	-	-	-	-	[173]	-	[86]	-	-
Argyrazi et al., 2018	(vineyard area in Nemea)	7300-25400	11700-37500	48700-276500	3100-10100	-	-	481-3489	-	31-145	28-92	56.7-232	33.1-291	4.9-14.3	10-44.7
Kelepertzis et al., 2018	(industrial area of Volos)	20722-66152 (39230)	18520-54299 (31488)	-	-	-	-	484-1309 (762)	-	133-1169 (438)	52-89 (69)	101-1159 (327)	20-60 (40)	42-66152 (100)	17-71 (35)
Antoniadis et al., 2019															

**Table 4.10.** Results from other studies occurred worldwide. The range, the mean values (in parenthesis) and the median values [in brackets] of the elemental concentrations in soil ( $\mu\text{g g}^{-1}$ ) are presented.

study	Area of study	Al	Fe	Ca	Mg	Na	K	Mn	Sr	Cr	Zn	Ni	Cu	As	Co
This study	(Northern Greece)	9175-84454 (241223) [47038]	5936-76966 (23956) [22099]	1307-503000 (48435) [18571]	2262-149100 (18761) [11484]	338-15147 (5134) [4637]	2070-28478 (11644) [11057]	101-6473 (1214) [1108]	0-989 (184) [139]	0-1721 (156) [62]	0-339 (98) [100]	0-1982 (140) [0]	0-414 (39) [0]	0-306 (10) [0]	0-112 (10) [0]
(Kabata Pendias, 2011)	World soil average	-	-	-	-	-	-	(488)	(175)	(59.5)	(70)	(29)	(38.9)	(6.83)	(11.3)
FOREGS, 2005 Kabata-Pendias, 2011	(top soils of Europe)	-	-	-	-	-	-	(524)	(130)	(94.8)	(68.1)	(37)	(17.3)	(11.6)	(10.4)
CEC, 1986	(EU soil limits)	-	-	-	-	-	-	-	-	-	150-300	30-75	50-140	-	-
Paterson et al., 1996	(rural soil, Scotland)	(21843)	(18613)	(3579)	(3781)	(859)	(3605)	(385)	(21.9)	(29.4)	(392)	(11.5)	(4.8)	-	(5.3)
Birke & Rauch, 2000	(urban soil, Berlin)	-	-	-	-	-	-	-	-	..-1840 (35)	..-25210 (243)	..-769 (119)	..-12300 (79.5)	..-126 (5.1)	-
Manta et al., 2002	(soil from parks, Palermo)	-	-	-	-	-	-	[519]	-	[34]	[138]	[17.8]	[63]	-	[5.2]
Tijhuis et al., 2002	(urban soil, Oslo)	2080-43200 (17468)	2200-50200 (21852)	1330-37900 (7375)	698-24700 (6145)	..-1040 (328)	638-6960 (3258)	71.4-2230 (486)	9.23-243 (45.2)	2.85-224 (32.5)	22.9-1150 (160)	2.23-232 (28.4)	4.76-437 (31.7)	..-69.6 (5.48)	..-29.5 (9.98)
Romic & Romic, 2003	(agricultural soil, Zagreb)	-	5850-51782 (27041)	-	-	-	-	79.2-1282 (613)	-	-	15.2-277 (77.9)	1-282 (49.5)	4.3-183 (20.8)	-	-
Li et al., 2004	(urban soil, Hong Kong)	-	-	-	-	-	-	-	-	[21.6]	[92.1]	[11.2]	[16]	-	[3.02]
Zhang, 2006	(urban soil, Ireland)	11400-80800 (39600)	4400-56100 (17000)	2700-222000 (40200)	900-10500 (3600)	1500-17500 (7900)	3600-33000 (14200)	69-6902 (674)	50-365 (129)	8-129 (33.3)	23-656 (99.3)	2-86 (20.7)	9-272 (33.2)	..-30 (8.6)	0.5-14 (5.6)
Morton et al., 2009	(urban soil, Mexico city)	-	-	-	-	-	-	-	-	50-265 [116]	36-1641 [219]	20-146 [39]	15-398 [54]	-	-
Bi et al., 2018	(suburban soil, Shanghai)	-	-	-	-	-	-	-	-	-	79-223 (131.9)	-	5.9-94.2 (27.8)	3.3-17.1 (7.8)	-
Varol et al., 2020	(Harran plain, Turkey)	23850-85916 (42692)	21859-65237 (37505)	-	-	-	-	420-1409 (679)	-	-	40-197 (68)	5.8-16.5 (89)	15-47 (27)	0.13-18.31 (6.36)	9-34 (16)

## Chapter 5 Radionuclides

### 5.1 Radionuclides concentrations in mosses

Ninety-five (95) moss samples were collected from Northern Greece (Figure 5.1). After the sampling preparation in the lab according to the instructions of the ICP Vegetation Protocol, mosses were analyzed by means of gamma spectrometry for the determination of the radionuclides (natural and artificial) activities.

During the analysis of the gamma spectrums, several peaks were identified and the concentrations of six radioactive nuclides were determined. More specifically the activities of natural ( $^7\text{Be}$ ,  $^{40}\text{K}$ ,  $^{226}\text{Ra}$ ,  $^{232}\text{Th}$ ,  $^{210}\text{Pb}_{\text{uns}}$ ) and artificial ( $^{137}\text{Cs}$ ) nuclides were calculated and are presented with details in Table G1 in the Appendix G.

The peaks that were used for the determination of the radionuclides are the following ones: the 477.6 keV gamma line ( $^7\text{Be}$ ), the 661.6 keV ( $^{137}\text{Cs}$ ) and the 1460 keV ( $^{40}\text{K}$ ). In addition, assuming the existence of the radioactive equilibrium, the activity of  $^{226}\text{Ra}$  was specified using the weighted mean activity of the progenies  $^{214}\text{Pb}$  and  $^{214}\text{Bi}$ . The unsupported  $^{210}\text{Pb}$  ( $^{210}\text{Pb}_{\text{uns}}$ ) was calculated by subtracting the intensity of the supported  $^{210}\text{Pb}$  (which was calculated from the decay of  $^{214}\text{Bi}$  and  $^{214}\text{Pb}$ ) from the intensity of 45 keV gamma line (from the decay of  $^{210}\text{Pb}$ ) under the assumption of secular equilibrium. Finally, the intensity of gamma lines from the decay of  $^{228}\text{Ac}$ ,  $^{212}\text{Pb}$ , and  $^{212}\text{Bi}$  were used to define the activity of  $^{232}\text{Th}$ .

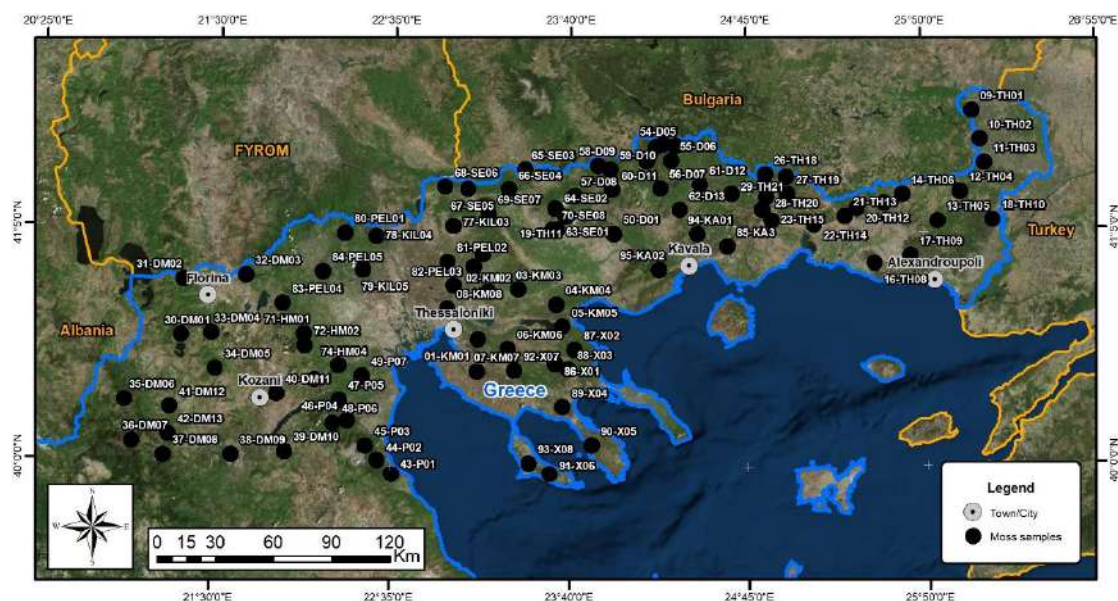


Figure 5.1. The sampling sites where the moss samples were collected from.

The study of the above radionuclides activities consists a useful tool for understanding the different environmental processes and can improve the knowledge about monitoring the radionuclides that are released into the environment. Finally, illustrating the spatial distributions of the radionuclides across Northern Greece, will reveal areas of interest giving a clue for their deposition processes in mosses.

### 5.1.1 Spatial distributions of radionuclides in mosses

#### *Beryllium-7*

Beryllium-7 is a naturally occurring radionuclide of cosmogenic origin with a relative short half-life ( $T_{1/2}=53.3$  d). It is formed in the upper troposphere and lower stratosphere by spallation reactions among cosmic rays and light atmospheric nuclei of nitrogen and oxygen (Lal et al., 1958; Brost et al., 1991; Papastefanou and Ioannidou, 1995b; 1996; Masarik and Beer, 1999).

The flux of  $^7\text{Be}$  to the Earth's surface depends on the latitude (Lal and Peters, 1958; Ioannidou et al., 2005; Ioannidou and Paatero; 2014), while its production has negligible dependence on season and longitude. The production rate of  $^7\text{Be}$  is two times higher in the stratosphere than in the troposphere (Masarik and Beer, 1999; Ioannidou et al., 2019). Additionally, it is modulated by the 11-year solar cycle and the atmospheric depth (Hötzl et al., 1991; O'Brien et al., 1991; Ioannidou and Papastefanou, 2005; Papastefanou, 2009; Ioannidou and Paatero, 2014). The calculated global average production rate of  $^7\text{Be}$  per unit surface area of the earth is  $810$  atoms/m<sup>2</sup>/s and the average concentration of  $^7\text{Be}$  in the troposphere is  $12.5$  mBq/m<sup>3</sup> (UNSCEAR 2000; Papastefanou, 2009).

Once  $^7\text{Be}$  (inorganic ion) is formed in the troposphere, it rapidly attaches to atmospheric aerosol particles and participates in the formation and growth of the accumulation mode (from  $0.07$  to  $2$  mm) aerosols which consist a major source of pollutants in the atmosphere (Bondietti et al. 1987; Porstendörfer et al., 1991; Papastefanou and Ioannidou, 1995a; Papastefanou and Ioannidou, 1996a; Ioannidou and Paatero, 2014). As soon as  $^7\text{Be}$  is attached to the aerosols, the fate of  $^7\text{Be}$  will become the fate of the carrier aerosols (Bondietti et al. 1988; Papastefanou and Ioannidou, 1996a; Ioannidou et al., 2019). So, it can be used as a tracer in atmospheric science taking into advantage its short half-life and the relatively easy determination. Its life-time is long enough to enhance long-distance transport (both horizontally and vertically) but not so long to permit long-term accumulation of the isotope in large reservoirs (Usoskin et al., 2009; Ioannidou and Paatero, 2014). The residence time of  $^7\text{Be}$  in the troposphere is of the order of a week (Papastefanou and Ioannidou, 1995a; Ioannidou, 2011). Finally,  $^7\text{Be}$ , while being attached to aerosols, can enter the marine and the terrestrial environment as well as the vegetation through wet and dry deposition (Papastefanou and Ioannidou, 1991; 1996a).

Beryllium-7 was identified in all the moss samples that were collected during the current study. It ranges between  $69$  and  $1280$  Bq kg<sup>-1</sup>, while its mean value is  $388$  Bq kg<sup>-1</sup>. Its spatial distribution is presented in Figure 5.2. The areas that present higher activity concentrations are those close to the city of Thessaloniki and in the west direction of it (towards Pella Region). No connection of  $^7\text{Be}$  with the altitude as well as with the precipitation has been found. It should be noted that during the sampling period, the precipitation rate was very low (the usual dry Greek summer), and there weren't any remarkable rainfall events recorded that would influence its concentration. Thus,  $^7\text{Be}$  was deposited on mosses mainly through the dry deposition and less through precipitation events. Finally, no season variability could be estimated, as all the samples were collected during a specific time interval (summer 2016).

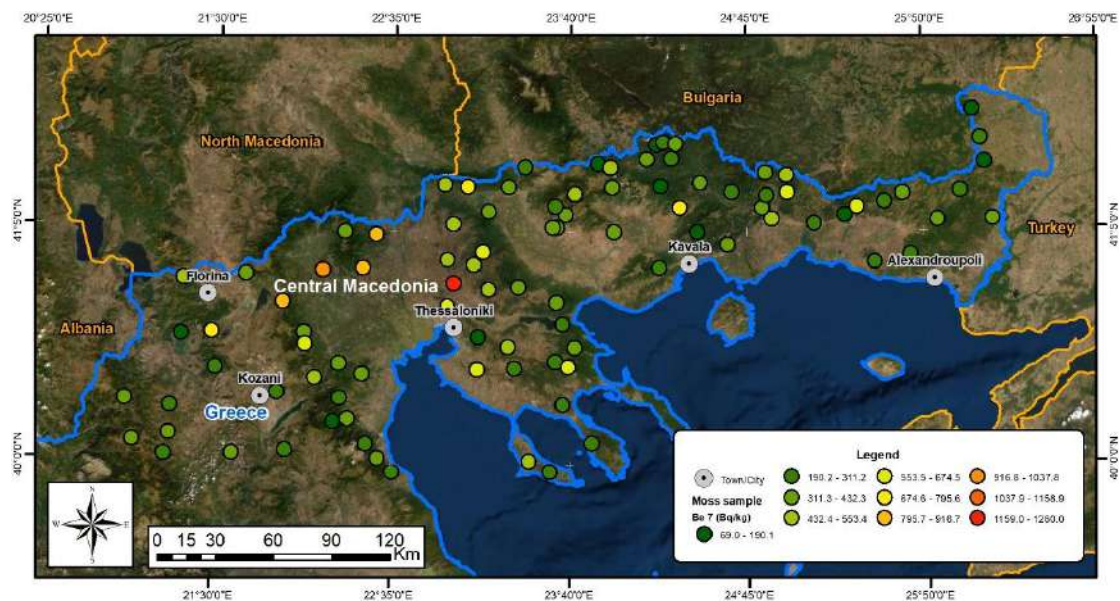


**Figure 5.2.** The activity concentrations of  $^7\text{Be}$  across Northern Greece.

### *Lead-210*

Crust minerals which contain U, are the main source of  $^{226}\text{Ra}$ , as it comes from the  $^{238}\text{U}$  decay chain.  $^{226}\text{Ra}$  has a half-life of 1620 years and decays with alpha decay to  $^{222}\text{Rn}$  (half-life: 3.8 d) in soil.  $^{222}\text{Rn}$  as a noble gas escapes from all the chemical bounds and diffuses in the atmosphere. Then, after some subsequent decays (three alpha and two beta decays) the long-living nuclide Pb-210 is formed (Ioannidou et al., 2005; Krmar et al., 2013; 2014; Wattanavatee et al., 2017; Stoulos and Ioannidou, 2020). Lead-210 is chemically more active than the noble radon gas and has a 22.6 years' half-life. After it is formed in the atmosphere, it is usually attached to aerosol particles, and is transported and deposited together with them. Therefore,  $^{210}\text{Pb}$  can be used as a tracer for investigation of certain atmospheric processes like atmospheric transport and deposition processes (Koch et al., 1996; Baskaran, 2011; Ioannidou et al., 2012a; Krmar et al., 2016).

The presence of  $^{210}\text{Pb}$  and other radon daughters in the lower atmosphere depends on the rate of  $^{222}\text{Rn}$  emanation. The geological properties of the ground; the ability of radon to leak from the crust and enter the atmosphere; the conditions of the ground surface layer (soil wetness, the presence and thickness of snow cover, the thickness of the frozen soil layer etc.) and finally the distribution of underground water reservoirs, are the factors that may influence the emanation rate of  $^{222}\text{Rn}$  (Koch et al., 1996; Stoulos et al., 2004; Ioannidou et al., 2012a; Krmar et al., 2014). The concentrations of  $^{210}\text{Pb}$  are higher near the land surface, while they decrease with both altitude and distance from the ground surface (Ioannidou et al., 2012a). So the main source of  $^{210}\text{Pb}$  in the atmosphere is the emanation of  $^{222}\text{Rn}$  from the ground. However,  $^{210}\text{Pb}$  can also be released to the environment through industrial processes such as the sintering of ores containing some amount of  $^{238}\text{U}$ , the burning of coal (Delfanti et al., 1999) or the production and use of agricultural phosphate fertilizers (Krmar et al., 2013) and volcanic eruptions (Lambert et al., 1982; Ioannidou et al., 2012a).

Lead-210 ( $^{210}\text{Pb}_{\text{tot}}$ ) can be distinguished to Pb supported ( $^{210}\text{Pb}_{\text{sup}}$ ) and Pb unsupported ( $^{210}\text{Pb}_{\text{uns}}$ ). If  $^{222}\text{Rn}$  decays within solid or liquid environmental media, its short-lived progeny (comprising Po-218, Pb-214, Bi-214, and Po-214) do not have time to migrate far from their site of production. Thus, they can generally be treated as being present in secular equilibrium with  $^{222}\text{Rn}$  and the decay goes on till  $^{210}\text{Pb}_{\text{sup}}$  is formed (Mittell et al., 2013). However, due to the fact that  $^{222}\text{Rn}$  is an inert gas and can easily escape from soils and the surfaces of water bodies, it often decays in the above-ground atmosphere, forming the unsupported Pb ( $^{210}\text{Pb}_{\text{uns}}$ ) which subsequently is attached to ambient aerosol particles and they are subsequently subjected to dry or wet deposition (Mittell et al., 2013). In this thesis, the concentrations of the unsupported Pb are being studied and reported as we are only interested in the atmospheric deposition of the different elements and radionuclides on mosses.

Lead was measured in all samples and its activity concentration ranges between 147 and 2049 Bq kg<sup>-1</sup>, with an average value of 829 Bq kg<sup>-1</sup>. The distribution of  $^{210}\text{Pb}$  is also presented in Figure 5.3. The same site like in the  $^7\text{Be}$  case at the north-west direction of Thessaloniki, presents high activity concentration of  $^{210}\text{Pb}_{\text{uns}}$ , indicating that they both ended up in mosses through the aerosol deposition. Although, no correlation has been observed between the natural radionuclides  $^7\text{Be}$  and  $^{210}\text{Pb}_{\text{uns}}$  activities, despite the fact that the atmospheric deposition is the main way of their transfer to mosses. Moreover, it should be noticed that the soil structure is one factor that can influence the concentration of  $^{210}\text{Pb}_{\text{uns}}$  in the atmosphere, through the emanation of  $^{222}\text{Rn}$ . This indicates that there are different mechanisms that govern the levels of the concentrations of  $^{210}\text{Pb}_{\text{uns}}$  and  $^7\text{Be}$  in the surface air which are not related to each other.

Furthermore, no temperature or altitude dependence of  $^{210}\text{Pb}_{\text{uns}}$  is noticed, as well as there is no connection with the precipitation or any other meteorological factor. It is reasonable that the influence of precipitation on the activity concentrations of  $^{210}\text{Pb}$  (as well as of  $^7\text{Be}$ ) in mosses cannot be identified (no-linear correlation), as mosses accumulate radionuclides over time. Thus, their concentration variability can't be explained based on individual precipitation events, but on cumulative values of precipitation and activities in mosses collected on a regular basis from the same location (Křmar et al., 2016), which was not possible during this study, but may be investigated in a future study.

In order to understand better the origin of  $^{210}\text{Pb}$  measured in mosses (supported or unsupported), the correlation between  $^{210}\text{Pb}_{\text{tot}}$ ,  $^{210}\text{Pb}_{\text{uns}}$  and  $^{210}\text{Pb}_{\text{sup}}$  is studied. The unsupported lead ( $^{210}\text{Pb}_{\text{uns}}$ ) present a linear relationship with the total lead ( $^{210}\text{Pb}_{\text{tot}}$ ) ( $R^2=0.99$ ), whereas the supported lead ( $^{210}\text{Pb}_{\text{sup}}$ ) has no correlation with the  $^{210}\text{Pb}_{\text{tot}}$ . This proves that most of the  $^{210}\text{Pb}$  in mosses comes from the decay of radon in the air and not in the soil. Thus,  $^{210}\text{Pb}$  after it is released into the atmosphere, it follows the path of the aerosols to whom it is attached and it returns to the earth surface mainly through sedimentation, and in some cases through rainfall.

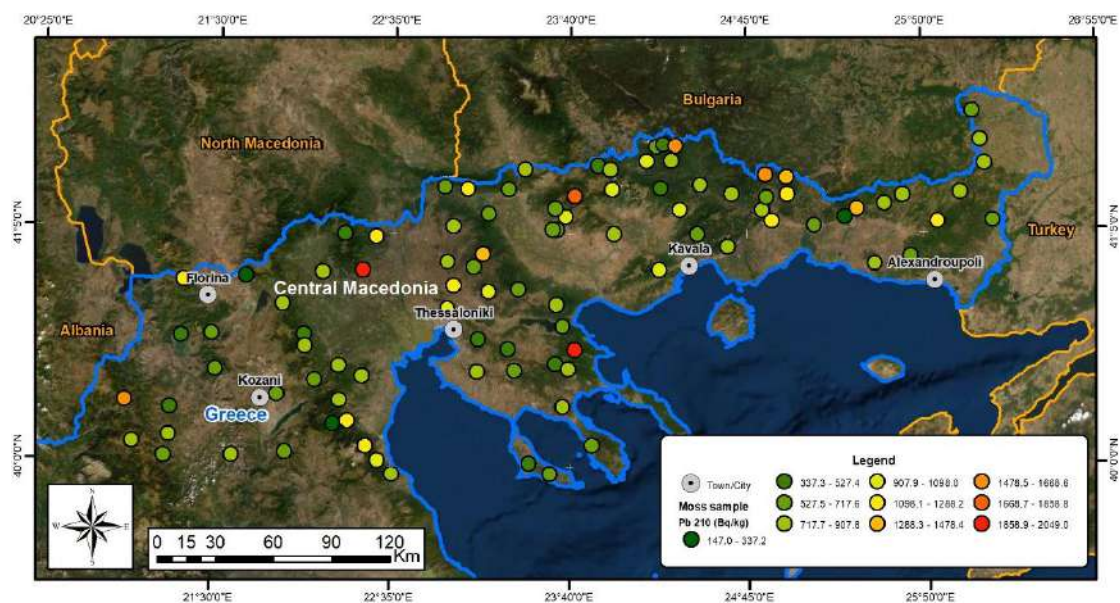


**Figure 5.3.** The activity concentrations of  $^{210}\text{Pb}$  across Northern Greece.

### *Radium-226*

Radium-226 activity concentration in mosses ranges from 0 to 126  $\text{Bq kg}^{-1}$  and its mean value was measured in 18  $\text{Bq kg}^{-1}$ . The spatial distribution of  $^{226}\text{Ra}$  is presented in Figure 5.4. The same lack of correlations among  $^{226}\text{Ra}$ , altitude, rainfall events and temperature exist here too. In addition,  $^{226}\text{Ra}$  nuclide is not correlated with  $^7\text{Be}$  nuclide and it is weakly correlated with  $^{210}\text{Pb}_{\text{uns}}$  nuclide. This indicates that  $^{226}\text{Ra}$  and  $^{210}\text{Pb}$  in mosses do not have exactly the same origin. The majority of  $^{210}\text{Pb}$  that was measured in mosses comes from the decay of  $^{222}\text{Rn}$  in the atmosphere (Krmar et al., 2009; Krmar et al., 2013; Wattanavatee et al., 2017), while  $^{226}\text{Ra}$  is deposited on mosses mainly through the soil dust particles and the aerosol deposition of  $^{214}\text{Bi}$  and  $^{214}\text{Pb}$ . Therefore,  $^{226}\text{Ra}$  and  $^{210}\text{Pb}$  do not follow the same procedure before they are deposited on mosses. The first one is due to a mixture of soil dust particles and  $^{214}\text{Bi}$  and  $^{214}\text{Pb}$  aerosol deposition on mosses, while the second one is only due to the decay of  $^{222}\text{Rn}$  in the air, which afterwards is deposited through aerosols on mosses.

### *Thorium-232*

Thorium-232 is a natural occurring radionuclide with half-life  $1.4 \times 10^{10}$  y. It decays to different progenies (such as  $^{228}\text{Ac}$ ,  $^{212}\text{Pb}$  and  $^{212}\text{Bi}$ ); whose activities helped to determine the activity of  $^{232}\text{Th}$  assuming the equilibrium existence.  $^{232}\text{Th}$  nuclide was not measured in all samples, while its max and mean activities are 66  $\text{Bq kg}^{-1}$  and 15  $\text{Bq kg}^{-1}$  respectively. The spatial distribution of the  $^{232}\text{Th}$  activity is shown in Figure 5.5. Thorium is deposited on mosses through the windspread soil particles and the aerosol deposition of  $^{212}\text{Pb}$  and  $^{212}\text{Bi}$ .

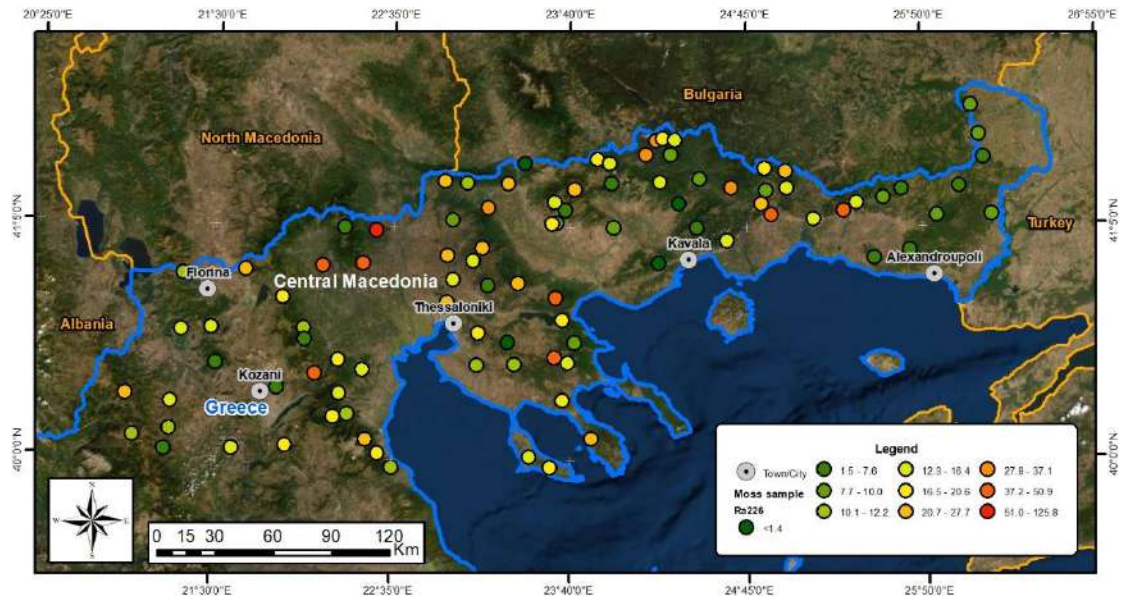


Figure 5.4. The activity concentrations of  $^{226}\text{Ra}$  across Northern Greece.

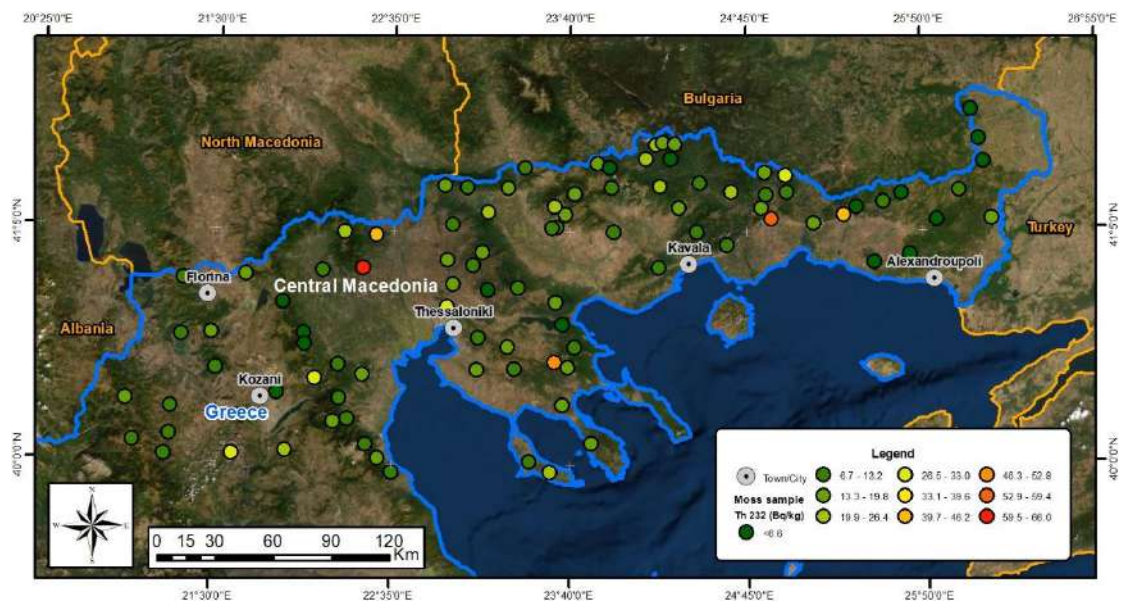


Figure 5.5. The activity concentrations of  $^{232}\text{Th}$  across Northern Greece.

### Potassium-40

Potassium-40 is a natural occurring radionuclide with half-life  $1.28 \times 10^9$  years. It is a natural component of the Earth's crust and its abundance in soil reaches 2.59% of the Earth's crust (Mason, 1966; Papastefanou et al., 1999a). Potassium is also necessary for the metabolism of the plants (Krmár et al., 2017; Zhong et al., 2019).  $^{40}\text{K}$  was measured in all samples and it ranges between 120 and 1060  $\text{Bq kg}^{-1}$ . The mean value of  $^{40}\text{K}$  is 278  $\text{Bq kg}^{-1}$ .

In Figure 5.6 the distribution of the activity concentrations of  $^{40}\text{K}$  is presented. It seems that  $^{40}\text{K}$  follows a similar distribution like those of  $^{226}\text{Ra}$  and  $^{232}\text{Th}$  nuclides, indicating

that it attends similar deposition processes on mosses like  $^{226}\text{Ra}$  and  $^{232}\text{Th}$  nuclides. Its activity concentrations are mainly influenced by the geological properties of each area. Although, due to the fact that  $^{40}\text{K}$  is an element that is found in all plants, its concentration in mosses might be affected also by the leaves' leaching and the decayed plant matter that could have covered the mosses. Furthermore, there is no correlation between  $^{40}\text{K}$  and any meteorological parameter, or the nuclides  $^7\text{Be}$  and  $^{210}\text{Pb}^{\text{uns}}$ , as they have different origins. Therefore,  $^{40}\text{K}$  was transferred to mosses through the deposition of soil dust particles from the surrounding area. The arid climate of Greece favors the transfer of soil dust particles even in far distances.

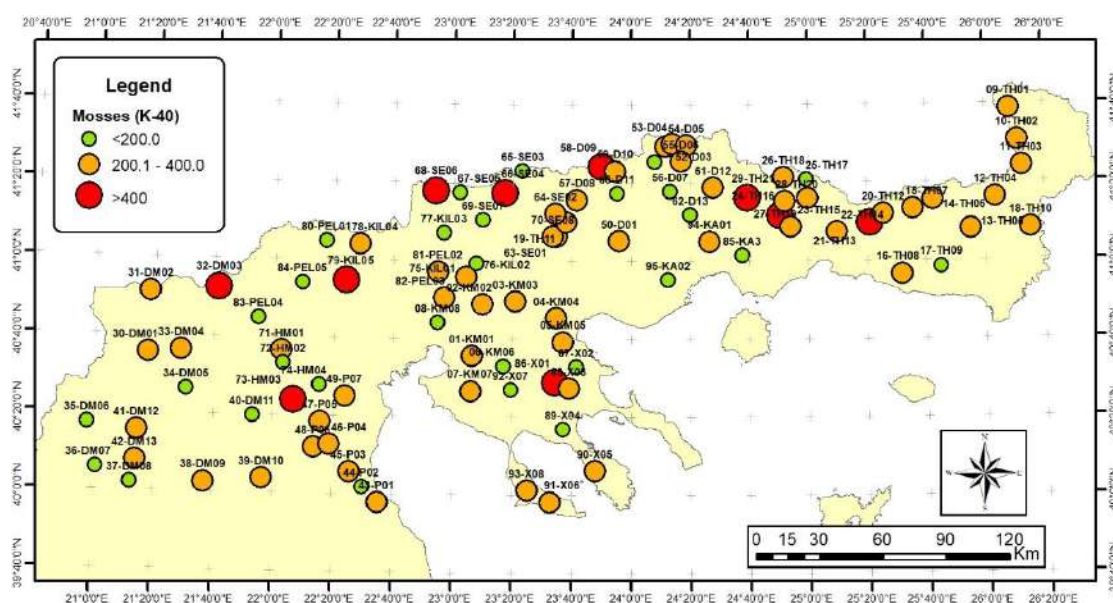


Figure 5.6. The activity concentrations of  $^{40}\text{K}$  across Northern Greece.

### Caesium-137

Caesium-137 is an artificial radionuclide with a 30 years' half-life. It is associated with nuclear fission and was released into the environment through atmospheric deposition (Ritchie et al., 1990; De Court et al., 1998; Stoulos et al., 2014; Krmar et al., 2017). More specifically,  $^{137}\text{Cs}$  was mostly deposited in the atmosphere during nuclear weapon tests and the Chernobyl nuclear power plant accident (Petropoulos et al., 2001; Ioannidou and Papastefanou, 2006; Krmar et al., 2013; Courtier et al., 2017; Savino et al., 2017). The prevailing atmospheric conditions of each area affected the deposition pattern of  $^{137}\text{Cs}$  during the first weeks right after the nuclear accident and the weapons tests (Figure 5.7).

In Greece, the radioactive cloud from Chernobyl, arrived in the beginning of May 1986; on 2 May 1986 it was detected in Thessaloniki (Papastefanou et al., 1988; Ioannidou and Papastefanou, 2005). Heavy rainfall was coincident with the passage of this radioactive cloud over the Greek territory and as a result highly-radioactive deposits of

$^{137}\text{Cs}$  occurred. This fallout of radionuclides on the ground and their capacity to be transported into the ecosystem lead to their use as tracers in the ecological cycle for a long time now and especially of the long-lived  $^{137}\text{Cs}$  (Papastefanou et al., 2005).

After the Chernobyl accident, there were not any other significant  $^{137}\text{Cs}$  emissions and the atmospheric  $^{137}\text{Cs}$  was exposed to physical decay, as well as to wet and dry deposition (Papastefanou et al., 1995b; Alonso Hernández et al., 2004; Papastefanou et al., 2005; Krmar et al., 2013; Beresford et al., 2016). In addition, the soil resuspension and the atmospheric transport favored the subsequent deposition of  $^{137}\text{Cs}$  (Todorović et al., 1999; Pham et al., 2011; Krmar et al., 2013) into the environment. In recent years, the Fukushima nuclear accident followed and contributed to the release of  $^{137}\text{Cs}$  in the atmosphere but with minor influence in areas that are far from Japan (Manolopoulou et al., 2011; Ioannidou et al., 2012b; Steinhäuser et al., 2014; Oguri and Deguchi, 2018).

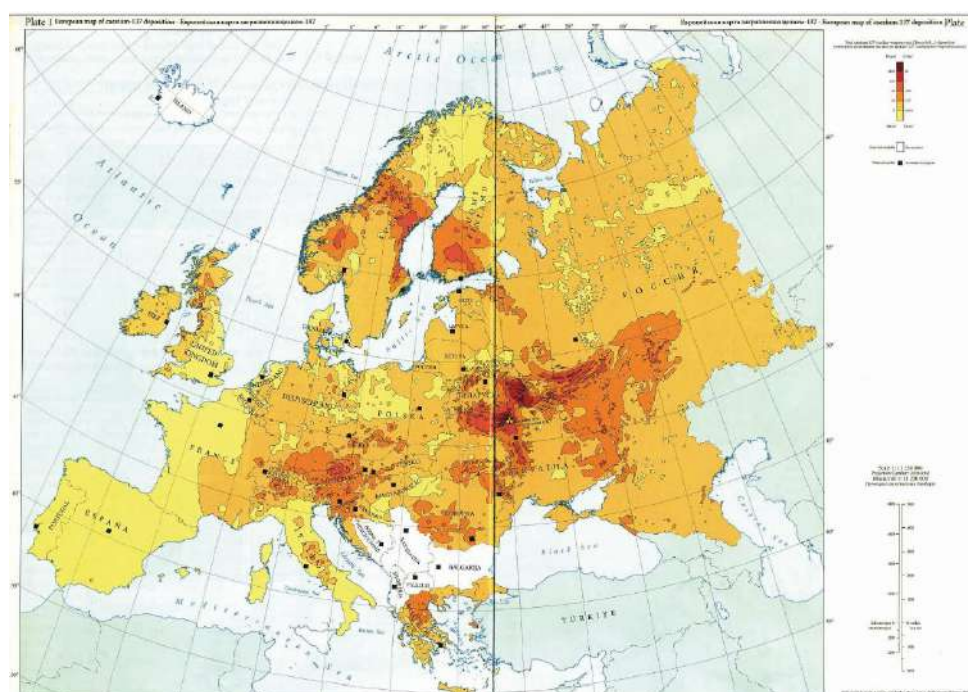


**Figure 5.7.** The total deposition of  $^{137}\text{Cs}$  (nuclear weapons tests, Chernobyl accident, ...) in Europe according to De Cort et al. (1998). Heavy rainfalls enhanced the  $^{137}\text{Cs}$  fallout after the Chernobyl accident in Greek territory too.

Since the Chernobyl accident a lot of studies have taken place around the world regarding the activity concentrations of  $^{137}\text{Cs}$  in different matrices (soil, air, water, food, vegetation, mosses, lichens, e.t.c) (Misaelides et al., 1987; Sawidis, 1988; Simopoulos, 1989; Smith, 1989; Smith and Ellis, 1990; Raes et al., 1990; Steinnes and Njåstad, 1993; De Court et al., 1998; Petropoulos et al., 1996, 2001, Papastefanou et al., 1989, 1995b, 1999b, 2001; 2005; Kulan, 2006; Marović et al., 2008; Popovic et al., 2008; Cevik and Celik, 2009; Celik et al., 2009; Sawidis et al., 2009; Zhiyanski et al., 2010; Pham et al., 2011; Stoulos et al., 2014; Konoplev et al., 2016; Papadakos et al., 2017; Savino et al., 2017; Andrović et al., 2017). Regarding this research, the sampling of mosses was

coincident with the anniversary of the three decades since the Chernobyl accident (one half-life of  $^{137}\text{Cs}$ ), thus it was considered very important to study the  $^{137}\text{Cs}$  activity concentrations in mosses and its distribution across Northern Greece.

$^{137}\text{Cs}$  nuclide was not detected in all of the moss samples. Some of the them show really low and even zero concentrations while others show much higher concentrations, depending on the area and how much it was affected mostly during the radioactive cloud thirty years ago. More specifically, the activity of  $^{137}\text{Cs}$  in moss samples ranges from 0 to  $590 \text{ Bq kg}^{-1}$ , with a mean value of  $41 \text{ Bq kg}^{-1}$ . The spatial distribution of  $^{137}\text{Cs}$  activity concentrations is presented in Figure 5.8. The most remarkable observation about this map, is that there is a match between the areas that present high concentrations of  $^{137}\text{Cs}$  in mosses and those that had accepted highly-radioactive deposits of  $^{137}\text{Cs}$  after the Chernobyl accident and the prior above-ground weapons testing (Figure 5.9). This indicates that the origin of  $^{137}\text{Cs}$  which was accumulated in the body of mosses is the soil dust particles that were resuspended, redeposited and transferred to mosses through the wet and dry deposition process.

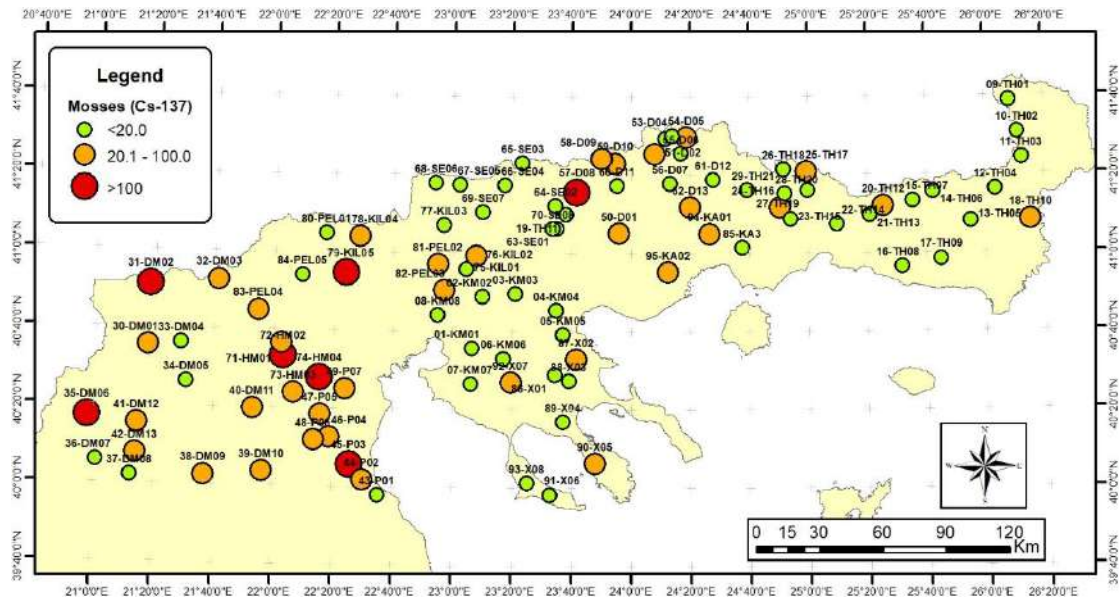


**Figure 5.8.** The activity concentrations of  $^{137}\text{Cs}$  across Northern Greece.

There is no correlation between the manmade nuclide  $^{137}\text{Cs}$  and the natural nuclides  $^{40}\text{K}$ ,  $^{210}\text{Pb}_{\text{uns}}$ ,  $^{226}\text{Ra}$  and  $^{232}\text{Th}$ , which is reasonable as they have different emission sources (natural and artificial ones). Furthermore, no correlation between  $^{137}\text{Cs}$  activity concentrations and precipitation is recorded. Therefore, the resuspended and redeposited soil is responsible for the activity concentrations of  $^{137}\text{Cs}$  in moss samples.

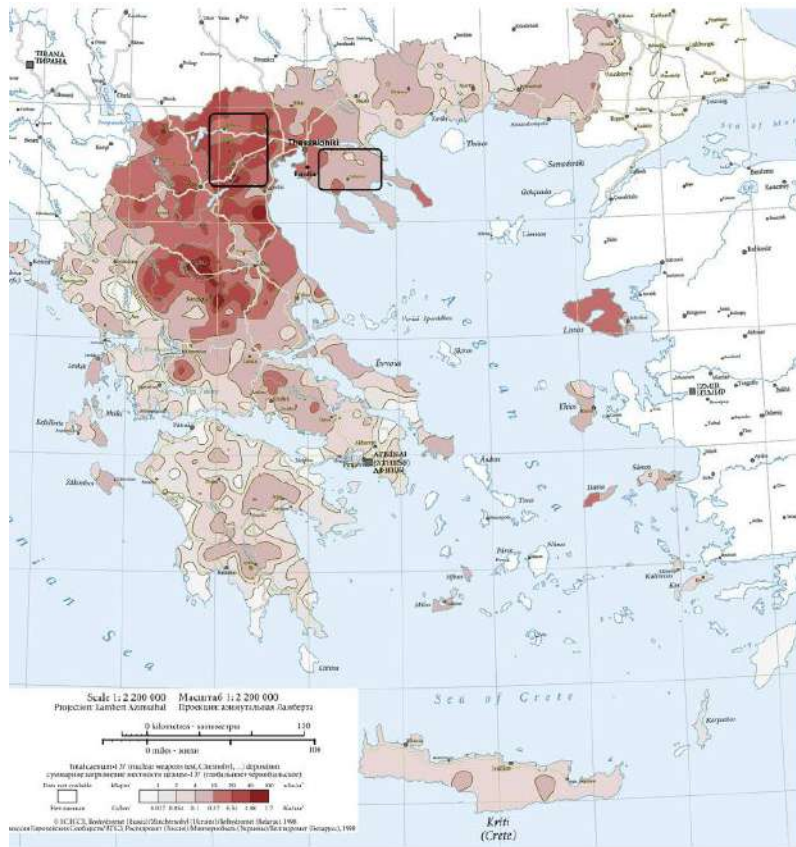


**Figure 5.9.** The total deposition of  $^{137}\text{Cs}$  (nuclear weapons tests, Chernobyl accident, ...) in Northern Greece according to De Cort et al. (1998). The photo was published by Stoulos et al. (2014).

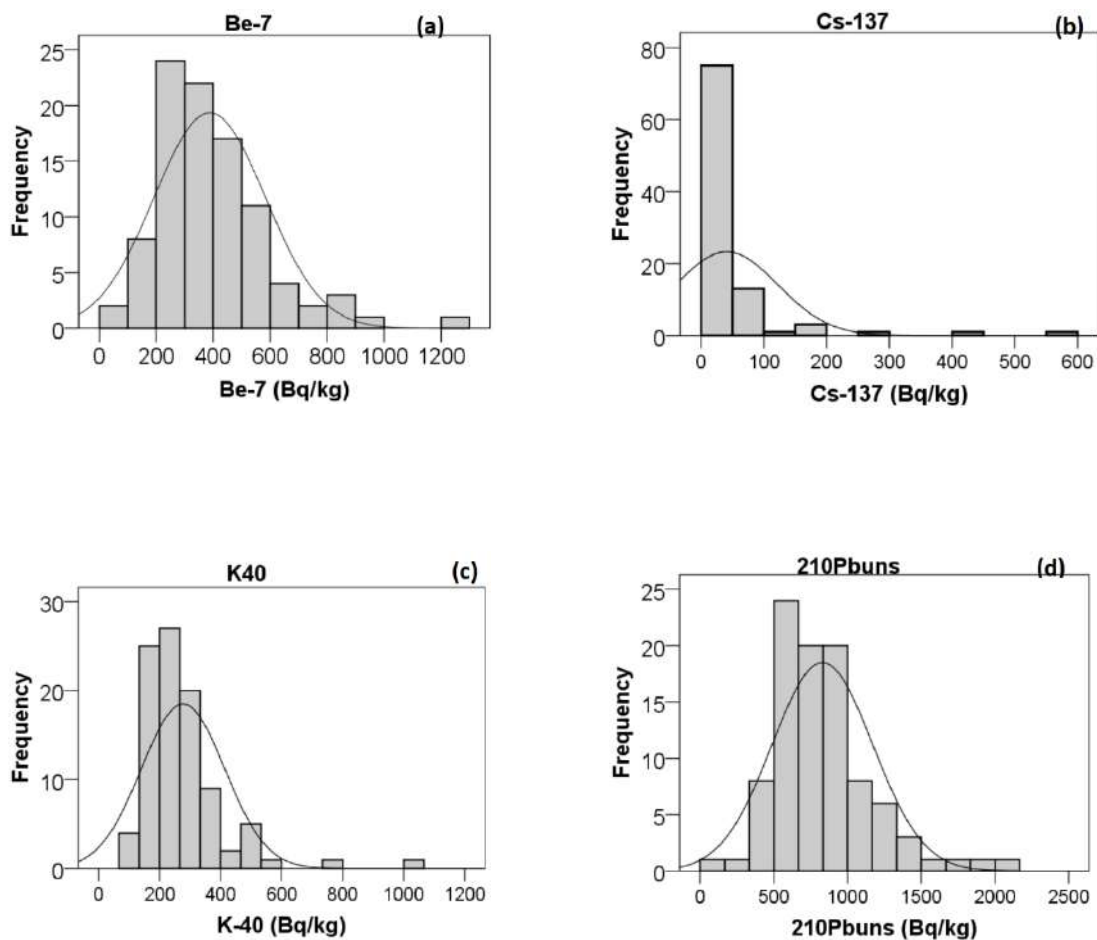
### 5.1.2 General statistic of the radionuclides activities

The results of the descriptive statistical analysis of  $^{137}\text{Cs}$ ,  $^7\text{Be}$ ,  $^{40}\text{K}$ ,  $^{210}\text{Pb}_{\text{uns}}$ ,  $^{226}\text{Ra}$  and  $^{232}\text{Th}$  radionuclides concentrations in mosses (mean, median, min, max, standard deviation, kurtosis and skewness) are presented in Table 5.1. The uncertainties ( $1\sigma$ ) of the max and min values are also shown.

**Table 5.1.** The descriptive analysis of  $^7\text{Be}$ ,  $^{137}\text{Cs}$ ,  $^{210}\text{Pb}_{\text{uns}}$ ,  $^{232}\text{Th}$ ,  $^{226}\text{Ra}$  and  $^{40}\text{K}$  radionuclides in mosses. The min and max values and their uncertainties are given in  $\text{Bq kg}^{-1}$ .

	<i>Be-7</i>	<i>Cs-137</i>	<i>Pb-210</i>	<i>Th-232</i>	<i>Ra-226</i>	<i>K-40</i>
Min	69±14	0	147±19	0	0	120±11
Max	1280±100	590±40	2049±80	66±10	126±4	1060±60
Median	350	15.7	796	13	14	256
Mean	388	41	829	15	18	278
Std Dev.	196	81	341	11	16	137
Kurtosis	4.02	26.89	2.14	6.29	24.54	11.71
Skewness	1.52	4.81	1.18	2.20	3.98	2.73

The highest measured values of  $^{40}\text{K}$  is within a  $3\sigma$  interval about the mean value, of  $^7\text{Be}$ ,  $^{232}\text{Th}$ ,  $^{210}\text{Pb}_{\text{uns}}$  are within  $4\sigma$  interval about the mean values and finally of  $^{226}\text{Ra}$  and  $^{137}\text{Cs}$  are within  $7\sigma$  interval about the mean values. All the nuclides have positive skewness and kurtosis, indicating a non-linear distribution (Cramer, 1998; Cramer & Howitt, 2004; Doane & Seward, 2011). Only  $^{210}\text{Pb}_{\text{uns}}$  seems to be less skewed than the other nuclides, but still its distribution cannot be characterized totally as normal. A Shapiro-Wilk's test (Shapiro & Wilk, 1965; Razali & Wah, 2011) and a visual inspection of their histograms and normal Q-Q plots (Appendix I) confirm the previous observations about the non-normality of the distributions. The frequency distributions of the aforementioned nuclides in mosses are presented in Figure 5.10 (a)-(f). All the above statistical analysis, as well as the Pearson analysis that follows, were carried out using the IBM SPSS statistics 23 software.



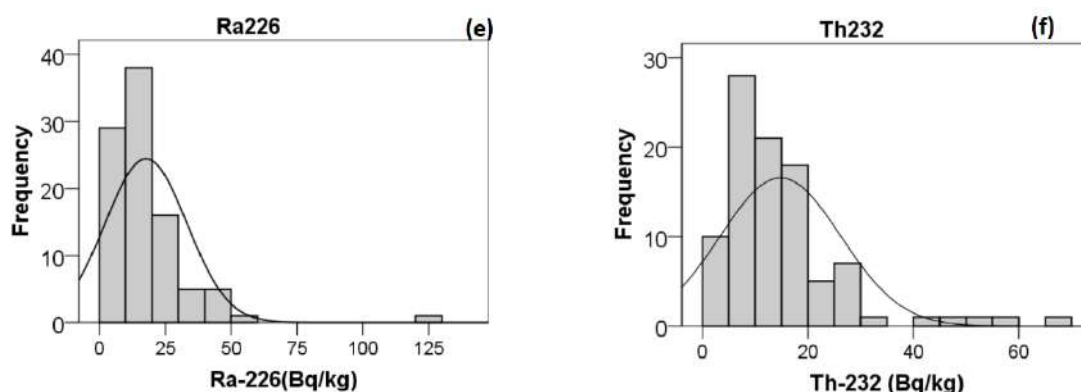


**Figure 5.10 (a)-(f).** The frequency distributions of  $^7\text{Be}$ ,  $^{137}\text{Cs}$ ,  $^{40}\text{K}$ ,  $^{210}\text{Pb}_{\text{uns}}$ ,  $^{226}\text{Ra}$  and  $^{232}\text{Th}$  radionuclides.

Pearson correlation analysis was performed in order to study the degree of the linear relationship between the above radionuclides. The correlation coefficients ( $r$  values) and their statistical significance levels ( $p$ -values- in parenthesis) are shown in Table 5.2. According to Evans (1996), the strength of correlation can be defined by the absolute value of the correlation coefficient  $r$ . More specifically, when:

$0 < r < 0.19$  is a very weak correlation

$0.2 < r < 0.39$  is a weak correlation

$0.4 < r < 0.59$  is a moderate correlation

$0.60 < r < 0.79$  is a strong correlation

$0.80 < r < 1.0$  is a very strong correlation

In addition, the  $p$ -values give the significance level between two nuclides. When they are lower than 0.01, it indicates that, statistically speaking, the correlation between two nuclides (weak, moderate, strong) does exist on the studied population of mosses.

The Pearson correlations between the terrestrial nuclides  $^{232}\text{Th}$ ,  $^{40}\text{K}$  and  $^{226}\text{Ra}$  as well as the atmospheric radionuclides  $^7\text{Be}$  and  $^{210}\text{Pb}_{\text{uns}}$  show a moderate behaviour.  $^{232}\text{Th}$  and  $^{226}\text{Ra}$  radionuclides present a strong relationship, while the rest ones show a weak or even a very weak correlation. Only  $^{210}\text{Pb}_{\text{tot}}$  and  $^{210}\text{Pb}_{\text{uns}}$  are very strongly correlated. The significance of all these correlations is also confirmed by the  $p$ -values. The results from the Pearson analysis additionally verify some of the earlier expressed observations about the radionuclides relationships and their origins.

More specifically, according to Pearson analysis,  $^{226}\text{Ra}$  has a very weak correlation with  $^{210}\text{Pb}_{\text{tot}}$  and with  $^{210}\text{Pb}_{\text{uns}}$ . This probably means that the majority of the  $^{210}\text{Pb}$  that was measured in mosses is unsupported, coming possibly from the decay of radon in the atmosphere (Wattanavatee et al., 2017; Krmar et al., 2013; Krmar et al., 2009). This can also be explained based on the fact that, if the source of  $^{210}\text{Pb}_{\text{tot}}$  was the soil dust or even the substrate (bedrock) on which mosses were lying, then  $^{210}\text{Pb}_{\text{tot}}$  should be deposited on mosses following the same procedure as  $^{226}\text{Ra}$ . And if the previous

assumption had occurred, then  $^{226}\text{Ra}$  and  $^{210}\text{Pb}_{\text{tot}}$  would have a strong correlation. The same would have happened with  $^{210}\text{Pb}_{\text{uns}}$ . But in this case, they do not have any correlation, while  $^{210}\text{Pb}_{\text{tot}}$  and  $^{210}\text{Pb}_{\text{uns}}$  do have a very strong one, so most of  $^{210}\text{Pb}_{\text{tot}}$  in mosses comes from the decay of radon in the air.

**Table 5.2.** Pearson correlation analysis of  $^7\text{Be}$ ,  $^{210}\text{Pb}_{\text{uns}}$ ,  $^{210}\text{Pb}_{\text{tot}}$ ,  $^{137}\text{Cs}$ ,  $^{232}\text{Th}$ ,  $^{226}\text{Ra}$  and  $^{40}\text{K}$  radionuclides in mosses. The correlation coefficients and the p-values (in italics in brackets) give the significance level between two variables.

	$^7\text{Be}$	$^{137}\text{Cs}$	$^{210}\text{Pb}_{\text{uns}}$	$^{210}\text{Pb}_{\text{tot}}$	$^{232}\text{Th}$	$^{226}\text{Ra}$	$^{40}\text{K}$
$^7\text{Be}$	1	0.252 (0.014)	0.453 ( <i>&lt;0.01</i> )	0.462 ( <i>&lt;0.01</i> )	0.095 (0.363)	0.253 (0.013)	0.005 (0.962)
$^{137}\text{Cs}$	0.252 (0.014)	1	0.488 ( <i>&lt;0.01</i> )	0.490 ( <i>&lt;0.01</i> )	0.287 (0.005)	0.116 (0.262)	0.366 ( <i>&lt;0.01</i> )
$^{210}\text{Pb}_{\text{uns}}$	0.453 ( <i>&lt;0.01</i> )	0.488 ( <i>&lt;0.01</i> )	1	0.999 ( <i>&lt;0.01</i> )	0.147 (0.155)	0.100 (0.334)	-0.020 (0.844)
$^{210}\text{Pb}_{\text{tot}}$	0.462 ( <i>&lt;0.01</i> )	0.490 ( <i>&lt;0.01</i> )	0.999 ( <i>&lt;0.01</i> )	1	0.177 (0.086)	0.145 (0.160)	-0.002 (0.981)
$^{232}\text{Th}$	0.183 (0.075)	0.287 (0.005)	0.147 (0.155)	0.177 (0.086)	1	0.669 ( <i>&lt;0.01</i> )	0.577 ( <i>&lt;0.01</i> )
$^{226}\text{Ra}$	0.253 (0.013)	0.116 (0.262)	0.145 (0.160)	0.091 (0.381)	0.669 ( <i>&lt;0.01</i> )	1	0.421 ( <i>&lt;0.01</i> )
$^{40}\text{K}$	0.005 (0.962)	0.366 ( <i>&lt;0.01</i> )	-0.020 (0.844)	-0.002 (0.981)	0.577 ( <i>&lt;0.01</i> )	0.421 ( <i>&lt;0.01</i> )	1

Finally, the strong correlation between  $^{232}\text{Th}$  and  $^{226}\text{Ra}$  indicates that both nuclides are deposited on mosses with the same process, mostly through the deposition of soil dust particles, but also through the aerosol deposition. The activity concentrations of these nuclides depends also on the kind of substrate (bedrock) where the mosses were situated. For example, in some samples  $^{226}\text{Ra}$  could be higher than thorium, due to granite substrate, while thorium is risen when the bedrock is sedimentary (Wattanavatee et al., 2017; Krmar, 2013).

In addition, the Principle Component Analysis (PCA) with VARIMAX rotation is applied for the determination of the relationship between the aforementioned studied radionuclides. The PCA analysis results that were extracted are presented in Table 5.3 and verify on their turn the Pearson correlations analysis results that were performed earlier. More specifically, the total variances of seven components are presented by applying Kaiser's criteria with accepted eigenvalues higher than unity. The first three are selected and explained 82.25% of the total variance of the dataset.

The factor loading of the radionuclides were also calculated and are presented in Table 5.4. High positive loading values of the variables in each component are observed. The first component (PC1), which accounts for 41.97% of the variance, includes the radionuclides,  $^7\text{Be}$ ,  $^{210}\text{Pb}_{\text{uns}}$  and  $^{210}\text{Pb}_{\text{tot}}$  with high positive loadings of 71.5%, 92.4% and 92.6%. The second component (PC2) accounts for 27.15% of the variance and includes the terrestrial radionuclides with high positive loadings of 89.6% ( $^{226}\text{Ra}$ ), 85.2% ( $^{232}\text{Th}$ ) and 62.1% ( $^{40}\text{K}$ ). Finally, the third component (PC3), accounts for the 13.3% of the variance. The major contributor to this component is the  $^{137}\text{Cs}$

radionuclide, with a high positive loading of 78.6%. The PCA solution which includes three components can also be seen in Figure 5.11. The component plot reveals three different groups that have been distinguished during the analysis. Each axis represents one component, and the closest to the axis are the variables, the more are associated to this component. Thus, the radionuclides  $^7\text{Be}$ ,  $^{210}\text{Pb}_{\text{uns}}$  and  $^{210}\text{Pb}_{\text{tot}}$  seem to hang together (PC1). This indicates that all of them are deposited on mosses following similar processes and that the majority of lead that is measured in mosses comes mainly from the decay of  $^{222}\text{Rn}$  in the atmosphere. The nuclides  $^{226}\text{Ra}$ ,  $^{232}\text{Th}$  and  $^{40}\text{K}$  are loading quite nicely on the second component, while  $^{137}\text{Cs}$  characterize the last component.

**Table 5.3.** The Total Variance Explained from the Principle Component Analysis Extraction Method. Four Components are identified concerning the studied radionuclides in mosses.

Component	Total Variance Explained								
	Initial Eigenvalues			Extraction Sums of Squared Loadings			Rotation Sums of Squared Loadings		
	Total	% of Variance	Cumulative %	Total	% of Variance	Cumulative %	Total	% of Variance	Cumulative %
1	2.938	41.969	41.969	2.938	41.969	41.969	2.459	35.126	35.126
2	1.901	27.152	69.121	1.901	27.152	69.121	2.017	28.815	63.941
3	.919	13.131	82.252	.919	13.131	82.252	1.282	18.311	82.252
4	.596	8.520	90.772						
5	.357	5.106	95.877						
6	.289	4.122	100.000						
7	6.282E-6	8.975E-5	100.000						

**Table 5.4.** The Factor Loadings extracted from the PCA analysis in moss samples. The rotation method that was used is the VARIMAX with Kaiser Normalization.

	Component		
	1	2	3
$^{210}\text{Pb}_{\text{uns}}$	.924	-.036	.270
$^{210}\text{Pb}_{\text{tot}}$	.926	.005	.264
$^{226}\text{Ra}$	.137	.896	-.071
$^{232}\text{Th}$	.089	.852	.265
$^{40}\text{K}$	-.191	.621	.620
$^7\text{Be}$	.715	.305	-.250
$^{137}\text{Cs}$	.416	.090	.786

The PCA results are also verified by the Cluster Analysis results, performed by the SPSS software as well. The Cluster Analysis results are illustrated in a dendrogram (Figure 5.12). Three statistically significant separated clusters are distinguished. The first one (Cluster 1) includes the radionuclides  $^7\text{Be}$ ,  $^{210}\text{Pb}_{\text{uns}}$  and  $^{210}\text{Pb}_{\text{tot}}$ . In the second branch (Cluster 2), the radionuclides  $^{226}\text{Ra}$ ,  $^{232}\text{Th}$  and  $^{40}\text{K}$  are grouped together, while  $^{137}\text{Cs}$  belongs to the last branch (Cluster 3). The first Cluster 1 reveals the atmospheric origin of the radionuclides which are placed on mosses through wet and dry deposition. The second cluster concerns the nuclides which are accumulated into mosses through the dispersed soil dust particles ( $^{226}\text{Ra}$  and  $^{232}\text{Th}$  may also come from the aerosol deposition of their daughters  $^{214}\text{Pb}$ ,  $^{214}\text{Bi}$ ,  $^{212}\text{Pb}$ ,  $^{212}\text{Bi}$  respectively). Finally, the last cluster has manmade characteristics, and is expressed only by the  $^{137}\text{Cs}$  nuclide which traveled through the resuspended soil particles to mosses.

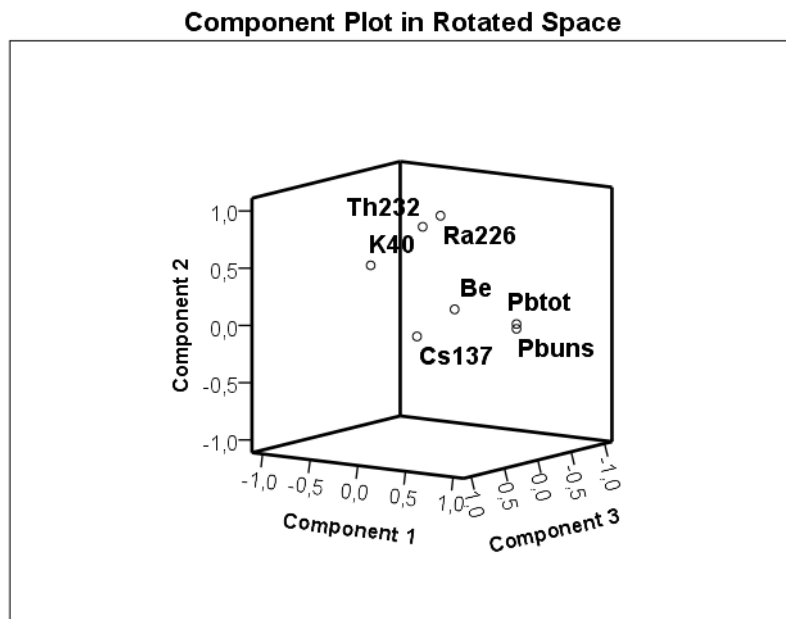


**Figure 5.11.** Plot representing the component solution extracted by the PCA.

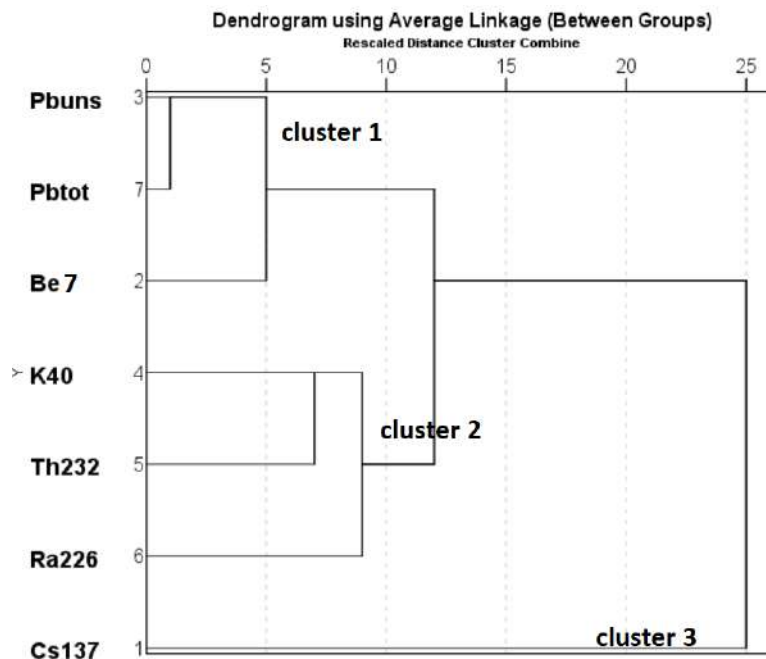


**Figure 5.12.** A dendrogram obtained by Cluster Analysis, revealing the correlation between the different radionuclides measured in mosses. The distance between the branches expresses the correlation between the radionuclides.

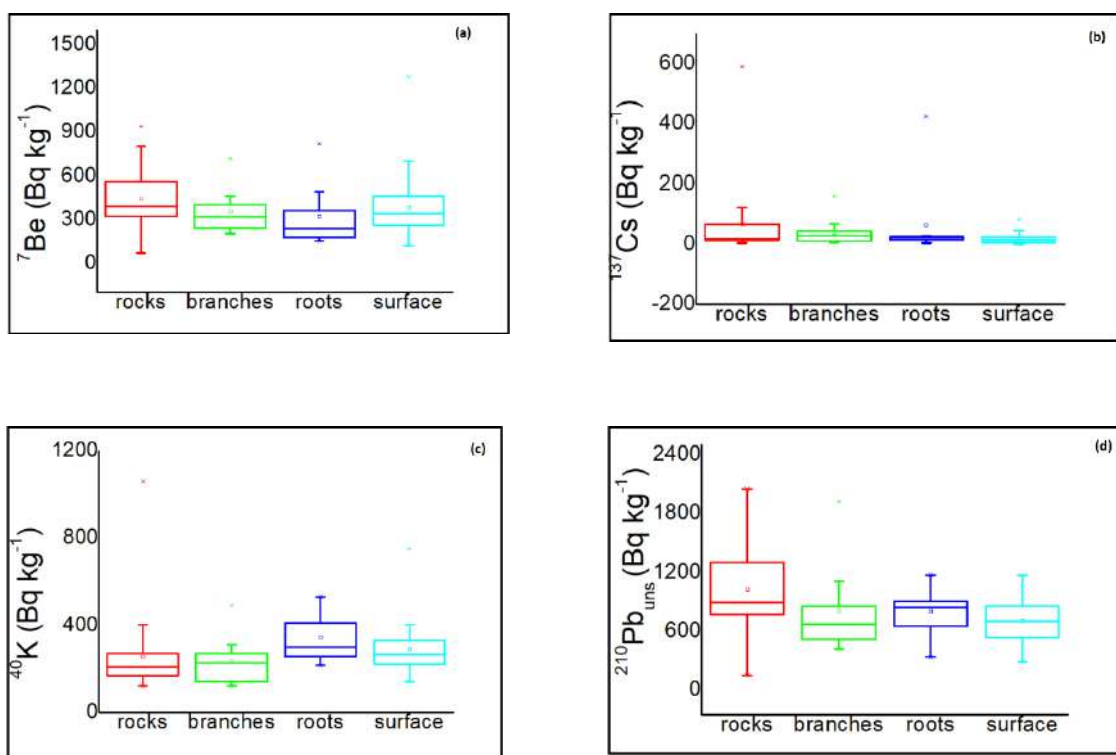
As it was previously said, till the end of this thesis the concentrations of  $^{210}\text{Pb}$  nuclide correspond only to the concentrations of the  $^{210}\text{Pb}_{\text{uns}}$  nuclide, as we are interested only in the amount of lead that comes from the atmosphere.

### 5.1.3 The role of the substrate surfaces in radionuclides concentrations

Moss sampling took place in the whole territory of Northern Greece. The collected mosses were grown naturally under different environmental features. Based on the different characteristics of the environment, such as the substrate type where mosses grew and collected (rocks, branches, near roots, ground surface), some plots describing the radionuclides activities distributions are made and presented in Figure 5.13(a)-(f).

Slight differences can be observed in the activity concentrations of the studied radionuclides. For example, the cosmogenic nuclide  $^7\text{Be}$  presents higher activities in mosses collected from the ground surface and rocks, than those that were collected near roots. The nuclides  $^{210}\text{Pb}$ ,  $^{226}\text{Ra}$ ,  $^{232}\text{Th}$  do not present any significant difference between those collected on surface and near roots. There is a homogeneity for the concentrations of the artificial radionuclide  $^{137}\text{Cs}$ , while  $^{40}\text{K}$  is found in higher concentrations in those mosses that were picked up mostly near roots.

The above remarks are reasonable if someone thinks that  $^7\text{Be}$  and  $^{210}\text{Pb}$  come from the aerosol deposition on mosses, while  $^{40}\text{K}$  and  $^{137}\text{Cs}$  come from the resuspension of soil and its deposition on mosses. These observations are also verified by the ratio of the activity concentrations between mosses collected from the surface and near roots. The ratio of the activity concentrations between mosses taken from the surface versus roots are higher than 1 for  $^7\text{Be}$ , around 1 for  $^{210}\text{Pb}$ ,  $^{232}\text{Th}$  and  $^{226}\text{Ra}$ , and lower than 1 for  $^{137}\text{Cs}$ , indicating the association of the last one to the dispersed soil dust particles.



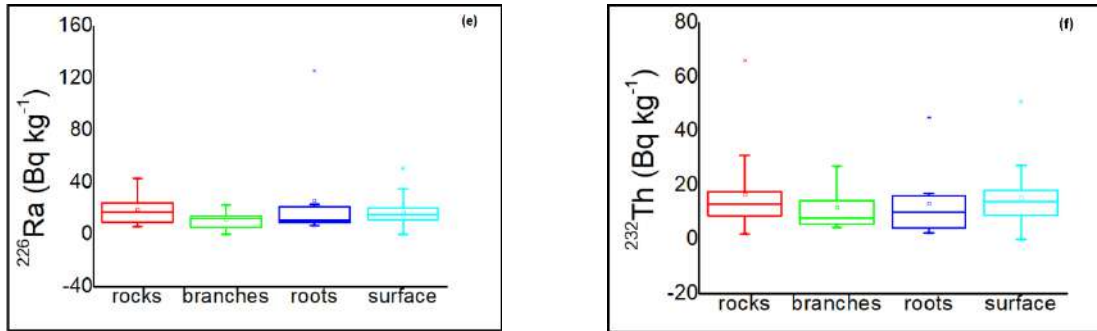


**Figure 5.13 (a)-(f).** “Box/whisker” plots of the radionuclides activities ( $^7\text{Be}$ ,  $^{137}\text{Cs}$ ,  $^{40}\text{K}$ ,  $^{210}\text{Pb}$ ,  $^{226}\text{Ra}$  and  $^{232}\text{Th}$ ) based on the different surface types from where mosses were collected.

#### 5.1.4 Results from other Greek studies

In the literature a few studies are found about the activities concentrations of radionuclides in mosses in Greek territory. All of them concern some specific areas of the vicinity of Northern Greece, and mostly the area of Thessaloniki and Ptolemaida in West Macedonia. Their results are shown in Table 5.5.

According to Table 5.5, the activity concentrations of  $^{137}\text{Cs}$  are much lower than in most of the studies, and in some cases even 1 order of magnitude lower. This is reasonable, as most of these studies were performed some years right after the Chernobyl accident in 1986, while this research occurred 30 years later- after the passage of one half-life time. Additionally, the concentrations of  $^{137}\text{Cs}$  that are now measured in mosses concern the concentrations due to the atmospheric deposition of  $^{137}\text{Cs}$  during the last three years, which was deposited on mosses through the resuspended soil particles of the surrounding area.

Furthermore, the max concentrations of  $^{40}\text{K}$  of this study are 3-18 times higher than those from the other studies, while its mean concentration is 1.5 times higher than Tsikritzis (2002) results. Finally,  $^{226}\text{Ra}$  in mosses was only measured by Tsikritzis (2002) and Tsigaridas (2014). The max concentration of  $^{226}\text{Ra}$  of the current study is 30% higher than Tsikritzis concentration, and it's two times higher than Tsigaridas max concentration. These differences can be explained due to the different geological characteristics of each area, as well as to the possible leaching of decayed plant matter on mosses.

**Table 5.5.** The results of other studies performed in Greece compared to the results of the current study. Mostly the activities of  $^{137}\text{Cs}$ ,  $^{40}\text{K}$  and in some cases  $^{226}\text{Ra}$  were measured. The min, max values are presented accompanied by the mean values (in parenthesis). All the concentrations are given in  $\text{Bq kg}^{-1}$ .

study	place	$^{137}\text{Cs}$	$^{40}\text{K}$	$^{226}\text{Ra}$
(Current study)	Northern Greece	0-590 (41)	120-1060 (277)	0-126 (18)
(Sawidis, 1988)	Thessaloniki	(2612)	-	-
(Papastefanou et al., 1989)	Thessaloniki	2390-4500	61-128	-
	Grevena	803-2457	43-56	-
(Papastefanou & Manolopoulou, 1992)	Thessaloniki	(8040)	-	-
	Grevena	(8150)	-	-
(Tsikritzis, 2002)	W. Macedonia (Kozani basin)	512-4182 (2213)	0-352 (178)	0.3-97.6 (56.7)
(Sawidis et al., 2009)	W. Macedonia (Mt. Vermio)	227-2050	-	-
(Sawidis et al., 2010)	W. Macedonia (Mt. Vermio)	(954.4)	-	-
(Tsigaridas, 2014)	W. Macedonia Ptolemaida	(1660)	(412)	(69.7)

### 5.1.5 Results from other studies around the world

The concentrations of radionuclides in mosses were being studied since the 90's across the world. The results of different surveys performed worldwide are presented in Table 5.6. Differences can be observed between the radionuclide concentrations of the current study and the other ones.

More specifically, the max concentrations of  $^7\text{Be}$  are 2 times to 1 order of magnitude higher than the concentrations of most of the studies, while there is a 20% difference with the results of Karunakara et al. (2003) in India and Krmar et al (2009; 2017) in Serbia. Additionally, the mean values of  $^7\text{Be}$  present differences in the range of 7- 40% among the other studies results. The latitude of each sampling site affects the concentrations of  $^7\text{Be}$  in mosses and explains the differences that are noticed among different surveys.

The activity concentrations of  $^{137}\text{Cs}$  present also a variance according to Table 5.5. In most of the cases, the concentrations of  $^{137}\text{Cs}$  are higher in the Greek samples (2 times to 1 order of magnitude higher) than in the other studies, with some exceptions like in the studies of Dragović et al. (2004; 2010), Marović et al. (2008), Celik et al. (2009), Ziembik et al. (2013), Aleksiyenek et al. (2017) and Andrović et al. (2017). These differences could be explained based on the fact that as a) each study refers to a different

period of measurement of  $^{137}\text{Cs}$  deposited from the atmosphere to mosses and b) the resuspension of the soil particles especially in dry climates is a factor that should be seriously taken under consideration.

Lead-210 concentrations were referred in a lot of studies around the world. In some cases, like in Krmar et al. (2013; 2014), Sert et al. (2011) and Aleksiyayenek et al. (2017) studies, the max concentrations of the Greek results are 2 to 4 times higher compared to them. On the other hand,  $^{210}\text{Pb}$  is 40% lower than in China as it was reported by Zhong et al. (2019). Lead as it was already reported, depends on the emanation rate of  $^{222}\text{Rn}$ . Additionally, the geological characteristics of each area consist a major factor that influences its concentrations. Thus, the fact that the values of  $^{210}\text{Pb}$  reported in the literature differ between each other is justified based on the above reasons.

Pottassium-40 is a radionuclide that was quite often announced in moss samples. The max value of the current dataset is almost twice those reported in Serbia by Dragović et al. (2010) and in Norway by Dowdall et al. (2005), while it's 40% lower than those announced by Egili et al. (2003) in Turkey. The mean value of  $^{40}\text{K}$  is similar to those published by Krmar et al. (2007), Popović et al. (2008), Ziembik et al. (2013). Therefore,  $^{40}\text{K}$  as a natural component of the Earth's crust can be found everywhere in the world, but in different proportions depending on the geology of each area. Finally,  $^{232}\text{Th}$  and  $^{226}\text{Ra}$  nuclides are higher than in most of the studies, except of those published by Krmar et al. (2013) and Wattanavatee et al. (2017).

**Table 5.6.** The results of other international studies performed around the world. The min, max values are presented accompanied by the mean values (in parenthesis). All the concentrations are given in  $\text{Bq kg}^{-1}$ .

Studies ( $\text{Bq kg}^{-1}$ )	place	$^7\text{Be}$	$^{210}\text{Pb}$	$^{40}\text{K}$	$^{226}\text{Ra}$	$^{232}\text{Th}$	$^{137}\text{Cs}$
(Current study)	(Northern Greece)	69-1280 (388)	147-2049 (829)	120-1060 (277)	0-126 (18)	0-66 (15)	0-590 (41)
(Kwalpuski & Sarosiek., 1988)	(Poland)	-	-	187-247	181-1303	-	65-98
(Nifontova, 1995)	(Russia)	-	-	-	-	-	80-410
(Godoy et al., 1998)	(Archipelagos)	-	17-150	32.5-138	-	-	6.3-43.7 (14)
(Oğur et al., 2003)	(Turkey)	-	200-650	-	-	-	-
(Eğilli et al., 2003)	(Turkey)	-	-	170-1471	-	-	43-139
(Karunakara et al., 2003)	(India)	235-1061 (680)	-	12-40 (22)	0-2.2 (1.5)	-	-
(Dragović et al., 2004)	(Serbia)	-	-	-	-	-	1000-6954
(Dowdall et al., 2005)	(Norway)	-	-	42-369	6-42	4-21	11-292
(Popović et al., 2008)	(Serbia)	(228)	(210)	(298)	-	-	(226)
(Marović et al., 2008)	(Croatia)	-	-	-	-	-	-955 (172)

(Krmr et al., 2009)	(Serbia)	201-920	347-885	-	-	-	(8.9)
(Celik et al., 2009)	(Turkey)	-	-	-	-	-	67-1396 (362.3)
(Cevik & Celik, 2009)	(Turkey)	-	-	345-1435 (814)	-	-	31-469 (122)
(Belivermiş & Çotuk, 2010)	(Turkey)	-	-	17-181	-	1.5-6.2	0.36-8.13
(Dragović et al., 2010)	(Serbia)			44-692	0.9-25.8	0.8-13.7	112-1248
(Sert et al., 2011)	(Turkey)	-	113-490	-	-	-	-
(Krmr et al., 2013)	(Serbia)	217-494 (314)	526-881 (695)	-	2.2-36 (24)	0-17	-
(Krmr et al., 2013)	(Thailand)	130-340 (226)	199-660 (351)	-	0-300	2.5-327 (67)	-
(Park et al., 2013)	(South Korea)	-	-	-	-	-	15-41
(Ziembik et al., 2013)	(Croatia)	-	475-1245	170-364	-	-	44-1115
(Aleksiayenak et al., 2013)	(Belarus)	-	163-575 (312)	-	-	-	5-4833 (34)
(Aleksiayenak et al., 2013)	(Slovakia)	-	330-1521 (771)	-	-	-	-
(Thinova et al., 2014)	(Czech)	-	-	-	-	-	3.8-263.1
(Krmr et al., 2014)	(Serbia)	-	280-850	-	-	-	-
(Čučulović et al., 2014)	(Serbia)	41-122	-	100-500	5-50	5-50	-
(Krmr et al., 2016)	(Serbia)	277-590	(556)	-	-	-	-
(Mitrović et al., 2016)	(Serbia)	-	-	104-386	0-39	0-37	9.4-228
(Wattanavatee et al., 2017)	(Thailand)	0-1220 (295)	135-1630 (660)	34-1157 (385)	9-432 (145)	4-422 (95)	-
(Andrović et al., 2017)	(Bosnia and Herzegovina)	-	-	-	-	-	4-1612
(Konstantinova et al., 2017)	(Lithuania)	-	-	-	-	-	1.06-43.16
(Krmr et al., 2017)	(Serbia)	260-1170 (542)	256-1480 (744)	-	-	-	-
(Zhong et al., 2019)	(China)	13-1442	47-2897	26-284	-	-	2-144
(Malikova et al., 2019)	(Siberia)	-	-	-	-	-	0-216

## 5.2 Radionuclides concentrations in soil

During the moss sampling, from the exact same locations (Figure 5.14), ninety-five (95) surface soil samples were collected, prepared and measured in the AUTH laboratory using gamma spectrometry for the determination of the radionuclides concentrations. The intensities of the 46.5 keV ( $^{210}\text{Pb}$ ), 661.6 keV ( $^{137}\text{Cs}$ ) and the 1460 keV ( $^{40}\text{K}$ ) peaks were used for the determination of the activities of the above natural and artificial radionuclides.

The study of the radionuclides activities in soil samples in combination with their activities in mosses, consists a useful tool for understanding the different environmental processes. and monitoring the radionuclides that are released into the environment. Moreover, by performing the spatial distributions of the radionuclides in soil across Northern Greece, and by achieving any possible fit between the corresponding spatial distributions in mosses and soil, will give additional information about the deposition processes of specific radionuclides in mosses.

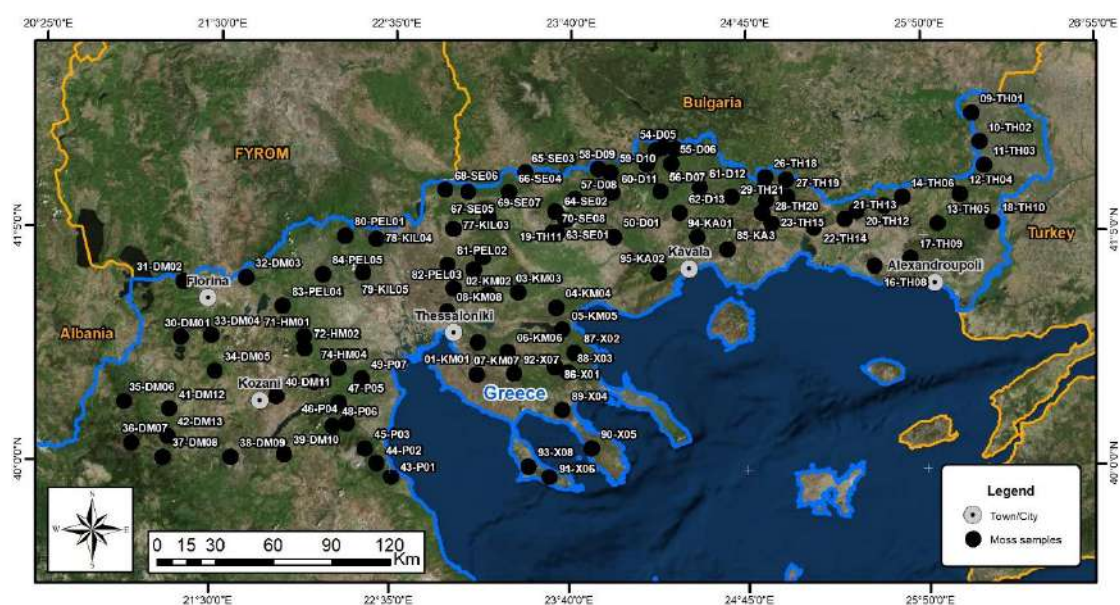


Figure 5.14. The sampling sites where the moss samples were collected from.

### 5.2.1 Spatial distributions of radionuclides in soil

The origin of the radionuclides  $^{137}\text{Cs}$ ,  $^{40}\text{K}$  and  $^{210}\text{Pb}$  has already been mentioned with details in the paragraph 5.1. The concentrations of the above radionuclides with their uncertainties are presented in Appendix, in Table J1. The descriptive analysis of the radionuclides activities in soil was performed and is presented in Table 5.7. The spatial distributions of the under studied radionuclides are shown in Figures 5.15- 5.17.

**Table 5.7.** The results of the descriptive analysis of the radionuclides concentrations in soil ( $\text{Bq kg}^{-1}$ ).

	<i>Cs-137</i>	<i>Pb-210</i>	<i>K-40</i>
Min	0.34±0.26	11.46±1.00	52.79±2.61
Max	2568.8±64.5	1380.87±55.45	1148.30±43.85
Median	17.57	80.47	479.23
Mean	72.96	123.54	512.45
Std Dev.	270.08	165.11	250.74
Kurtosis	79.69	37.32	-0.09
Skewness	8.63	5.46	0.45

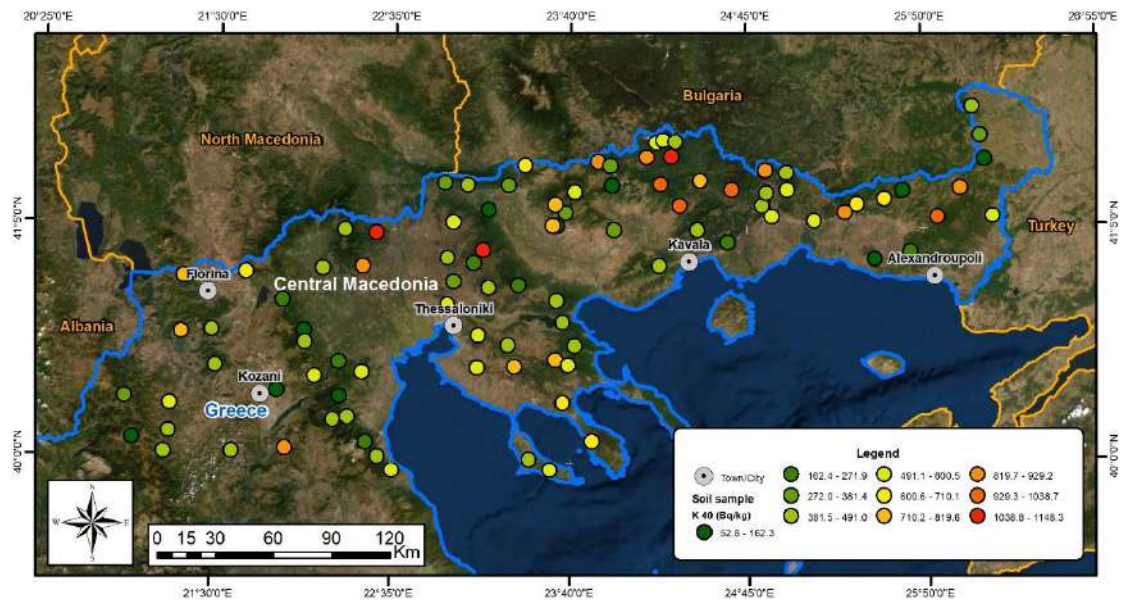


**Figure 5.15.** The spatial distribution of  $^{40}\text{K}$  ( $\text{Bq kg}^{-1}$ ) in soil samples across Northern Greece.

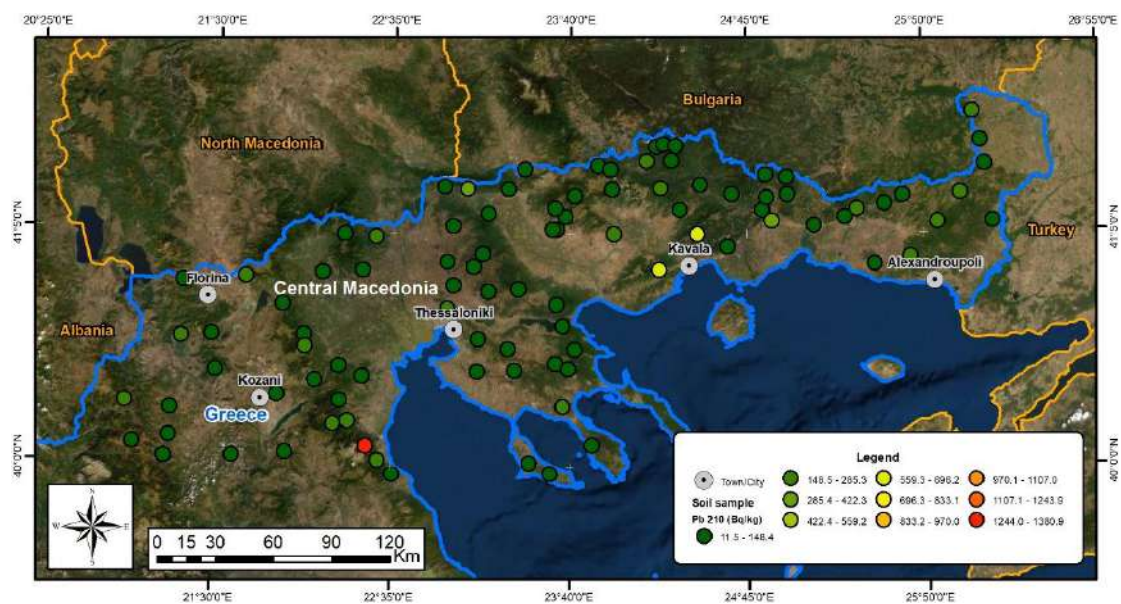


**Figure 5.16.** The spatial distribution of  $^{210}\text{Pb}$  ( $\text{Bq kg}^{-1}$ ) in soil samples across Northern Greece.

There is a variance in the activity concentrations of  $^{40}\text{K}$  in soil, but according to its spatial distribution, no specific sampling sites are highlighted. On the other hand,  $^{210}\text{Pb}$  spatial distribution does not present such a wide variance, despite the fact that some sites show much higher concentrations than the rest ones (e.g. the area of Kavala and Olympus). The different concentrations of both  $^{40}\text{K}$  and  $^{210}\text{Pb}$  in soil samples are based on the geological characteristics and the soil structure of each area. Although, there is no correlation between these two radionuclides. No special fit is identified between the concentrations of  $^{40}\text{K}$  or  $^{210}\text{Pb}$  in mosses and the corresponding soil samples (Figures 5.3 and 5.6).

The last radionuclide that was measured in soil samples is  $^{137}\text{Cs}$ . Cesium, as it has been mentioned in the previous paragraph, is an artificial radionuclide and was released in the environment due to the nuclear weapon tests and the Chernobyl accident. It is known that when  $^{137}\text{Cs}$  is deposited on soil, it becomes strongly absorbed by clay fractions, clay minerals and organic matter, and can migrate quite slowly in soil. Its mobility and thus its migration rate can be decreased by increased contents in clay fraction, organic matter and Fe and Mn contents (Arapis et al., 1997). Moreover, the soil organic matter, and especially this characterized by high molecular weight, is likely to accumulate a large proportion of  $^{137}\text{Cs}$  and therefore it influences its relative low mobility (Grytsyuk et al., 2006).

The spatial distribution of  $^{137}\text{Cs}$  is presented in Figure 5.17. Some areas present really high concentrations of  $^{137}\text{Cs}$  while others have very low concentrations. The areas with high concentrations of  $^{137}\text{Cs}$  in soil in the current study match with the areas that were characterized as the most influenced after the accident, and are confirmed by the study of Petropoulos et al. (2001) (Figure 5.19). The distribution of  $^{137}\text{Cs}$  across the Greek territory was affected by the precipitation events and the dry depositions of  $^{137}\text{Cs}$  that followed during the passage of the radioactive cloud through our country after the Chernobyl accident.

Except of this agreement between the sites characterized by high  $^{137}\text{Cs}$  concentrations of the current study and the previous one, there is a similar fit between the concentrations of  $^{137}\text{Cs}$  in soil and moss samples across Northern Greece. By looking at both their spatial distributions (Figure 5.17 and 5.18), someone can observe a match between these sites. This indicates that the origin of  $^{137}\text{Cs}$  in mosses is the dispersed and resuspended soil particles from the surrounding area of mosses, and their deposition on them is favored by the arid climate that characterizes Greece. Finally, there is no correlation between the radionuclides  $^{137}\text{Cs}$ ,  $^{40}\text{K}$  and  $^{210}\text{Pb}$  measured in soil samples.

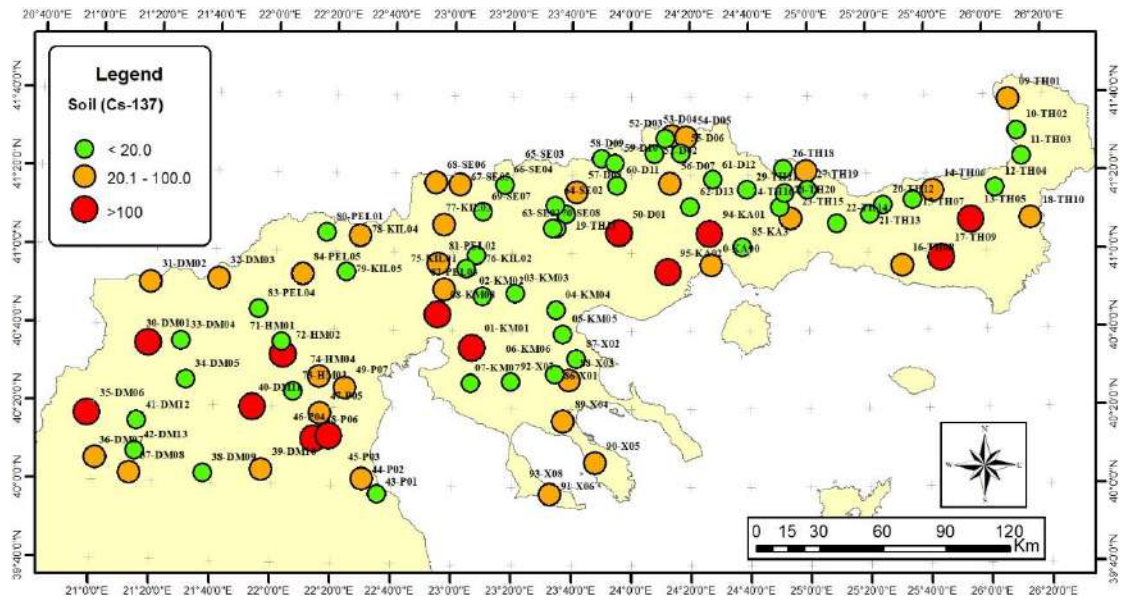


Figure 5.17. The spatial distribution of  $^{137}\text{Cs}$  (Bq  $\text{kg}^{-1}$ ) in soil samples across Northern Greece.

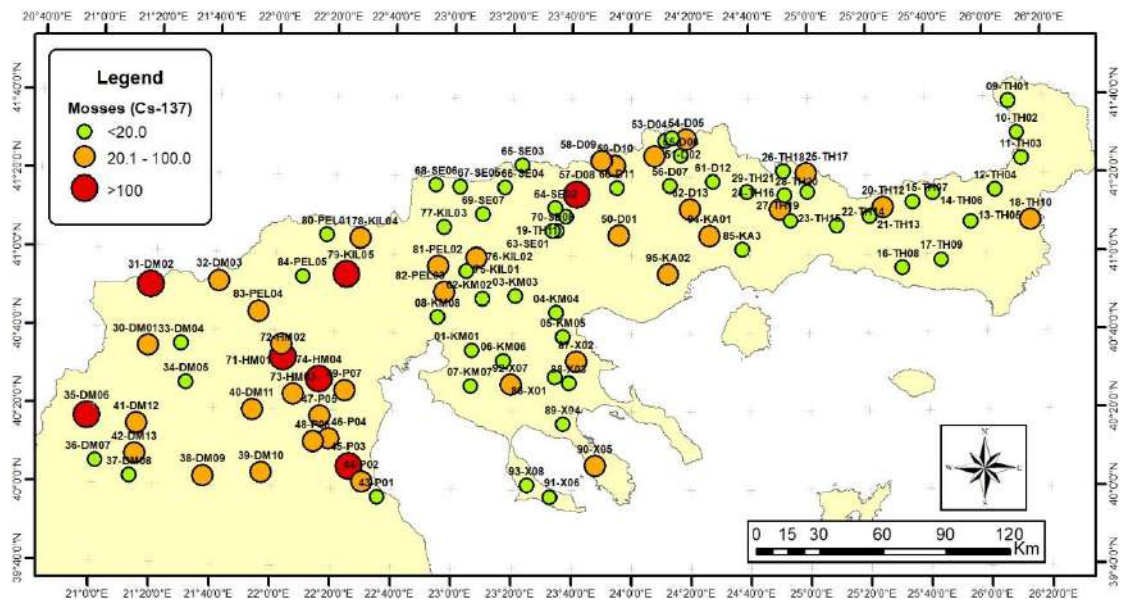
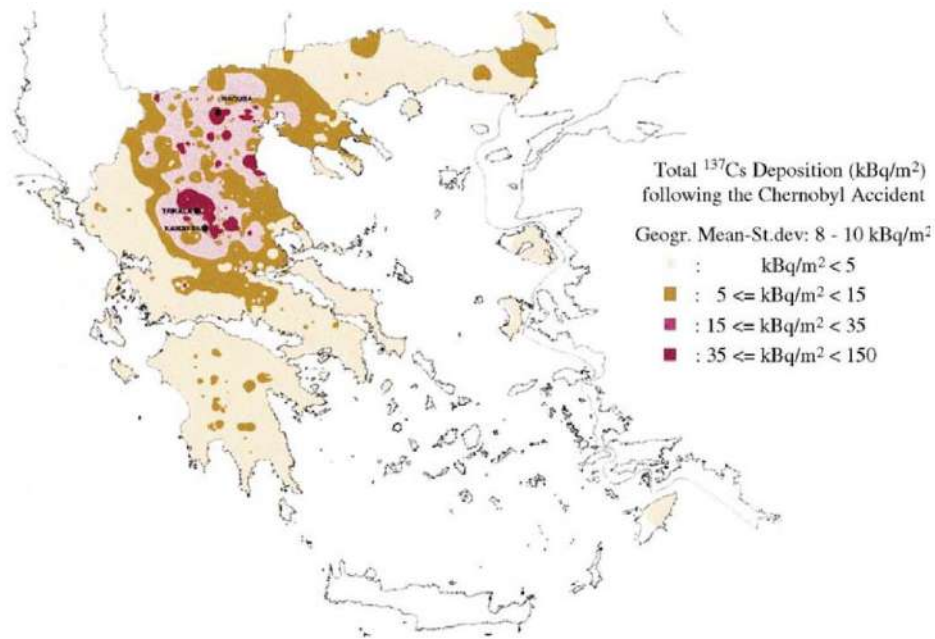


Figure 5.18. The spatial distribution of  $^{137}\text{Cs}$  (Bq  $\text{kg}^{-1}$ ) in moss samples across Northern Greece.



**Figure 5.19.** The total deposition of  $^{137}\text{Cs}$  (nuclear weapons tests, Chernobyl accident, ...) in Greece according to Petropoulos et al. (2001).

### 5.2.2 Transfer of resuspended soil to mosses

Radionuclides that occur naturally in soil are incorporated metabolically into plants. The artificial ones have the same behavior. In addition to root uptake, direct deposition may occur on foliar surfaces, and when this happens the radionuclides may be absorbed metabolically by the plants (Papastefanou et al., 1999a). In the case of mosses, where no roots exist, the root uptake of radionuclides is impossible, but radionuclides can be transferred to mosses through the atmospheric deposition. Thus, the determination of the transfer of the radionuclides from soil to mosses is considered important.

The transfer of radionuclides from soil to plants is measured by the Transfer Factor (Papastefanou et al., 1999a; Jalil et al., 2002; Tsikritzis, 2002; IAEA 2006; Eslava-Gomez and Brown, 2013; Elywa et al., 2016; Tuo et al., 2017; Ivanić et al., 2019; Li et al., 2019; Ibikunle et al., 2019), which reveals the relationship between the radionuclide contents in soil and plant (Sarap et al., 2014). In the case of mosses, the transfer of resuspended soil to moss bodies for radionuclides is calculated according to the ratio:

$$\frac{A_{Moss}}{A_{Soil}}$$

where

$A_{Moss}$  is the radionuclide's activity concentration in moss sample in  $\text{Bq kg}^{-1}$

$A_{Soil}$  is the radionuclide's activity concentration in soil in  $\text{Bq kg}^{-1}$ .

The transfer of resuspended soil to mosses and their uncertainties concerning all the sampling sites are presented in Appendix in Table K1. In Table 5.8, the descriptive analysis of the transfer values is shown.

**Table 5.8.** The results of the descriptive analysis of the radionuclides transfer values of resuspended soil to moss are presented.

	<i>Cs-137</i>	<i>Pb-210</i>	<i>K-40</i>
Min	0	0.8±0.08	0.16±0.01
Max	531±209	86.73±8.73	4.51±0.47
Median	0.92	9.85	0.56
Mean	8.93	11.92	0.74
Std Dev.	55.2	10.73	0.69
Kurtosis	87.89	24.68	14.66
Skewness	9.25	3.96	3.44

The transfer of resuspended soil to mosses of the radionuclides  $^{137}\text{Cs}$  and  $^{210}\text{Pb}$  were found to be high in the majority of the studied samples with a mean value in the order of 8.93 and 11.92 respectively. High values of  $^{210}\text{Pb}$  transfer values are observed in the cases where the corresponding concentrations in moss samples are higher than in soil samples, indicating that the majority of lead that was deposited on mosses came from the decay of  $^{222}\text{Rn}$  in the atmosphere. High values of  $^{137}\text{Cs}$  transfer values correspond to sites where  $^{137}\text{Cs}$  concentrations in soil are low, while  $^{40}\text{K}$  concentrations are high. These sites reveal that these two radionuclides are inversely proportional (Papastefanou et al., 1999a; Tsikritzis, 2002; Tsigaridas, 2014) and this kind of relationship can also be observed in their transfer factor values.

The relationship between each radionuclide concentration in soil and their transfer values is presented in the following scatter plots (Figure 5.20-5.21). There is an exponential relationship between  $^{210}\text{Pb}$  and  $^{40}\text{K}$  nuclides and the transfer value which points out that the transfer of resuspended soil to mosses decreases with increasing soil activity concentration. Thus, the results show that the soil-to-plant transfer values are higher at low soil concentrations, and decrease with an increasing soil concentration. For  $^{137}\text{Cs}$ , no special relationship could be extracted between its activity and transfer factor values.

Finally, as it was already said, there is no relationship between the radionuclides in soil and mosses. The lack of any kind of relationship between the activities in soil and mosses points out that the existence of different factors (moisture, organic content matter, soil structure) that influence the “uptake” from soil to mosses (no rooting system-just through the atmospheric deposition).

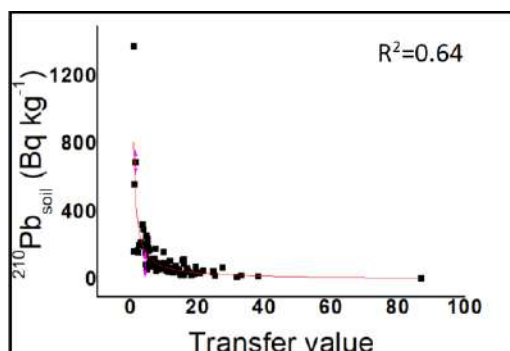


**Figure 5.20.** The scatter plot between  $^{210}\text{Pb}$  in soil and its transfer value of resuspended soil to mosses.

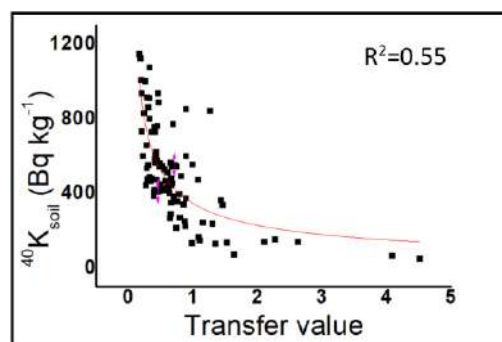


**Figure 5.21.** The scatter plot between  $^{40}\text{K}$  in soil and its transfer value of resuspended soil to mosses.

### 5.2.3 Comparison with other data in the literature

In the literature there are a lot of studies concerning the activity concentrations of radionuclides in soil. In the Greek territory and since the Chernobyl accident a lot of studies have been conducted (Simopoulos, 1989; Antonopoulos-Domis et al., 1990; Papastefanou et al., 1999a; Petropoulos et al., 2001; Anagnostakis et al., 1996; Tsikritzis et al., 2002, 2008; Manolopoulou et al., 2003; Arapis and Karandinos, 2004; Papaefthymiou et al., 2004; Florou et al., 2007; Psychoudaki and Papaefthymiou, 2008; Kritidis et al., 2012; Tsigaridas et al., 2014; Kourtidis et al., 2015).

The mean value of  $^{40}\text{K}$  is around 1.5 times higher than the values reported by Tsikritzis (2002) and Anagnostakis et al. (1996) results for the Greek soils, while they are similar to those announced by Psychoudaki and Papaefthymiou (2008). Cesium mean value and its transfer factor from soil to mosses are 4 times to one order of magnitude lower than those recorded by Tsikritzis (2002) and Sawidis et al. (2010), whereas the max value is almost 10% higher compared to Arapis and Karandinos results (2004). So, the levels of  $^{137}\text{Cs}$  nowadays is one order of magnitude lower than it was reported immediately after the accident, due to radioisotope decay as well as to the resuspension factor, movement in soils due to chemical or biological processes and other physical processes, such as erosion.

Across the world, there are many studies investigating the radioactivity in soil and with which the results of the current study can be compared (Dragović et al., 2004; Fujiyoshi and Sawamura, 2004; Dowdall et al., 2005; Popovic et al., 2008; Celik et al., 2009; Cevik and Celik, 2009; Matissof et al., 2011; Park et al., 2013; Krmar et al., 2014; Mitrović et al., 2016; Ivanić et al., 2019; Zhong et al., 2019). In the current study, the mean  $^{40}\text{K}$  concentration in soil is 17% higher than the mean concentration reported by UNSCEAR 2000, 1.5 higher than those from Dragović et al. (2010) and Popovic et al. (2010) studies, whereas it is 10 and 30% lower than Mitrović et al., (2016) and Celik et al. (2009) respectively.

Lead-210 max concentration is one order of magnitude higher than those reported by Krmar et al. (2014), while it is 3 times lower compared to Zhong (2019) measurements. The soil structure and its geological characteristics influence the terrestrial radionuclides concentrations and explain these variances. The mean concentration of the artificial nuclide  $^{137}\text{Cs}$  is 2 to 6 times lower than the corresponding activities published by Popovic et al. (2008;2010), Celik et al. (2009), Dragović et al. (2010) and Ivanić et al. (2019). The differences that are observed in the cesium concentrations, are based on how much each area was influenced by the Chernobyl accident and the nuclear weapon tests that occurred in the previous century. Finally, based on the possible erosion and resuspension events, the climate of each area and other factors that may influence the horizontal and vertical distribution of  $^{137}\text{Cs}$ , a fluctuation in its concentration is totally justified.

## Chapter 6

## Conclusions

Mosses are ideal bioindicators of trace elements and radionuclides. They are widely used for monitoring their deposition from the atmosphere, as they do not have roots and all the nutrients and water they need, are taken directly from wet and dry deposition. They can grow up in all the environments but not all the moss species are found everywhere.

In Northern Greece, the most widespread moss species is *Hypnum cupressiforme* Hedw., a pleurocarpous moss which is usually found living in forests, forming thick mats on the forest floor (Tsakiri, 2009). It can get easily wet due to the fact that it grows horizontally on the substrate. Moreover, *Hypnum cupressiforme* Hedw. moss species, is the most studied and analyzed moss species in the ICP Vegetation Programme (Frontasyeva et al., 2015), in which Greece participates for the first time with our group consisted by Professor Dr. Alexandra Ioannidou and Dr. Evdoxia Tsakiri. These characteristics made it ideal for biomonitoring in the 2015/2016 moss survey coordinated by the Joint Institute of Nuclear Research (JINR; Dubna, Russian Federation), under the auspice of the ICP Vegetation Programme.

The current survey was conducted at the end of summer till middle of autumn of 2016. Ninety-five moss samples of *Hypnum cupressiforme* Hedw. were collected from the Regions of West, Central and East Macedonia & Thrace. After sampling, mosses were cleaned manually and were prepared for ENAA and gamma ray measurements for the determination of trace elements and radionuclides respectively.

The elemental concentrations of forty-four (44) trace elements (Al, As, Ni, V, Cr, Zn, Fe, Br, Cl, I, Mg, Na, K, Sc, Ti, Mn, Co, Se, Rb, Sb, Au, Th, U, Si, Sr, Ca, Zr, Cs, Ba, La, Ce, Nd, Sm, Gd, Tb, Dy, Tm, Yb, Lu, Hf, Ta, In, Mo, Ag) were measured and consist the first concentrations that are recorded in mosses in the Greek territory and are included in the European moss data base. The concentrations of Al, As, Ni, V, Cr, Zn and Fe range between 1350-46100  $\mu\text{g g}^{-1}$ , 0.52-17.90  $\mu\text{g g}^{-1}$ , 1.72-90.20  $\mu\text{g g}^{-1}$ , 2.61-33.4  $\mu\text{g g}^{-1}$ , 2.04- 222  $\mu\text{g g}^{-1}$ , 14.60-282  $\mu\text{g g}^{-1}$  and 1010-28700  $\mu\text{g g}^{-1}$  respectively. Higher elemental concentrations are observed in mosses collected from the surface and not near roots, indicating that most of them are transferred to mosses though the resuspended soil.

Additional to the study of ninety-five moss samples collected from the vicinity of Northern Greece, a special case study was also performed, including trace elements measurements in ten moss samples collected from the area of Skouries, close to active mining facilities. The elemental concentrations of Al, As, Ni, V, Cr, Zn and Fe range between 7170- 17300  $\mu\text{g g}^{-1}$ , 7.5- 15.4  $\mu\text{g g}^{-1}$ , 52- 138  $\mu\text{g g}^{-1}$ , 14- 30  $\mu\text{g g}^{-1}$ , 66- 200  $\mu\text{g g}^{-1}$ , 35- 72  $\mu\text{g g}^{-1}$  and 6350- 14300  $\mu\text{g g}^{-1}$  respectively. The moss species *Isoetium alopecuroides* and *Dicranum scoparium* present the highest elemental concentrations of As, Al, Co, Fe, V and Cr, Mg, Ni, Sb respectively. The concentrations of Au, Mn, and Ni in Skouries mosses, are much higher than the concentrations of all ninety-five (95) samples collected from Northern Greece, highlighting the impact of the activities that occur in the gold mine of Skouries.

Different studies have been occurred in the area of Skouries using different kind of samples: sediment (Papa et al., 2016), surface water (Chantzi et al., 2016), edible fish (Lazaridou- Dimitriadou et al., 2004), limpets (Kelepertsis, 2013) and soil (Kelepertsis et al., 2006; Argyraki et al., 2017). In most of these studies, the elemental concentrations that were determined were high enough and sometimes they exceeded the global mean values (Kelepertsis et al., 2006; Chantzi et al., 2016). Although, there is no study in the literature that uses moss as a matrix for the determination of the elemental concentrations in the area. Therefore, this moss survey will add useful data in the literature and it could also be the basis for future moss bioindicator studies in the area.

In the rest part of Greece only a limited number of studies exist concerning the atmospheric deposition of trace elements in mosses. This survey is the first attempt of studying the atmospheric deposition of trace elements by using mosses collected in such a big territory in Greece, during a five years' period. The present study verifies the results of Yurukova et al. (2009) investigation regarding the pollutants' chemical composition in the region of Northeastern part of Greece, next to the Bulgarian borders. Areas that are characterized by high concentrations of Al, As, Fe and V are observed in both of the studies, with some differences concerning the concentration levels of each element.

Furthermore, the concentrations of Cr, Mn and Ni elements in the region of West Macedonia and close to the coal power plants in the basin of Ptolemaida are around 30% lower than the concentrations reported by Tsikritzis (2002) study. The same reduction of the order up to 50% is noticed between the results of the current study and those announced by Tsigaridas (2014). Our results do not agree with the conclusions of the study conducted by Saitanis et al. (2012) regarding the origin of Mn in mosses. In our research, Mn is associated to antropogenic activities like mining activities in the regions enriched in Mn, while in Saitanis study, Mn is assumed to be originally present in mosses as an essential element.

According to the 2005/2006 moss survey results, Greece presents lower maximum concentrations of Zn, Mn, Co than Norway, while Ni levels are lower than Norway's, Poland's and Albania's and similar to the Bulgarian's ones. Chromium in Greece is higher than almost all the countries, except of Serbia which has similar median value and Poland which is 30% higher. Al and Sb min values are 5% and 50% times lower in Greece than Republic of North Macedonia. Finally, the levels of V and Zn are comparable to those in Serbia and Croatia.

A possible transboundary transfer of the elements Fe, V, Zn, As, Co, Ni and Cr is observed close to the Greek- Republic of North Macedonian borders (around the Kavadarci region), as well as in the region between Bulgarian and Greek borders (transfer especially of Zn element).

In order to identify the possible sources of the elements in mosses, the Positive Matrix Factorization (PMF) analysis was performed by means of the PMF 5.0 model. Based on different criteria, and after running the model for 100 times for different number of factors (4 to 10) each time, five different factors-sources were extracted: *The Soil Dust, the Aged Sea Salt, the Road Dust, the Lignite Power Plant and the Mn-rich source.*

The *first* source is the Soil Dust source and includes the elements Mg, Al, Ti, Si, Ca, Th, Ba, La, K and Fe. More than 40% of the mass of Si, Ca, Cl, K, and Mg is assigned to this Soil dust source. All these elements were transferred to mosses through the resuspension of the soil from fields by local winds. The Aged sea salt factor is the *second* source and it is represented by the elements Na, Rb, Sr, Hf and Ta, with Na contributing the most. The *third* factor contains high loadings of Sb and As and is characterized as the dispersed Road dust source. The *fourth* factor is identified as the Lignite power plant source where there is high contribution of Ni, Cr and Co. This factor could also be related to heavy oil combustion emissions. The *last* factor that was produced by the model, is characterized as the Mn-rich source and it is possibly connected with mining activities. The soil dust and the sea salt sources contribute more than 60% to many of the moss samples. Similar relative contributions of the road dust source occur to almost all mosses.

Two areas can be distinguished according to the relative source contribution for each sampling site. The first one is the region of W. Macedonia, where the Ptolemaida-Amyntaio complex Lignite power plants are located and are characterized by high concentrations of Ni, V, Cr and Co. The second one is the area of Skouries, where there are high contributions of the Mn-rich source, the lignite power plant source as well as the road dust source. The majority of the elements is deposited on mosses through the resuspended soil, which is also verified. Finally, the soil dust source contributes the most in all mosses (52%).

The elemental concentrations in soil samples collected from the same sampling sites like mosses, were also determined. The elements Al, K, Si and Ti have similar concentrations in almost all sites, proving that there is no impact of anthropogenic activities on them and the majority are just typical components of the soil. This is also verified by the comparison of the chemical composition of the soil samples with the one of a reference's chemical composition. The areas that present high concentrations of Ni, Mn, Fe, Mg and Cr in mosses correspond to those with high concentrations in soil, indicating that the origins of the trace elements in both of the matrices are the same. These results are also verified by the calculation of the Transfer Factor of resuspended soil to mosses, which is a useful tool for the identification of the "soil dust" elements.

In Greek territory, the elemental concentrations of Zn, Cu and As in soil are found in lower levels than those provided by Nikolaidis et al. (2013) and Argyraki-Kelepertzis, (2014), while the elements Al, Ca, Fe, Mg, Si, Ti and K present higher concentrations than those reported by Pentari et al. (2006), Papastergios et al. (2011), Skordas et al. (2013) and Botsou et al. (2016). On the other hand, the mean concentrations of the elements Mn, Cr, Zn, As and Ni are higher (1.5 to 5 times) than the worldwide average soil concentrations (Kabata-Pendias; 2011), while they are similar to the European mean values of the topsoils. The different natural processes and the anthropogenic activities are those which influence the elemental concentrations in soil of each area.

The activity concentrations of  $^7\text{Be}$ ,  $^{210}\text{Pb}_{\text{uns}}$ ,  $^{40}\text{K}$ ,  $^{232}\text{Th}$ ,  $^{226}\text{Ra}$  and  $^{137}\text{Cs}$  in mosses are also studied. The cosmogenic nuclide  $^7\text{Be}$  ranges from 69 to 1280 Bq kg<sup>-1</sup>, while  $^{210}\text{Pb}_{\text{uns}}$  ranges from between 147 to 2049 Bq kg<sup>-1</sup>. The terrestrial nuclides  $^{40}\text{K}$ ,  $^{232}\text{Th}$  and  $^{226}\text{Ra}$  range between 120 to 1060 Bq kg<sup>-1</sup>, 0 to 66 Bq kg<sup>-1</sup> and 0 to 126 Bq kg<sup>-1</sup> respectively.

The artificial nuclide  $^{137}\text{Cs}$  is found between 0 to  $590 \text{ Bq kg}^{-1}$ . There is no correlation between the altitude, the temperature and the above radionuclides, as well as between precipitation or any other meteorological characteristics and their activities. No seasonal variability could be estimated for  $^7\text{Be}$  and  $^{210}\text{Pb}_{\text{uns}}$ , as all the samples were collected during a specific time interval (summer 2016).

The cosmogenic nuclide  $^7\text{Be}$  ends up in mosses through wet and dry deposition of aerosols to which it was attached right after its formation in the troposphere. The radionuclide  $^{210}\text{Pb}_{\text{uns}}$  in mosses comes from the decay of radon in the air and not in the soil and after its release into the atmosphere, it follows the path of the aerosols to which it is attached and it is deposited on mosses mainly through sedimentation, and in some cases through rainfall.  $^{40}\text{K}$ , is placed on mosses via the soil dust particles that are dispersed in the atmosphere through the wind, while  $^{232}\text{Th}$  and  $^{226}\text{Ra}$  are deposited on mosses both through soil particles and aerosol deposition. The artificial nuclide  $^{137}\text{Cs}$  is deposited on mosses through the resuspended soil particles. The arid climate of Greece favors the transfer of soil dust particles even in far distances.

The correlations between the radionuclides is also studied. According to Pearson Correlation and to Principle Component Analysis, the aforementioned radionuclides could be distinguished into three groups- components, based on their origin and correlations. The first component includes the radionuclides  $^7\text{Be}$ ,  $^{210}\text{Pb}_{\text{uns}}$ ,  $^{210}\text{Pb}_{\text{tot}}$  which are deposited on mosses through dry deposition and precipitation. The nuclides  $^{226}\text{Ra}$ ,  $^{232}\text{Th}$  and  $^{40}\text{K}$  are loading quite nicely on the second component, while  $^{137}\text{Cs}$  characterize the last component. The Cluster Analysis results reveal the same three groups- clusters as the previous analysis.

Mosses were collected from different substrate types (rocks, branches, surface soil and near roots). The substrate type influences their activities. Slight differences can be observed in the activity concentrations of the studied radionuclides. For example, the cosmogenic nuclide  $^7\text{Be}$  presents higher activities in mosses collected from the ground surface than those that were collected near roots. The nuclides  $^{210}\text{Pb}$ ,  $^{226}\text{Ra}$ ,  $^{232}\text{Th}$  do not present any significant difference between those collected from surface and near roots. There is a homogeneity for the concentrations of the artificial radionuclide  $^{137}\text{Cs}$ , while  $^{40}\text{K}$  is found in higher concentrations in those mosses that were picked up mostly near roots. The ratio of the activity concentrations between mosses taken from the surface versus roots are higher than 1 for  $^7\text{Be}$ , around 1 for  $^{210}\text{Pb}$ ,  $^{232}\text{Th}$  and  $^{226}\text{Ra}$ , and lower than 1 for  $^{137}\text{Cs}$ , indicating the association of the last one to the dispersed soil dust particles.

In the literature a few studies are found about the activities concentrations of radionuclides in mosses in Greek territory. The concentrations of  $^{137}\text{Cs}$  are much lower than in most of the studies (up to 1 order of magnitude lower). However, the concentrations of  $^{40}\text{K}$  and  $^{226}\text{Ra}$  are higher (more than 3 times higher) than those reported by Tsikritzis (2002) and Tsigaridas (2014). Concerning other international studies,  $^7\text{Be}$  and  $^{210}\text{Pb}$  nuclides are found more than 2 times higher than in Serbia's and India's mosses (Krmr et al. 2017; Karanakura et al. (2013), while  $^{210}\text{Pb}$  is 40% lower than in China (Zhong et al., 2019).  $^{137}\text{Cs}$  concentrations are more than two times higher than in the other studies with some exceptions like in the studies of Dragović et al.

(2004; 2010), Marović et al. (2008) and Celik et al. (2009). The concentrations of  $^{40}\text{K}$  vary in most of the countries depending on the soil properties of each area.

Additionally, the radionuclides concentrations in surface soil samples are also studied. The concentrations of  $^{137}\text{Cs}$  range between 0.34 to 2569  $\text{Bq kg}^{-1}$ , of  $^{40}\text{K}$  between 52.79 to 1148  $\text{Bq kg}^{-1}$ , and of  $^{210}\text{Pb}$  from 11.46 to 1381  $\text{Bq kg}^{-1}$ . No special fit is identified between the concentrations of  $^{40}\text{K}$  or  $^{210}\text{Pb}$  in mosses and the corresponding soil samples. On the other hand, there is a match between areas that present high concentrations of  $^{137}\text{Cs}$  in soil and mosses of the current survey with those areas that were characterized as the most influenced after the Chernobyl accident (Petropoulos et al., 2001). This indicates that the origin of  $^{137}\text{Cs}$  in mosses is the dispersed and resuspended soil particles from the surrounding area of mosses. Moreover, there is no correlation between the radionuclides  $^{137}\text{Cs}$ ,  $^{40}\text{K}$  and  $^{210}\text{Pb}$  measured in soil samples. The calculation of the Transfer Factor of resuspended soil to mosses verifies the above results. The resuspension of the soil is the main source of trace elements and nuclides in mosses, which is also verified by the PMF model.

The data in soil of the current study are compared with other results in Greece and around the world.  $^{40}\text{K}$  is higher than the mean value reported for Greek soils (Anagnostakis et al., 1996) as well as the international levels announced by UNSCEAR 2000.  $^{137}\text{Cs}$  nowadays is one order of magnitude lower than it was reported immediately after the accident (both in Greece and around the world), due to radioisotope decay as well as to the resuspension factor and other physical processes, such as erosion. Finally, lead-210 max concentration is one order of magnitude higher than those reported by Krmar et al. (2014), while it is 3 times lower compared to Zhong (2019) measurements. The soil structure and its geological characteristics influence the terrestrial radionuclides concentrations and explain these variances.

To sum up, moss and soil samples were collected from the vicinity of Northern Greece. The determination of trace elements and radionuclides concentrations in both matrices was simultaneously achieved. Their detailed spatial distributions reveal the areas of interest. The PMF model was run for the determination of the origins of trace elements in mosses, while the Principle Component Analysis in combination with the Cluster Analysis grouped together the radionuclides of the same origins deposited on mosses. Attention should be given to the area of Skouries where the impact of the mining activities on the area is revealed.

This thesis consists the basis for future research on trace elements and radionuclides concentrations on mosses in the Greek territory. Also, gives the possibility of comparing data between the different countries in Europe and around the world, while putting a small piece in the puzzle of the European moss database concerning the accumulation of trace elements in mosses. Some suggestions for the future are: the collection of mosses in the whole territory of Greece for the same purposes, covering areas that couldn't be afforded during this study and the use of mosses in perforated bags or in other mediums for measurements in areas where mosses cannot grow up naturally.

## References

- Adamo, P., Giordano, S., Sforza, A., Bargagli, R., 2011. Implementation of airborne trace element monitoring with devitalized transplants of *Hypnum cupressiforme* Hedw.: assessment of temporal trends and element contribution by vehicular traffic in Naples city. *Environ Pollut*, 159,1620–1628.
- Aleksiyayenak, Yu. V., Frontasyeva, M. V., Florek, M., Sykora, I., Holy, K., Masarik, J., Brestakova, L., Jeskovsky, M., Steinnes, E., Faanhof, A., Ramatlhape, K. I., 2013. Distributions of  $^{137}\text{Cs}$  and  $^{210}\text{Pb}$  in moss collected from Belarus and Slovakia. *Journal of Environmental Radioactivity*, 117, 19-24.
- Almeida, S. M., Pio, C. A., Freitas, M. C., Reis, M. A., Trancoso, M. A., 2005. Source apportionment of fine and coarse particulate matter in a sub-urban area at the Western European Coast. *Atmospheric Environment*, 39, 3127–3138.
- Alloway, B.J., 1995. *Heavy Metals in Soils*. Blackie Academic and Professional, London.
- Alonso Hernández, C. M., Cartas Águila, H., Díaz Asencio, M., Muñoz Caravaca, A., 2004. Reconstruction of  $^{137}\text{Cs}$  signal in Cuba using  $^7\text{Be}$  as tracer of vertical transport processes in the atmosphere. *Journal of Environmental Radioactivity* 75,133–142.
- Anagnostakis, M.J., Xinis, E.P., Simopoulos, S.E., Angelopoulos, M.G., 1996. Natural radioactivity mapping of Greek surface soils. *Environmental International*, 22 (1), S3-S8.
- Aničić, M., Frontasyeva, M.V., Tomašević, M., Popović, A., 2007. Assessment of Atmospheric Deposition of Heavy Metals and Other Elements in Belgrade Using the Moss Biomonitoring Technique and Neutron Activation Analysis. *Environ Monit Assess*, 129,207–219. DOI 10.1007/s10661-006-9354-y
- Aničić, M., Tasić, M., Frontasyeva, M.V., Tomašević, M., Rajšić, S., Mijić, Z., Popović, A., 2009a. Active moss biomonitoring of trace elements with *Sphagnum girgensohnii* moss bags in relation to atmospheric bulk deposition in Belgrade, Serbia. *Environmental Pollution* 157, 673–679.
- Aničić, M., Tomašević, M., Tasić, M., Rajšić, S., Popović, A., Frontasyeva, M.V., Lierhagen, S., Steinnes, S., 2009b. Monitoring of trace element atmospheric deposition using dry and wet moss bags: Accumulation capacity versus exposure time. *Journal of Hazardous Materials* 171, 182–188.
- Aničić Urošević, M., Vuković, G., Tomašević, M., 2017. *Biomonitoring of Air Pollution Using Mosses and Lichens, A Passive and Active Approach, State of the Art Research and Perspectives*. Nova Science Publishers, New York, USA, ISBN: 978-1-53610-212-3.
- Andrović, F., Damjanović, A., Adrović, J., Kamberović, J., Hadžiselimović, N., 2017. Study of  $^{137}\text{Cs}$  concentration activity in mosses of Bosnia and Herzegovina. *International Journal of Modern Biological Research*, 5, 32-41.

Anttila, P., Paatero, P., Tapper, U., Järvinen, O., 1995. Source identification of bulk wet deposition in Finland by positive Matrix Factorization. *Atmospheric Environment*, 14, 1705–1718.

Antoniadis, V., Golia, E.E., Liu, Y.T., Wang, S.L., Shaheen, S.M., Rinklebe, J., 2019. Soil and maize contamination by trace elements and associated health risk assessment in the industrial area of Volos, Greece. *Environment International*, 124, 79–88. <https://doi.org/10.1016/j.envint.2018.12.053>

Antonopoulos-Domis, M., Clouvas, A., Gagianas, A., 1990. Derivation of Soil to Plant Transfer Factors of Radiocesium in Northern Greece after the Chernobyl Accident, and Comparison with Greenhouse Experiments. *Environmental Pollution*, 68, 119-128.

Arapis, G.D., Petrayev, E., Shagalova, E., Zhukova, O., Sokolik, G., Ivanova, T., 1997. Effective migration velocity of  $^{137}\text{Cs}$  and  $^{90}\text{Sr}$  as a function of type of soils in Belarus. *Journal of Environmental Radioactivity*, 34 (2), 171-185.

Arapis, G.D., Karandinos, M.G., 2004. Migration of  $^{137}\text{Cs}$  in the soil of sloping semi-natural ecosystems in Northern Greece. *Journal of Environmental Radioactivity*, 77, 133–142.

Argyaki, A., Kelepertzis, E., 2014. Urban soil geochemistry in Athens, Greece: the importance of local geology in controlling the distribution of potentially harmful trace elements. *Sci. Total Environ.* 482-483, 366–377.

Argyaki, A., Boutsis, Z., Zotiadis, V., 2017. Towards sustainable remediation of contaminated soil by using diasporicbauxite: Laboratory experiments on soil from the sulfide mining village of Stratoni, Greece. *Journal of Geochemical Exploration*, 183, 214-222.

Argyaki, A., Kelepertzis, E., Botsou, F., Paraskevopoulou, V., Katsikis, I., Trigoni, M., 2018. Environmental availability of trace elements (Pb, Cd, Zn, Cu) in soil from urban, suburban, rural and mining areas of Attica, Hellas. *Journal of Geochemical Exploration*, 187, 201–213.

Bačeva, K., Stafilov, T., Šajn, R., Tănăselia, C., 2012. Moss biomonitoring of air pollution with heavy metals in the vicinity of a ferronickel smelter plant. *J Environ Sci Health A*, 47, 645–656.

Barandovski, L., Cekova, M., Frontasyeva, M. V., Pavlov, S. S., Stafilov, T., Steinnes, E., Urumov, V., 2008. Atmospheric deposition of trace element pollutants in Macedonia studied by the moss biomonitoring technique. *Environ Monit Assess*, 138, 107-118.

Barandovski, L., Frontasyeva, M. V., Stafilov, T., Šajn, R., Pavlov, S., Enimiteva, V., 2012. Trends of atmospheric deposition of trace elements in Macedonia studied by the moss biomonitoring technique. *J Environ Sci Health A*, 47(13), 2000–2015.

Barandovski, L., Frontasyeva, M. V., Stafilov, T., Šajn, T., Ostrovnyaya, R., 2015. Multi-element atmospheric deposition in Macedonia studied by the moss biomonitoring

technique. *Environ Sci Pollut Res*, 22, 16077–16097. DOI 10.1007/s11356-015-4787-x.

Bargagli, R., Brown, D.H., Nelli, L., 1995a. Metal biomonitoring with mosses: procedures for correcting for soil contamination. *Environ Pollut*, 89(2), 169–175.

Bargagli, R., 1995b. The elemental composition of vegetation and the possible incidence of soil contamination of samples. *The Science of the Total Environment*, 176, 121-128.

Bargagli, R., 1998. Trace elements in terrestrial plants. An Ecophysiological approach to biomonitoring and Biorecovery. Springer, Berlin, pp. 324.

Baskaran, M., 2011. Po-210 and Pb-210 as atmospheric tracers and global atmospheric Pb-210 fallout: a review. *J. Environ. Radioact.*, 102, 500-513.

Begum, B.A., Kim, E., Biswas, S.K., Hopke, P.K., 2004. Investigation of sources of atmospheric aerosol at urban and semi-urban areas in Bangladesh. *Atmospheric Environment*, 38, 3025-3038.

Bekteshi, L., Lazo, P., Qarri, F., Stafilov, T., 2015. Application of the normalization process in the survey of atmospheric deposition of heavy metals in Albania through moss biomonitoring. *Ecol Indic*, 56, 50–59.

Belis, C.A., Larsen, R., Amato, F., El Hadad, I., Olivier, F., Harisson, R.M., Hopke, P.K., Nava, S., Paatero, P., Prévôt, A., Quass, U., Vecchi, R., Viana, M., 2014. Reference Report of the European Guide on Air Pollution Source Apportionment with Receptor Models. Joint Research Centre Institute for Environment and Sustainability, pp 1-92, doi: 10.2788/9307

Belivermiş, M., Çotuk, Y., 2010. Radioactivity measurements in moss (*Hypnum cupressiforme*) and lichen (*Cladonia rangiformis*) samples collected from Marmara region of Turkey. *Journal of Environmental Radioactivity*, 101, 945-951.

Bell, M.L., Ebisu, K., Peng, R.D., Walker, J., Samet, J.M., Zeger, S.L., Dominici, F., 2008. Seasonal and regional short-term effects of fine particles on hospital admissions in 202 US counties, 1999-2005. *Am. J. Epidemiol.*, 168 (11), 1301–1310.

Beresford, N.A., Fesenko, S., Konoplev, A., Skuterud, L., Smith, J.T., Voigt, G., 2016. Thirty years after the Chernobyl accident: What lessons have we learnt? *Journal of Environmental Radioactivity*, 157, 77-89. <http://dx.doi.org/10.1016/j.jenvrad.2016.02.003>

Berg, T., Røyset, O., Steinnes, E., 1995. Moss (*Hylocomium splendens*) used as biomonitor of atmospheric trace element deposition: estimation of uptake efficiencies. *Atmos Environ*, 29(3), 353–360.

Berg, T., Steinnes, E., 1997. Use of mosses (*Hylocomium splendens* and *Pleurozium schreberi*) as biomonitors of heavy metal deposition: from relative to absolute values. *Environ Pollut*, 98, 61–71.

Berg, T., Hjellbrekke, A., Röhling, E., Steinnes, E., Kubin, E., Larsen, M.M., Piispanen, J., 2003. Absolute deposition maps of heavy metals for the Nordic countries based on the moss survey. TemaNord 2003: 505, Nordic Council of Ministers, Copenhagen, Denmark.

Betsou, Ch., 2015. Study of the reaction  ${}^6\text{Li}+\text{p}\rightarrow{}^3\text{He}+{}^4\text{He}$  with DINEX telescope. Master Thesis. University of Ioannina, Ioannina, Greece, pp. 27-29.

Betsou, Ch., Tsakiri, E., Kazakis, N., Vasilev, A., Frontasyeva, M., Ioannidou, A., 2019. Atmospheric deposition of trace elements in Greece using moss *Hypnum cupressiforme* Hedw. as biomonitors. Journal of Radioanalytical and Nuclear Chemistry, 320(3), 597-608. <https://doi.org/10.1007/s10967-019-06535-4>.

Bi, C., Zhou, Y., Chen, Z., Jia, J., Bao, X., 2018. Heavy metals and lead isotopes in soil, road dust and leafy vegetables and health risks via vegetable consumption in the industrial areas of Shanghai, China. Sci. Total Environ., 619-690, 1349–1357.

Birke, M., Rauch, U., 2000. Urban Geochemistry: Investigations in the Berlin metropolitan area. Environmental Geochemistry and Health, 22, 233–248.

Bitterli, C., Bañuelos, G.S., Schulin, R., 2010. Use of transfer factors to characterize uptake of selenium by plants. Journal of Geochemical Exploration, 107, 206–216. doi:10.1016/j.gexplo.2010.09.009

Botsou, F., Sungur, A., Kelepertzis, E., Soylak, M., 2016. Insights into the chemical partitioning of trace metals in roadside and off-road agricultural soils along two major highways in Attica's region, Greece. Ecotoxicol. Environ. Saf. 132, 101-110.

Bondiatti, E.A.; Brantley, J.N.; Rangarajan, C., 1988. Size distributions and growth of natural and Chernobyl-derived submicron aerosols in Tennessee. J. Environ. Radioact., 6, 99-120.

Boubel, R.W, Fox, D.L, Turner, D.B, Stern, A.C., 1994. Fundamentals of air pollution. Academic Press, San Diego.

Boryło, A., Romańczyk, G., Skwarzec, B., 2017. Lichens and mosses as polonium and uranium biomonitors on Sobieszewo Island. J Radioanal Nucl Chem., 311, 859–869. DOI 10.1007/s10967-016-5079-8

Brost, R. A., Feichter, J., Heimann, M., 1991. Three-dimensional simulation of  ${}^7\text{Be}$  in a global climate model. Journal of Geophysical Research Atmospheres, 96 (D12), 22423–22445, doi:10.1029/91JD02283.

Bzdusek, P.A., Christensen, E.R., Lee, C.M., Pakadeesusuk, U., Freedman, D.C., 2006. PCB congeners and dechlorination in sediments of Lake Hartwell, South Carolina, determined from cores collected in 1987 and 1988. Environmental Science and Technology, 40, 109–119.

Canberra, 2003. Germanium Detectors.

- Capozzi, F., Giordano, S., Di Palma, A., Spagnuolo, V., De Nicola, F., Adamo, P., 2016a. Biomonitoring of atmospheric pollution by moss bags: Discriminating urban-rural structure in a fragmented landscape. *Chemosphere* 149, 211-218
- Capozzi, F., Giordano, S., Aboal, J.R., Adamo, P., Bargagli, R., Boquete, T., Di Palma, A., Real, C., Reski, R., Spagnuolo, V., Steinbauer, K., Tretiach, M., Varela, Z., Zechmeister, H., Fernández, J.A., 2016b. Best options for the exposure of traditional and innovative moss bags: A systematic evaluation in three European countries. *Environmental Pollution* 214, 362-373.
- Celik, N., Cevik, U., Celik, A., Koz, B., 2009. Natural and artificial radioactivity measurements in Eastern Black Sea region of Turkey. *Journal of Hazardous Materials*, 162, 146–153. doi:10.1016/j.jhazmat.2008.05.017
- Cevik, U., Celik, N., 2009. Ecological half-life of  $^{137}\text{Cs}$  in mosses and lichens in the Ordu province, Turkey by Cevik and Celik. *Journal of Environmental Radioactivity*, 100, 23–28.
- Chakraborty, S., Paratkar, G.T., 2006. Biomonitoring of trace element air pollution using mosses. *Aeros Air Qual Res*, 6(3), 247–258.
- Chakraborty, S.R., Azim, R., Rezaur Rahman, A.K.M., Sarker, R., 2013. Radioactivity concentrations in soil and transfer factors of radionuclides from soil to grass and plants in the Chittagong city of Bangladesh. *Journal of Physical Science*, 24(1), 95–113.
- Challan, M. H., 2013. Gamma-ray efficiency of a HPGe detector as a function of energy and geometry. *Applied Radiation and Isotopes* 82, 166–169.
- Chantzi, P., Dotsika, E., Raco, B., 2016. Isotope Geochemistry Survey in Ierissos Gulf Basin, North Greece. *IOP Conf. Ser.: Earth Environ. Sci.* 44 052036. doi:10.1088/1755-1315/44/5/052036
- Chettri, M.K. and Sawidis, T., 1995. Impact of heavy metals on water loss from lichen *Thalli*. *Ecotoxicology and Environmental Safety*, 37, 103-111.
- Chettri, M.K., Sawidis, T., Karataglis, S., 1997a. Lichens as a tool for Biogeochemical Prospecting. *Ecotoxicology and Environmental Safety*, 38, 322-335.
- Chettri, M.K., Sawidis, T., Zachariadis, G.A., Stratis, J.A., 1997b. Uptake of heavy metals by living and dead *Cladonia thalli*. *Environmental and Experimental Botany*, 37, 39-52.
- Chettri, M.K., Cook, C.M., Vardaka, E., Sawidis, T., Lanaras, T., 1998. The effect of Cu, Zn and Pb on the chlorophyll content of the lichens *Cladonia convoluta* and *Cladonia rangiformis*. *Environmental and Experimental Botany*, 39, 1-10.
- Christensen, E.R., Steinnes, E., Eggen, O.A., 2018. Anthropogenic and geogenic mass input of trace elements to moss and natural surface soil in Norway. *Science of the Total Environment*, 613-614, 371-378. <http://dx.doi.org/10.1016/j.scitotenv.2017.09.094>

- Comero, S., Capitani, L., Gawlik, B.M., 2009. Positive Matrix Factorization: An Introduction to the chemometric evaluation of environmental monitoring data using PMF. JRC Scientific and Technical Reports, JRC 52754, pp 18, DOI 10.2788/2497.
- Conti, M.E., Cecchetti, G., 2001. Biological monitoring: lichens as bioindicators of air pollution assessment – a review. *Environ Pollut*, 114, 471–492.
- Courtier, J., Sdrauling, S., Hirth, G., 2017.  $^7\text{Be}$  and  $^{210}\text{Pb}$  wet/dry deposition in Melbourne, Australia and the development of deployable units for radiological emergency monitoring. *Journal of Environmental Radioactivity*, 1-7. <http://dx.doi.org/10.1016/j.jenvrad.2017.07.004>
- Cramer, D. 1998. *Fundamental statistics for social research*. London. Rudledge.
- Cramer, D., & Howitt, D. L., 2004. *The SAGE Dictionary of Statistics: A Practical Resource for Students in Social Sciences*. London: SAGE Publications Ltd. <https://doi.org/10.4135/9780857020123>
- Čučulović, A., Sabovljević, M., Veselinović, D., 2014. The activity concentrations of  $^{40}\text{K}$ ,  $^{226}\text{Ra}$ ,  $^{232}\text{Th}$ ,  $^{238}\text{U}$  and  $^7\text{Be}$  in moss from spas in eastern Serbia in the period 2000-2012. *Arch. Biol. Sci.*, 66, 691-700. <https://doi.org/10.2298/ABS1402691C>.
- Cucu-Man, S., Mocanu, R., Culicov, O., Steinnes, E., Frontasyeva, M., 2004. Atmospheric deposition of metals in Romania studied by biomonitoring using the epiphytic moss *Hypnum cupressiforme*. *Int J Environ Anal Chem*, 84(11), 845–854.
- Culicov, O.A., Mocanu, R., Frontasyeva, M.V., Yurukova, L., Steinnes, E., 2005. Active moss biomonitoring applied to an industrial site in Romania: Relative accumulation of 36 elements in moss-bags. *Environmental Monitoring and Assessment*, 108, 229–240.
- Czarnowska, K., Rejment-Grochowska, I., 1974. Concentration of heavy metals- iron, manganese, zinc and copper in mosses. *Acta Soc Bot Pol* XLIII (1), 39–44.
- Decker, E.L., Frank, W., Sarnighausen, E., Reski, R., 2006. Moss systems biology en route: phytohormones in *Physcomitrella* development. *Plant Biol*, 8, 397–406. <https://doi.org/10.1055/s-2006-923952>.
- De Cort, M., Dubois, G., Fridman, Sh., Germenchuk, M., Izrael, Yu, Janssens, A., Jones, A., Kelly, G., Kvasnikova, E., Matveenko, I., Nazarov, I., Pokumeiko, Yu, Sitak, V., Stukin, E., Tabachny, L., Tsaturov, Yu, Avdyushin, S., 1998. *Atlas of Caesium Deposition in Europe after the Chernobyl Accident*. Office for Official Publications of the European Communities.
- Delfanti, R., Papucci, C., Benco, C., 1999. Mosses as indicators of radioactivity deposition around a coal-fired power station. *The Science of the Total Environment* 227, 49–56.
- De Wit, H.A., Hettelingh, J.P., Harmens, H., 2015. Trends in ecosystem and health responses to long-range transported atmospheric pollutants. *International Cooperative Programme on Assessment and Monitoring Effects of Air Pollution on Rivers and*

Lakes. ICP Waters Programme Centre, Norwegian Institute for Water Research. NIVA 6946-2015, pp 13.

Diapouli, E., Manousakas, M., Vratolis, S., Vasilatou, V., Maggos, Th., Saraga, T., Grigoratos, Th., Argyropoulos, G., Voutsas, D., Samara, C., Eleftheriadis, K., 2017. Evolution of air pollution source contributions over one decade, derived by PM<sub>10</sub> and PM<sub>2.5</sub> source apportionment in two metropolitan urban areas in Greece. *Atmospheric Environment*, 164, 416-430. <http://dx.doi.org/10.1016/j.atmosenv.2017.06.016>

Di Palma, A., Crespo Pardo, D., Spagnuolo, V., Adamo, P., Bargagli, R., Cafasso, D., Capozzi, F., Aboal, J.R., González, A.G., Pokrovsky, O., Beike, A.K., Reski, R., Tretiach, M., Varela Z., Giordano, S., 2016. Molecular and chemical characterization of a *Sphagnum palustre* clone: key steps towards a standardized and sustainable moss bag technique. *Ecol Indic*, 71, 388–39.

Di Palma, A., Capozzi, F., Spagnuolo, V., Giordano, S., Adamo, P., 2017. Atmospheric particulate matter intercepted by moss-bags: Relations to moss trace element uptake and land use. *Chemosphere*, 176, 361-368.

Dmitriev, A.Y, Pavlov, S.S., 2013. Automation of the quantitative determination of elemental content in samples using neutron activation analysis on the IBR-2 reactor at the Frank Laboratory for Neutron Physics, Joint Institute for Nuclear Research. *Physics of Particles and Nuclei Letters* 10 (1)1, 33-36. DOI:10.1134/S1547477113010056.

Doane, D.P., Seward, L.E., 2011. Measuring Skewness: A Forgotten Statistic? *Journal of Statistics Education*, 19 (2),1-18.

Dowdall, M., Gwynn, J.P., Moran, C., O’dea, J., Davids, C., Lind, B., 2005. Uptake of radionuclides by vegetation at a High Arctic location. *Environ. Pollut.*, 133, 327-332.

Dragović, S., Nedić, O., Stanković, S., Bačić, G., 2004. Radiocesium accumulation in mosses from highlands of Serbia and Montenegro: chemical and physiological aspects. *Journal of Environmental Radioactivity*, 77, 381–388.

Dragović, S., Michailović, N., Gajić, B., 2010. Quantification of transfer of <sup>238</sup>U, <sup>226</sup>Ra, <sup>232</sup>Th, <sup>40</sup>K and <sup>137</sup>Cs in mosses of a semi-natural ecosystem. *Journal of Environmental Radioactivity*, 101, 159–164. doi:10.1016/j.jenvrad.2009.09.011

Duffus, H.J., 2002. “HEAVY METALS” – A MEANINGLESS TERM? *International Union of Pure and Applied Chemistry*, 74,793–807.

Dutton, S.J., Vedal, S., Piedrahita, R., Milford, J.B., Miller, S.L., Hannigan, M.P., 2010. Source Apportionment Using Positive Matrix Factorization On Daily Measurements of Inorganic and Organic Speciated PM<sub>2.5</sub>. *Atmos Environ.*, 44(23), 2731–2741. doi:10.1016/j.atmosenv.2010.04.038.

Eğilli, E., Topsuoğlu, S., Kut, D., Kirbaşoğlu, C., Esen, N., 2003. Heavy Metals and Radionuclides in Lichens and Mosses in Thrace, Turkey. *Bull. Environ. Contam. Toxicol.*, 70, 502–508.

Eleftheriadis, K., KM, O., Lympelopoulou, T., Karanasiou, A., Razos, P., Ochsenkuhn-Petropoulou, M., 2014. Influence of local and regional sources on the observed spatial and temporal variability of size resolved atmospheric aerosol mass concentrations and water-soluble species in the Athens metropolitan area. *Atmospheric Environment*, 97, 252–61. <http://dx.doi.org/10.1016/j.atmosenv.2014.08.013>

Eliopoulos, D.G., Economou-Eliopoulos, M., Apostolikas, A., Golightly, J.P., 2012. Geochemical features of nickel-laterite deposits from the Balkan Peninsula and Gordes, Turkey: The genetic and environmental significance of arsenic. *Ore Geology Reviews*, 48, 413-427.

Elywa, M., Mubarak, F., Omar, H.A., Nassif, A., Mansour, Selem, E., Marwaan, N., 2016. Determination of Soil-Plant Transfer Factor of Edible Plants Grown in a Contaminated Soil with Europium – 152. *Middle-East Journal of Scientific Research*, 24 (10), 3278-3283.

Eslava-Gomez, A., Brown, J., 2013. Determination of Root Uptake to Vegetables Grown in Soil Contaminated for Twenty-Five Years. Report for the Health Protection Agency Centre for Radiation, Chemical and Environmental Hazards, Chilton, 2013. ISBN 978- 0- 85951-732- 4

EU 2008. Directive 2008/50/EC of the European Parliament and of the Council of 21 May 2008 on ambient air quality and cleaner air for Europe. Off J 1–44. 11.062008, L152.

Evans, J. D., 1996. Straightforward statistics for the behavioral sciences. Pacific Grove, CA: Brooks/Cole Publishing.

Falla, J., Laval-Gilly, P., Henryon, M., Morlot, D., Ferard, J.F., 2000. Biological air quality monitoring: a review. *Environ Monit Assess*, 64, 627–644.

Ferreira, V.V.M., Fonseca, R.L.M., Rocha, Z., L. Oliveira, A., Moreira, R.M., Lemos, N.C., Chagas, C.J., Menezes, M.A., Santos, T.O., 2015. Use of Radon as Water Tracer at Juatuba Basin. *Journal of Geography and Geology*; Vol. X, No. X; ISSN 1916-9779 E-ISSN 1916-9787

Filippidis, A., Georgakopoulos, A., Kassoli-Fourmaraki, A., Misaelides, P., YiakKoupis, P., Broussoulis, J., 1996. Trace element contents in composited samples of three lignite seams from the centrl part of the Drama lignite deposit, Macedonia, Greece. *International Journal of Coal Geology*, 29, 219-234.

Florou, H., Travidou, G., Nicolaou, G., 2007. An assessment of the external radiological impact in areas of Greece with elevated natural radioactivity. *Journal of Environmental Radioactivity*, 93. 74-83.

Foscolos, A.E., Goodarzi, F., Koukouzas, C.N., Hatziyannis, G., 1989. Reconnaissance study of mineral matter and trace elements in Greek lignites. *Chemical Geology* ,76, 107-130.

FOREGS, 2005. Forum of the European Geological Survey Directors. *Geochemical Atlas of Europe*, Geological Survey of Finland, Espoo.

Frontasyeva, M.V., Steinnes, E., 1997. Epithermal neutron activation analysis for studying the environment. Proc. Int. Symposium on Harmonization of Health Related Environmental Measurements Using Nuclear and Isotopic Techniques (Hyderabad, India, 4-7 November, 1996), IAEA 1997, p. 301-311.

Frontasyeva, M. V. and Pavlov, S. S., 1999. in Problems of Modern Physics, Ed. by A. N. Sisakyan and V. I. Trubetskov, JINR, Dubna, 152–158 [in Russian].

Frontasyeva, M.V., Pavlov, S.S., 2000. Analytical investigations at the IBR-2 Reactor in Dubna, Proceedings of the VIII International Seminar on Interactions of Neutrons with Nuclei, 17-20 May 2000, Dubna, Russia, code E14-2000-177, published by the Joint Institute for Nuclear Research, pages 35-43.

Frontasyeva, M. V., Galinskaya, T. Ye., Krmar, M., Matavuly, M., Pavlov, S. S., Povtoreyko, E. A., Radnovic, D., and Steinnes, E., 2004 Atmospheric deposition of heavy metals in northern Serbia and Bosnia-Herzegovina studied by the moss biomonitors, neutron activation analysis and GIS technology. Journal Radioanalytical Nuclear Chemistry, 259, 141-147.

Frontasyeva, M.V., 2008. Epithermal Neutron Activation Analysis at the IBR-2 Reactor of the Frank Laboratory of Neutron Physics at the Joint Institute for Nuclear Research (Dubna), Physics of Atomic Nuclei, 71 (10), 1684-1693.

Frontasyeva, M.V., 2011. Neutron Activation Analysis in the Life Sciences. Physics of Particles and Nuclei, 42 (2), 332-378.

Frontasyeva, M., Harmens, H., and the participants of the ICP Vegetation Programme, 2015. Heavy metals, Nitrogen and POP's in European mosses: 2015 Survey Monitoring manual. United Nations Economic Commission for Europe Convention on Long-Range Transboundary Air Pollution. International Cooperative Programme on Effects of Air Pollution on Natural Vegetation and Crops. pp. 1-26. <http://icpvegetation.ceh.ac.uk>

Frontasyeva, M., Harmens, H., 2020. Heavy metals, nitrogen and POPs in European mosses: 2020 survey - Monitoring Manual. Bangor, UK, ICP Vegetation. <https://icpvegetation.ceh.ac.uk/sites/default/files/ICP%20Vegetation%20moss%20monitoring%20manual%202020.pdf>

Fujiyoshi, R, Sawamura, S., 2004. Mesoscale variability of vertical profiles of environmental radionuclides ( $^{40}\text{K}$ ,  $^{226}\text{Ra}$ ,  $^{210}\text{Pb}$  and  $^{137}\text{Cs}$ ) in temperate forest soils in Germany. Science of the Total Environment, 320, 177–188.

Gerdol, R., Marchesini, R., Iacumin, P., Brancaleoni, L., 2014. Monitoring temporal trends of air pollution in an urban area using mosses and lichens as biomonitors. Chemosphere, 108, 388–395.

Gilmore, G.R., 2008. Practical Gamma-ray Spectrometry, second edition, John Wiley & Sons, England, pp. 143-163.

Giordano, S., Adamo, P., Monaci, F., Pittao, E., Tretiach, M., Bargagli, R., 2009. Bags with oven-dried moss for the active monitoring of airborne trace elements in urban areas. Environmental Pollution 157, 2798–2805.

Giordano, S., Adamo, P., Spanguolo, V., Tretiach, M., Bargagli, R., 2013. Accumulation of airborne trace elements in mosses, lichens and synthetic materials exposed at urban monitoring stations: Towards a harmonization of the moss-bag technique. *Chemosphere* 90, 292–299.

Gjengedal, E., Steinnes, E., 1990. Uptake of metal ions in moss from artificial precipitation. *Environ Monit Assess*, 14(1), 77–87.

Glime, J.M., 2017. Bryophyte ecology. Volume 1. *Physiological Ecology*. Ebook sponsored by Michigan Technological University and the International Association of Bryologists. Last updated 25 March 2017 and available at <http://digitalcommons.mtu.edu/bryophyte-ecology/>

Glime, J. M. 2017a. *Bryophyte Ecology*. Volume 1. *Physiological Ecology*. Ebook sponsored by Michigan Technological University and the International Association of Bryologists. Last updated 9 May 2017 and available at <<http://digitalcommons.mtu.edu/bryophyte-ecology/>>.

Glime, J. M., 2017b. *Bryophyte Ecology*. Volume 1, Chapter 7.1. *Physiological Ecology*. Ebook sponsored by Michigan Technological University and the International Association of Bryologists. Last updated 9 May 2017 and available at <<http://digitalcommons.mtu.edu/bryophyte-ecology/>>.

Glime, J. M., 2017c. *Bryophyte Ecology*. Volume 1, Chapter 2.7. *Physiological Ecology*. Ebook sponsored by Michigan Technological University and the International Association of Bryologists. Last updated 9 May 2017 and available at <<http://digitalcommons.mtu.edu/bryophyte-ecology/>>.

Glime, J. M., 2017d. *Bryophyte Ecology*. Volume 1, Chapter 7.2. *Physiological Ecology*. Ebook sponsored by Michigan Technological University and the International Association of Bryologists. Last updated 9 May 2017 and available at <<http://digitalcommons.mtu.edu/bryophyte-ecology/>>.

Glime, J. M., 2017e. *Bryophyte Ecology*. Volume 1, Chapter 7.5. *Physiological Ecology*. Ebook sponsored by Michigan Technological University and the International Association of Bryologists. Last updated 9 May 2017 and available at <<http://digitalcommons.mtu.edu/bryophyte-ecology/>>.

Glime, J. M., 2017f. *Bryophyte Ecology*. Volume 1, Chapter 8.1, p. 9. *Physiological Ecology*. Ebook sponsored by Michigan Technological University and the International Association of Bryologists. Last updated 9 May 2017 and available at <<http://digitalcommons.mtu.edu/bryophyte-ecology/>>.

Godoy, J.M., Schuch, L.A., Nordemann, D.J.R., Reis, V.R.G., Ramalho, M., Reico, J.C., Brito, R.R.A., Olech, M.A., 1998.  $^{137}\text{Cs}$ ,  $^{226,228}\text{Ra}$ ,  $^{210}\text{Pb}$  and  $^{40}\text{K}$  concentrations in Antarctic soil, sediment and selected moss and lichen samples. *Journal of Environmental Radioactivity* 41, 33–45.

González Ortiz, A., Guerreiro, C., Soares, J., all the contributors of EEA and the European Topic Centre on Air Pollution, Noise, Transport and Industrial Pollution (ETC/ATNI), 2019. Air quality in Europe-2019 report. European Environmental

Agency, Luxembourg: Publications Office of the European Union, ISBN 978-92-9480-088-6, ISSN 1977-8449, doi:10.2800/822355.

Goryainova, Z., Vuković, G., Aničić -Urošević, M., Vergel, K., Ostrovnaya, T., Frontasyeva, M.V., Zechmeister, H., 2016. Assessment of vertical element distribution in street canyons using the moss *Sphagnum girgensohnii*: A case study in Belgrade and Moscow cities. *Atmospheric Pollution Research* 7, 690-697.

Grytsyuk, N., Arapis, G., Davydchuk, V., 2006. Root uptake of <sup>137</sup>Cs by natural and semi-natural grasses as a function of texture and moisture of soils. *Journal of Environmental Radioactivity*, 85, 48-58.

Gusev, A., Ilyin, I., Rozovskaya, O., Shatalov, V., Sokovych, V., Travnikov, O., 2009. Modelling of heavy metals and persistent organic pollutants: New developments. EMEP/MSCE Technical Report 1/2009. Meteorological Synthesizing Centre e East, Moscow, Russian Federation. <http://www.mscea.st.org>.

Harmens H, Norris D A, The Participants of the Moss Survey, 2008. Spatial and Temporal Trends in Heavy Metal Accumulation in Mosses in Europe (1990-2005). ICP Vegetation Programme Coordination Centre, Centre for Ecology and Hydrology, Bangor, UK.

Harmens, H., Norris, D.A., Steinnes, E., Kubin, E., Piispanen, J., Alber, R., Aleksiyaynak, Y., Blum, O., Coşkun, M., Dam, M., De Temmerman, L., Fernández, J.A., Frolova, M., Frontasyeva, M., Gonzalez- Miqueo, L., Grodzińska, K., Jeran, Z., Korzekwa, S., Krmar, M., Kvietskus, K., Leblond, S., Liiv, S., Magnússon, S.H., Maňkovská, B., Pesch, R., Rühling, A., Santamaria, J.M., Schröder, W., Spiric, Z., Suchara, I., Thöni, L., Urumov, V., Yurukova, L., Zechmeister, H.G., 2010. Mosses as biomonitors of atmospheric heavy metal deposition: spatial patterns and temporal trends in Europe. *Environ Pollut*, 158, 3144–3156.

Harmens, H., Norris, D.A., Cooper, D.M., Mills, G., Steinnes, E., Kubin, E., Thöni, L., Aboal, J.R., Alber, R., Carballeira, A., Coşkun, M., De Temmerman, L., Frolova, M., Gonzalez-Miqueo, L., Jeran, Z., Leblond, S., Liiv, S., Maňkovská, B., Pesch, R., Poikolainen, J., Rühling, A., Santamaria Simonè, P., Schröder, W., Suchara, I., Yurukova, L., Zechmeister, H.G., 2011. Nitrogen concentrations in mosses indicate the spatial distribution of atmospheric nitrogen deposition in Europe. *Environ Pollut*, 159, 2852–2860.

Harmens, H., Ilyin, I., Mills, G., Aboal, J.R., Alber, R., Blum, O., Coşkun, M., De Temmerman, L., Fernández, J.A., Figueira, R., Frontasyeva, M., Godzik, B., Goltsova, N., Jeran, Z., Korzekwa, S., Kubin, E., Kvietskus, K., Leblond, S., Liiv, S., Magnússon, S.H., Maňkovská, B., Nikodemus, O., Pesch, R., Poikolainen, J., Radnović, D., Rühling, A., Santamaria, J.M., Schroder, W., Špirić, Z., Stafilov, T., Steinnes, E., Suchara, I., Tabors, G., Thöni, L., Turcsanyi, G., Yurukova, L., Zechmeister, H.G., 2012. Country-specific correlations across Europe between modelled atmospheric cadmium and lead deposition and concentrations in mosses. *Environ Pollut*, 166, 1–9.

Harmens, H., Norris, D. A., Mills, G., The Participants of the Moss Survey, 2013. Heavy Metals and Nitrogen in Mosses: Spatial Patterns in 2010/2011 and Long-term

Temporal Trends in Europe. ICP Vegetation Programme Coordination Centre, Centre for Ecology and Hydrology, Bangor, UK.

Harmens, H., Mills, G., Hayes, F., Norris, D. A., Sharps, K., 2015. Twenty-eight years of ICP Vegetation: an overview of its activities. *Annali di Botanica (Roma)*, 5, 31-43, doi: 10.4462/annbotrm-13064.

Herpin, U., Berlekamp, J., Markert, B., Wolterbeek, B., Grodzinska, K., Siewers, U., Lieth, H., Weckert, V., 1996. The distribution of heavy metals in a transect of the three states the Netherlands, Germany and Poland, determined with the aid of moss monitoring. *Sci Total Environ*, 187, 185–198.

Herrmann, R., 1976. Modellvorstellungen zur räumlichen Verteilung von Spurenmetall-verunreinigungen in der Bundesrepublik Deutschland, angezeigt durch den Metallgehalt in epiphytischen Moosen. *Erdkunde (Sonderdruck)*, Archiv fuer wissenschaftliche Geographie, Band 30, Lfg. 4, Bonn

Holy, M., Pesch, R., Schröder, W., Harmens, H., Ilyin, I., Alber, R., Aleksiyenak, Y., Blum, O., Coşkun, M., Dam, M., De Temmerman, L., Fedorets, N., Figueira, R., Frolova, M., Frontasyeva, M., Goltsova, N., Gonzalez Miqueo, L., Grodzińska, K., Jeran, Z., Korzekwa, S., Krmar, M., Kubin, E., Kvietkus, K., Larsen, M., Leblond, S., Liiv, S., Magnússon, S.H., Maňková, B., Mocanu, R., Piispanen, J., Rühling, A., Santamaria, J.M., Steinnes, E., Suchara, I., Thöni, L., Turcsanyi, G., Urumov, V., Wolterbeek, B., Yurukova, L., Zechmeister, H.G., 2009. First thorough identification of factors associated with Cd, Hg and Pb concentrations in mosses sampled in the European Surveys 1990, 1995, 2000 and 2005. *J Atmos Chem*, 63, 109–124.

Hoodaji, M., Ataabadi, M., Najafi, P., 2012. Biomonitoring of Airborne Heavy Metal Contamination. *Air Pollution- Monitoring, Modelling, Health and Control*, Chapter, 97-122. DOI: 10.5772/32963

Hötzl, H., Rosner, G., Winkler, R., 1991. Correlation of <sup>7</sup>Be concentrations in surface air and precipitation with the solar cycle. *Naturwissenschaften* 78, 215-217.

Hovardas, T., 2017. “Battlefields” of blue flags and seahorses: Acts of “fencing” and “defencing” place in a gold mining controversy. *Journal of Environmental Psychology* 53, 100-111. <http://dx.doi.org/10.1016/j.jenvp.2017.07.005>

Hovardas, T., 2019. Discursive positioning of actors in a gold mining conflict in Northern Greece: Risk calculus, subjectification and place. *The Extractive Industries and Society*, <https://doi.org/10.1016/j.exis.2019.12.001>

IAEA, 2003. Guidelines for radioelement mapping using gamma ray spectrometry data. Technical report, International Atomic Energy Agency. IAEA-TECDOC-1363.

IAEA 2006, Classification of soil systems on the basis of transfer factors of radionuclides from soil to reference plants. Proceedings of a final research coordination meeting organized by the Joint FAO/IAEA Programme of Nuclear Techniques in Food and Agriculture and held in Chania, Crete, 22–26 September 2003

Ibikunle, S.B., Arogunjo, A.M., Ajayi, O.S., 2019. Characterization of radiation dose and soil-to-plant transfer factor of natural radionuclides in some cities from south-

- western Nigeria and its effect on man. *Scientific African*, 3, e00062.  
<https://doi.org/10.1016/j.sciaf.2019.e00062>
- Ilyin, I., Rozovskaya, O., Travnikov, O., Varygina, M., Aas, W., Uggerud, H. T., 2013. Heavy metals: transboundary pollution of the environment (No. Status Report 2/2013). EMEP/MS-C-E/CCC/CEIP.
- Ioannidou, A., Manolopoulou, M., Papastefanou, C., 2005. Temporal changes of  $^7\text{Be}$  and  $^{210}\text{Pb}$  concentrations in surface air at temperate latitudes ( $40^\circ\text{N}$ ). *Applied Radiation and Isotopes*, 63, 277–284. doi:10.1016/j.apradiso.2005.03.010
- Ioannidou, A., Papastefanou, C., 2006. Precipitation scavenging of  $^7\text{Be}$  and  $^{137}\text{Cs}$  radionuclides in air. *Journal of Environmental Radioactivity*, 85, 121-136.
- Ioannidou, A., 2011. Activity size distribution of  $^7\text{Be}$  in association with trace metals in the urban area of the city of Thessaloniki, Greece. *Atmospheric Environment*, 45, 1286-1290. doi:10.1016/j.atmosenv.2010.12.006
- Ioannidou, A., Kotsopoulou, E., Karanatsiou, A., Papastefanou, C., 2012a. Variations of  $^{210}\text{Pb}$  concentrations in surface air at Thessaloniki, Greece ( $40^\circ\text{N}$ ). *EPJ Web of Conferences*, 24, 05003, 1-9. DOI: 10.1051/epjconf/20122405003
- Ioannidou, A., Manenti, S., Gini, L., Groppi, F., 2012b. Fukushima fallout at Milano, Italy. *Journal of Environmental Radioactivity*, 114, 119-125. doi:10.1016/j.jenvrad.2012.01.006
- Ioannidou, A., Paatero, J., 2014. Activity size distribution and residence time of  $^7\text{Be}$  aerosols in the Arctic atmosphere. *Atmospheric Environment*, 88, 99-106.  
<http://dx.doi.org/10.1016/j.atmosenv.2013.12.046>
- Ioannidou, A., Eleftheriadis, K., Gini, M., Manenti, S., Groppi, F., 2019. Activity size distribution of radioactive nuclide  $^7\text{Be}$  at different locations and under different meteorological conditions. *Atmospheric Environment*, 212, 272–280.  
<https://doi.org/10.1016/j.atmosenv.2019.05.044>
- Ivanić, M., Fiket, Z., Medunić, G., Furdek Turk, M., Marović, G., Senčar, J., Kniewald, G., 2019. Multi-element composition of soil, mosses and mushrooms and assessment of natural and artificial radioactivity of a pristine temperate rainforest system (Slavonia, Croatia). *Chemosphere*, 215, 668-677.
- Jalil, A., Rahman, M.M., Chand, M.M., Koddus, A., Zaman, M.A., Ahmad, G.U., 2002. Soil to plant transfer factor of radiocesium by pot experiment. IAEA-CN-90/10. XA0300139, pp. 43-46.
- Juntto, S., Paatero, P., 1994. Analysis of daily precipitation data by positive matrix factorization. *Environmetrics*, 5, 127–144.
- Kabata-Pendias, A., 2004. Soil-plant transfer of trace elements- an environmental issue. *Geoderma*, 122, 143–149. doi:10.1016/j.geoderma.2004.01.004
- Kabata-Pendias, A., 2011. Trace Elements in Soil and Plants. Fourth Edition. Taylor and Francis Group, LLC, ISBN 978-1-4200-9368-1 (hardback), pp 37-60.

Kadovic, R., Belanovic, S., Obratov-Petkovic, D., Bjedov, I., Dragovic, N., 2011. Assessment of heavy metal content in soil and grasslands in national park of the lake plateau of the N. P. “Durmitor” Montenegro. *African Journal of Biotechnology*, 10(26), 5157-5165. DOI: 10.5897/AJB10.2129

Kalfas, C.A., Axiotis, M., Tsabaris, C., 2016. SPECTRW: A software package for nuclear and atomic spectroscopy. *Nuclear Instruments and Methods in Physics Research A* (830), 265-274.

Kaniu, I., 2017. *In-Situ* Gamma-Ray Spectrometry and Associated Radiometric Assessment of the Mrima-Kiruku Complex (Kenya) High Background Radiation Anomaly. – PhD Thesis. Department of Physics, University of Nairobi, Nairobi, pp. 13-36.

Karunakara, N., Somashekarappa, H.M., Narayana, Y., Avadhani, D.N., Mahesh, H.M., Siddappa, K., 2003.  $^{226}\text{Ra}$ ,  $^{40}\text{K}$  and  $^7\text{Be}$  activity concentrations in plants in the environment of Kaiga, India. *Journal of Environmental Radioactivity*, 65, 255–266.

Kelepertsis, A., Argyraki, A., Alexakis, D., 2006. Multivariate statistics and spatial interpretation of geochemical data for assessing soil contamination by potentially toxic elements in the mining area of Stratoní, north Greece. *Geochemistry: Exploration, Environment, Analysis*, 6, 349–355.

Kelepertsis, A., 2013. Heavy metals baseline concentrations in soft tissues of *Patella* sp. from the Stratoní coastal environment, NE Greece. *ECOL CHEM ENG S*, 20(1), 141-149. DOI: 10.2478/eces-2013-0011

Kelepertsis, E., Botsou, F., Patinha, C., Argyraki, A., Massas, I., 2018. Agricultural geochemistry in viticulture: An example of Cu accumulation and geochemical fractionation in Mediterranean calcareous soils (Nemea region, Greece). *Applied Geochemistry*, 88, 23-39.

Knoll, G.F., 2000. *Radiation Detection and Measurement*. John Wiley & Sons, New York, 3<sup>rd</sup> edition, pp. 40-60.

Koch, D.M., Jacob, D.L., Graustein, W.C., 1996. Vertical transport of troposphere aerosols as indicated by  $^7\text{Be}$  and  $^{210}\text{Pb}$  in a chemical tracer model. *J. Geophys. Res.*, 101, 18651–18666.

Konoplev, A., Golosov, V., Laptev, G., Nanba, K., Onda, Y., Takase, T., Wakiyama, Y., Yoshimura, K., 2016. Behavior of accidentally released radiocesium in soil- water environment: Looking at Fukushima from a Chernobyl perspective. *Journal of Environmental Radioactivity*, 151, 568-578. <http://dx.doi.org/10.1016/j.jenvrad.2015.06.019>

Konstantinova, M., Lukšienė, B., Tarasiuk, N., Maceika, E., 2017. Estimation of Cs isotope accumulation by litter, moss and grass in Lithuania attributed to the Fukushima Daiichi NPP accident. *Journal of Geochemical Exploration*, 174, 159–163. <http://dx.doi.org/10.1016/j.gexplo.2015.11.001>

- Kritidis, P., Florou, H., Eleftheriadis, K., Evangelidou, N., Gini, M., Sotiropoulou, M., Diapouli, E., Vratolis, S., 2012. Radioactive pollution in Athens, Greece due to the Fukushima nuclear accident. *Journal of Environmental Radioactivity*, 114, 100-104.
- Krmar, M., Radnović, D., Rakic, S., Matavuly, M., 2007. Possible use of terrestrial mosses in detection of atmospheric deposition of  $^7\text{Be}$  over large areas. *Journal of Environmental Radioactivity*, 95, 53-61.
- Krmar, M., Radnović, D., Michailović, D.T., Lalić, B., Slivka, J., Bikit, I., 2009. Temporal variations of  $^7\text{Be}$ ,  $^{210}\text{Pb}$  and  $^{137}\text{Cs}$  in moss samples over 14 month period. *Applied Radiation and Isotopes*, 67, 1139–1147. doi:10.1016/j.apradiso.2009.01.001
- Krmar, M., Wattanavatee, K., Radnović, D., Slivka, J., Bhongsuwan, T., Frontasyeva, M.V., Pavlov, S.S., 2013. Airborne radionuclides in mosses collected at different latitudes. *Journal of Environmental Radioactivity*, 117, 45-48.
- Krmar, M., Radnović, D., Hansman, J., 2014. Correlation of unsupported  $^{210}\text{Pb}$  in soil and moss. *Journal of Environmental Radioactivity*, 129, 23-26. <http://dx.doi.org/10.1016/j.jenvrad.2013.11.009>
- Krmar, M., Michailović, D.T., Arsenić, I., Radnović, D., Pap, I., 2016. Beryllium-7 and  $^{210}\text{Pb}$  atmospheric deposition measured in moss and dependence on cumulative precipitation. *Science of the Total Environment*, 541, 941–948.
- Krmar, M., Radnović, D., Hansman, J., Repić, P., 2017. Influence of broadleaf forest vegetation on atmospheric deposition of airborne radionuclides. *J. Environ. Radioact.*, 177, 32–36.
- Kulan, A., 2006. Seasonal  $^7\text{Be}$  and  $^{137}\text{Cs}$  activities in surface air before and after the Chernobyl event. *Journal of Environmental Radioactivity*, 90, 140-150. doi:10.1016/j.jenvrad.2006.06.010
- Lal, D., Malhotra, P.K., Peters, B., 1958. On the production of radioisotopes in the atmosphere by cosmic radiation and their application to meteorology. *Journal of Atmospheric and Terrestrial Physics*, 12, 306-328.
- Lambert, G., Polian, G., Sanak, J., Ardouin, B., Buisson, A., Jegou, A. and Le Roulley, J. C., 1982. Cycle du radon et de ses descendants. Application à l' étude des échanges troposphere-stratosphère. *Ann. Géophys.*, 38, 497-531.
- Laço, A., Radulov, I., Berbecea, A., Laço, K., Crista, F., 2012. The transfer factor in metals in soil plant system. *Research Journal of Agricultural Science*, 44 (3), 67-72.
- Lazaridou- Dimitriadou, M., Koukoumides, C., Lekka, E., Gaidagis, G., 2004. Integrative evaluation of the ecological quality of metalliferous streams (Chalkidiki, Macedonia, Hellas). *Environ. Monit. Assess.*, 90, 59–86.
- Lazić, L., Aničić-Urošević, M., Mijić, Z., Vuković, G., Ilić, L., 2016. Traffic contribution to air pollution in urban street canyons: Integrated application of the OSPM, moss biomonitoring and spectral analysis. *Atmospheric Environment*, 141, 347-360.

- Lee, E., Chan, C.K., Paatero, P., 1999. Application of positive matrix factorization in source apportionment of particulate pollutants in Hong Kong. *Atmospheric Environment*, 33, 3201–3212.
- Lehto, J., Paatero, J., Pehrman, R., Kulmala, S., Suksi, J., Koivula, T., Jaakkola, T., 2008. Deposition of gamma emitters from Chernobyl accident and their transfer in lichen–soil columns. *J Environ Radioact*, 99, 1656–1664.
- Leo, W.R., 1994. *Techniques for Nuclear and Particle Physics Experiments*, second edition, Springer-Verlag, Berlin, pp 6-15, 121-122, 215-245.
- Li, X., Lee, S.I., Wong, S., Shi, W., Thornton, I., 2004. The study of metal contamination in urban soils of Hong Kong using a GIS-based approach. *Environmental Pollution*, 129, 113-124.
- Li, P., Gong, Y., Komatsuzaki, M., 2019. Temporal dynamics of  $^{137}\text{Cs}$  distribution in soil and soil-to-crop transfer factor under different tillage systems after the Fukushima Daiichi Nuclear Power Plant accident in Japan. *Science of the Total Environment*, 697, 134060.
- Little, P., Martin, M.H., 1974. Biological monitoring of heavy metal pollution. *Environ Pollut*, 6, 1–19.
- Loppi, S., Riccobono, F., Zhang, Z., Savic, S., Ivanov, D., Pirintsos, S., 2003. Lichens as biomonitors of uranium in the Balkan area. *Environ. Pollut.*, 125, 277–280.
- Lu, J., Jiang, P., Wu, L., Chang, A.C., 2008. Assessing soil quality data by positive matrix factorization. *Geoderma*, 145, 259-266.
- Malikova, I.N., Strahkonevko, V.D., Shcherbov, B.L., 2019. Distribution of radionuclides in moss-lichen cover and needles on the same grounds of landscape-climatic zones of Siberia. *Journal of Environmental Radioactivity*, 198, 64–78.
- Malizia, D., Giuliano, A., Ortaggi, G., Masotti, A., 2012. Common plants as alternative analytical tools to monitor heavy metals in soil. *Chem Cent J* 6 (Suppl. 2), S6. <https://doi.org/10.1186/1752-153X-6-S2-S6>.
- Manolopoulou, M., Stoulos, S., Mironaki, D., Papastefanou, C., 2003. A new technique for the accurate measurement of  $^{226}\text{Ra}$  by gamma spectroscopy in voluminous samples. *Nuclear Instruments and Methods in Physics Research A*, 508, 362–366.
- Manolopoulou, M., Vagena, E., Stoulos, S., Ioannidou, A., Papastefanou, C., 2011. Radioiodine and radiocesium in Thessaloniki, Northern Greece due to the Fukushima nuclear accident. *Journal of Environmental Radioactivity*, 102, 796-797. doi:10.1016/j.jenvrad.2011.04.010
- Manousakas, M., Diapouli, E., Papaefthymiou, H., Migliori, A., Karydas, Padilla-Alvarez, R., Bogovac, M., Kaiser, R.B., Jaksic, M., Bogdanovic-Radovic, I., Eleftheriadis, K., 2015. Source apportionment by PMF on elemental concentrations obtained by PIXE analysis of PM10 samples collected at the vicinity of lignite power plants and mines in Megalopolis, Greece. *Nuclear Instruments and Methods in Physics Research B*, 349, 114–124. <http://dx.doi.org/10.1016/j.nimb.2015.02.037>

- Manousakas, M., Papaefthymiou, H., Diapouli, E., Migliori, A., Karydas, A.G., Bogdanovic-Radovic, I., Eleftheriadis, K., 2017a. Assessment of PM<sub>2.5</sub> sources and their corresponding level of uncertainty in a coastal urban area using EPA PMF 5.0enhanced diagnostics. *Science of the Total Environment*, 574, 155–164. <http://dx.doi.org/10.1016/j.scitotenv.2016.09.047>
- Manousakas, M., Diapouli, E., Papaefthymiou, H., Kantarelou, V., Zarkadas, C., Kalogridis, A.-C., Karydas, A.-G., Eleftheriadis, K., 2017b. XRF characterization and source apportionment of PM<sub>10</sub> samples collected in a coastal city. *X - Ray Spectrometry*, 1–11.DOI: 10.1002/xrs.2817.
- Manta, D.S., Angelone, M., Bellanca, A., Neri, R., Sprovieri, M., 2002. Heavy metals in urban soils: a case study from the city of Palermo (Sicily), Italy. *Sci. Total Environ.*, 300 (1-3), 229-243.
- Matissof, G., Ketterer, M.E., Rosen, K., Mietelski, J.W., Vitko, L.F., Persson, H., Lokas, E., 2011. Downward migration of Chernobyl-derived radionuclides in soils in Poland and Sweden. *Applied Geochemistry*, 26, 105–115.
- Marenco, F., Bonasoni, P., Calzolari, F., Ceriani, M., Chiari, M., Cristofanelli, P., 2006. Characterization of atmospheric aerosols at Monte Cimone, Italy during summer 2004: Source apportionment and transport mechanisms. *Journal of Geophysical Research*, 111, D24202.
- Marinova, S., Yurukova, L., Frontasyeva, M.V., Steinnes, E., Strelkova, L.P., Marinov, A., Karadzinova, A.G., 2010. Air pollution studies in Bulgaria using the moss biomonitoring technique. *Ecological Chemistry and Engineering S*, 17, 1, 37-52.
- Markert, B., 1993. *Plants as Biomonitors; Indicators for Heavy Metals in the Terrestrial Environment*, Weinheim: VCH, pp.1–23.
- Markert, B.A., Breure, A.M., Zechmeister, H.G., 2003. *Bioindicators and biomonitors: principles, concepts, and applications*. Elsevier, Amsterdam.
- Marović, G., Franić, Z., Senčar, J., Bituh, T., Vugrinec, O., 2008. Mosses and Some Mushroom Species as Bioindicators of Radiocaesium Contamination and Risk Assessment. *Coll. Antropol.*, 32 (2), 109–114.
- Masarik, J., Beer, J., 1999. Simulation of particle fluxes and cosmogenic nuclide production in the Earth's atmosphere. *Journal of Geophysical Research* 104, 12099-12111.
- Mason, B., 1966. *Principles of geochemistry*. New York: Wiley.
- Mbong, E.O., Apkan, E.E., Osu, S.R., 2014. Soil-plant heavy metal relations and transfer factor index of habitats densely distributed with *Citrus reticulata* (tangerine). *Journal of Research in Environmental Science and Toxicology*, 3(4), 61-65. DOI: <http://dx.doi.org/10.14303/jrest.2014.014>

- Meng, Y.Y., Wilhelm, M., Rull, R.P., English, P., Ritz, B., 2007. Traffic and outdoor air pollution levels near residences and poorly controlled asthma in adults. *Ann. Allergy Asthma Immunol.* 98 (5), 455–463.
- Mermier, P. & Seldon, E., 1969. Physics of Nuclei and Particles. In: *Physics of Nuclei and Particles*. New York: Academic Press, pp. 274.
- Metzger, K.B., Tolbert, P.E., Klein, M., Peel, J.L., Flanders, W.D., Todd, K., Mulholland, J.A., Ryan, P.B., Frumkin, H., 2004. Ambient air pollution and cardiovascular emergency department visits. *Epidemiology*, 15 (1), 46–56.
- Meyer, C., Diaz-de-Quijano, M., Monna, F., Franchi, M., Toussaint, M., Gilbert, D., Bernard, N., 2015. Characterization and distribution of deposited trace elements transported over long and intermediate distances in north-eastern France using Sphagnum peatlands as a sentinel ecosystem. *Atmos Environ*, 101, 286–293.
- Mirabelli, M.C., Ebelt, S., Damon, S.A., 2020. Air Quality Index and air quality awareness among adults in the United States. *Environmental Research*, 183, 109185. <https://doi.org/10.1016/j.envres.2020.109185>
- Mirecki, N., Agič, R., Šunić, L., Milenković, L., Ilić, Z. S., 2015. Transfer factor as indicator of heavy metals content in plants. *Fresenius Environmental Bulletin*, 24 (11c), 4212-4219.
- Misaelides, P., Sikalidis, S., Tsitouridou, R., Aexiades, C., 1987. Distribution of Fission Products in Dust Samples from the Region of Thessaloniki, Greece, after the Chernobyl Nuclear Accident. *Environmental Pollution*, 47, 1-8.
- Mitcell, N., Pérez-Sánchez, D., Thorne, M.C., 2013. A review of the behavior of U-238 series radionuclides in soils and plants. *Journal of Radioecological Protection*, 33, R17-R48. doi:10.1088/0952-4746/33/2/R17
- Mitrović, B., Ajtić, J., Lazić, M., Andrić, V., Krstić, N., Vranješ B., Vićentijević, M., 2016. Natural and anthropogenic radioactivity in the environment of Kopaonik mountain, Serbia. *Environmental Pollution*, 215, 273-279.
- Moens, L., De Donder, J., De Corte, F., De Wispelaere, A., Simonits, A., Hoste, J., 1981. Calculation of the absolute peak efficiency of gamma-ray detectors for different counting geometries. *Nuclear Instruments and Methods* 187, 451.
- Morton-Bermea, O., Hernández-Álvarez, E., González-Hernández, G., Romero, F., Lozano, R., Beramendi-Orosco, L.E., 2009 Assessment of heavy metal pollution in urban topsoils from the metropolitan area of Mexico City. *J Geochem Explor*, 101, 218–224.
- Nifontova, M., 1995. Radionuclides in the moss-lichen cover of tundra communities in the Yamal Peninsula. *The Science of the Total Environment*, 160/161, 749-752.
- Nikolaidis, C., Orfanidis, M., Hauri, D., Mylonas, S., Constantinidis, T., 2013. Public health risk assessment associated with heavy metal and arsenic exposure near an abandoned mine (Kirki, Greece). *Int. J. Environ. Health Res.* 23, 219–507.

- Noli, F., Tsamos, P., 2016. Concentration of heavy metals and trace elements in soils, waters and vegetables and assessment of health risk in the vicinity of a lignite-fired power plant. *Science of the Total Environment*, 563–564, 377–385. <http://dx.doi.org/10.1016/j.scitotenv.2016.04.098>
- O'Brien, K., De La Zerda Lerner, A., Shea, M.A., Smart, D.F., 1991. The production of cosmogenic isotopes in the earth's atmosphere and their inventories. *The Sun in Time*. University of Arizona Press, Tucson, AZ, 317-342.
- Ogoko, E.C., 2015. Accumulation of Heavy Metal in Soil and Their Transfer to Leafy Vegetables with Phytoremediation Potential. *American Journal of Chemistry*, 5(5), 125-131. DOI: 10.5923/j.chemistry.20150505.01
- Oguri, E., Hironori Deguchi, H., 2018. Radiocesium contamination of the moss *Hypnum plumaeforme* caused by the Fukushima Dai-ichi Nuclear Power Plant accident. *Journal of Environmental Radioactivity*, 192, 648-653. <https://doi.org/10.1016/j.jenvrad.2018.02.013>
- Oğur, A., Özden, B., Saç, M. M., Yener, G., 2003. Biomonitoring of  $^{210}\text{Po}$  and  $^{210}\text{Pb}$  using lichens and mosses around a uraniumiferous coal-fired power plant in western Turkey. *Atmospheric Environment*, 37, 2237–2245.
- Olivier, F., Belis, C.A., Amato, F., Decesari, S., Diapouli, E., El Hadad, I., Gilardoni, S., Harisson, R.M., Hopke, P.K., Larsen, R., Manousakas, M.I., Mocnik, G., Moolbroek, D., Nava, S., Paatero, P., Paglione, M., Prévôt, A., Quass, U., Salvador, P., Takahama, S., Vecchi, R., Viana, M., Vratolis, S., 2019. Reference Report of the European Guide on Air Pollution Source Apportionment with Receptor Models. Joint Research Centre Institute for Environment and Sustainability, pp 3-170.
- Onianwa, P.C., 2001. Monitoring atmospheric metal pollution: a review of the use of mosses as indicators. *Environ Monit Assess*, 71, 13–50.
- Paatero, P., Tapper, U., 1993. Analysis of different modes of factor analysis as least squares fit problems. *Chemometric and Intelligent Laboratory Systems*, 18, 183–194.
- Paatero P, Tapper, U., 1994. Positive Matrix Factorization - a Nonnegative Factor Model with Optimal Utilization of Error-Estimates of Data Values. *Environmetrics*, 5, 111–126.
- Paatero, P., 1997. Least squares formulation of robust non-negative factor analysis. *Chemometrics and Intelligent Laboratory Systems*, 37, 23–35.
- Paatero, J., Jaakkola, T., Kulmala, S., 1998. Lichen (sp. *Cladonia*) as a deposition indicator for transuranium elements investigated with the Chernobyl fallout. *J Environ Radioact*, 38, 2, 223–247.
- Paatero, P, Hopke, PK, Begum, BA, Biswas, SK. A graphical diagnostic method for assessing the rotation in factor analytical models of atmospheric pollution. *Atmospheric Environment*. 2005; 39:193–201.

Paatero, P., Eberly, S., Brown, S. G., and Norris, G. A., 2014. Methods for estimating uncertainty in factor analytic solutions, *Atmos. Meas. Tech.*, 7, 781–797, <https://doi.org/10.5194/amt-7-781-2014>.

Papadakos, G.N., Karangelos, D.J., Petropoulos, N.P., Anagnostakis, M.J., Hinis, E.P., 2017. Uncertainty assessment method for the Cs-137 fallout inventory and penetration depth. *Journal of Environmental Radioactivity*, 171, 234-245. <http://dx.doi.org/10.1016/j.jenvrad.2017.02.009>

Papaefthymiou, H., Kritidis, P., Anousis, J., Sarafidou, J., 2004. Comparative Assessment of natural radioactivity in fallout samples from Patras and Megalopolis, Greece. *Journal of Environmental Radioactivity*, 78, 249–265.

Papaioannou, D., Kalavrouziotis, I.K., Koukoulakis, P.H., Papadopoulos, F., Psoma, P., 2018. Interrelationships of metal transfer factor under wastewater reuse and soil pollution. *Journal of Environmental Management*, 216, 328-336. <http://dx.doi.org/10.1016/j.jenvman.2017.04.008>

Papastefanou, C., Manolopoulou, M., Charalambous, S., 1988. Radiation measurements and Radioecological aspects of fallout from the Chernobyl reactor accident. *Journal of Environmental Radioactivity*, 7 (1), 49-64.

Papastefanou, C., Manolopoulou, M., Sawidis, T., 1989. Lichens and mosses: biological monitors of radioactive fallout from the Chernobyl reactor accident. *Journal of Environmental Radioactivity*, 9, 199–207.

Papastefanou, C., Ioannidou, A., 1991. Depositional fluxes and other physical characteristics of atmospheric Beryllium-7 in the temperate zones (40°N) with a dry (precipitation-free) climate. *Atmospheric Environment*, 25A (10), 2335-2343.

Papastefanou, C., Manolopoulou, M., 1992a. Residence time and uptake rates of <sup>137</sup>Cs in lichens and mosses at temperate latitude (40°N). *Environment International*, 18, 397-401.

Papastefanou, C., Manolopoulou, M., 1992b. Behavior of Natural Radionuclides in Lignites and Fly Ashes. *Journal of Environmental Radioactivity* 16, 261-27.

Papastefanou, C., Ioannidou, A., 1995a. Aerodynamic size association of <sup>7</sup>Be in ambient aerosols. *Journal of Environmental Radioactivity*, 26(3), 273-282.

Papastefanou, C., Ioannidou, A., Stoulos, S., Manolopoulou, M., 1995b. Atmospheric deposition of cosmogenic <sup>7</sup>Be and <sup>137</sup>Cs from fallout of the Chernobyl accident. *The Science of the Total Environment*, 170, 151-156.

Papastefanou, C., Ioannidou, A., 1996a. Beryllium-7 aerosols in ambient air. *Environment International*, 22 (1), S125-S130.

Papastefanou, C., 1996b. Radiological Impact from Atmospheric Releases of <sup>226</sup>Ra from Coal-Fired Power Plants. *J. Environ. Radioactivity*, 32, (1-2), 105-114.

- Papastefanou, C., Manolopoulou, M., Stoulos, S., Ioannidou, A., Gerasopoulos, E., 1999a. Soil-to-plant transfer of  $^{137}\text{Cs}$ ,  $^{40}\text{K}$  and  $^7\text{Be}$ . *Journal of Environmental Radioactivity*, 45, 59-65.
- Papastefanou, C., Manolopoulou, M., Stoulos, S., Ioannidou, A., Gerasopoulos, E., 1999b. Background radiation measurements in the lower atmosphere before and after Chernobyl. *Journal of Environmental Radioactivity*, 42, 87-92.
- Papastefanou, C., Manolopoulou, M., Stoulos, S., Ioannidou, A., Gerasopoulos, E., 2001. Coloured rain dust from Sahara Desert is still radioactive. *Journal of Environmental Radioactivity*, 55, 109–112.
- Papastefanou, C., Manolopoulou, M., Stoulos, S., Ioannidou, A., Gerasopoulos, E., 2005. Cesium-137 in grass from Chernobyl fallout. *Journal of Environmental Radioactivity*, 83, 253-257.
- Papastefanou, C., 2009. Beryllium-7 in Ambient Air. *Aerosol and Air Quality Research*, 9 (2), 187-197.
- Papastefanou, C., 2010. Escaping radioactivity from coal-fired power plants (CPPs) due to coal burning and the associated hazards: a review. *Journal of Environmental Radioactivity* 101, 191–200.
- Papastergios, G., Filippidis, A., Fernandez-Touriel, J.-L., Gimeno, D., Sikalidis, C., 2011. Surface soil geochemistry for environmental assessment in Kavala area, northern Greece. *Water Air Soil Pollut.* 216, 141–152.
- Pappa, F.K., et al., 2016. Radioactivity and metal concentrations in marine sediments associated with mining activities in Ierissos Gulf, North Aegean Sea, Greece. *Appl. Radiat. Isotopes*, <http://dx.doi.org/10.1016/j.apradiso.2016.07.006i>
- Pappa, F.K., 2018. Study and dispersion of radionuclides and heavy metals in coastal areas of Greece, characterized by active and past mining activities. –PhD Thesis. National Technical University of Athens, School of Applied Mathematical and Physical Sciences, Athens, pp. 10-15.
- Park, K.H., Kang, T.W., Kim, W.J., Park, J.W., 2013.  $^{134}\text{Cs}$  and  $^{137}\text{Cs}$  radioactivity in soil and moss samples of Jeju Island after Fukushima nuclear reactor accident. *Applied Radiation and Isotopes*, 81, 379–382.
- Paterson, E., Sanka, M., Clark, L., 1996. Urban soils as pollutant sinks- a case study from Aberdeen, Scotland. *App Geochem*, 11, 129-131.
- Pavlov, S.S., Dmtriev, A.Y., Chepurchenko, I.A., Frontasyeva, M.V., 2014. Automation System for Measurement of Gamma-Ray Spectra of Induced Activity for Multi-Element High Volume Neutron Activation Analysis at the Reactor IBR-2 of Frank Laboratory of Neutron Physics at the Joint Institute for Nuclear Research. ISSN 1547-4771, *Physics of Particles and Nuclei Letters*, 11 (6), 737–742.
- Pavlov, S.S., Dmtriev, A.Y., Frontasyeva, M.V., 2016. Automation system for neutron activation analysis at the reactor IBR-2, Frank Laboratory of Neutron Physics, Joint

Institute for Nuclear Research, Dubna, Russia, J Radioanal Nucl Chem 309, 27–38, DOI 10.1007/s10967-016-4864-8.

Pentari, D., Typou, J., Goodarzi, F., Foscolos, A.E., 2006. Comparison of elements of environmental concern in regular and reclaimed soils, near abandoned coal mines Ptolemaida –Amynteon, northern Greece: impact on wheat crops. *Int. J. Coal Geol.* 65, 51–58.

Peresedov, V.F., Rogov, A.D., 1996. Simulation and analysis of neutron energy spectra from irradiation channels of the IBR-2 reactor. *J. of Radioanal. Nucl. Chem., Letters*, 214(4), 277-283.

Petropoulos, N.P., Hinis, E.P., Simopoulos, S.E., 1996.  $^{137}\text{Cs}$  Chernobyl fallout in Greece and its associated radiological impact. *Environmental International*, 22 (1), S369-S373.

Petropoulos, N.P., Anagnostakis, M.J., Hinis, E.P., Simopoulos, S.E., 2001. Geographical mapping and associated fractal analysis of the long-lived Chernobyl fallout radionuclides in Greece. *Journal of Environmental Radioactivity*, 53, 59-66.

Pham, M.K., Betti, M., Nies, H., Povinec, P.P., 2011. Temporal changes of  $^7\text{Be}$ ,  $^{137}\text{Cs}$  and  $^{210}\text{Pb}$  activity concentrations in surface air at Monaco and their correlation with meteorological parameters. *Journal of Environmental Radioactivity*, 102, 1045-1054. doi:10.1016/j.jenvrad.2011.06.002

Polissar, A.V., Hopke, P.K., Malm, W.C., Sisler, J.F., 1998. Atmospheric aerosol over Alaska: 2. Elemental composition and sources. *Journal of Geophysical Research*, 103, 19 045–19 057.

Polissar, A.V., Hopke, P.K., Paatero, P., Kaufmann, Y.J., Hall, D.K., Bodhaine, B.A., Dutton, E.G., Harris, J.M., 1999. The aerosol at Barrow, Alaska: long-term trends and source locations. *Atmospheric Environment*, 33, 2441–2458.

Popovic, D., Todorovic, D., Frontasyeva, M.V., Ajtic, J., Tasic, M., Rajsic, S., 2008. Radionuclides and heavy metals in Borovac, Southern Serbia. *Environ Sci Pollut Res*, 15, 509–520. DOI 10.1007/s11356-008-0003-6

Popovic, D., Todorovic, D., Aničić, M., Tomasević, M., Nikolić, J., Ajtć, J., 2010. Trace Elements and Radionuclides in Urban Air Monitored by Moss and Tree Leaves, *Air Quality*, Ashok Kumar (Ed.), ISBN: 978-953-307-131-2, InTech, Available from: <http://www.intechopen.com/books/airquality/biomonitoring-of-trace-elements-and-radionuclides-in-urban-air>

Porstendörfer, J., Butterweck, G., Reineking, A., 1991. Diurnal variation of the concentrations of radon and its short-lived daughters in the atmosphere near the ground. *Atmos. Environ.*, 25A (3/4), 709-713.

Pott, U., Turpin, D.H., 1998. Assessment of atmospheric heavy metals by moss monitoring with *isothecium stoloniferum* brid. In the Fraser Valley B.C., Canada. *Water Air Soil Pollut*, 101,25–44.

- Psichoudaki, M., Papaefthymiou, H., 2008. Natural radioactivity measurements in the city of Ptolemais (Northern Greece). *Journal of Environmental Radioactivity*, 99, 1011-1017.
- Puschenreiter, M., Horak, O., 2000. Influence of different soil parameters on the transfer factor soil to plant of Cd, Cu and Zn for wheat and rye. *Die Bodenkultur*. 51(1), 3-10.
- Qarri, F., Lazo, P., Stafilov, T., Frontasyeva, M., Harmens, H., Bekteshi, L., Baceva, K., Goryainov, Z., 2014. Multi-elements atmospheric deposition in Albania. *Environ Sci Pollut Res*, 21, 2506–2518. DOI 10.1007/s11356-013-2091-1.
- Qarri, F., Lazo, P., Bekteshi, L., Stafilov, T., Frontasyeva, M., Harmens, H., 2015. The effect of sampling scheme in the survey of atmospheric deposition of heavy metals in Albania by using moss biomonitoring. *Environ Sci Pollut Res*, 22, 2258–2271. DOI 10.1007/s11356-014-3417-3.
- Raes, F., Graziani, G., Satnners, D., Girardi, F., 1990. Radioactivity measurements in air over Europe after the Chernobyl Accident. *Atmospheric Environment*, 24A(4), 909-916.
- Raman, R.S., Ramachadran, S., Rastogi, N., 2010. Source identification of ambient aerosols over an urban region in western India. *Journal of Environmental Monitoring*, 12, 1330-1340.
- Razali, N.M, & Wah, Y.B., 2011. Power comparisons of Shapiro Wilk, Kolmogorov-Smirnov, Liliefors and Aderson darling tests. *Journal of statistical modeling and Analytics* 2 (1), 21-33.
- Riga-Karandinos, A.N. and Karandinos M.G., 1998. Assessment of air pollution from a lignite power plant in the plain of Megalopolis (Greece) using as biomonitors three species of lichens; impacts on biochemical parameters of lichens. *The Science of the Total Environment*, 215, 167-183.
- Ritchie, S.W., Nguyen, H.T., Holaday, A.S., 1990. Leaf water content and gas exchanges parameters of two wheat genotypes differing in drought resistance. *Crop. Sci.*, 30, 105-111. <http://dx.doi.org/10.2135/cropsci1990.0011183X003000010025x>.
- Romic, M., Romic, D., 2003. Heavy metals distributions in agricultural topsoils in urban areas. *Environmental Geology*, 43, 795-805.
- Rühling, E., Tyler, G., 1968. An ecological approach to the lead problem. *Bot Notiser*, 121, 321–342.
- Saitanis, C. J., Frontasyeva, M. V., Steinnes, E., Palmer, M. W., Ostrovnaya, T. M., Gundorina, S. F., 2012. Spatiotemporal distribution of airborne elements monitored with the moss bags technique in the Greater Thriasion Plain, Attica, Greece. *Environ Monit Assess* DOI 10.1007/s10661-012-2606-0.

- Sarap, N.B., Janković, M.M., Dolijanović, Z.K., Kovačević, D.D., Rajačić, M.M., Nikolić, J.D., Todorović, D.J., 2014. Soil-to-plant transfer factor for  $^{90}\text{Sr}$  and  $^{137}\text{Cs}$ . J Radioanal Nucl Chem, DOI 10.1007/s10967-014-3809-3
- Sardans, J., Peñuelas, J., 2005. Trace element accumulation in the moss *Hypnum cupressiforme* Hedw. And the trees *Quercus ilex* L and *pinushalepensis* mill. In Catalonia. Chemosphere, 60, 1293-1307.
- Savino, F., Pugliese, M., Quarto, M., Adamo, P., Loffredo, F., De Cicco, F., Roca, V., 2017. Thirty years after Chernobyl: Long-term determination of  $^{137}\text{Cs}$  effective half-life in the lichen *Stereocaulon vesuvianum*. Journal of Environmental Radioactivity, 172, 201-206. <http://dx.doi.org/10.1016/j.jenvrad.2017.03.002>
- Skordas, K., Papastergios, G., Filippidis, A., 2013. Major and trace element contents in apples from a cultivated area of Central Greece. Environ. Monit. Assess. 185, 8465–8471.
- Sawidis, T., 1988. Uptake of Radionuclides by Plants after the Chernobyl Accident. Environmental Pollution, 50, 317-324.
- Sawidis, T., Tsikritzis, L., Tsigaridas, K., 2009. Cesium-137 monitoring using mosses from W. Macedonia, N. Greece. Journal of Environmental Management, 90, 2620–2627. doi:10.1016/j.jenvman.2009.02.010
- Sawidis, T., Tsigaridas, K., Tsikritzis, L., 2010. Cesium-137 monitoring using lichens from W. Macedonia, N. Greece. Ecotoxicology and Environmental Safety 73, 1789-1796.
- Schröder, W., Pesch, R., Englert, C., Harmens, H., Suchara, I., Zechmeister, H.G., Thöni, L., Maňková, B., Jeran, Z., Grodzińska, K., Alber, R., 2008. Metal accumulation in mosses across national boundaries: uncovering and ranking causes of spatial variation. Environ Pollut, 151, 377–388.
- Schröder, W., Holy, M., Pesch, R., Harmens, H., Ilyin, I., Steinnes, E., Alber, R., Aleksiyenak, Y., Blum, O., Coşkun, M., Dam, M., De Temmerman, L., Frolova, M., Frontasyeva, M., Gonzalez Miqueo, L., Grodzińska, K., Jeran, Z., Korzekwa, S., Krmar, M., Kubin, E., Kvičkus, K., Leblond, S., Liiv, S., Magnússon, S.H., Maňková, B., Piispanen, J., Rühling, A., Santamaria, J.M., Špirić, Z., Suchara, I., Thöni, L., Urumov, V., Yurukova, L., Zechmeister, H.G., 2010. Are cadmium, lead and mercury concentrations in mosses across Europe primarily determined by atmospheric deposition of these metals? J Soils Sedim, 10, 1572–1584.
- Schwartzberg, K., 2006. Moss biology and phytohormones— Cytokinins in *Physcomitrella*. Plant Biol, 8, 382–388. <https://doi.org/10.1055/s-2006-923962>
- Seinfeld, J.H., Pandis, S.N., 2006. Atmospheric chemistry and physics—from air pollution to climate change, 2nd edn. Wiley, Hoboken.
- Sert, E., Uğur, A., Özden, B., Saç, M. M., Camğoz, B., 2011. Biomonitoring of  $^{210}\text{Po}$  and  $^{210}\text{Pb}$  using lichens and mosses around coal-fired power plants in Western Turkey. J. Environ. Radioact., 102, 535-542. [http://dx.doi.org/10.1016/j.jenvrad](http://dx.doi.org/10.1016/j.jenvrad.2011.02.005). 2011.02.005.

- Shapiro, S.S. and Wilk, M.B., 1965. An analysis of variance test for normality (complete samples). *Biometrika*, 52(3/4), 591-611.
- Shaw, A.J., Goffinet, B., 2000. *Bryophyte Biology*. Cambridge University Press. p. 476.
- Shrivastav, R., 2001. Atmospheric Heavy Metal Pollution (Development of Chronological Records and Geochemical Monitoring). Study in department of chemistry faculty of science, Dayalbagh Educational Institute, Agra, India. *Resonance*, 62-68. ISSN 0971-8044
- Simopoulos, S.E., 1989. Soil Sampling and <sup>137</sup>Cs Analysis of the Chernobyl Fallout in Greece. *Applied Radiation Isotopes*, 40 (7), 607-613.
- Smith, A.J.E., 1982. *Bryophyte Ecology*. Chapman and Hall. London and New York. p. 511.
- Smith, F.B., 1989. The deposition of Chernobyl Caesium-137 in heavy rain and its persistent uptake by grazing sheep. *Agricultural and Forest Meteorology*, 47, 163-177.
- Smith, F.B., Ellis, K.M., 1990. Time Dependent Transport of Chernobyl Radioactivity between Atmospheric and Lichen Phases in Eastern Canada. *Journal of Environmental Radioactivity*, 11, 151-168.
- Sofianska, E., Michailidis, K., 2015. Chemical assessment and fractionation of some heavy metals and arsenic in agricultural soils of the mining affected Drama plain, Macedonia, North Greece. *Environ. Monit. Assess.* 187, 101.
- Spiegel, H., 2002. Trace Element Accumulation in Selected Bioindicators Exposed to Emissions along the Industrial Facilities of Danube Lowland. *Turkish Journal of Chemistry*, 26 (6), 815 – 823, ISSN 1300-0527
- Špirić, Z., Frontasyeva, M., Steinnes, E., Stafilov, T., 2012. Multi-element atmospheric deposition study in Croatia. *Int J Environ Anal Chem.*, 92 (10), 1200–1214.
- Špirić, Z., Vučković, I., Stafilov, T., Kušan, V., Frontasyeva, M. 2013. Air Pollution Study in Croatia Using Moss Biomonitoring and ICP–AES and AAS Analytical Techniques. *Arch Environ Contam Toxicol*, 65, 33–46. DOI 10.1007/s00244-013-9884-6.
- Stamatis, N., Ioannidou, D., Christoforidis, A., Koutrakis, E., 2001. Sediment pollution by heavy metals in the Strymonikos and Ierissos Gulf, North Aegean Sea, Greece. *Environmental Monitoring and Assessment*, 80, 33–49.
- Stamatis, N., Kamidis, N., Pigada, P., Sylaios, G., Koutrakis, E., 2019. Quality Indicators and Possible Ecological Risks of Heavy Metals in the Sediments of three Semi-closed East Mediterranean Gulfs. *Toxics*, 7, 30, 1-16. doi:10.3390/toxics7020030
- Steinnes, E., Rambaek, J., Hanssen, E., 1992. Large scale multi-element survey of atmospheric deposition using naturally growing moss as biomonitor. *Chemos*, 25(5), 735–752.

Steinnes, E., Njåstad, O., 1993. Use of Mosses and Lichens for Regional Mapping of  $^{137}\text{Cs}$  Fallout from the Chernobyl Accident. *J. Environ. Radioactivity*, 21, 65-73.

Steinnes, E., Berg, T., Uggerud, H., Vadset, M., 2007. Atmospheric Deposition of Heavy Metals in Norway. Nation-wide survey in 2005, State Program for Pollution Monitoring, Report 980/2007. Norwegian State Pollution Control Authority, Oslo (in Norwegian).

Steinnes, E., Berg, T., Uggerud, H. T., Pfaffhuber, K. A., 2011. Atmospheric deposition of heavy metals in Norway, National Study in 2010, Rapport 1109/2011 [in Norwegian]. Norwegian University of Science and Technology, Trondheim.

Stoulos, S., Manolopoulou, M., Papastefanou, S., 2004. Measurement of radon emanation factor from granular samples: effects of additives in cement. *Applied Radiation and Isotopes*, 60, 49–54.

Stoulos, S., Ioannidou, A., Vagena, E., Koseoglou, P., Manolopoulou, M., 2014. Post-Chernobyl  $^{137}\text{Cs}$  in the atmosphere of Thessaloniki: a consequence of the financial crisis in Greece. *Journal of Environmental Radioactivity*, 128, 68-74. <http://dx.doi.org/10.1016/j.jenvrad.2013.11.007>

Stoulos, S., Ioannidou, A., 2020. Radon and its progenies variation in the urban polluted atmosphere of the Mediterranean city of Thessaloniki, Greece. *Environmental Science and Pollution Research*, 27, 1160–1166. <https://doi.org/10.1007/s11356-019-07051-4>

Thinova, L., Frontasyeva, M., Vergel, K., Bayushkina, E., 2014. Assessment of contamination with trace elements and man-made radionuclides around Temelin Nuclear Power Plant in Czech Republic. *Radiation Physics and Chemistry*, 104, 432–435.

Thomas, W., 1986. Representativity of mosses as biomonitor organisms for the accumulation of environmental chemicals in plants and soils. *Ecotoxicol Environ Saf*, 11, 339–346.

Thorne, R., Roberts, S., Herrington, R., 2012. The formation and evolution of the Bitincke nickel laterite deposit, Albania. *Mineralium Deposita*, DOI 10.1007/s00126-012-0411-x.

Thöni L., Yurukova L., Bergamini A., Ilyin I., Matthaei D., 2011. Temporal trends and spatial patterns of heavy metal concentrations in mosses in Bulgaria and Switzerland: 1990-2005. *Atmos Environ*, 45, 1899-1912.

Todorović, D., Popović, D., Djurić, G., 1999. Concentration measurements of  $^7\text{Be}$  and  $^{137}\text{Cs}$  in ground level air in the Belgrade city area. *Environmental International*, 25, 59-66.

Tomassini, F.D., Puckett, K.J., Nieboer, E., Richardson, D.H.S., Grace, B., 1976. Determination of copper, iron, nickel and sulphur by X-ray fluorescence in lichens from the Mackenzie Valley, Northwest Territories and the Sudbury district, Ontario. *Can J Bot*, 54, 1591–1603.

Tørseth, K., Aas, W., Breivik, K., Fjaraa, A.M., Fiebig, M., Hjellbrekke, A.G., Lund Myhre, C., Solberg, S., Yttri, K.E., 2012. Introduction to the European Monitoring and Evaluation Programme (EMEP) and observed atmospheric composition change during 1972–2009. *Atmos Chem Phys*, 12, 5447–5481.

Topalidis, V., Harris, A., Hardaway, C. J., Benipal, G., Douvris, C., 2017. Investigation of selected metals in soil samples exposed to agricultural and automobile activities in Macedonia, Greece using inductively coupled plasma-optical emission spectrometry. *Microchemical Journal*, 130, 213–220.

Tsakiri, E., 2009: Bryophyte flora of Greece: phytogeographical and ecological study of bryophytes at the aquatic system of the Ano Aliakmonas River (Western Macedonia). –PhD Thesis, School of Biology, Faculty of Sciences, Aristotle University, Thessaloniki, 356 pp. (in Greek with English summary).

Tsavdaroglou, C., Petrakos, K., Makrygianni, V., 2017. The golden ‘saltomortale’ in the era of crisis. *City*, 21:3-4, 428-447, DOI:10.1080/13604813.2017.1331563, <https://doi.org/10.1080/13604813.2017.1331563>

Tsigaridas, K., 2014. Study of heavy metal and radionuclide contamination in Kozani-Ptolemais basin with the use of bioindicators, water and microorganisms. Doctoral dissertation, Faculty of Sciences, School of Biology, Aristotle University of Thessaloniki, Thessaloniki.

Tsikritzis, L., 2002. Study of the bioaccumulation of heavy metals and radionuclides of plants in West Macedonia. Doctoral dissertation, Technical University of Thessaloniki, Aristotle University of Thessaloniki, Thessaloniki, ISSN 1101-5049.

Tsikritzis, L.I., Fotakis, M., Tzimkas, N., Kolovos, N., Tsikritzi, R., 2008. Distribution and correlation of the natural radionuclides in a coal mine of the West Macedonia Lignite Center (Greece). *Journal of Environmental Radioactivity*, 99, 230-237.

Tsirampides, A., Filippidis, A., 2016. Gold Metallogeny of the SerboMacedonian Rhodope Metallogenic Belt (SRMB). Proceedings of the 14th International Congress, Thessaloniki, May 2016. *Bulletin of the Geological Society of Greece*, vol. L, p. 2037-2046.

Tsoufanidis, N., Landsberger, S., 2010. Measurement and Detection of Radiation, third edition, CRC Press, Boca Raton, pp 72-85.

Tuo, F., Zhang, J., Li, W., Yao, S., Zhou, Q., Li, Z., 2017. Radionuclides in mushrooms. and soil-to-mushroom transfer factors in certain areas of China. *Journal of Environmental Radioactivity*, 180, 59-64.

Tyler, G., 1990. Bryophytes and heavy-metals: a literature review. *Bot J Linn Soc*, 104, 231–253.

Uchida, S., Tagami, K., Hirai, I., 2007. Soil-to-Plant Transfer Factors of Stable Elements and Naturally Occurring Radionuclides (1) Upland Field Crops Collected in Japan. *Journal of NUCLEAR SCIENCE and TECHNOLOGY*, 44 (4), 628–640.

Uğur, A., Özden, B., Saç, M.M., Yener, G., 2003. Biomonitoring of  $^{210}\text{Po}$  and  $^{210}\text{Pb}$  using lichens and mosses around uraniumiferous coal-fired power plant in western Turkey. *Atmospheric Environmental* 37, 2237–2245.

UNSCEAR (2000). Sources and Effects of Ionizing Radiation. United Nations Scientific Committee on the Effects of Atomic Radiation, Vol. I, United Nations, New York.

Vaccaro, S., Sobiecka, E., Contini, S., Locoro, G., Free, G., Gawlik, B.M., 2007. The application of positive matrix factorization in the analysis, characterization and detection of contaminated soils. *Chemosphere*, 69, 1055-1063.

Vagena, E., 2016. Study of the ionizing radiation field around accelerators. PhD Thesis. Aristotle University of Thessaloniki, Thessaloniki, pp. 2.16-21.

Van Grieken, R. & Markowicz, A., 2002. *Handbook of X-ray spectrometry*. New York: Marcel Dekker Inc.

Varol, M., Sünbül, M.R., Aytıp, H., Yilmaz, C.H., 2020. Environmental, ecological and health risks of trace elements and their sources in soils of Harran Plain, Turkey. *Chemosphere*, 245, 125592.

Viana, M., Kyhlbusch, T.A.J., Querol, X., Alastuey, A., Harrison, R.M., Hopke, P.K., Winiwarter, W., Vallius, M., Szidat, S., Prévôt, A.S.H., Hueglin, C., Bloemen, H., Wählin, P., Vecchi, R., Miranda, A.I., Kasper-Giebl, A., Maenhaut, W., Hitzenberger, R., 2008. Source apportionment of particulate matter in Europe: A review of methods and results. *Aerosol Science*, 39, 827-849. doi:10.1016/j.jaerosci.2008.05.007.

Vuković, G., 2015. Biomonitoring of urban air pollution (particulate matter, trace elements and polycyclic aromatic hydrocarbons) using mosses *Spagnum girgensohnii* and *Hypnum cupressiforme* Hedw. Doctoral dissertation, Belgrade, 2015.

Wattanavatee, K., Krmar, M., Bhongsuwan, T., 2017. A survey of natural terrestrial and airborne radionuclides in moss samples from the peninsular Thailand. *Journal of Environmental Radioactivity*, 177, 113-127. <http://dx.doi.org/10.1016/j.jenvrad.2017.06.009>

Wolterbeek, B., 2002. Biomonitoring of trace element air pollution: principles, possibilities and perspectives. *Environ Pollut*, 120, 11–21.

Yin, J., Allen, A. G., Harrison, R. M., Jennings, S. G., Wright, E., Fitzpatrick, M., 2005. Major component composition of urban PM10 and PM2.5 in Ireland. *Atmospheric Research*, 78, 149–165.

Yurukova, L., 2007. Bulgarian experience during the last 3 EU moss surveys. In Proceedings of the 7th Subregional Meeting on Effect-Oriented Activities in the Countries of Eastern and South-Eastern Europe, September 28-October 1, 2006. Risoprint Cluj-Napoca, Baie Mare, Romania, pp. 157-164.

Yurukova, L., Tsakiri, E., Çayır, A., 2009. Cross-Border Response of Moss, *Hypnum cupressiforme* Hedw. to Atmospheric Deposition in Southern Bulgaria and

Northeastern Greece. Bull Environ Contam Toxicol., 83:174–179. DOI 10.1007/s00128-008-9601-8

Zabalza, J., Ogulei, D., Hopke, P. K., Lee, J. H., Hwang, I., Querol, X., 2006. Concentration and sources of PM10 and its constituents in Alsasua, Spain. Water, Air and Soil Pollution, 174, 385–404.

Zechmeister, H.G., Grodzińska, K., Szarek-Łukaszewska, G., 2003. Bryophytes. In: Markert, B.A., Breure, A.M., Zechmeister, H.G. (Eds.), Bioindicators and biomonitors. Elsevier Science Ltd., Amsterdam, pp. 329-375.

Zhang, C., 2006. Using multivariate analyses and GIS to identify pollutants and their spatial patterns in urban soils in Galway, Ireland. Environ Pollut, 142, 501–511.

Zhong, Q., Du, Z., Puigcorbé, V., Wang, J., Wand, Q., Deng, B., Zhang, F., 2019. Accumulation of natural and anthropogenic radionuclides in body profiles of Bryidae, a subgroup of mosses. Environmental Science and Pollution Research. <https://doi.org/10.1007/s11356-019-05993-3>

Zhiyanski, M., Sokolovska, M., Bech, J., Clouvas, A., Penev, I., Badulin, V., 2010. Cesium-137 contamination of oak (*Quercus petrae* Liebl.) from sub-mediterranean zone in South Bulgaria. Journal of Environmental Radioactivity, 101, 864-868. doi:10.1016/j.jenvrad.2010.05.011

Ziembik, Z., Dołhańczuk-Śródka, A., Majcherczyk, T., Waclawek, M., 2013. Illustration of constrained composition statistical methods in the interpretation of radionuclide concentrations in the moss *Pleurozium schreberi*. Journal of Environmental Radioactivity, 117, 13-18.

[https://en.wikipedia.org/wiki/Climate\\_of\\_Greece#/media/File:Greece\\_map\\_of\\_K%C3%B6ppen\\_climate\\_classification\\_\(new\).svg](https://en.wikipedia.org/wiki/Climate_of_Greece#/media/File:Greece_map_of_K%C3%B6ppen_climate_classification_(new).svg)

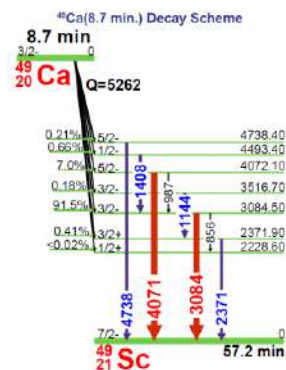
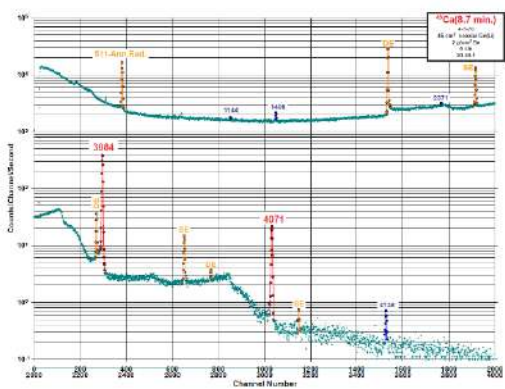
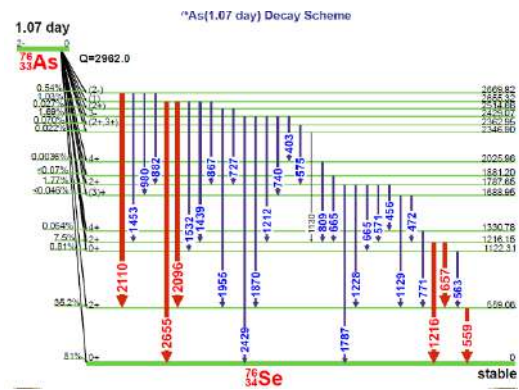
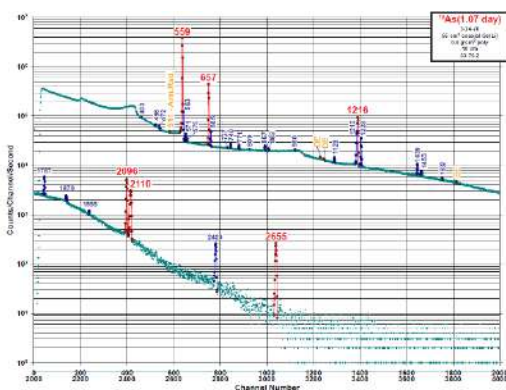
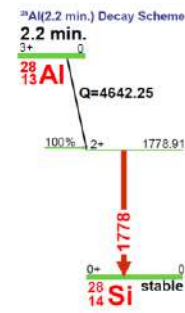
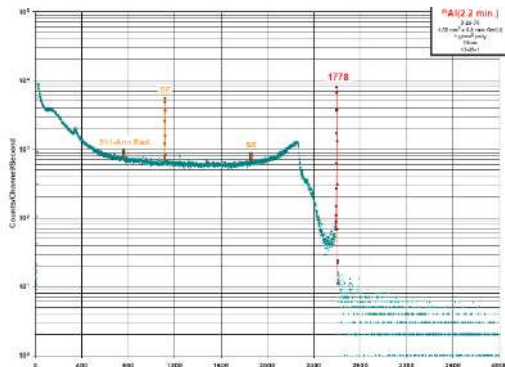
<https://en.wikipedia.org/wiki/Greece#/media/File:EU-Greece.svg>

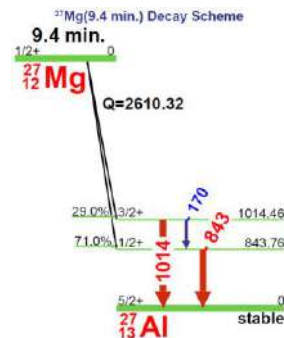
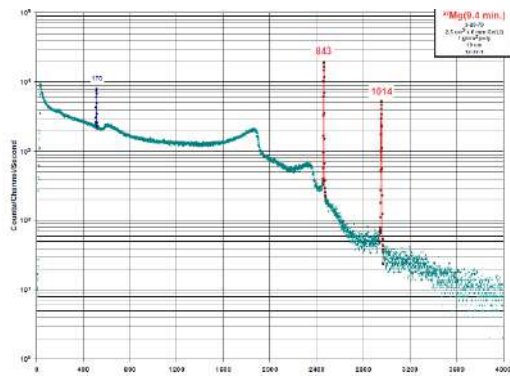
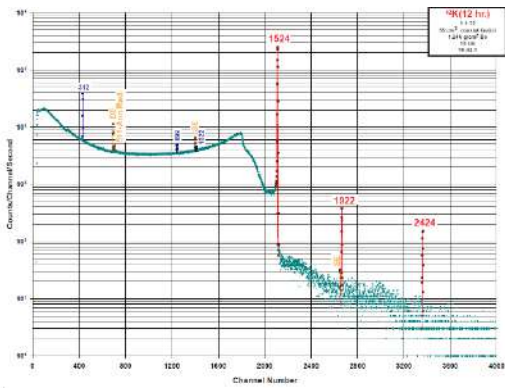
<https://www.miningreece.com/mining-greece/mining-projects/kassandras-mines/>

# APPENDIX

## A.a. Spectra of elements produced after irradiation

Some gamma spectra and decay schemes of different elements (Al, As, Ca, K, Mg) after irradiation of samples are presented (Figures Aa1-10). In reality, the spectra that are produced after the irradiation of samples include plenty of gamma lines and some examples are presented in the main part of this thesis, in Chapter 3.





### A<sub>b</sub>. Trace elements concentrations in mosses

In Table A1 the most frequently analyzed and announced in studies elemental concentrations are presented, while in Table A2 the rest twenty one elemental concentration are shown. The uncertainties of all the elemental concentrations are presented in parenthesis, next to each concentration, and they range from 3% to 44%. The reason why some elemental concentrations have such high uncertainties like those from Rb, Au, Zr, Lu, Cs, I, Br and others is due to the big uncertainties of the standard materials that were irradiated simultaneously with the samples, measured by gamma spectrometry, and involved in the calculation of the elemental concentrations of the samples.

**Table A1.** The concentrations ( $\mu\text{g g}^{-1}$ ) and the uncertainties (%) of the 23 most frequently analyzed and announced in studies elements. that were measured in mosses collected in Northern Greece determined using Epithermal Neutron Activation Analysis (ENAA).

Sampl ing site	Na	Mg	Al	Cl	K	Sc	Ti	V	Cr	Mn	Fe	Co	Ni	Zn	As	Se	Br	Rb	Sb	I	Au	Th	U
x-01	9210(3)	11000(3)	25200(5)	140(10)	7590(8)	4.7(12)	1190(8)	25.6(5)	33(6)	374(6)	10600(5)	3.9(5)	17(5)	28(5)	5.3(5)	0.09(16)	5(30)	23(34)	0.28(8)	1.9(36)	0.0010(40)	4.17(6)	1.31(9)
x-02	902(3)	2320(3)	3270(5)	151(10)	4720(8)	1.4(12)	201(8)	5.5(5)	11(6)	162(6)	3480(5)	1.7(5)	9(5)	34(5)	1.4(5)	0.25(16)	7(30)	13(34)	0.25(8)	1.8(36)	0.0007(40)	0.99(6)	0.25(9)
x-03	4500(3)	7790(3)	2855(5)	164(10)	5850(8)	8.6(12)	200(8)	5.4(5)	33(6)	386(6)	19400(5)	8.5(5)	14(5)	41(5)	2.1(5)	0.14(16)	6(30)	16(34)	0.18(8)	1.8(36)	0.0003(40)	1.85(6)	0.54(9)
x-04	2110(3)	2480(3)	3830(5)	176(10)	4960(8)	2.3(12)	229(8)	8.2(5)	9(6)	160(6)	8190(5)	3.9(5)	5(5)	32(5)	1.6(5)	0.24(16)	6(30)	15(34)	0.34(8)	1.7(36)	0.0008(40)	0.72(6)	0.22(9)
x-05	549(3)	2760(3)	2530(5)	200(10)	4790(8)	0.9(12)	188(8)	5.0(5)	8(6)	44(6)	2470(5)	1.2(5)	5(5)	25(5)	1.8(5)	0.31(16)	9(30)	8(34)	0.36(8)	2.3(36)	0.0005(40)	0.63(6)	0.15(9)
x-06	341(3)	2120(3)	4870(5)	112(10)	3190(8)	0.8(12)	351(8)	7.8(5)	7(6)	70(6)	2250(5)	0.9(5)	5(5)	22(5)	1.3(5)	0.25(16)	6(30)	7(34)	0.17(8)	2.2(36)	0.0003(40)	0.82(6)	0.16(9)
x-07	3690(3)	5010(3)	12100(5)	108(10)	8510(8)	3.2(12)	810(8)	14.2(5)	17(6)	286(6)	7900(5)	2.7(5)	11(5)	46(5)	8.3(5)	0.14(16)	5(30)	42(34)	0.47(8)	1.8(36)	0.0007(40)	2.88(6)	1.13(9)
x-08	320(3)	2410(3)	3190(5)	260(10)	3990(8)	0.6(12)	201(8)	6.3(5)	8(6)	110(6)	1730(5)	0.8(5)	6(5)	37(5)	1.0(5)	0.21(16)	5(30)	6(34)	0.28(8)	1.8(36)	0.0007(40)	0.48(6)	0.10(9)
x-09	207(3)	1730(3)	1810(5)	236(10)	5260(8)	0.3(12)	104(8)	3.3(5)	2(6)	733(6)	1010(5)	0.5(5)	3(5)	19(5)	0.5(5)	0.26(16)	4(30)	8(34)	0.08(8)	1.5(36)	0.0001(40)	0.35(6)	0.07(9)
x-10	606(3)	2560(3)	3610(5)	172(10)	4230(8)	1.5(12)	225(8)	5.4(5)	25(6)	269(6)	3760(5)	2.7(5)	14(5)	26(5)	1.4(5)	0.33(16)	8(30)	15(34)	0.20(8)	1.6(36)	0.0003(40)	1.51(6)	0.23(9)
x-11	569(3)	2170(3)	3200(5)	80(10)	4690(8)	1.7(12)	237(8)	5.6(5)	11(6)	183(6)	3450(5)	1.4(5)	6(5)	174(5)	1.0(5)	0.36(16)	6(30)	11(34)	0.27(8)	2.1(36)	0.0012(40)	0.69(6)	0.21(9)
x-12	507(3)	2070(3)	4050(5)	308(10)	4870(8)	1.1(12)	219(8)	6.4(5)	7(6)	142(6)	2600(5)	1.4(5)	6(5)	247(5)	1.1(5)	0.34(16)	7(30)	7(34)	0.20(8)	2.2(36)	0.0005(40)	0.53(6)	0.20(9)
x-13	567(3)	2440(3)	4590(5)	203(10)	4060(8)	1.0(12)	266(8)	6.5(5)	6(6)	111(6)	2310(5)	0.9(5)	4(5)	144(5)	1.7(5)	0.28(16)	5(30)	17(34)	0.17(8)	2.8(36)	0.0005(40)	0.68(6)	0.12(9)
x-14	363(3)	2680(3)	4030(5)	85(10)	3790(8)	1.1(12)	162(8)	5.3(5)	11(6)	149(6)	2470(5)	1.3(5)	13(5)	124(5)	0.9(5)	0.26(16)	4(30)	15(34)	0.22(8)	1.9(36)	0.0003(40)	0.47(6)	0.15(9)
x-15	386(3)	2760(3)	4110(5)	111(10)	4130(8)	1.0(12)	274(8)	6.5(5)	7(6)	294(6)	2190(5)	0.9(5)	5(5)	154(5)	0.7(5)	0.24(16)	5(30)	10(34)	0.15(8)	2.0(36)	0.0003(40)	0.51(6)	0.16(9)
x-16	724(3)	2450(3)	4030(5)	230(10)	3380(8)	1.4(12)	264(8)	8.2(5)	6(6)	89(6)	2710(5)	1.1(5)	4(5)	142(5)	1.2(5)	0.29(16)	5(30)	6(34)	0.15(8)	2.1(36)	0.0005(40)	0.49(6)	0.14(9)
x-17	1020(3)	3260(3)	5190(5)	118(10)	4440(8)	3.1(12)	349(8)	11.1(5)	8(6)	438(6)	4970(5)	2.4(5)	5(5)	181(5)	15.1(5)	0.18(16)	7(30)	12(34)	0.33(8)	2.0(36)	0.0025(40)	0.55(6)	0.17(9)
x-18	624(3)	3260(3)	5490(5)	164(10)	4290(8)	1.2(12)	304(8)	8.3(5)	8(6)	438(6)	2590(5)	1.9(5)	7(5)	192(5)	1.2(5)	0.34(16)	8(30)	10(34)	0.16(8)	3.0(36)	0.0006(40)	0.77(6)	0.23(9)
x-19	653(3)	4690(3)	9970(5)	271(10)	5820(8)	4.5(12)	529(8)	14.4(5)	28(6)	491(6)	8600(5)	4.7(5)	22(5)	282(5)	17.9(5)	0.16(16)	6(30)	30(34)	2.20(8)	2.4(36)	0.0015(40)	4.08(6)	0.99(9)
x-20	833(3)	3910(3)	6100(5)	193(10)	4800(8)	1.5(12)	385(8)	9.8(5)	9(6)	512(6)	3510(5)	1.3(5)	6(5)	243(5)	1.1(5)	0.33(16)	8(30)	13(34)	0.21(8)	3.3(36)	0.0013(40)	0.85(6)	0.40(9)
x-21	3260(3)	4670(3)	12900(5)	111(10)	7640(8)	4.1(12)	860(8)	18.2(5)	20(6)	167(6)	10200(5)	3.1(5)	11(5)	80(5)	3.1(5)	0.33(16)	6(30)	30(34)	0.26(8)	2.8(36)	0.0012(40)	4.92(6)	0.75(9)
x-22	7780(3)	6440(3)	19600(5)	135(10)	9440(8)	5.4(12)	876(8)	18.9(5)	47(6)	324(6)	12100(5)	5.9(5)	30(5)	112(5)	3.7(5)	0.20(16)	10(30)	50(34)	0.58(8)	2.5(36)	0.0013(40)	7.86(6)	1.31(9)
x-23	679(3)	3110(3)	6100(5)	233(10)	5720(8)	1.2(12)	305(8)	9.3(5)	5(6)	276(6)	2690(5)	1.0(5)	3(5)	39(5)	0.8(5)	0.28(16)	4(30)	10(34)	0.13(8)	2.4(36)	0.0004(40)	1.17(6)	0.34(9)
x-24	5630(3)	7600(3)	20800(5)	147(10)	10200(8)	6.6(12)	1570(8)	14.9(5)	15(6)	1090(6)	16500(5)	3.7(5)	5(5)	88(5)	2.0(5)	0.27(16)	8(30)	49(34)	0.29(8)	2.3(36)	0.0003(40)	5.79(6)	1.30(9)
x-25	848(3)	3770(3)	6520(5)	219(10)	5580(8)	2.9(12)	507(8)	12.6(5)	15(6)	610(6)	6950(5)	3.0(5)	10(5)	76(5)	1.7(5)	0.24(16)	9(30)	19(34)	0.34(8)	2.9(36)	0.0017(40)	1.42(6)	0.47(9)
x-26	7850(3)	8350(3)	30800(5)	91(10)	15300(8)	3.7(12)	873(8)	16.5(5)	12(6)	524(6)	10100(5)	2.8(5)	6(5)	90(5)	5.4(5)	0.33(16)	9(30)	79(34)	0.03(8)	3.6(36)	0.0013(40)	8.93(6)	2.58(9)
x-27	7060(3)	7670(3)	19700(5)	87(10)	16000(8)	6.7(12)	984(8)	20.2(5)	28(6)	361(6)	15300(5)	5.6(5)	13(5)	67(5)	3.6(5)	0.18(16)	5(30)	66(34)	0.21(8)	3.0(36)	0.0013(40)	7.35(6)	1.93(9)
x-28	577(3)	1720(3)	3080(5)	119(10)	3830(8)	0.6(12)	127(8)	3.3(5)	3(6)	66(6)	1470(5)	0.4(5)	2(5)	23(5)	0.9(5)	0.14(16)	4(30)	5(34)	0.08(8)	1.8(36)	0.0002(40)	0.52(6)	0.15(9)
x-29	2170(3)	3010(3)	6890(5)	86(10)	6240(8)	1.5(12)	219(8)	5.7(5)	8(6)	389(6)	3780(5)	1.2(5)	4(5)	53(5)	1.6(5)	0.19(16)	5(30)	25(34)	0.16(8)	2.7(36)	0.0004(40)	1.85(6)	0.45(9)
x-30	3630(3)	2150(3)	3790(5)	47(10)	6370(8)	2.5(12)	174(8)	4.2(5)	22(6)	104(6)	7090(5)	2.7(5)	13(5)	49(5)	1.8(5)	0.19(16)	8(30)	35(34)	0.32(8)	1.8(36)	0.0009(40)	5.01(6)	0.97(9)

x-31	854(3)	3670(3)	6600(5)	107(10)	5430(8)	1.4(12)	463(8)	11.4(5)	15(6)	541(6)	4810(5)	2.3(5)	12(5)	39(5)	1.2(5)	0.35(16)	8(30)	31(34)0.22(8)	4.0(36)	0.0005(40)	1.45(6)	0.48(9)
x-32	625(3)	3780(3)	8310(5)	56(10)	5670(8)	1.0(12)	471(8)	10.6(5)	8(6)	216(6)	2990(5)	1.4(5)	6(5)	20(5)	1.2(5)	0.13(16)	3(30)	13(34)0.07(8)	2.8(36)	0.0003(40)	0.88(6)	0.30(9)
x-33	513(3)	2780(3)	3640(5)	90(10)	4870(8)	0.6(12)	198(8)	4.9(5)	7(6)	146(6)	1880(5)	0.9(5)	5(5)	17(5)	0.7(5)	0.20(16)	3(30)	6(34)0.08(8)	1.8(36)	0.0001(40)	0.51(6)	0.19(9)
x-34	7180(3)	6340(3)	21200(5)	65(10)	14500(8)	8.9(12)	1480(8)	29.3(5)	68(6)	511(6)	28700(5)	13.7(5)	24(5)	40(5)	3.3(5)	0.38(16)	3(30)	76(34)0.07(8)	3.8(36)	0.0006(40)	9.54(6)	2.31(9)
x-35	1830(3)	871(3)	12500(5)	122(10)	5040(8)	2.2(12)	871(8)	19.6(5)	64(6)	473(6)	6670(5)	4.0(5)	31(5)	37(5)	1.7(5)	0.34(16)	13(30)	16(34)0.16(8)	7.4(36)	0.0003(40)	1.89(6)	0.83(9)
x-36	932(3)	11300(3)	7830(5)	125(10)	4290(8)	2.9(12)	478(8)	16.4(5)	174(6)	179(6)	10600(5)	10.4(5)	25(5)	30(5)	1.6(5)	0.31(16)	11(30)	14(34)0.17(8)	3.9(36)	0.0003(40)	1.55(6)	0.93(9)
x-37	643(3)	4670(3)	4730(5)	145(10)	5830(8)	1.2(12)	304(8)	7.6(5)	19(6)	251(6)	3770(5)	1.8(5)	12(5)	19(5)	0.9(5)	0.28(16)	12(30)	14(34)0.15(8)	3.8(36)	0.0002(40)	0.93(6)	0.27(9)
x-38	327(3)	2450(3)	2870(5)	75(10)	4740(8)	0.6(12)	180(8)	4.6(5)	13(6)	158(6)	2090(5)	1.1(5)	9(5)	16(5)	0.6(5)	0.17(16)	3(30)	15(34)0.08(8)	1.8(36)	0.0002(40)	0.47(6)	0.15(9)
x-39	1590(3)	705(3)	7010(5)	87(10)	5970(8)	1.0(12)	393(8)	7.8(5)	16(6)	709(6)	3320(5)	1.5(5)	10(5)	29(5)	0.9(5)	0.26(16)	5(30)	23(34)0.10(8)	3.0(36)	0.0003(40)	1.62(6)	0.65(9)
x-40	344(3)	3080(3)	5560(5)	130(10)	5760(8)	1.1(12)	323(8)	9.3(5)	29(6)	356(6)	3700(5)	2.3(5)	23(5)	22(5)	1.1(5)	0.27(16)	5(30)	24(34)0.02(8)	3.6(36)	0.0000(40)	0.90(6)	0.80(9)
x-41	1540(3)	5120(3)	7170(5)	100(10)	7740(8)	2.0(12)	447(8)	11.1(5)	35(6)	280(6)	6370(5)	2.9(5)	23(5)	28(5)	0.9(5)	0.16(16)	4(30)	26(34)0.22(8)	2.5(36)	0.0003(40)	1.67(6)	0.43(9)
x-42	3580(3)	12000(3)	15100(5)	69(10)	6590(8)	3.7(12)	941(8)	23.7(5)	190(6)	269(6)	11600(5)	8.1(5)	90(5)	30(5)	1.6(5)	0.12(16)	4(30)	31(34)0.21(8)	2.6(36)	0.0001(40)	2.10(6)	0.60(9)
x-43	1160(3)	3130(3)	3770(5)	369(10)	6390(8)	2.0(12)	199(8)	7.3(5)	31(6)	381(6)	5800(5)	3.2(5)	32(5)	51(5)	2.0(5)	0.31(16)	13(30)	16(34)0.35(8)	6.0(36)	0.0003(40)	1.22(6)	0.08(9)
x-44	366(3)	2490(3)	3730(5)	184(10)	3930(8)	0.9(12)	243(8)	7.2(5)	10(6)	74(6)	2790(5)	1.3(5)	7(5)	44(5)	1.4(5)	0.28(16)	5(30)	8(34)0.18(8)	3.1(36)	0.0000(40)	0.65(6)	0.23(9)
x-45	270(3)	3130(3)	5620(5)	196(10)	3760(8)	0.7(12)	420(8)	9.7(5)	8(6)	133(6)	2560(5)	0.9(5)	6(5)	35(5)	0.9(5)	0.44(16)	5(30)	8(34)0.17(8)	5.5(36)	0.0001(40)	0.55(6)	0.19(9)
x-46	1320(3)	13500(3)	7660(5)	105(10)	4620(8)	3.7(12)	498(8)	17.4(5)	222(6)	280(6)	13800(5)	15.0(5)	30(5)	38(5)	1.6(5)	0.21(16)	4(30)	14(34)0.23(8)	2.6(36)	0.0007(40)	1.20(6)	0.42(9)
x-47	270(3)	4950(3)	3210(5)	84(10)	3600(8)	0.6(12)	242(8)	6.6(5)	32(6)	109(6)	1870(5)	1.8(5)	26(5)	17(5)	0.8(5)	0.24(16)	2(30)	7(34)0.09(8)	2.7(36)	0.0012(40)	0.28(6)	0.10(9)
x-48	3470(3)	8690(3)	11700(5)	212(10)	6000(8)	4.2(12)	954(8)	21.8(5)	42(6)	285(6)	13900(5)	20.3(5)	40(5)	37(5)	1.0(5)	0.14(16)	5(30)	18(34)0.02(8)	3.4(36)	0.0011(40)	1.77(6)	0.46(9)
x-49	1750(3)	5420(3)	8110(5)	181(10)	5830(8)	2.5(12)	532(8)	13.2(5)	28(6)	262(6)	7410(5)	5.1(5)	30(5)	40(5)	3.2(5)	0.15(16)	4(30)	19(34)0.24(8)	2.8(36)	0.0005(40)	1.90(6)	0.47(9)
x-50	1270(3)	5720(3)	15100(5)	119(10)	8680(8)	2.3(12)	833(8)	16.4(5)	20(6)	170(6)	7470(5)	3.0(5)	13(5)	38(5)	6.1(5)	0.13(16)	6(30)	33(34)0.34(8)	4.9(36)	0.0030(40)	3.55(6)	0.86(9)
x-51	1590(3)	3320(3)	6920(5)	117(10)	5600(8)	1.6(12)	399(8)	8.1(5)	8(6)	166(6)	3470(5)	1.3(5)	3(5)	26(5)	1.7(5)	0.10(16)	4(30)	20(34)0.15(8)	2.5(36)	0.0002(40)	2.39(6)	0.79(9)
x-52	1610(3)	2770(3)	5840(5)	83(10)	5750(8)	1.7(12)	359(8)	6.7(5)	4(6)	117(6)	4200(5)	1.6(5)	2(5)	38(5)	0.7(5)	0.02(16)	3(30)	13(34)0.10(8)	1.5(36)	0.0006(40)	2.79(6)	0.60(9)
x-53	8290(3)	6140(3)	13800(5)	134(10)	11100(8)	6.0(12)	869(8)	13.3(5)	11(6)	243(6)	15500(5)	4.6(5)	5(5)	58(5)	1.6(5)	0.27(16)	6(30)	60(34)0.02(8)	1.8(36)	0.0003(40)	13.60(6)	3.38(9)
x-54	939(3)	3550(3)	6160(5)	226(10)	5610(8)	1.9(12)	432(8)	8.7(5)	8(6)	190(6)	4240(5)	1.7(5)	4(5)	44(5)	1.4(5)	0.16(16)	10(30)	14(34)0.20(8)	5.2(36)	0.0007(40)	1.93(6)	0.42(9)
x-55	791(3)	3410(3)	6320(5)	127(10)	5130(8)	2.3(12)	389(8)	10.0(5)	13(6)	188(6)	5270(5)	2.4(5)	10(5)	66(5)	4.8(5)	0.15(16)	15(30)	19(34)0.44(8)	4.7(36)	0.0011(40)	1.87(6)	0.52(9)
x-56	1980(3)	4510(3)	7460(5)	206(10)	8700(8)	1.9(12)	388(8)	9.2(5)	9(6)	515(6)	6950(5)	2.6(5)	4(5)	42(5)	0.9(5)	0.28(16)	6(30)	37(34)0.19(8)	2.5(36)	0.0079(40)	3.19(6)	0.88(9)
x-57	1250(3)	4550(3)	9450(5)	117(10)	6840(8)	1.2(12)	442(8)	9.1(5)	7(6)	247(6)	4970(5)	1.5(5)	4(5)	32(5)	0.8(5)	0.21(16)	6(30)	19(34)0.16(8)	3.0(36)	0.0010(40)	0.99(6)	0.35(9)
x-58	482(3)	2620(3)	3090(5)	113(10)	5820(8)	1.0(12)	186(8)	4.3(5)	8(6)	258(6)	3270(5)	1.2(5)	5(5)	28(5)	0.8(5)	0.25(16)	7(30)	15(34)0.24(8)	2.1(36)	0.0011(40)	0.88(6)	0.26(9)
x-59	391(3)	2410(3)	3660(5)	58(10)	4610(8)	0.9(12)	217(8)	5.2(5)	8(6)	274(6)	2950(5)	1.3(5)	5(5)	24(5)	0.9(5)	0.27(16)	8(30)	26(34)0.17(8)	2.9(36)	0.0007(40)	0.87(6)	0.22(9)
x-60	231(3)	4710(3)	4790(5)	133(10)	5050(8)	0.7(12)	305(8)	6.6(5)	6(6)	147(6)	2260(5)	0.9(5)	3(5)	39(5)	0.9(5)	0.22(16)	3(30)	13(34)0.18(8)	3.6(36)	0.0023(40)	0.59(6)	0.15(9)
x-61	878(3)	3600(3)	5850(5)	92(10)	6070(8)	1.0(12)	348(8)	6.8(5)	7(6)	271(6)	3540(5)	1.2(5)	4(5)	35(5)	0.9(5)	0.23(16)	5(30)	11(34)0.16(8)	2.8(36)	0.0005(40)	0.98(6)	0.31(9)
x-62	225(3)	3030(3)	3060(5)	137(10)	4060(8)	0.5(12)	178(8)	4.0(5)	5(6)	188(6)	1780(5)	0.7(5)	3(5)	33(5)	0.7(5)	0.21(16)	5(30)	9(34)0.15(8)	2.1(36)	0.0004(40)	0.47(6)	0.12(9)
x-63	184(3)	1980(3)	2410(5)	190(10)	6430(8)	0.3(12)	135(8)	3.6(5)	3(6)	46(6)	1060(5)	0.5(5)	2(5)	135(5)	1.3(5)	0.11(16)	2(30)	7(34)0.11(8)	1.7(36)	0.0008(40)	0.36(6)	0.09(9)
x-64	2370(3)	5120(3)	12200(5)	133(10)	10700(8)	1.5(12)	343(8)	5.7(5)	6(6)	216(6)	4870(5)	1.7(5)	4(5)	49(5)	1.3(5)	0.29(16)	5(30)	42(34)0.20(8)	2.7(36)	0.0002(40)	6.18(6)	0.88(9)
x-65	258(3)	1530(3)	2190(5)	65(10)	2920(8)	0.6(12)	123(8)	3.4(5)	6(6)	34(6)	2110(5)	0.8(5)	3(5)	18(5)	0.9(5)	0.18(16)	4(30)	8(34)0.19(8)	1.9(36)	0.0009(40)	0.63(6)	0.15(9)
x-66	1240(3)	6110(3)	9370(5)	156(10)	7870(8)	3.2(12)	803(8)	16.4(5)	24(6)	142(6)	9410(5)	4.4(5)	12(5)	42(5)	10.3(5)	0.19(16)	10(30)	23(34)0.53(8)	4.2(36)	0.0019(40)	1.88(6)	0.63(9)

x-67	697(3)	7760(3)	7680(5)	125(10)	7860(8)	1.7(12)	514(8)	13.2(5)	41(6)	210(6)	5510(5)	5.8(5)	25(5)	58(5)	2.2(5)	0.36(16)	10(30)	13(34)0.38(8)	6.4(36)	0.0017(40)	1.20(6)	0.37(9)
x-68	8900(3)	9220(3)	16600(5)	108(10)	12000(8)	7.8(12)	1100(8)	24.9(5)	42(6)	358(6)	19900(5)	8.6(5)	18(5)	51(5)	5.7(5)	0.13(16)	7(30)	34(34)0.28(8)	2.8(36)	0.0012(40)	3.41(6)	1.72(9)
x-69	234(3)	1480(3)	1350(5)	71(10)	2160(8)	0.6(12)	97(8)	2.6(5)	5(6)	38(6)	1800(5)	1.3(5)	3(5)	15(5)	2.3(5)	0.26(16)	4(30)	5(34)0.17(8)	1.3(36)	0.0007(40)	0.30(6)	0.11(9)
x-70	3090(3)	6790(3)	14500(5)	164(10)	9580(8)	3.3(12)	700(8)	16.7(5)	22(6)	129(6)	9980(5)	4.4(5)	11(5)	62(5)	6.7(5)	0.12(16)	6(30)	44(34)0.59(8)	3.0(36)	0.0051(40)	4.29(6)	1.92(9)
x-71	292(3)	3840(3)	2800(5)	340(10)	6580(8)	0.7(12)	173(8)	4.6(5)	23(6)	47(6)	2420(5)	1.7(5)	19(5)	25(5)	1.7(5)	0.24(16)	7(30)	11(34)0.17(8)	4.4(36)	0.0072(40)	0.48(6)	0.20(9)
x-72	568(3)	4670(3)	7410(5)	140(10)	7360(8)	1.8(12)	528(8)	11.4(5)	28(6)	200(6)	6380(5)	3.4(5)	21(5)	82(5)	2.7(5)	0.28(16)	7(30)	41(34)0.34(8)	4.9(36)	0.0019(40)	1.43(6)	0.54(9)
x-73	9140(3)	17800(3)	46100(5)	140(10)	16500(8)	5.2(12)	1760(8)	33.4(5)	46(6)	566(6)	16000(5)	5.9(5)	25(5)	89(5)	2.7(5)	0.14(16)	8(30)	83(34)0.20(8)	4.4(36)	0.0019(40)	0.50(6)	0.15(9)
x-74	751(3)	3460(3)	3760(5)	99(10)	5270(8)	1.6(12)	253(8)	8.0(5)	61(6)	221(6)	4680(5)	4.3(5)	32(5)	33(5)	1.6(5)	0.22(16)	4(30)	8(34)0.20(8)	2.9(36)	0.0008(40)	0.58(6)	0.24(9)
x-75	327(3)	2180(3)	2060(5)	144(10)	6660(8)	0.6(12)	144(8)	3.6(5)	5(6)	156(6)	1860(5)	1.0(5)	4(5)	22(5)	0.8(5)	0.19(16)	3(30)	7(34)0.10(8)	2.1(36)	0.0010(40)	0.30(6)	0.10(9)
x-76	269(3)	2280(3)	2260(5)	98(10)	5930(8)	0.4(12)	167(8)	4.4(5)	6(6)	119(6)	1470(5)	0.8(5)	4(5)	32(5)	0.8(5)	0.24(16)	4(30)	9(34)0.13(8)	1.7(36)	0.0004(40)	0.35(6)	0.09(9)
x-77	327(3)	3680(3)	4480(5)	152(10)	4740(8)	0.7(12)	221(8)	6.0(5)	7(6)	280(6)	2430(5)	1.0(5)	7(5)	24(5)	1.7(5)	0.16(16)	6(30)	7(34)0.14(8)	1.8(36)	0.0013(40)	0.56(6)	0.15(9)
x-78	1140(3)	3280(3)	6140(5)	99(10)	7330(8)	1.0(12)	244(8)	6.2(5)	12(6)	219(6)	3200(5)	1.5(5)	13(5)	32(5)	1.1(5)	0.14(16)	5(30)	28(34)0.19(8)	1.4(36)	0.0005(40)	3.51(6)	0.90(9)
x-79	1760(3)	4430(3)	14500(5)	108(10)	10500(8)	2.3(12)	706(8)	15.7(5)	22(6)	759(6)	8310(5)	4.7(5)	14(5)	76(5)	6.2(5)	0.22(16)	10(30)	48(34)3.23(8)	1.9(36)	0.0006(40)	6.37(6)	1.50(9)
x-80	241(3)	2430(3)	4190(5)	86(10)	4770(8)	0.5(12)	219(8)	5.9(5)	5(6)	152(6)	1560(5)	0.8(5)	6(5)	20(5)	0.8(5)	0.21(16)	4(30)	10(34)0.08(8)	1.3(36)	0.0009(40)	0.36(6)	0.09(9)
x-81	478(3)	4390(3)	6510(5)	158(10)	4580(8)	1.1(12)	364(8)	9.7(5)	18(6)	323(6)	4010(5)	2.0(5)	18(5)	48(5)	1.6(5)	0.26(16)	9(30)	17(34)0.23(8)	2.0(36)	0.0010(40)	1.04(6)	0.26(9)
x-82	449(3)	4590(3)	5610(5)	98(10)	4400(8)	1.3(12)	310(8)	8.5(5)	57(6)	228(6)	4630(5)	3.4(5)	39(5)	28(5)	1.5(5)	0.17(16)	6(30)	18(34)0.15(8)	1.4(36)	0.0011(40)	0.90(6)	0.22(9)
x-83	322(3)	4020(3)	5230(5)	71(10)	4290(8)	1.0(12)	305(8)	8.0(5)	26(6)	131(6)	3480(5)	2.0(5)	20(5)	23(5)	1.3(5)	0.14(16)	4(30)	12(34)0.13(8)	1.4(36)	0.0004(40)	0.86(6)	0.27(9)
x-84	1240(3)	4180(3)	7200(5)	208(10)	17200(8)	8.2(12)	344(8)	10.6(5)	98(6)	118(6)	23600(5)	10.8(5)	47(5)	79(5)	8.0(5)	0.17(16)	8(30)	69(34)0.48(8)	1.7(36)	0.0079(40)	6.80(6)	1.08(9)
x-85	286(3)	2660(3)	4360(5)	117(10)	4570(8)	0.8(12)	243(8)	5.7(5)	8(6)	121(6)	2910(5)	1.1(5)	4(5)	30(5)	2.4(5)	0.25(16)	8(30)	16(34)0.21(8)	2.1(36)	0.0007(40)	0.85(6)	0.23(9)
x-86	4800(3)	7250(3)	17900(5)	149(10)	9070(8)	1.8(12)	642(8)	9.3(5)	12(6)	299(6)	5930(5)	1.7(5)	5(5)	32(5)	2.1(5)	0.34(16)	9(30)	37(34)0.30(8)	1.5(36)	0.0011(40)	8.47(6)	1.76(9)
x-87	300(3)	2920(3)	3230(5)	160(10)	4230(8)	0.8(12)	170(8)	4.7(5)	7(6)	189(6)	2590(5)	1.1(5)	5(5)	33(5)	2.5(5)	0.34(16)	14(30)	20(34)0.26(8)	1.8(36)	0.0013(40)	0.66(6)	0.18(9)
x-88	1870(3)	4010(3)	6300(5)	113(10)	6540(8)	2.6(12)	425(8)	9.3(5)	25(6)	235(6)	7720(5)	3.3(5)	14(5)	57(5)	13.3(5)	0.23(16)	5(30)	20(34)0.67(8)	1.2(36)	0.0172(40)	2.02(6)	0.52(9)
x-89	616(3)	3530(3)	5430(5)	196(10)	4920(8)	1.8(12)	282(8)	7.9(5)	18(6)	253(6)	5540(5)	3.0(5)	12(5)	49(5)	2.1(5)	0.48(16)	15(30)	16(34)0.36(8)	1.8(36)	0.0017(40)	1.47(6)	0.37(9)
x-90	420(3)	2990(3)	4980(5)	95.2(10)	3960(8)	1.0(12)	301(8)	6.5(5)	9(6)	72(6)	3130(5)	1.2(5)	5(5)	23(5)	0.9(5)	0.20(16)	6(30)	10(34)0.15(8)	1.3(36)	0.0004(40)	0.92(6)	0.24(9)
x-91	3210(3)	8220(3)	16400(5)	311(10)	7660(8)	2.5(12)	753(8)	20.0(5)	56(6)	313(6)	7120(5)	4.0(5)	27(5)	44(5)	1.4(5)	0.29(16)	15(30)	20(34)0.24(8)	2.0(36)	0.0011(40)	2.95(6)	0.64(9)
x-92	274(3)	3600(3)	6170(5)	92(10)	4230(8)	0.8(12)	322(8)	8.1(5)	8(6)	148(6)	2410(5)	1.3(5)	6(5)	22(5)	1.8(5)	0.19(16)	5(30)	8(34)0.23(8)	1.0(36)	0.0011(40)	0.79(6)	0.18(9)
x-93	687(3)	5370(3)	5380(5)	380(10)	6070(8)	1.0(12)	327(8)	8.3(5)	18(6)	81(6)	3110(5)	1.6(5)	11(5)	30(5)	0.8(5)	0.23(16)	7(30)	8(34)0.12(8)	1.9(36)	0.0009(40)	0.68(6)	0.17(9)
x-94	223(3)	2670(3)	4230(5)	136(10)	4170(8)	0.6(12)	252(8)	5.7(5)	6(6)	86(6)	2070(5)	0.8(5)	4(5)	22(5)	1.0(5)	0.20(16)	7(30)	14(34)0.16(8)	1.5(36)	0.0007(40)	0.49(6)	0.16(9)
x-95	777(3)	5830(3)	8250(5)	163(10)	5860(8)	1.1(12)	372(8)	9.7(5)	9(6)	1080(6)	3460(5)	1.5(5)	6(5)	31(5)	1.4(5)	0.42(16)	12(30)	24(34)0.28(8)	2.6(36)	0.0010(40)	1.27(6)	0.30(9)

**Table A2.** The concentrations ( $\mu\text{g g}^{-1}$ ) and the uncertainties (%) of the rest 21 elements that were measured in mosses collected in Northern Greece determined using Epithermal Neutron Activation Analysis (ENAA).

Sampl ing site	Si	Sr	Ca	Zr	Cs	Ba	La	Ce	Nd	Sm	Gd	Tb	Dy	Yb	Tm	Hf	Lu	Ta	In	Mo	Ag
x-01	211000(20)	112(7)	14200(11)	69(30)	0.87(30)	224(5)	10.70(7)	22(7)	10.00(21)	0.010(12)	0.217(21)	0.293(14)	1.26(25)	0.57(18)	0.153(22)	1.69(30)	0.340(44)	0.406(30)	0.06(31)	0.26(31)	0.049(14)
x-02	61000(20)	32(7)	6680(11)	18(30)	0.42(30)	59(5)	3.09(7)	6(7)	2.40(21)	0.005(12)	1.080(21)	0.087(14)	0.22(25)	0.15(18)	0.049(22)	0.51(30)	0.057(44)	0.135(30)	0.03(31)	0.37(31)	0.029(14)
x-03	83700(20)	60(7)	9730(11)	68(30)	0.69(30)	123(5)	7.67(7)	15(7)	9.16(21)	0.010(12)	3.230(21)	0.438(14)	1.43(25)	0.89(18)	0.229(22)	1.63(30)	0.275(44)	0.253(30)	0.10(31)	0.46(31)	0.060(14)
x-04	62400(20)	90(7)	6480(11)	13(30)	1.53(30)	55(5)	3.67(7)	8(7)	3.98(21)	0.006(12)	0.644(21)	0.110(14)	0.25(25)	0.19(18)	0.050(22)	0.36(30)	0.077(44)	0.084(30)	0.03(31)	0.24(31)	0.037(14)
x-05	49300(20)	36(7)	7880(11)	4(30)	0.30(30)	31(5)	1.84(7)	4(7)	1.76(21)	0.004(12)	0.292(21)	0.055(14)	0.20(25)	0.07(18)	0.028(22)	0.24(30)	0.023(44)	0.065(30)	0.03(31)	0.14(31)	0.024(14)
x-06	45100(20)	22(7)	8770(11)	13(30)	0.31(30)	33(5)	2.45(7)	5(7)	1.66(21)	0.005(12)	0.337(21)	0.061(14)	0.31(25)	0.09(18)	0.013(22)	0.31(30)	0.026(44)	0.081(30)	0.01(31)	0.15(31)	0.023(14)
x-07	94400(20)	33(7)	7640(11)	103(30)	2.01(30)	104(5)	13.30(7)	27(7)	12.00(21)	0.012(12)	1.600(21)	0.458(14)	1.57(25)	0.94(18)	0.202(22)	2.25(30)	0.225(44)	0.517(30)	0.15(31)	0.09(31)	0.048(14)
x-08	56500(20)	22(7)	10500(11)	3(30)	0.22(30)	27(5)	1.48(7)	3(7)	1.34(21)	0.004(12)	0.190(21)	0.037(14)	0.16(25)	0.04(18)	0.006(22)	0.21(30)	0.014(44)	0.066(30)	0.03(31)	0.26(31)	0.021(14)
x-09	63000(20)	29(7)	9180(11)	5(30)	0.27(30)	72(5)	0.50(7)	2(7)	1.82(21)	0.003(12)	0.180(21)	0.022(14)	0.36(25)	0.03(18)	0.010(22)	0.14(30)	0.029(44)	0.038(30)	0.04(31)	0.10(31)	0.018(14)
x-10	62900(20)	46(7)	6880(11)	29(30)	0.78(30)	149(5)	5.88(7)	12(7)	4.98(21)	0.007(12)	0.592(21)	0.154(14)	0.29(25)	0.27(18)	0.052(22)	0.71(30)	0.111(44)	0.141(30)	0.03(31)	0.02(31)	0.032(14)
x-11	59400(20)	32(7)	5110(11)	5(30)	0.45(30)	61(5)	2.87(7)	6(7)	2.43(21)	0.006(12)	0.389(21)	0.065(14)	0.26(25)	0.05(18)	0.028(22)	0.41(30)	0.036(44)	0.098(30)	0.03(31)	0.21(31)	0.049(14)
x-12	65500(20)	23(7)	4900(11)	10(30)	0.33(30)	62(5)	3.61(7)	7(7)	3.07(21)	0.006(12)	0.169(21)	0.066(14)	0.31(25)	0.03(18)	0.022(22)	0.31(30)	0.034(44)	0.081(30)	0.04(31)	0.25(31)	0.046(14)
x-13	20300(20)	27(7)	6570(11)	12(30)	0.47(30)	60(5)	2.37(7)	5(7)	1.75(21)	0.006(12)	0.358(21)	0.052(14)	0.06(25)	0.11(18)	0.017(22)	0.34(30)	0.119(44)	0.111(30)	0.04(31)	0.22(31)	0.045(14)
x-14	65400(20)	29(7)	5040(11)	5(30)	1.30(30)	49(5)	2.15(7)	4(7)	1.73(21)	0.005(12)	0.242(21)	0.050(14)	0.27(25)	0.04(18)	0.023(22)	0.25(30)	0.066(44)	0.066(30)	0.04(31)	0.13(31)	0.047(14)
x-15	71500(20)	34(7)	7080(11)	11(30)	0.30(30)	76(5)	2.04(7)	4(7)	2.01(21)	0.005(12)	0.171(21)	0.046(14)	0.32(25)	0.19(18)	0.016(22)	0.26(30)	0.024(44)	0.064(30)	0.04(31)	0.18(31)	0.044(14)
x-16	46600(20)	26(7)	6290(11)	5(30)	0.27(30)	25(5)	2.15(7)	5(7)	1.92(21)	0.006(12)	0.233(21)	0.064(14)	0.27(25)	0.07(18)	0.027(22)	0.25(30)	0.082(44)	0.059(30)	0.04(31)	0.22(31)	0.044(14)
x-17	55700(20)	36(7)	6030(11)	6(30)	0.75(30)	56(5)	2.19(7)	5(7)	1.85(21)	0.006(12)	0.175(21)	0.081(14)	0.36(25)	0.13(18)	0.045(22)	0.35(30)	0.062(44)	0.065(30)	0.04(31)	0.13(31)	0.057(14)
x-18	72500(20)	36(7)	7010(11)	12(30)	0.38(30)	49(5)	2.77(7)	6(7)	2.74(21)	0.006(12)	0.291(21)	0.061(14)	0.15(25)	0.11(18)	0.026(22)	0.34(30)	0.078(44)	0.079(30)	0.04(31)	0.25(31)	0.045(14)
x-19	80300(20)	50(7)	6790(11)	9(30)	1.79(30)	135(5)	9.12(7)	19(7)	7.35(21)	0.011(12)	1.580(21)	0.183(14)	0.74(25)	0.24(18)	0.077(22)	1.31(30)	0.171(44)	0.289(30)	0.05(31)	0.71(31)	0.075(14)
x-20	84200(20)	49(7)	8190(11)	16(30)	0.50(30)	150(5)	3.19(7)	7(7)	2.59(21)	0.007(12)	0.376(21)	0.069(14)	0.45(25)	0.12(18)	0.016(22)	0.47(30)	0.033(44)	0.130(30)	0.04(31)	0.26(31)	0.051(14)
x-21	74600(20)	69(7)	6560(11)	57(30)	1.30(30)	188(5)	9.55(7)	15(7)	8.69(21)	0.007(12)	0.156(21)	0.185(14)	0.96(25)	0.15(18)	0.050(22)	1.64(30)	0.148(44)	0.384(30)	0.04(31)	0.36(31)	0.077(14)
x-22	209000(20)	186(7)	10600(11)	108(30)	2.24(30)	204(5)	13.80(7)	15(7)	12.20(21)	0.009(12)	0.174(21)	0.242(14)	1.06(25)	0.28(18)	0.082(22)	3.08(30)	0.144(44)	0.487(30)	0.18(31)	0.48(31)	0.088(14)
x-23	81200(20)	41(7)	7450(11)	22(30)	0.39(30)	41(5)	2.08(7)	14(7)	1.96(21)	0.004(12)	0.089(21)	0.060(14)	0.34(25)	0.13(18)	0.013(22)	0.60(30)	0.055(44)	0.084(30)	0.10(31)	0.31(31)	0.048(14)
x-24	163000(20)	141(7)	10300(11)	96(30)	1.26(30)	284(5)	11.80(7)	14(7)	12.70(21)	0.009(12)	0.275(21)	0.313(14)	1.67(25)	0.45(18)	0.091(22)	2.65(30)	0.233(44)	0.492(30)	0.09(31)	0.48(31)	0.091(14)
x-25	50300(20)	62(7)	9230(11)	22(30)	2.20(30)	89(5)	3.81(7)	14(7)	3.19(21)	0.005(12)	0.099(21)	0.115(14)	0.47(25)	0.10(18)	0.029(22)	0.69(30)	0.072(44)	0.160(30)	0.21(31)	0.35(31)	0.066(14)
x-26	128000(20)	151(7)	8630(11)	100(30)	5.08(30)	352(5)	15.70(7)	14(7)	14.00(21)	0.010(12)	0.238(21)	0.255(14)	1.49(25)	0.26(18)	0.071(22)	2.77(30)	0.187(44)	0.539(30)	0.04(31)	0.59(31)	0.087(14)
x-27	75400(20)	144(7)	6290(11)	100(30)	2.14(30)	397(5)	14.00(7)	15(7)	11.90(21)	0.009(12)	0.261(21)	0.251(14)	0.82(25)	0.35(18)	0.089(22)	2.68(30)	0.198(44)	0.491(30)	0.22(31)	0.40(31)	0.091(14)
x-28	14500(20)	40(7)	6350(11)	10(30)	0.17(30)	46(5)	1.25(7)	13(7)	1.10(21)	0.003(12)	0.068(21)	0.040(14)	0.26(25)	0.08(18)	0.012(22)	0.31(30)	0.011(44)	0.051(30)	0.03(31)	0.10(31)	0.038(14)
x-29	29800(20)	79(7)	6240(11)	24(30)	0.81(30)	108(5)	3.82(7)	14(7)	2.56(21)	0.005(12)	0.138(21)	0.080(14)	0.24(25)	0.05(18)	0.022(22)	0.65(30)	0.049(44)	0.151(30)	0.16(31)	0.33(31)	0.053(14)
x-30	30700(20)	107(7)	5330(11)	69(30)	1.00(30)	163(5)	3.69(7)	14(7)	3.93(21)	0.006(12)	0.220(21)	0.097(14)	0.30(25)	0.09(18)	0.021(22)	1.78(30)	0.061(44)	0.294(30)	0.03(31)	0.32(31)	0.064(14)

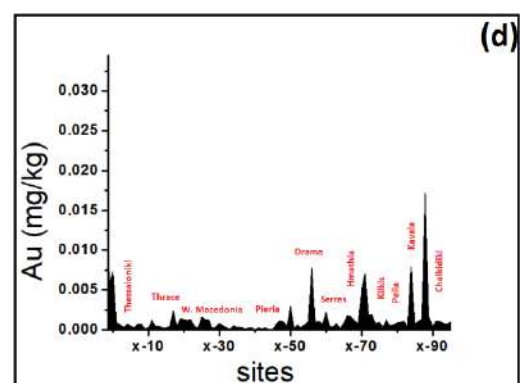
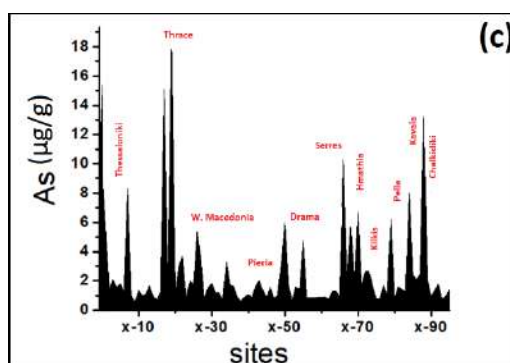
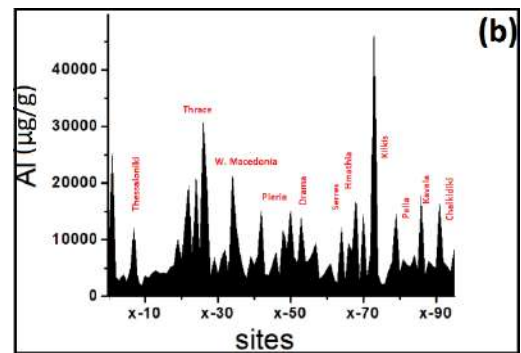
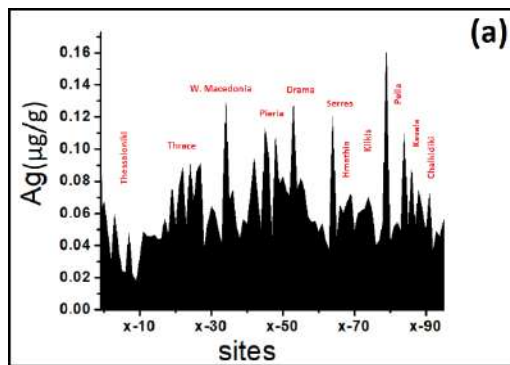
x-31	15200(20)	64(7)	7000(11)	22(30)	0.71(30)	158(5)	4.06(7)	8(7)	3.76(21)	0.564(12)	0.114(21)	0.085(14)	0.47(25)	0.58(18)	0.033(22)	0.55(30)	0.169(44)	0.120(30)	0.19(31)	0.25(31)	0.061(14)
x-32	37000(20)	27(7)	4700(11)	13(30)	0.47(30)	59(5)	2.37(7)	5(7)	2.22(21)	0.352(12)	0.098(21)	0.057(14)	0.53(25)	0.46(18)	0.029(22)	0.37(30)	0.053(44)	0.089(30)	0.03(31)	0.15(31)	0.049(14)
x-33	30600(20)	37(7)	5450(11)	13(30)	0.23(30)	52(5)	1.80(7)	3(7)	1.36(21)	0.247(12)	0.086(21)	0.040(14)	0.31(25)	0.13(18)	0.016(22)	0.28(30)	0.039(44)	0.050(30)	0.03(31)	0.15(31)	0.041(14)
x-34	82400(20)	74(7)	6320(11)	192(30)	2.61(30)	294(5)	21.00(7)	46(7)	17.90(21)	3.680(12)	0.232(21)	0.549(14)	1.79(25)	1.96(18)	0.213(22)	4.60(30)	0.474(44)	0.909(30)	0.23(31)	0.36(31)	0.129(14)
x-35	54700(20)	39(7)	13500(11)	36(30)	0.71(30)	78(5)	5.23(7)	11(7)	4.01(21)	0.822(12)	0.126(21)	0.136(14)	1.07(25)	0.74(18)	0.062(22)	0.89(30)	0.149(44)	0.190(30)	0.15(31)	0.19(31)	0.068(14)
x-36	29300(20)	43(7)	10800(11)	35(30)	0.68(30)	57(5)	4.03(7)	9(7)	3.36(21)	0.651(12)	0.119(21)	0.105(14)	0.39(25)	0.68(18)	0.040(22)	0.77(30)	0.121(44)	0.156(30)	0.16(31)	0.23(31)	0.074(14)
x-37	37000(20)	61(7)	7580(11)	18(30)	0.43(30)	195(5)	2.37(7)	5(7)	2.76(21)	0.349(12)	0.105(21)	0.055(14)	0.28(25)	0.49(18)	0.022(22)	0.47(30)	0.091(44)	0.092(30)	0.04(31)	0.15(31)	0.052(14)
x-38	28500(20)	21(7)	7440(11)	8(30)	0.41(30)	44(5)	1.26(7)	3(7)	0.86(21)	0.186(12)	0.082(21)	0.030(14)	0.31(25)	0.30(18)	0.013(22)	0.22(30)	0.020(44)	0.051(30)	0.03(31)	0.09(31)	0.044(14)
x-39	49100(20)	30(7)	9640(11)	23(30)	0.39(30)	76(5)	2.36(7)	6(7)	2.88(21)	0.344(12)	0.120(21)	0.108(14)	0.91(25)	1.10(18)	0.068(22)	0.69(30)	0.172(44)	0.224(30)	0.04(31)	0.21(31)	0.056(14)
x-40	39600(20)	27(7)	13900(11)	17(30)	1.00(30)	43(5)	2.14(7)	5(7)	1.43(21)	0.275(12)	0.101(21)	0.053(14)	0.26(25)	0.43(18)	0.021(22)	0.32(30)	0.044(44)	0.076(30)	0.04(31)	0.25(31)	0.053(14)
x-41	43500(20)	37(7)	11400(11)	29(30)	0.85(30)	91(5)	5.02(7)	10(7)	3.84(21)	0.731(12)	0.426(21)	0.117(14)	0.62(25)	0.39(18)	0.048(22)	0.73(30)	0.064(44)	0.171(30)	0.05(31)	0.16(31)	0.072(14)
x-42	65400(20)	42(7)	9750(11)	46(30)	1.37(30)	100(5)	6.32(7)	13(7)	4.87(21)	0.961(12)	0.481(21)	0.162(14)	0.88(25)	0.43(18)	0.093(22)	1.03(30)	0.128(44)	0.251(30)	0.04(31)	0.21(31)	0.094(14)
x-43	28500(20)	38(7)	7910(11)	22(30)	0.69(30)	66(5)	4.43(7)	9(7)	3.78(21)	0.003(12)	0.389(21)	0.101(14)	0.12(25)	0.12(18)	0.082(22)	0.62(30)	0.001(44)	0.115(30)	0.03(31)	0.27(31)	0.070(14)
x-44	19100(20)	26(7)	8370(11)	13(30)	0.38(30)	48(5)	2.38(7)	5(7)	2.03(21)	0.327(12)	0.306(21)	0.053(14)	0.34(25)	0.17(18)	0.033(22)	0.31(30)	0.079(44)	0.075(30)	0.04(31)	0.31(31)	0.049(14)
x-45	38400(20)	19(7)	6180(11)	11(30)	0.34(30)	33(5)	2.30(7)	5(7)	2.06(21)	0.315(12)	0.305(21)	0.049(14)	0.31(25)	0.03(18)	0.024(22)	0.29(30)	0.036(44)	0.069(30)	0.04(31)	0.22(31)	0.113(14)
x-46	34500(20)	38(7)	10000(11)	25(30)	0.71(30)	50(5)	4.06(7)	8(7)	3.86(21)	0.006(12)	0.414(21)	0.113(14)	0.42(25)	0.13(18)	0.062(22)	0.61(30)	0.055(44)	0.134(30)	0.04(31)	0.21(31)	0.095(14)
x-47	30200(20)	15(7)	6170(11)	4(30)	0.17(30)	17(5)	0.99(7)	2(7)	1.41(21)	0.003(12)	0.245(21)	0.023(14)	0.32(25)	0.02(18)	0.012(22)	0.13(30)	0.014(44)	0.030(30)	0.03(31)	0.08(31)	0.041(14)
x-48	32600(20)	89(7)	10500(11)	47(30)	0.84(30)	164(5)	11.60(7)	18(7)	11.60(21)	0.011(12)	0.512(21)	0.439(14)	2.11(25)	0.71(18)	0.327(22)	1.05(30)	0.256(44)	0.260(30)	0.21(31)	0.48(31)	0.107(14)
x-49	30800(20)	53(7)	10100(11)	40(30)	1.03(30)	115(5)	5.55(7)	11(7)	4.66(21)	0.006(12)	0.421(21)	0.124(14)	0.46(25)	0.13(18)	0.055(22)	0.93(30)	0.054(44)	0.164(30)	0.04(31)	0.11(31)	0.078(14)
x-50	94000(20)	42(7)	23400(11)	77(30)	1.30(30)	170(5)	9.97(7)	19(7)	7.87(21)	0.008(12)	0.519(21)	0.182(14)	0.99(25)	0.17(18)	0.067(22)	1.86(30)	0.087(44)	0.283(30)	0.04(31)	0.27(31)	0.083(14)
x-51	61500(20)	44(7)	16200(11)	28(30)	0.62(30)	56(5)	3.83(7)	14(7)	4.19(21)	0.007(12)	0.294(21)	0.090(14)	0.40(25)	0.17(18)	0.040(22)	0.68(30)	0.071(44)	0.179(30)	0.04(31)	0.30(31)	0.074(14)
x-52	60300(20)	46(7)	5000(11)	41(30)	0.45(30)	55(5)	9.21(7)	13(7)	6.40(21)	0.008(12)	0.286(21)	0.108(14)	0.60(25)	0.16(18)	0.036(22)	0.86(30)	0.049(44)	0.162(30)	0.17(31)	0.19(31)	0.071(14)
x-53	129000(20)	178(7)	13100(11)	219(30)	2.19(30)	245(5)	35.20(7)	15(7)	28.90(21)	0.018(12)	0.433(21)	0.407(14)	0.53(25)	0.30(18)	0.091(22)	4.70(30)	0.202(44)	1.090(30)	0.05(31)	0.40(31)	0.127(14)
x-54	57000(20)	72(7)	10300(11)	33(30)	0.53(30)	146(5)	5.64(7)	13(7)	4.53(21)	0.007(12)	0.278(21)	0.093(14)	0.54(25)	0.15(18)	0.043(22)	0.69(30)	0.053(44)	0.139(30)	0.15(31)	0.32(31)	0.074(14)
x-55	58800(20)	41(7)	15500(11)	28(30)	1.31(30)	63(5)	5.67(7)	13(7)	5.50(21)	0.008(12)	0.281(21)	0.117(14)	0.60(25)	0.17(18)	0.019(22)	0.70(30)	0.058(44)	0.188(30)	0.04(31)	0.45(31)	0.082(14)
x-56	67400(20)	75(7)	8170(11)	41(30)	1.16(30)	138(5)	9.58(7)	18(7)	6.36(21)	1.110(12)	0.222(21)	0.121(14)	0.72(25)	0.30(18)	0.051(22)	1.09(30)	0.115(44)	0.232(30)	0.04(31)	0.20(31)	0.075(14)
x-57	66800(20)	95(7)	9090(11)	36(30)	0.49(30)	110(5)	2.81(7)	6(7)	3.33(21)	0.433(12)	0.343(21)	0.062(14)	0.58(25)	0.32(18)	0.038(22)	0.90(30)	0.175(44)	0.089(30)	0.04(31)	0.11(31)	0.058(14)
x-58	11500(20)	36(7)	6100(11)	17(30)	0.42(30)	97(5)	3.22(7)	6(7)	2.98(21)	0.467(12)	0.387(21)	0.062(14)	0.22(25)	0.20(18)	0.034(22)	0.51(30)	0.058(44)	0.107(30)	0.08(31)	0.22(31)	0.055(14)
x-59	47600(20)	32(7)	6270(11)	25(30)	0.47(30)	84(5)	3.13(7)	6(7)	2.57(21)	0.441(12)	0.291(21)	0.058(14)	0.55(25)	0.24(18)	0.033(22)	0.58(30)	0.055(44)	0.104(30)	0.03(31)	0.19(31)	0.055(14)
x-60	32800(20)	26(7)	11400(11)	11(30)	0.26(30)	34(5)	2.09(7)	4(7)	1.61(21)	0.323(12)	0.496(21)	0.044(14)	0.46(25)	0.19(18)	0.023(22)	0.33(30)	0.095(44)	0.068(30)	0.03(31)	0.16(31)	0.048(14)
x-61	58600(20)	117(7)	13700(11)	25(30)	0.41(30)	102(5)	3.08(7)	8(7)	2.99(21)	0.434(12)	0.322(21)	0.059(14)	0.61(25)	0.29(18)	0.028(22)	0.63(30)	0.115(44)	0.102(30)	0.04(31)	0.19(31)	0.054(14)
x-62	44100(20)	33(7)	10800(11)	10(30)	0.29(30)	37(5)	1.66(7)	4(7)	1.55(21)	0.242(12)	0.765(21)	0.032(14)	0.52(25)	0.15(18)	0.020(22)	0.25(30)	0.026(44)	0.052(30)	0.03(31)	0.27(31)	0.043(14)
x-63	37400(20)	13(7)	13300(11)	5(30)	0.17(30)	16(5)	1.04(7)	2(7)	0.88(21)	0.153(12)	0.201(21)	0.022(14)	0.41(25)	0.10(18)	0.015(22)	0.14(30)	0.026(44)	0.031(30)	0.03(31)	0.29(31)	0.037(14)
x-64	106000(20)	61(7)	7960(11)	61(30)	0.68(30)	160(5)	9.12(7)	16(7)	6.25(21)	0.971(12)	0.249(21)	0.157(14)	0.92(25)	0.57(18)	0.101(22)	1.70(30)	0.156(44)	0.313(30)	0.08(31)	0.25(31)	0.120(14)
x-65	36000(20)	33(7)	5960(11)	11(30)	0.26(30)	37(5)	1.89(7)	4(7)	1.80(21)	0.285(12)	0.592(21)	0.039(14)	0.40(25)	0.16(18)	0.022(22)	0.31(30)	0.063(44)	0.064(30)	0.03(31)	0.23(31)	0.043(14)
x-66	42100(20)	60(7)	15300(11)	52(30)	1.67(30)	116(5)	6.41(7)	12(7)	3.29(21)	0.009(12)	0.318(21)	0.149(14)	0.87(25)	0.53(18)	0.080(22)	1.06(30)	0.071(44)	0.191(30)	0.05(31)	0.43(31)	0.065(14)

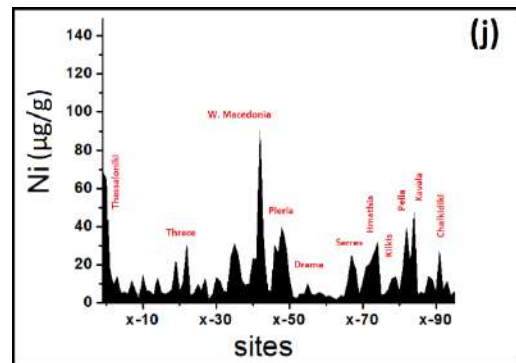
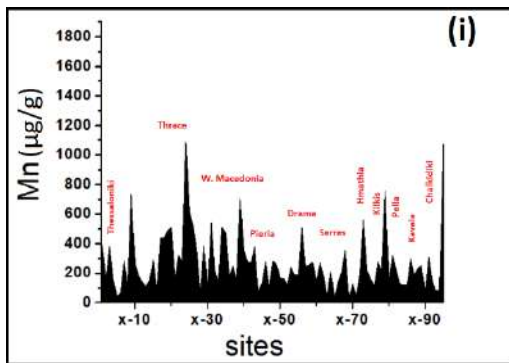
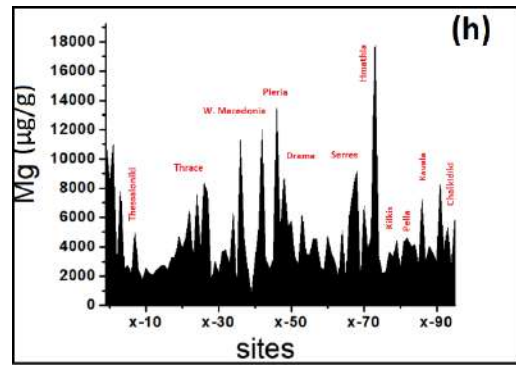
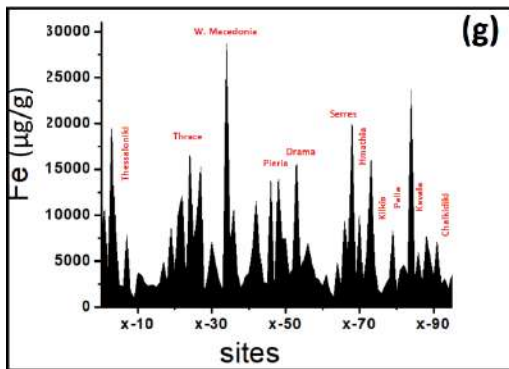
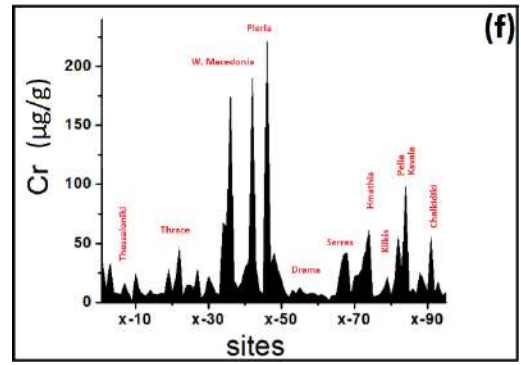
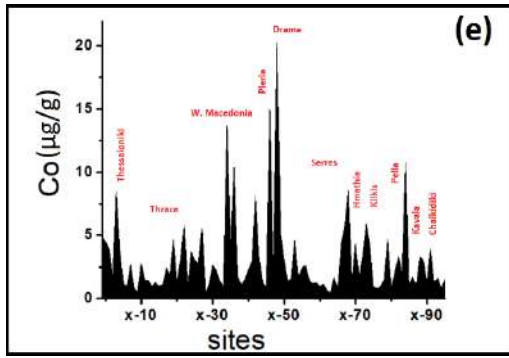
x-67	62200(20)	50(7)	9210(11)	25(30)	1.02(30)	86(5)	4.48(7)	9(7)	3.45(21)	0.005(12)	0.276(21)	0.101(14)	0.42(25)	0.34(18)	0.047(22)	0.51(30)	0.062(44)	0.130(30)	0.04(31)	0.54(31)	0.060(14)
x-68	110000(20)	118(7)	14600(11)	113(30)	1.41(30)	264(5)	11.90(7)	24(7)	10.90(21)	0.013(12)	0.424(21)	0.339(14)	1.53(25)	1.23(18)	0.172(22)	2.03(30)	0.318(44)	0.425(30)	0.05(31)	0.35(31)	0.067(14)
x-69	31000(20)	21(7)	5310(11)	7(30)	0.96(30)	32(5)	1.18(7)	3(7)	0.94(21)	0.003(12)	0.172(21)	0.029(14)	0.41(25)	0.10(18)	0.013(22)	0.15(30)	0.019(44)	0.043(30)	0.03(31)	0.13(31)	0.072(14)
x-70	83100(20)	83(7)	10500(11)	59(30)	2.91(30)	171(5)	9.55(7)	22(7)	9.20(21)	0.012(12)	0.420(21)	0.231(14)	0.90(25)	0.68(18)	0.078(22)	1.14(30)	0.206(44)	0.408(30)	0.07(31)	2.31(31)	0.049(14)
x-71	41500(20)	48(7)	14700(11)	13(30)	0.34(30)	24(5)	1.55(7)	3(7)	1.08(21)	0.003(12)	0.186(21)	0.031(14)	0.46(25)	0.11(18)	0.012(22)	0.21(30)	0.024(44)	0.049(30)	0.03(31)	0.23(31)	0.060(14)
x-72	63000(20)	39(7)	11700(11)	33(30)	0.94(30)	69(5)	4.90(7)	10(7)	3.82(21)	0.005(12)	0.275(21)	0.096(14)	0.66(25)	0.32(18)	0.039(22)	0.67(30)	0.090(44)	0.176(30)	0.05(31)	0.23(31)	0.062(14)
x-73	321000(20)	197(7)	11600(11)	133(30)	2.53(30)	451(5)	21.00(7)	42(7)	16.70(21)	0.028(12)	0.547(21)	0.392(14)	1.80(25)	0.81(18)	0.111(22)	2.70(30)	0.336(44)	0.919(30)	0.16(31)	0.55(31)	0.063(14)
x-74	49000(20)	23(7)	6510(11)	21(30)	0.36(30)	45(5)	1.07(7)	4(7)	1.84(21)	0.003(12)	0.200(21)	0.049(14)	0.57(25)	0.19(18)	0.025(22)	0.33(30)	0.035(44)	0.067(30)	0.04(31)	0.03(31)	0.070(14)
x-75	36400(20)	19(7)	5450(11)	8(30)	0.17(30)	41(5)	1.08(7)	2(7)	0.59(21)	0.003(12)	0.171(21)	0.028(14)	0.45(25)	0.10(18)	0.027(22)	0.15(30)	0.024(44)	0.039(30)	0.03(31)	0.06(31)	0.060(14)
x-76	37100(20)	27(7)	3960(11)	6(30)	0.24(30)	32(5)	1.14(7)	17(7)	1.16(21)	0.003(12)	0.431(21)	0.041(14)	0.44(25)	0.14(18)	0.017(22)	0.17(30)	0.026(44)	0.046(30)	0.03(31)	0.13(31)	0.040(14)
x-77	113000(20)	33(7)	7160(11)	12(30)	0.31(30)	82(5)	1.85(7)	17(7)	1.76(21)	0.003(12)	0.458(21)	0.054(14)	0.39(25)	0.28(18)	0.020(22)	0.29(30)	0.014(44)	0.074(30)	0.03(31)	0.17(31)	0.043(14)
x-78	89100(20)	32(7)	5500(11)	20(30)	0.49(30)	56(5)	4.59(7)	17(7)	3.37(21)	0.005(12)	0.678(21)	0.069(14)	0.42(25)	0.29(18)	0.021(22)	0.66(30)	0.057(44)	0.271(30)	0.03(31)	0.26(31)	0.054(14)
x-79	300000(20)	84(7)	5880(11)	10(30)	2.58(30)	519(5)	11.00(7)	19(7)	9.06(21)	0.008(12)	0.835(21)	0.161(14)	0.71(25)	0.45(18)	0.065(22)	1.91(30)	0.073(44)	0.387(30)	0.05(31)	0.61(31)	0.160(14)
x-80	66600(20)	23(7)	7140(11)	7(30)	0.25(30)	34(5)	1.24(7)	17(7)	1.56(21)	0.003(12)	0.425(21)	0.041(14)	0.39(25)	0.19(18)	0.017(22)	0.16(30)	0.021(44)	0.044(30)	0.03(31)	0.13(31)	0.040(14)
x-81	94400(20)	30(7)	11600(11)	15(30)	0.66(30)	50(5)	2.95(7)	17(7)	2.34(21)	0.004(12)	0.531(21)	0.075(14)	0.42(25)	0.12(18)	0.026(22)	0.40(30)	0.028(44)	0.110(30)	0.03(31)	0.36(31)	0.051(14)
x-82	93900(20)	19(7)	8350(11)	19(30)	0.77(30)	46(5)	2.86(7)	17(7)	3.36(21)	0.004(12)	0.513(21)	0.076(14)	0.35(25)	0.11(18)	0.027(22)	0.52(30)	0.029(44)	0.097(30)	0.03(31)	0.23(31)	0.054(14)
x-83	83600(20)	23(7)	7120(11)	14(30)	0.55(30)	46(5)	2.77(7)	17(7)	3.19(21)	0.005(12)	0.504(21)	0.075(14)	0.39(25)	0.12(18)	0.019(22)	0.39(30)	0.017(44)	0.093(30)	0.02(31)	0.20(31)	0.049(14)
x-84	145000(20)	42(7)	8370(11)	91(30)	2.86(30)	215(5)	17.50(7)	18(7)	16.50(21)	0.011(12)	0.878(21)	0.363(14)	0.64(25)	1.64(18)	0.206(22)	2.51(30)	0.202(44)	0.516(30)	0.03(31)	0.53(31)	0.110(14)
x-85	98600(20)	30(7)	11100(11)	13(30)	0.52(30)	38(5)	2.60(7)	17(7)	2.57(21)	0.004(12)	0.497(21)	0.071(14)	0.39(25)	0.34(18)	0.024(22)	0.36(30)	0.044(44)	0.099(30)	0.03(31)	0.16(31)	0.047(14)
x-86	331000(20)	47(7)	8150(11)	102(30)	0.56(30)	82(5)	10.50(7)	28(7)	7.83(21)	1.900(12)	1.570(21)	0.567(14)	3.93(25)	2.83(18)	0.383(22)	3.64(30)	0.380(44)	0.989(30)	0.11(31)	0.49(31)	0.087(14)
x-87	44200(20)	26(7)	7380(11)	14(30)	0.77(30)	40(5)	2.25(7)	4(7)	2.19(21)	0.374(12)	0.673(21)	0.053(14)	0.24(25)	0.24(18)	0.016(22)	0.31(30)	0.059(44)	0.078(30)	0.02(31)	0.25(31)	0.051(14)
x-88	89000(20)	61(7)	10200(11)	55(30)	0.70(30)	124(5)	6.00(7)	8(7)	4.38(21)	1.070(12)	0.945(21)	0.149(14)	0.55(25)	0.35(18)	0.066(22)	1.18(30)	0.101(44)	0.179(30)	0.04(31)	0.35(31)	0.074(14)
x-89	128000(20)	37(7)	13000(11)	34(30)	0.83(30)	63(5)	4.59(7)	11(7)	3.33(21)	0.757(12)	0.821(21)	0.107(14)	0.35(25)	0.42(18)	0.044(22)	0.73(30)	0.082(44)	0.157(30)	0.03(31)	0.28(31)	0.063(14)
x-90	119000(20)	31(7)	6690(11)	25(30)	0.57(30)	36(5)	2.77(7)	6(7)	1.55(21)	0.434(12)	0.676(21)	0.061(14)	0.31(25)	0.25(18)	0.026(22)	0.50(30)	0.047(44)	0.103(30)	0.03(31)	0.17(31)	0.048(14)
x-91	340000(20)	68(7)	9640(11)	71(30)	0.76(30)	135(5)	8.13(7)	18(7)	5.73(21)	1.250(12)	1.000(21)	0.166(14)	1.18(25)	0.52(18)	0.073(22)	1.67(30)	0.199(44)	0.239(30)	0.04(31)	0.19(31)	0.072(14)
x-92	137000(20)	26(7)	6370(11)	18(30)	0.33(30)	33(5)	2.75(7)	5(7)	1.83(21)	0.499(12)	0.674(21)	0.074(14)	0.99(25)	0.33(18)	0.034(22)	0.42(30)	0.058(44)	0.079(30)	0.03(31)	0.17(31)	0.036(14)
x-93	88300(20)	35(7)	9870(11)	17(30)	0.29(30)	37(5)	1.90(7)	4(7)	1.09(21)	0.352(12)	0.662(21)	0.054(14)	0.39(25)	0.24(18)	0.027(22)	0.34(30)	0.033(44)	0.074(30)	0.03(31)	0.17(31)	0.049(14)
x-94	103000(20)	19(7)	9630(11)	12(30)	0.68(30)	30(5)	1.66(7)	3(7)	1.32(21)	0.263(12)	0.613(21)	0.035(14)	0.32(25)	0.17(18)	0.015(22)	0.24(30)	0.047(44)	0.061(30)	0.02(31)	0.17(31)	0.045(14)
x-95	151000(20)	40(7)	12600(11)	23(30)	0.70(30)	190(5)	3.40(7)	7(7)	3.45(21)	0.517(12)	0.779(21)	0.071(14)	0.63(25)	0.29(18)	0.031(22)	0.49(30)	0.040(44)	0.115(30)	0.04(31)	0.25(31)	0.056(14)

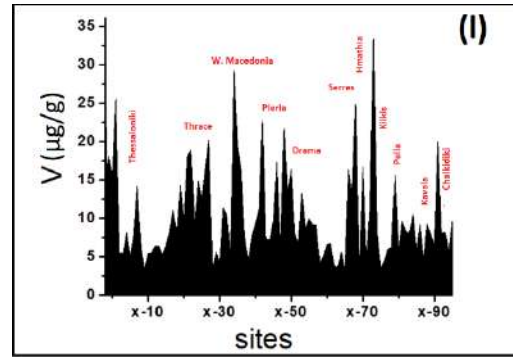
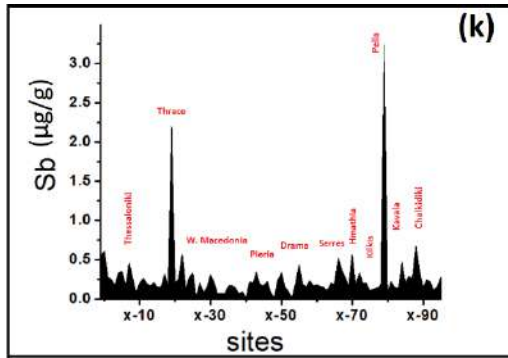
## B. Spatial distribution plots of the trace elements in mosses

Except of the visualization of the elemental concentrations using maps, the distributions of the elements are also presented in simple distribution diagrams (Figures B (a)-(1)). The same peaks-“hot” spots as in the corresponding maps are presented in the scatter plots. Some clarifications for the interpretations of the below diagrams follow.

In every diagram the location of each site is displayed with red labels. The sites named x01-x09 are about the vicinity of Thessaloniki, the sites x10-x29 are about Thrace, the sites x30-x42 are about West Macedonia and the sites x43-x49 concern the Pieria region. The sites x50-x63 concern the area of Drama, the sites x64-x70 are about the vicinity of Serres, the sites x71-x74 and the sites x75-x79 are about Hmathia and Kilkis region. The sites x80-x84 concern the area of Pella, and finally the sites x85-x95 are about Kavala and Chalkidiki vicinities respectively.







**Figures B.** The distributions of the different elements that were found in the ninety-five moss samples from the North Greece

### C. The case study of Skouries

In Table C1 the most frequently analyzed and announced in studies elemental concentrations are presented, while in Table C2 the rest twenty one elemental concentration are shown. The uncertainties of all the elemental concentrations are presented in parenthesis, next to each concentration, and they range from 3% to 44%.

**Table C1.** Skouries region-case study. The concentrations ( $\mu\text{g g}^{-1}$ ) and the uncertainties (%) of the 23 most frequently analyzed and announced in studies elements of the 10 moss samples that were collected close to mining activities.

Sampl ing site	Na	Mg	Al	Cl	K	Sc	Ti	V	Cr	Mn	Fe	Co	Ni	Zn	As	Se	Br	Rb	Sb	I	Au	Th	U
b-01	841(3)	6540(3)	7170(5)	284(10)	5930(8)	2.10(12)	352(8)	14.2(5)	83(6)	338(6)	7710(5)	4.82(5)	63(5)	35.2(5)	10.4(5)	0.46(16)	11.4(30)	20.2(34)	0.32(8)	5.54(36)	0.005(40)	1.49(6)	0.335(9)
b-02	1480(3)	13700(3)	17300(5)	794(10)	7370(8)	4.12(12)	915(8)	29.5(5)	146(6)	532(6)	14300(5)	10.6(5)	107(5)	58.3(5)	15.4(5)	0.51(16)	19.7(30)	31.5(34)	0.90(8)	8.47(36)	0.009(40)	2.92(6)	0.674(9)
b-03	961(3)	11600(3)	13200(5)	282(10)	5780(8)	2.86(12)	706(8)	24.0(5)	111(6)	468(6)	10200(5)	7.98(5)	86(5)	52.7(5)	11.0(5)	0.72(16)	16.7(30)	19.4(34)	0.69(8)	9.81(36)	0.014(40)	2.02(6)	0.465(9)
b-04	668(3)	1880(3)	13000(5)	271(10)	4910(8)	1.74(12)	1230(8)	14.0(5)	75(6)	1760(6)	6350(5)	4.64(5)	56(5)	44.8(5)	7.5(5)	0.48(16)	17.4(30)	24.9(34)	0.58(8)	9.06(36)	0.032(40)	1.27(6)	0.283(9)
b-05	1350(3)	11700(3)	11100(5)	2070(10)	14800(8)	3.55(12)	559(8)	21.2(5)	158(6)	543(6)	13000(5)	8.26(5)	111(5)	72.2(5)	14.1(5)	0.63(16)	59.2(30)	34.2(34)	0.91(8)	9.04(36)	0.007(40)	2.49(6)	0.609(9)
b-06	1710(3)	16400(3)	15400(5)	328(10)	7270(8)	3.85(12)	820(8)	29.3(5)	200(6)	599(6)	14000(5)	9.47(5)	138(5)	49.1(5)	15.3(5)	0.45(16)	8.2(30)	30.3(34)	0.93(8)	4.30(36)	0.005(40)	2.45(6)	0.520(9)
b-07	1550(3)	13600(3)	13500(5)	325(10)	6460(8)	3.44(12)	697(8)	24.5(5)	165(6)	432(6)	12300(5)	8.06(5)	116(5)	48.5(5)	14.4(5)	0.53(16)	9.0(30)	26.9(34)	1.03(8)	4.20(36)	0.004(40)	2.23(6)	0.470(9)
b-08	840(3)	6010(3)	8220(5)	377(10)	5750(8)	1.87(12)	575(8)	15.6(5)	66(6)	807(6)	6930(5)	4.48(5)	52(5)	44.2(5)	9.4(5)	0.47(16)	21.3(30)	29.3(34)	0.41(8)	9.19(36)	0.006(40)	1.49(6)	0.336(9)
b-09	687(3)	11100(3)	9500(5)	662(10)	6960(8)	1.91(12)	465(8)	18.1(5)	92(6)	567(6)	6930(5)	4.86(5)	69(5)	35.1(5)	7.7(5)	0.39(16)	5.5(30)	24.0(34)	0.54(8)	3.83(36)	0.006(40)	1.38(6)	0.155(9)
b-10	705(3)	8410(3)	7560(5)	597(10)	5550(8)	1.87(12)	378(8)	15.5(5)	86(6)	478(6)	6940(5)	4.47(5)	65(5)	34.9(5)	9.3(5)	0.38(16)	7.3(30)	22.4(34)	0.62(8)	5.32(36)	0.007(40)	1.33(6)	0.264(9)

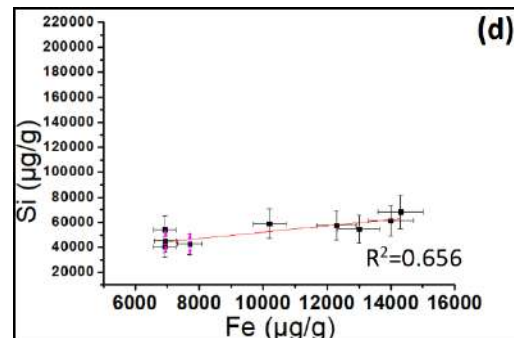
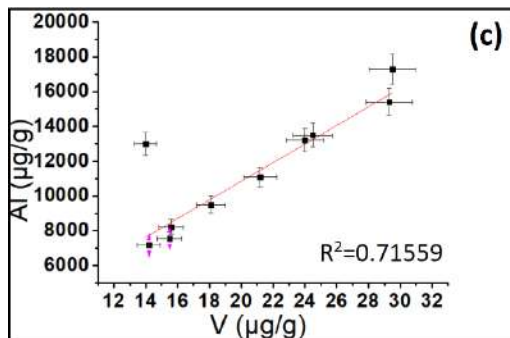
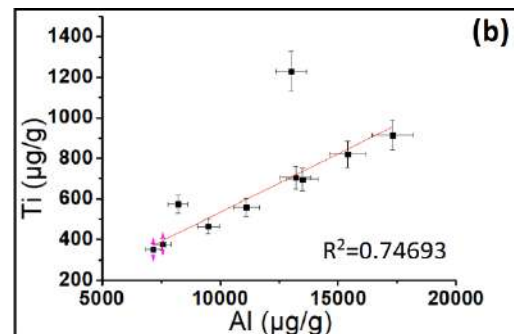
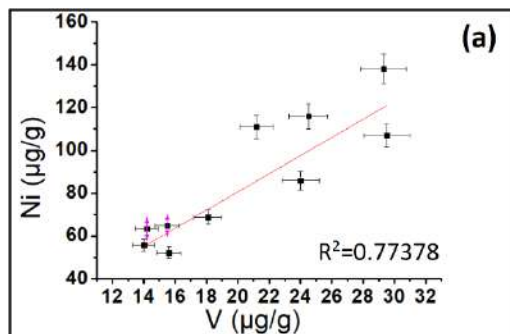
**Table C2.** Skouries region-case study. The concentrations ( $\mu\text{g g}^{-1}$ ) and the uncertainties (%) of the rest 21 elements of the moss samples that were collected close to mining activities.

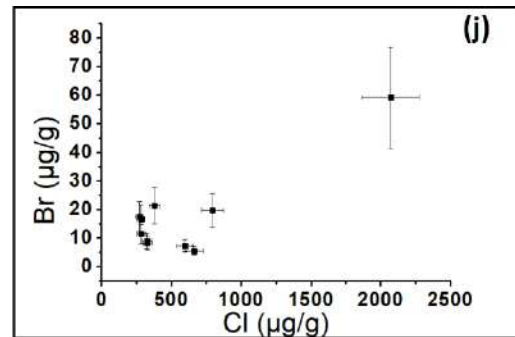
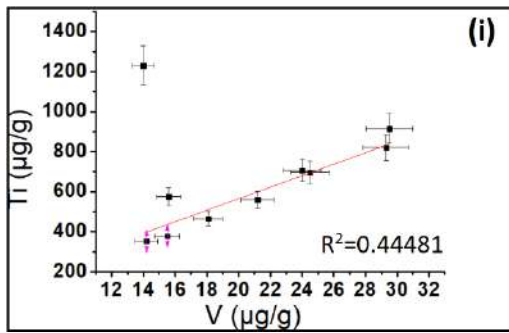
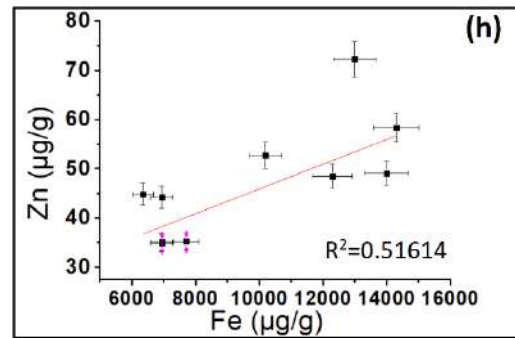
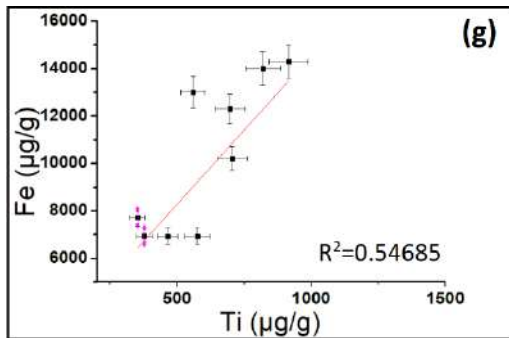
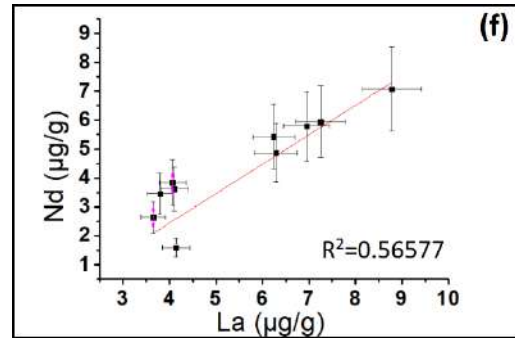
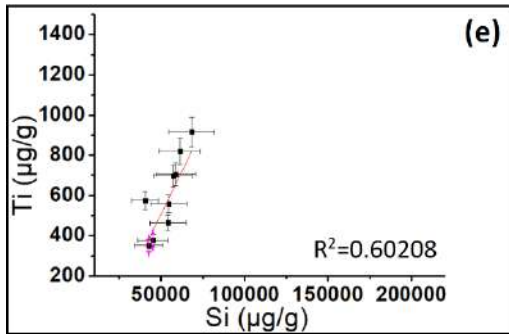
Sampl ing site	Si	Sr	Ca	Zr	Cs	Ba	La	Ce	Nd	Sm	Gd	Tb	Dy	Yb	Tm	Hf	Lu	Ta	In	Mo	Ag
b-01	42700(20)	46.0(7)	6090(11)	22.5(30)	0.88(30)	151(5)	4.07(7)	8.47(7)	3.84(21)	0.69(12)	0.48(21)	0.10(14)	0.46(25)	0.11(18)	0.07(22)	0.65(30)	0.13(44)	0.12(30)	0.202(31)	0.239(31)	0.073(14)
b-02	68300(20)	59.7(7)	8130(11)	50.7(30)	1.15(30)	201(5)	8.78(7)	17.5(7)	7.08(21)	1.42(12)	0.64(21)	0.18(14)	0.99(25)	0.18(18)	0.13(22)	1.71(30)	0.16(44)	0.27(30)	0.176(31)	0.237(31)	0.095(14)
b-03	58900(20)	46.6(7)	9300(11)	27.6(30)	0.83(30)	129(5)	6.29(7)	12.2(7)	4.87(21)	1.06(12)	0.54(21)	0.15(14)	0.71(25)	0.18(18)	0.10(22)	0.97(30)	0.13(44)	0.15(30)	0.195(31)	0.316(31)	0.090(14)
b-04	168000(20)	96.3(7)	16800(11)	16.6(30)	1.03(30)	182(5)	3.79(7)	7.41(7)	3.46(21)	0.62(12)	0.48(21)	0.09(14)	0.74(25)	0.07(18)	0.07(22)	0.54(30)	0.00(44)	0.09(30)	0.295(31)	0.202(31)	0.119(14)
b-05	54600(20)	47.9(7)	8080(11)	37.6(30)	1.18(30)	117(5)	7.25(7)	14.5(7)	5.95(21)	1.20(12)	0.62(21)	0.17(14)	0.63(25)	0.20(18)	0.09(22)	1.18(30)	0.14(44)	0.18(30)	0.092(31)	0.184(31)	0.141(14)
b-06	61400(20)	49.5(7)	10500(11)	40.9(30)	1.28(30)	108(5)	6.95(7)	14.1(7)	5.79(21)	1.20(12)	0.56(21)	0.16(14)	1.15(25)	0.20(18)	0.10(22)	1.23(30)	0.15(44)	0.16(30)	0.294(31)	0.139(31)	0.118(14)
b-07	57500(20)	50.2(7)	9970(11)	35.7(30)	1.13(30)	96(5)	6.24(7)	13.5(7)	5.42(21)	1.10(12)	0.55(21)	0.15(14)	0.91(25)	0.17(18)	0.10(22)	1.01(30)	0.09(44)	0.15(30)	0.173(31)	0.235(31)	0.110(14)
b-08	40400(20)	104(7)	13700(11)	21.2(30)	1.05(30)	367(5)	4.10(7)	8.27(7)	3.62(21)	0.68(12)	0.51(21)	0.01(14)	0.55(25)	0.11(18)	0.09(22)	0.68(30)	0.08(44)	0.12(30)	0.041(31)	0.327(31)	0.070(14)
b-09	54200(20)	36.7(7)	9240(11)	17.9(30)	0.74(30)	80(5)	4.14(7)	8.06(7)	1.59(21)	0.06(12)	0.46(21)	0.10(14)	0.56(25)	0.09(18)	0.06(22)	0.61(30)	0.06(44)	0.08(30)	0.037(31)	0.245(31)	0.061(14)
b-10	45200(20)	35.4(7)	9070(11)	18.1(30)	0.81(30)	75(5)	3.65(7)	7.39(7)	2.64(21)	0.01(12)	0.45(21)	0.08(14)	0.46(25)	0.08(18)	0.04(22)	0.56(30)	0.06(44)	0.09(30)	0.037(31)	0.0528(31)	0.067(14)

## D. Trace elements distribution plots in different species of moss samples from the “Skouries” region

In the following figures (Figures D (a)-(j)), the correlation plots among the elements Ni-V, Ti-Al, Al- V, Si-Fe, Ti-Si, Nd-La, Fe-Ti, Zn- Fe, Ti-V and Br-Cl are presented. Some of these correlations are almost strong linear correlations, while in some others plots, the linearity between the elements tend to get lost, and especially in the last one where it can not exist.

The linear relationship is an indicator of the common sources of the elements, such as the soil dust source for the elements (Ti-Al, Al-V, Si-Fe, Ti-Si, Nd-La, Fe-Ti, Ti-V), while the linearity between Ni and V elements shows that the human activities in the mining ore are their possible sources.





**Figures D.** The correlation between the different trace elements measured in the moss species collected from the Skouries region.

## E. Trace elements concentrations in surface soil samples

In Tables E1 and E2 the elemental concentrations of surface soil samples collected from the same locations like the moss samples are presented. The soil samples were analysed using the XRF analysis technique and only 19 elements were determined and are presented. In Figures E1(a) to (m). the distributions of the measured elements are shown.

**Table E1.** The concentrations (wt %) and the uncertainties (%) of the first 10 elements measured in surface soil samples using the XRF analysis technique.

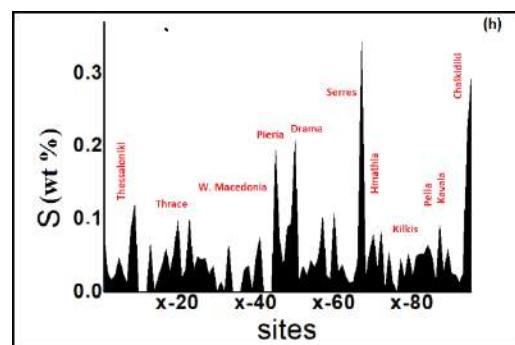
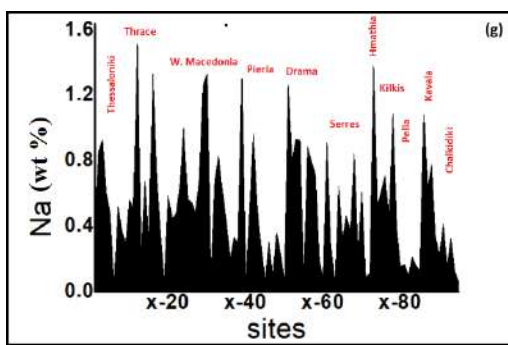
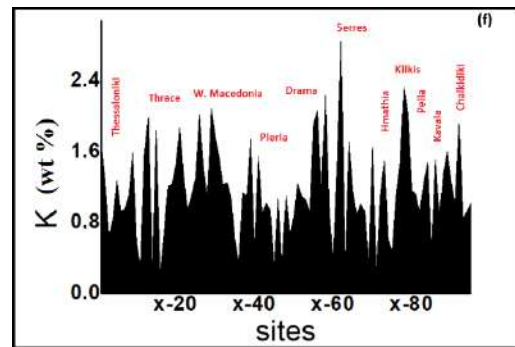
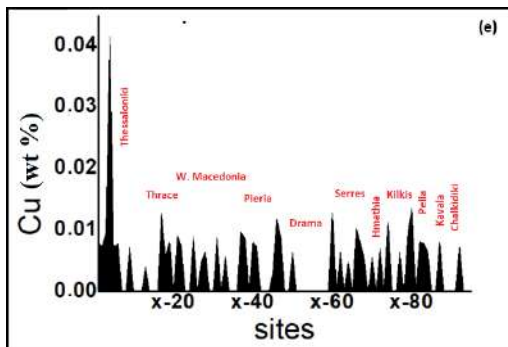
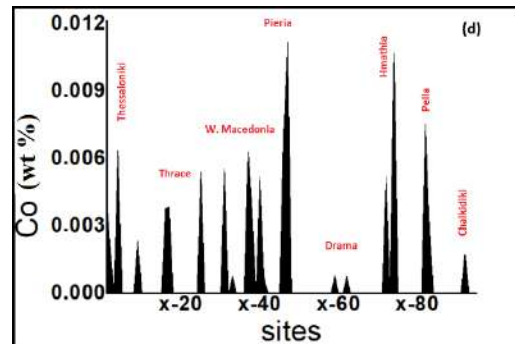
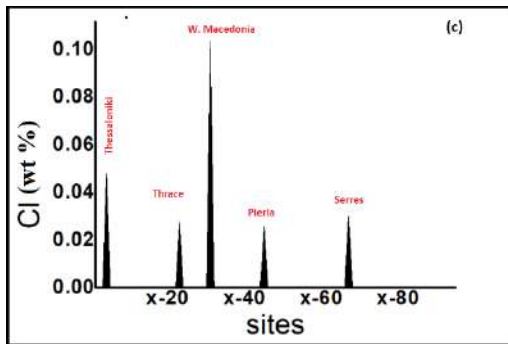
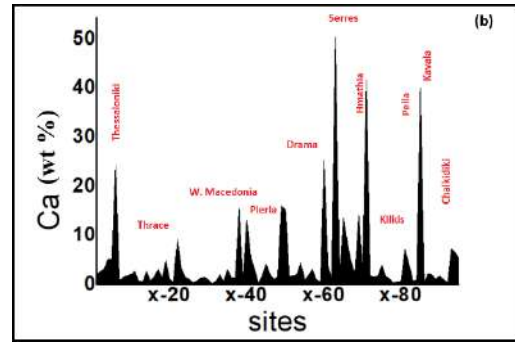
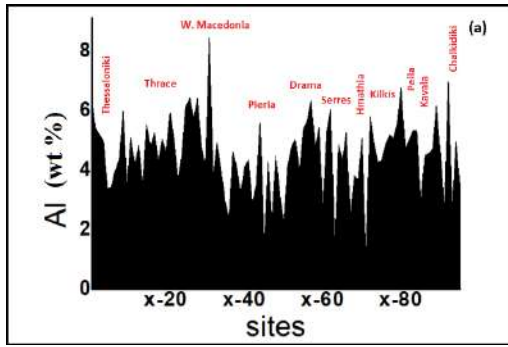
Sampling site	Si	Al	Fe	Ca	Mg	Na	Ti	K	Mn	Sr
x-01	23.08(0.04)	6.43(0.04)	3.16(0.14)	2.15(0.15)	3.83(0.54)	0.44(2.26)	0.46(1.06)	1.73(0.62)	0.30(1.31)	0.02(3.3)
x-02	25.00(0.04)	5.38(0.04)	3.91(0.14)	2.59(0.15)	2.31(0.54)	0.86(2.26)	0.79(1.06)	1.28(0.62)	0.14(1.31)	0.04(3.3)
x-03	22.93(0.04)	5.18(0.04)	5.18(0.14)	3.31(0.15)	3.34(0.54)	0.93(2.26)	0.91(1.06)	0.66(0.62)	0.16(1.31)	0.03(3.3)
x-04	22.61(0.04)	4.99(0.04)	4.79(0.14)	5.21(0.15)	2.44(0.54)	0.60(2.26)	0.86(1.06)	0.85(0.62)	0.24(1.31)	0.10(3.3)
x-05	24.26(0.04)	3.39(0.04)	2.19(0.14)	5.12(0.15)	1.70(0.54)	0.48(2.26)	0.47(1.06)	1.28(0.62)	0.10(1.31)	0.02(3.3)
x-06	15.19(0.04)	3.43(0.04)	1.85(0.14)	24.27(0.15)	0.75(0.54)	0.05(2.26)	0.43(1.06)	0.93(0.62)	0.03(1.31)	0.01(3.3)
x-07	20.73(0.04)	3.98(0.04)	3.16(0.14)	0.87(0.15)	0.92(0.54)	0.52(2.26)	1.00(1.06)	0.95(0.62)	0.03(1.31)	0.01(3.3)
x-08	22.32(0.04)	4.39(0.04)	2.80(0.14)	1.51(0.15)	2.90(0.54)	0.37(2.26)	0.43(1.06)	1.09(0.62)	0.21(1.31)	0.01(3.3)
x-09	27.74(0.04)	5.99(0.04)	2.03(0.14)	1.86(0.15)	0.52(0.54)	0.29(2.26)	0.58(1.06)	1.60(0.62)	0.65(1.31)	0.02(3.3)
x-10	33.02(0.04)	3.45(0.04)	1.90(0.14)	2.07(0.15)	0.72(0.54)	0.56(2.26)	0.52(1.06)	0.57(0.62)	0.12(1.31)	0.00(3.3)
x-11	27.72(0.04)	5.09(0.04)	3.49(0.14)	2.74(0.15)	2.13(0.54)	0.50(2.26)	0.35(1.06)	0.30(0.62)	0.07(1.31)	0.00(3.3)
x-12	30.92(0.04)	4.19(0.04)	1.81(0.14)	0.61(0.15)	0.79(0.54)	1.51(2.26)	0.40(1.06)	1.57(0.62)	0.07(1.31)	0.00(3.3)
x-13	24.47(0.04)	4.84(0.04)	1.14(0.14)	0.55(0.15)	0.59(0.54)	0.22(2.26)	0.23(1.06)	1.98(0.62)	0.05(1.31)	0.01(3.3)
x-14	27.93(0.04)	3.49(0.04)	3.03(0.14)	2.75(0.15)	5.22(0.54)	0.67(2.26)	0.39(1.06)	0.25(0.62)	0.13(1.31)	0.00(3.3)
x-15	31.22(0.04)	5.55(0.04)	1.26(0.14)	0.70(0.15)	0.35(0.54)	0.31(2.26)	0.28(1.06)	1.84(0.62)	0.04(1.31)	0.01(3.3)
x-16	28.04(0.04)	4.83(0.04)	3.96(0.14)	1.63(0.15)	1.73(0.54)	1.33(2.26)	0.55(1.06)	0.21(0.62)	0.21(1.31)	0.01(3.3)
x-17	26.01(0.04)	5.26(0.04)	3.92(0.14)	3.16(0.15)	2.29(0.54)	0.70(2.26)	0.51(1.06)	0.66(0.62)	0.20(1.31)	0.02(3.3)
x-18	25.24(0.04)	4.29(0.04)	1.92(0.14)	1.30(0.15)	1.15(0.54)	0.35(2.26)	0.41(1.06)	1.22(0.62)	0.05(1.31)	0.02(3.3)
x-19	27.69(0.04)	5.06(0.04)	2.90(0.14)	4.91(0.15)	1.06(0.54)	0.07(2.26)	0.64(1.06)	1.23(0.62)	0.12(1.31)	0.01(3.3)
x-20	20.71(0.04)	4.60(0.04)	1.61(0.14)	1.12(0.15)	0.65(0.54)	0.59(2.26)	0.35(1.06)	1.45(0.62)	0.12(1.31)	0.02(3.3)
x-21	22.47(0.04)	5.92(0.04)	2.58(0.14)	0.47(0.15)	0.45(0.54)	0.45(2.26)	0.66(1.06)	1.88(0.62)	0.09(1.31)	0.01(3.3)
x-22	23.70(0.04)	5.02(0.04)	2.46(0.14)	9.22(0.15)	0.93(0.54)	0.48(2.26)	0.48(1.06)	1.33(0.62)	0.12(1.31)	0.04(3.3)
x-23	18.70(0.04)	3.67(0.04)	1.97(0.14)	3.31(0.15)	1.14(0.54)	0.65(2.26)	0.45(1.06)	0.95(0.62)	0.13(1.31)	0.04(3.3)
x-24	23.53(0.04)	4.51(0.04)	1.93(0.14)	1.54(0.15)	0.72(0.54)	0.99(2.26)	0.53(1.06)	1.11(0.62)	0.12(1.31)	0.03(3.3)
x-25	25.89(0.04)	6.14(0.04)	3.44(0.14)	1.09(0.15)	1.92(0.54)	0.56(2.26)	0.76(1.06)	1.30(0.62)	0.22(1.31)	0.02(3.3)
x-26	29.82(0.04)	6.44(0.04)	0.96(0.14)	0.40(0.15)	0.40(0.54)	0.55(2.26)	0.26(1.06)	2.01(0.62)	0.10(1.31)	0.02(3.3)
x-27	29.26(0.04)	5.72(0.04)	1.96(0.14)	0.67(0.15)	0.77(0.54)	0.49(2.26)	0.55(1.06)	1.44(0.62)	0.12(1.31)	0.02(3.3)
x-28	26.91(0.04)	6.41(0.04)	1.91(0.14)	1.34(0.15)	0.80(0.54)	0.68(2.26)	0.42(1.06)	1.08(0.62)	0.06(1.31)	0.03(3.3)
x-29	29.83(0.04)	4.80(0.04)	0.59(0.14)	1.49(0.15)	0.23(0.54)	1.25(2.26)	0.11(1.06)	2.09(0.62)	0.05(1.31)	0.03(3.3)
x-30	31.59(0.04)	4.14(0.04)	1.03(0.14)	1.01(0.15)	0.62(0.54)	1.33(2.26)	0.33(1.06)	1.78(0.62)	0.04(1.31)	0.05(3.3)
x-31	22.52(0.04)	8.45(0.04)	3.45(0.14)	0.24(0.15)	1.01(0.54)	0.10(2.26)	0.73(1.06)	1.55(0.62)	0.20(1.31)	0.01(3.3)
x-32	32.77(0.04)	3.81(0.04)	1.76(0.14)	0.69(0.15)	0.69(0.54)	0.67(2.26)	0.54(1.06)	1.22(0.62)	0.12(1.31)	0.00(3.3)
x-33	29.05(0.04)	4.94(0.04)	2.00(0.14)	1.99(0.15)	0.99(0.54)	0.83(2.26)	0.53(1.06)	1.25(0.62)	0.12(1.31)	0.04(3.3)
x-34	30.44(0.04)	4.02(0.04)	3.24(0.14)	0.60(0.15)	1.01(0.54)	0.61(2.26)	0.77(1.06)	1.08(0.62)	0.08(1.31)	0.00(3.3)
x-35	27.56(0.04)	2.94(0.04)	3.25(0.14)	3.04(0.15)	6.56(0.54)	0.42(2.26)	0.33(1.06)	0.61(0.62)	0.08(1.31)	0.00(3.3)
x-36	24.48(0.04)	2.39(0.04)	3.65(0.14)	1.33(0.15)	13.36(0.54)	0.20(2.26)	0.35(1.06)	0.34(0.62)	0.19(1.31)	0.00(3.3)
x-37	26.43(0.04)	4.62(0.04)	3.29(0.14)	1.46(0.15)	4.59(0.54)	0.33(2.26)	0.48(1.06)	1.14(0.62)	0.11(1.31)	0.01(3.3)
x-38	20.72(0.04)	4.11(0.04)	3.12(0.14)	15.71(0.15)	2.04(0.54)	0.30(2.26)	0.47(1.06)	1.11(0.62)	0.10(1.31)	0.01(3.3)
x-39	34.86(0.04)	3.24(0.04)	0.60(0.14)	0.19(0.15)	0.31(0.54)	1.30(2.26)	0.16(1.06)	1.74(0.62)	0.08(1.31)	0.00(3.3)
x-40	23.11(0.04)	4.12(0.04)	3.41(0.14)	13.07(0.15)	2.67(0.54)	0.05(2.26)	0.51(1.06)	0.49(0.62)	0.14(1.31)	0.01(3.3)
x-41	26.34(0.04)	4.35(0.04)	2.39(0.14)	5.47(0.15)	2.03(0.54)	0.51(2.26)	0.49(1.06)	1.55(0.62)	0.11(1.31)	0.01(3.3)
x-42	31.16(0.04)	2.87(0.04)	1.81(0.14)	3.17(0.15)	2.82(0.54)	0.97(2.26)	0.42(1.06)	0.90(0.62)	0.08(1.31)	0.00(3.3)
x-43	32.33(0.04)	3.50(0.04)	2.40(0.14)	0.23(0.15)	2.21(0.54)	0.52(2.26)	0.44(1.06)	1.02(0.62)	0.12(1.31)	0.00(3.3)
x-44	27.15(0.04)	5.59(0.04)	3.21(0.14)	1.75(0.15)	1.34(0.54)	0.27(2.26)	0.69(1.06)	0.94(0.62)	0.12(1.31)	0.00(3.3)
x-45	8.58(0.04)	1.49(0.04)	0.62(0.14)	4.15(0.15)	1.53(0.54)	0.07(2.26)	0.15(1.06)	0.30(0.62)	0.08(1.31)	0.00(3.3)
x-46	26.40(0.04)	4.31(0.04)	3.57(0.14)	2.05(0.15)	5.95(0.54)	0.30(2.26)	0.43(1.06)	1.07(0.62)	0.20(1.31)	0.00(3.3)

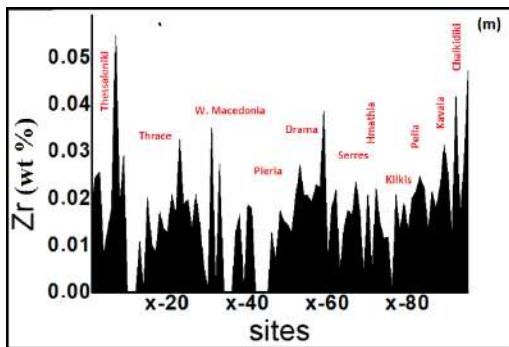
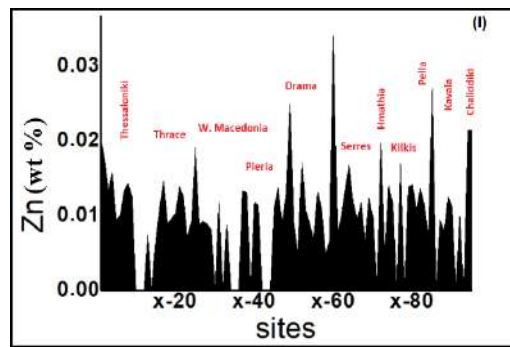
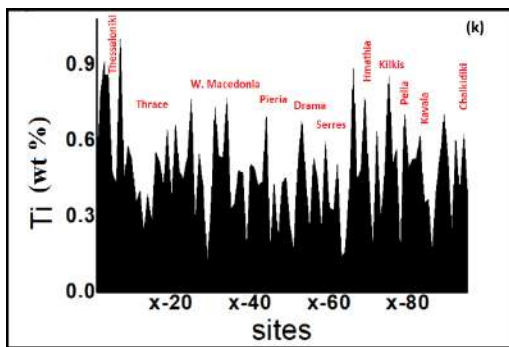
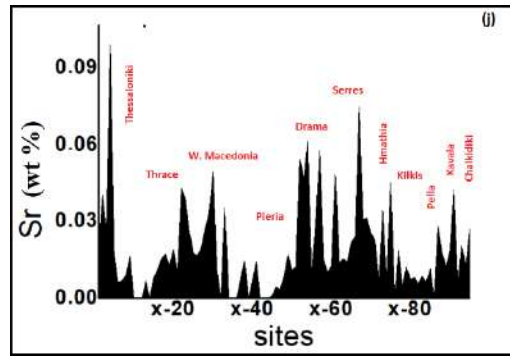
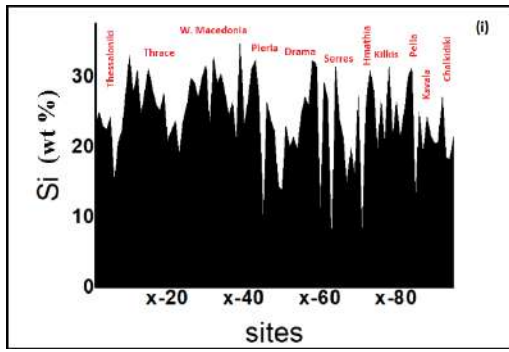
x-47	23.92(0.04)	2.28(0.04)	3.94(0.14)	1.09(0.15)	14.91(0.54)	0.09(2.26)	0.21(1.06)	0.32(0.62)	0.15(1.31)	0.00(3.3)
x-48	22.34(0.04)	4.46(0.04)	2.74(0.14)	1.56(0.15)	2.85(0.54)	0.36(2.26)	0.43(1.06)	1.10(0.62)	0.21(1.31)	0.01(3.3)
x-49	14.40(0.04)	3.15(0.04)	1.94(0.14)	16.04(0.15)	0.76(0.54)	0.22(2.26)	0.45(1.06)	0.66(0.62)	0.15(1.31)	0.02(3.3)
x-50	13.86(0.04)	2.25(0.04)	1.11(0.14)	15.20(0.15)	0.42(0.54)	0.07(2.26)	0.26(1.06)	0.88(0.62)	0.07(1.31)	0.01(3.3)
x-51	23.03(0.04)	4.12(0.04)	0.76(0.14)	1.64(0.15)	0.42(0.54)	1.26(2.26)	0.17(1.06)	1.24(0.62)	0.07(1.31)	0.01(3.3)
x-52	19.91(0.04)	4.78(0.04)	1.85(0.14)	1.86(0.15)	0.90(0.54)	0.79(2.26)	0.51(1.06)	1.10(0.62)	0.07(1.31)	0.05(3.3)
x-53	21.44(0.04)	5.04(0.04)	2.16(0.14)	2.04(0.15)	1.02(0.54)	0.93(2.26)	0.68(1.06)	1.06(0.62)	0.08(1.31)	0.05(3.3)
x-54	19.74(0.04)	3.95(0.04)	1.81(0.14)	4.42(0.15)	1.13(0.54)	0.92(2.26)	0.45(1.06)	0.92(0.62)	0.08(1.31)	0.06(3.3)
x-55	24.67(0.04)	5.38(0.04)	0.95(0.14)	0.90(0.15)	0.65(0.54)	0.07(2.26)	0.24(1.06)	1.92(0.62)	0.04(1.31)	0.01(3.3)
x-56	27.16(0.04)	5.66(0.04)	2.30(0.14)	1.92(0.15)	1.27(0.54)	0.88(2.26)	0.53(1.06)	2.06(0.62)	0.16(1.31)	0.03(3.3)
x-57	25.89(0.04)	6.36(0.04)	2.56(0.14)	3.18(0.15)	1.28(0.54)	0.80(2.26)	0.44(1.06)	1.14(0.62)	0.15(1.31)	0.06(3.3)
x-58	32.26(0.04)	4.76(0.04)	0.82(0.14)	1.01(0.15)	0.60(0.54)	0.71(2.26)	0.24(1.06)	2.24(0.62)	0.08(1.31)	0.02(3.3)
x-59	31.94(0.04)	5.44(0.04)	1.84(0.14)	0.57(0.15)	0.43(0.54)	0.19(2.26)	0.60(1.06)	0.92(0.62)	0.04(1.31)	0.01(3.3)
x-60	9.73(0.04)	2.66(0.04)	1.35(0.14)	25.24(0.15)	6.00(0.54)	0.08(2.26)	0.34(1.06)	0.37(0.62)	0.18(1.31)	0.01(3.3)
x-61	29.27(0.04)	5.30(0.04)	1.39(0.14)	3.90(0.15)	0.43(0.54)	0.91(2.26)	0.32(1.06)	1.45(0.62)	0.07(1.31)	0.05(3.3)
x-62	26.77(0.04)	6.04(0.04)	2.15(0.14)	1.34(0.15)	1.77(0.54)	0.29(2.26)	0.50(1.06)	2.85(0.62)	0.10(1.31)	0.01(3.3)
x-63	5.53(0.04)	1.43(0.04)	0.61(0.14)	50.30(0.15)	1.51(0.54)	0.03(2.26)	0.14(1.06)	0.33(0.62)	0.06(1.31)	0.02(3.3)
x-64	31.53(0.04)	4.85(0.04)	0.85(0.14)	1.34(0.15)	0.71(0.54)	0.64(2.26)	0.16(1.06)	1.71(0.62)	0.11(1.31)	0.01(3.3)
x-65	24.04(0.04)	4.31(0.04)	1.76(0.14)	13.52(0.15)	1.50(0.54)	0.32(2.26)	0.40(1.06)	1.15(0.62)	0.08(1.31)	0.02(3.3)
x-66	21.53(0.04)	5.27(0.04)	4.06(0.14)	8.89(0.15)	2.36(0.54)	0.46(2.26)	0.89(1.06)	0.88(0.62)	0.14(1.31)	0.02(3.3)
x-67	14.44(0.04)	2.46(0.04)	2.20(0.14)	4.83(0.15)	1.47(0.54)	0.37(2.26)	0.44(1.06)	1.01(0.62)	0.08(1.31)	0.07(3.3)
x-68	19.98(0.04)	3.82(0.04)	2.38(0.14)	2.39(0.15)	1.86(0.54)	0.84(2.26)	0.49(1.06)	0.93(0.62)	0.07(1.31)	0.03(3.3)
x-69	15.87(0.04)	3.68(0.04)	3.82(0.14)	14.29(0.15)	1.69(0.54)	0.24(2.26)	0.77(1.06)	0.33(0.62)	0.16(1.31)	0.03(3.3)
x-70	27.30(0.04)	5.09(0.04)	1.61(0.14)	2.31(0.15)	1.03(0.54)	0.61(2.26)	0.43(1.06)	1.65(0.62)	0.07(1.31)	0.03(3.3)
x-71	6.66(0.04)	0.97(0.04)	0.69(0.14)	41.65(0.15)	1.23(0.54)	0.09(2.26)	0.16(1.06)	0.22(0.62)	0.04(1.31)	0.02(3.3)
x-72	25.50(0.04)	5.82(0.04)	7.70(0.14)	1.82(0.15)	3.68(0.54)	0.11(2.26)	0.63(1.06)	1.09(0.62)	0.16(1.31)	0.01(3.3)
x-73	30.98(0.04)	4.94(0.04)	0.95(0.14)	1.52(0.15)	0.58(0.54)	1.38(2.26)	0.28(1.06)	1.50(0.62)	0.05(1.31)	0.03(3.3)
x-74	28.07(0.04)	4.27(0.04)	4.55(0.14)	1.83(0.15)	4.88(0.54)	0.52(2.26)	0.47(1.06)	0.60(0.62)	0.23(1.31)	0.01(3.3)
x-75	19.27(0.04)	4.32(0.04)	4.06(0.14)	4.06(0.15)	2.29(0.54)	0.61(2.26)	0.85(1.06)	0.48(0.62)	0.13(1.31)	0.04(3.3)
x-76	26.46(0.04)	4.84(0.04)	2.66(0.14)	1.72(0.15)	3.96(0.54)	0.71(2.26)	0.51(1.06)	1.10(0.62)	0.21(1.31)	0.00(3.3)
x-77	20.30(0.04)	5.19(0.04)	3.13(0.14)	1.18(0.15)	1.36(0.54)	0.46(2.26)	0.57(1.06)	1.46(0.62)	0.10(1.31)	0.02(3.3)
x-78	31.54(0.04)	5.07(0.04)	0.61(0.14)	0.34(0.15)	0.23(0.54)	1.09(2.26)	0.13(1.06)	2.33(0.62)	0.03(1.31)	0.00(3.3)
x-79	21.38(0.04)	5.59(0.04)	3.37(0.14)	0.50(0.15)	1.00(0.54)	0.39(2.26)	0.70(1.06)	2.02(0.62)	0.05(1.31)	0.01(3.3)
x-80	26.52(0.04)	6.77(0.04)	3.75(0.14)	0.60(0.15)	1.27(0.54)	0.15(2.26)	0.49(1.06)	1.16(0.62)	0.14(1.31)	0.01(3.3)
x-81	21.18(0.04)	4.72(0.04)	2.60(0.14)	7.21(0.15)	1.24(0.54)	0.16(2.26)	0.52(1.06)	1.12(0.62)	0.13(1.31)	0.01(3.3)
x-82	24.81(0.04)	5.02(0.04)	3.51(0.14)	4.38(0.15)	3.88(0.54)	0.10(2.26)	0.53(1.06)	0.91(0.62)	0.17(1.31)	0.01(3.3)
x-83	29.91(0.04)	5.32(0.04)	2.57(0.14)	0.78(0.15)	1.28(0.54)	0.21(2.26)	0.62(1.06)	1.25(0.62)	0.15(1.31)	0.01(3.3)
x-84	31.47(0.04)	5.32(0.04)	1.65(0.14)	0.85(0.15)	0.89(0.54)	0.16(2.26)	0.35(1.06)	1.48(0.62)	0.05(1.31)	0.01(3.3)
x-85	11.60(0.04)	2.89(0.04)	1.35(0.14)	40.14(0.15)	0.52(0.54)	0.13(2.26)	0.37(1.06)	0.47(0.62)	0.11(1.31)	0.01(3.3)
x-86	25.07(0.04)	4.50(0.04)	0.90(0.14)	0.13(0.15)	0.32(0.54)	1.08(2.26)	0.15(1.06)	1.51(0.62)	0.01(1.31)	0.00(3.3)
x-87	19.31(0.04)	4.55(0.04)	2.14(0.14)	2.21(0.15)	1.80(0.54)	0.63(2.26)	0.39(1.06)	0.88(0.62)	0.18(1.31)	0.03(3.3)
x-88	24.29(0.04)	4.70(0.04)	2.26(0.14)	1.97(0.15)	1.43(0.54)	0.78(2.26)	0.54(1.06)	1.36(0.62)	0.07(1.31)	0.02(3.3)
x-89	21.62(0.04)	6.17(0.04)	2.77(0.14)	1.04(0.15)	0.68(0.54)	0.34(2.26)	0.70(1.06)	1.60(0.62)	0.11(1.31)	0.01(3.3)
x-90	20.58(0.04)	4.49(0.04)	2.44(0.14)	1.79(0.15)	1.03(0.54)	0.23(2.26)	0.53(1.06)	1.26(0.62)	0.09(1.31)	0.02(3.3)
x-91	20.71(0.04)	2.67(0.04)	1.09(0.14)	1.06(0.15)	0.87(0.54)	0.41(2.26)	0.22(1.06)	1.01(0.62)	0.05(1.31)	0.04(3.3)
x-92	27.18(0.04)	6.99(0.04)	2.51(0.14)	0.28(0.15)	0.77(0.54)	0.15(2.26)	0.60(1.06)	1.92(0.62)	0.11(1.31)	0.01(3.3)
x-93	18.41(0.04)	2.63(0.04)	1.67(0.14)	7.30(0.15)	1.91(0.54)	0.33(2.26)	0.39(1.06)	0.85(0.62)	0.08(1.31)	0.02(3.3)
x-94	18.38(0.04)	4.94(0.04)	2.85(0.14)	6.58(0.15)	0.81(0.54)	0.13(2.26)	0.62(1.06)	0.93(0.62)	0.16(1.31)	0.01(3.3)
x-95	21.42(0.04)	3.41(0.04)	2.21(0.14)	5.30(0.15)	0.87(0.54)	0.06(2.26)	0.38(1.06)	1.02(0.62)	0.45(1.31)	0.03(3.3)

**Table E2.** The concentrations (wt %) and the uncertainties (%) of the rest nine elements measured in surface soil samples using the XRF analysis technique.

Sampl ing site	S	Cr	Zr	Zn	Ni	Cu	As	Cl	Co
x-01	0.08(7.69)	0.02(3.36)	0.02(1.84)	0.02(3.37)	0.02(2.39)	0.01(3.93)	0.00(8)	0.00(3.89)	0.00(3.45)
x-02	0.03(7.69)	0.01(3.36)	0.02(1.84)	0.02(3.37)	0.01(2.39)	0.01(3.93)	0.00(8)	0.00(3.89)	0.00(3.45)
x-03	0.02(7.69)	0.01(3.36)	0.03(1.84)	0.01(3.37)	0.01(2.39)	0.01(3.93)	0.00(8)	0.00(3.89)	0.00(3.45)
x-04	0.02(7.69)	0.00(3.36)	0.01(1.84)	0.02(3.37)	0.00(2.39)	0.04(3.93)	0.00(8)	0.05(3.89)	0.01(3.45)
x-05	0.05(7.69)	0.01(3.36)	0.01(1.84)	0.01(3.37)	0.01(2.39)	0.01(3.93)	0.0(8)0	0.00(3.89)	0.00(3.45)
x-06	0.02(7.69)	0.00(3.36)	0.02(1.84)	0.01(3.37)	0.00(2.39)	0.01(3.93)	0.00(8)	0.00(3.89)	0.00(3.45)
x-07	0.01(7.69)	0.02(3.36)	0.05(1.84)	0.01(3.37)	0.00(2.39)	0.00(3.93)	0.00(8)	0.00(3.89)	0.00(3.45)
x-08	0.09(7.69)	0.04(3.36)	0.02(1.84)	0.01(3.37)	0.02(2.39)	0.00(3.93)	0.00(8)	0.00(3.89)	0.00(3.45)
x-09	0.12(7.69)	0.01(3.36)	0.03(1.84)	0.01(3.37)	0.01(2.39)	0.01(3.93)	0.00(8)	0.00(3.89)	0.00(3.45)
x-10	0.00(7.69)	0.00(3.36)	0.00(1.84)	0.00(3.37)	0.00(2.39)	0.00(3.93)	0.00(8)	0.00(3.89)	0.00(3.45)
x-11	0.00(7.69)	0.00(3.36)	0.00(1.84)	0.00(3.37)	0.00(2.39)	0.00(3.93)	0.00(8)	0.00(3.89)	0.00(3.45)
x-12	0.00(7.69)	0.00(3.36)	0.00(1.84)	0.00(3.37)	0.00(2.39)	0.00(3.93)	0.00(8)	0.00(3.89)	0.00(3.45)
x-13	0.07(7.69)	0.00(3.36)	0.01(1.84)	0.01(3.37)	0.00(2.39)	0.00(3.93)	0.00(8)	0.00(3.89)	0.00(3.45)
x-14	0.00(7.69)	0.00(3.36)	0.00(1.84)	0.00(3.37)	0.00(2.39)	0.00(3.93)	0.00(8)	0.00(3.89)	0.00(3.45)
x-15	0.02(7.69)	0.01(3.36)	0.02(1.84)	0.01(3.37)	0.00(2.39)	0.00(3.93)	0.00(8)	0.00(3.89)	0.00(3.45)
x-16	0.04(7.69)	0.00(3.36)	0.01(1.84)	0.01(3.37)	0.00(2.39)	0.00(3.93)	0.00(8)	0.00(3.89)	0.00(3.45)
x-17	0.06(7.69)	0.00(3.36)	0.01(1.84)	0.01(3.37)	0.00(2.39)	0.01(3.93)	0.01(8)	0.00(3.89)	0.00(3.45)
x-18	0.03(7.69)	0.01(3.36)	0.02(1.84)	0.01(3.37)	0.01(2.39)	0.01(3.93)	0.00(8)	0.00(3.89)	0.00(3.45)
x-19	0.05(7.69)	0.01(3.36)	0.01(1.84)	0.01(3.37)	0.01(2.39)	0.01(3.93)	0.03(8)	0.00(3.89)	0.00(3.45)
x-20	0.10(7.69)	0.00(3.36)	0.01(1.84)	0.01(3.37)	0.00(2.39)	0.00(3.93)	0.00(8)	0.00(3.89)	0.00(3.45)
x-21	0.02(7.69)	0.01(3.36)	0.02(1.84)	0.01(3.37)	0.00(2.39)	0.01(3.93)	0.00(8)	0.00(3.89)	0.00(3.45)
x-22	0.03(7.69)	0.01(3.36)	0.02(1.84)	0.01(3.37)	0.02(2.39)	0.01(3.93)	0.00(8)	0.00(3.89)	0.00(3.45)
x-23	0.10(7.69)	0.00(3.36)	0.03(1.84)	0.01(3.37)	0.00(2.39)	0.00(3.93)	0.00(8)	0.03(3.89)	0.00(3.45)
x-24	0.03(7.69)	0.00(3.36)	0.02(1.84)	0.01(3.37)	0.00(2.39)	0.00(3.93)	0.00(8)	0.00(3.89)	0.00(3.45)
x-25	0.05(7.69)	0.01(3.36)	0.02(1.84)	0.02(3.37)	0.01(2.39)	0.01(3.93)	0.00(8)	0.00(3.89)	0.01(3.45)
x-26	0.04(7.69)	0.00(3.36)	0.01(1.84)	0.01(3.37)	0.00(2.39)	0.00(3.93)	0.00(8)	0.00(3.89)	0.00(3.45)
x-27	0.05(7.69)	0.00(3.36)	0.02(1.84)	0.01(3.37)	0.00(2.39)	0.00(3.93)	0.00(8)	0.00(3.89)	0.00(3.45)
x-28	0.02(7.69)	0.01(3.36)	0.02(1.84)	0.01(3.37)	0.00(2.39)	0.01(3.93)	0.00(8)	0.00(3.89)	0.00(3.45)
x-29	0.04(7.69)	0.00(3.36)	0.01(1.84)	0.01(3.37)	0.00(2.39)	0.00(3.93)	0.00(8)	0.00(3.89)	0.00(3.45)
x-30	0.00(7.69)	0.00(3.36)	0.00(1.84)	0.00(3.37)	0.00(2.39)	0.00(3.93)	0.00(8)	0.00(3.89)	0.00(3.45)
x-31	0.01(7.69)	0.01(3.36)	0.04(1.84)	0.01(3.37)	0.01(2.39)	0.01(3.93)	0.00(8)	0.10(3.89)	0.01(3.45)
x-32	0.00(7.69)	0.00(3.36)	0.00(1.84)	0.00(3.37)	0.00(2.39)	0.00(3.93)	0.00(8)	0.00(3.89)	0.00(3.45)
x-33	0.06(7.69)	0.01(3.36)	0.03(1.84)	0.01(3.37)	0.00(2.39)	0.01(3.93)	0.00(8)	0.00(3.89)	0.00(3.45)
x-34	0.00(7.69)	0.00(3.36)	0.00(1.84)	0.00(3.37)	0.00(2.39)	0.00(3.93)	0.00(8)	0.00(3.89)	0.00(3.45)
x-35	0.00(7.69)	0.12(3.36)	0.00(1.84)	0.00(3.37)	0.12(2.39)	0.00(3.93)	0.00(8)	0.00(3.89)	0.00(3.45)
x-36	0.00(7.69)	0.06(3.36)	0.00(1.84)	0.00(3.37)	0.09(2.39)	0.00(3.93)	0.00(8)	0.00(3.89)	0.00(3.45)
x-37	0.03(7.69)	0.03(3.36)	0.01(1.84)	0.01(3.37)	0.06(2.39)	0.01(3.93)	0.00(8)	0.00(3.89)	0.01(3.45)
x-38	0.04(7.69)	0.03(3.36)	0.02(1.84)	0.01(3.37)	0.04(2.39)	0.01(3.93)	0.00(8)	0.00(3.89)	0.00(3.45)
x-39	0.00(7.69)	0.00(3.36)	0.00(1.84)	0.00(3.37)	0.00(2.39)	0.00(3.93)	0.00(8)	0.00(3.89)	0.00(3.45)
x-40	0.05(7.69)	0.07(3.36)	0.02(1.84)	0.01(3.37)	0.07(2.39)	0.01(3.93)	0.00(8)	0.00(3.89)	0.01(3.45)
x-41	0.08(7.69)	0.02(3.36)	0.02(1.84)	0.01(3.37)	0.02(2.39)	0.01(3.93)	0.00(8)	0.00(3.89)	0.00(3.45)
x-42	0.00(7.69)	0.04(3.36)	0.00(1.84)	0.00(3.37)	0.04(2.39)	0.00(3.93)	0.00(8)	0.00(3.89)	0.00(3.45)
x-43	0.00(7.69)	0.00(3.36)	0.00(1.84)	0.00(3.37)	0.02(2.39)	0.00(3.93)	0.00(8)	0.00(3.89)	0.00(3.45)
x-44	0.00(7.69)	0.02(3.36)	0.00(1.84)	0.00(3.37)	0.02(2.39)	0.00(3.93)	0.00(8)	0.00(3.89)	0.00(3.45)
x-45	0.19(7.69)	0.00(3.36)	0.00(1.84)	0.01(3.37)	0.00(2.39)	0.00(3.93)	0.00(8)	0.03(3.89)	0.00(3.45)
x-46	0.07(7.69)	0.05(3.36)	0.01(1.84)	0.01(3.37)	0.08(2.39)	0.01(3.93)	0.00(8)	0.00(3.89)	0.01(3.45)
x-47	0.04(7.69)	0.17(3.36)	0.01(1.84)	0.01(3.37)	0.20(2.39)	0.01(3.93)	0.00(8)	0.00(3.89)	0.01(3.45)
x-48	0.09(7.69)	0.04(3.36)	0.02(1.84)	0.01(3.37)	0.02(2.39)	0.00(3.93)	0.00(8)	0.00(3.89)	0.00(3.45)
x-49	0.09(7.69)	0.00(3.36)	0.02(1.84)	0.02(3.37)	0.00(2.39)	0.00(3.93)	0.00(8)	0.00(3.89)	0.00(3.45)
x-50	0.21(7.69)	0.00(3.36)	0.01(1.84)	0.01(3.37)	0.00(2.39)	0.01(3.93)	0.00(8)	0.00(3.89)	0.00(3.45)
x-51	0.02(7.69)	0.00(3.36)	0.01(1.84)	0.00(3.37)	0.00(2.39)	0.00(3.93)	0.00(8)	0.00(3.89)	0.00(3.45)
x-52	0.04(7.69)	0.00(3.36)	0.02(1.84)	0.02(3.37)	0.00(2.39)	0.00(3.93)	0.00(8)	0.00(3.89)	0.00(3.45)
x-53	0.02(7.69)	0.00(3.36)	0.03(1.84)	0.01(3.37)	0.00(2.39)	0.00(3.93)	0.00(8)	0.00(3.89)	0.00(3.45)
x-54	0.04(7.69)	0.00(3.36)	0.02(1.84)	0.01(3.37)	0.00(2.39)	0.00(3.93)	0.00(8)	0.00(3.89)	0.00(3.45)
x-55	0.03(7.69)	0.01(3.36)	0.02(1.84)	0.01(3.37)	0.00(2.39)	0.00(3.93)	0.00(8)	0.00(3.89)	0.00(3.45)
x-56	0.05(7.69)	0.00(3.36)	0.02(1.84)	0.01(3.37)	0.00(2.39)	0.00(3.93)	0.00(8)	0.00(3.89)	0.00(3.45)







**Figures E (a)-(m).** The distributions of the different elements that were measured in the ninety-five surface soil samples collected in the North part of Greece.

## F. Transfer of resuspended soil to mosses for trace elements

The transfer of resuspended soil to mosses for the trace elements (Al. Si. Fe. Ca. Mg. Na. Ti. K. Mn. Sr. Cr. Zr. Zn. Ni and Co) was calculated and it is presented in Table D1.

**Table F1.** The transfer of resuspended soil to mosses for trace elements.

Sampling site	Al	Si	Fe	Ca	Mg	Na	Ti	K	Mn	Sr	Cr	Zr	Zn	Ni	Co
x-01	0.39(5)	0.91(20)	0.34(5)	0.66(11)	0.29(3)	2.10(4)	0.26(8)	0.44(8)	0.12(6)	0.58(8)	0.17(7)	0.37(30)	0.13(6)	0.07(6)	0.09(6)
x-02	0.06(5)	0.24(20)	0.09(5)	0.26(11)	0.10(3)	0.10(4)	0.03(8)	0.37(8)	0.11(6)	0.08(8)	0.13(7)	0.07(30)	0.19(6)	0.14(6)	0.08(6)
x-03	0.06(5)	0.36(20)	0.37(5)	0.29(11)	0.23(3)	0.48(4)	0.02(8)	0.89(8)	0.24(6)	0.23(8)	0.26(7)	0.27(30)	0.31(6)	0.20(6)	-
x-04	0.08(5)	0.28(20)	0.17(5)	0.12(11)	0.10(3)	0.35(4)	0.03(8)	0.59(8)	0.07(6)	0.09(8)	-	0.16(30)	0.20(6)	-	0.06(6)
x-05	0.07(5)	0.20(20)	0.11(5)	0.15(11)	0.16(3)	0.11(4)	0.04(8)	0.38(8)	0.04(6)	0.20(8)	0.05(7)	0.03(30)	0.27(6)	0.04(6)	-
x-06	0.14(5)	0.30(20)	0.12(5)	0.04(11)	0.28(3)	0.70(4)	0.08(8)	0.34(8)	0.22(6)	0.37(8)	-	0.07(30)	0.22(6)	-	-
x-07	0.30(5)	0.46(20)	0.25(5)	0.88(11)	0.55(3)	0.71(4)	0.08(8)	0.90(8)	0.94(6)	0.47(8)	0.07(7)	0.19(30)	0.34(6)	-	-
x-08	0.07(5)	0.25(20)	0.06(5)	0.69(11)	0.08(3)	0.09(4)	0.05(8)	0.37(8)	0.05(6)	0.24(8)	0.02(7)	0.02(30)	0.26(6)	0.03(6)	-
x-09	0.03(5)	0.23(20)	0.05(5)	0.49(11)	0.33(3)	0.07(4)	0.02(8)	0.33(8)	0.11(6)	0.18(8)	0.03(7)	0.02(30)	0.15(6)	0.03(6)	0.02(6)
x-10	0.10(5)	0.19(20)	0.20(5)	0.33(11)	0.35(3)	0.11(4)	0.04(8)	0.74(8)	0.22(6)	-	-	-	-	-	-
x-11	0.06(5)	0.21(20)	0.10(5)	0.19(11)	0.10(3)	0.11(4)	0.07(8)	1.54(8)	0.28(6)	-	-	-	-	-	-
x-12	0.10(5)	0.21(20)	0.14(5)	0.81(11)	0.26(3)	0.03(4)	0.05(8)	0.31(8)	0.20(6)	-	-	-	-	-	-
x-13	0.09(5)	0.08(20)	0.20(5)	1.19(11)	0.42(3)	0.25(4)	0.12(8)	0.20(8)	0.21(6)	0.41(8)	-	0.11(30)	1.93(6)	-	-
x-14	0.12(5)	0.23(20)	0.08(5)	0.18(11)	0.05(3)	0.05(4)	0.04(8)	1.55(8)	0.11(6)	-	-	-	-	-	-
x-15	0.07(5)	0.23(20)	0.17(5)	1.01(11)	0.79(3)	0.13(4)	0.10(8)	0.22(8)	0.78(6)	0.43(8)	0.13(7)	0.05(30)	2.26(6)	-	-
x-16	0.08(5)	0.17(20)	0.07(5)	0.39(11)	0.14(3)	0.05(4)	0.05(8)	1.63(8)	0.04(6)	0.23(8)	-	0.05(30)	1.26(6)	-	0.03(6)
x-17	0.10(5)	0.21(20)	0.13(5)	0.19(11)	0.14(3)	0.14(4)	0.07(8)	0.67(8)	0.22(6)	0.23(8)	-	0.07(30)	1.24(6)	-	0.06(6)
x-18	0.13(5)	0.29(20)	0.13(5)	0.54(11)	0.28(3)	0.18(4)	0.07(8)	0.35(8)	0.84(6)	0.21(8)	0.09(7)	0.07(30)	2.16(6)	0.08(6)	-
x-19	0.20(5)	0.29(20)	0.30(5)	0.14(11)	0.44(3)	0.97(4)	0.08(8)	0.47(8)	0.41(6)	0.39(8)	0.21(7)	0.07(30)	2.95(6)	0.25(6)	-
x-20	0.13(5)	0.41(20)	0.22(5)	0.73(11)	0.60(3)	0.14(4)	0.11(8)	0.33(8)	0.42(6)	0.26(8)	-	0.13(30)	2.35(6)	-	-
x-21	0.22(5)	0.33(20)	0.39(5)	1.39(11)	1.03(3)	0.73(4)	0.13(8)	0.41(8)	0.18(6)	0.70(8)	0.33(7)	0.27(30)	0.58(6)	-	-
x-22	0.39(5)	0.88(20)	0.49(5)	0.11(11)	0.69(3)	1.63(4)	0.18(8)	0.71(8)	0.27(6)	0.43(8)	0.37(7)	0.66(30)	0.89(6)	0.18(6)	-
x-23	0.17(5)	0.43(20)	0.14(5)	0.22(11)	0.27(3)	0.11(4)	0.07(8)	0.60(8)	0.21(6)	0.11(8)	-	0.07(30)	0.56(6)	-	-
x-24	0.46(5)	0.69(20)	0.86(5)	0.67(11)	1.06(3)	0.57(4)	0.30(8)	0.92(8)	0.90(6)	0.53(8)	-	0.51(30)	0.97(6)	-	-
x-25	0.11(5)	0.19(20)	0.20(5)	0.84(11)	0.20(3)	0.15(4)	0.07(8)	0.43(8)	0.28(6)	0.35(8)	0.11(7)	0.11(30)	0.41(6)	0.06(6)	0.06(6)
x-26	0.48(5)	0.43(20)	1.06(5)	2.15(11)	2.08(3)	1.44(4)	0.34(8)	0.76(8)	0.52(6)	0.91(8)	-	0.73(30)	1.03(6)	-	-

x-27	0.34(5)	0.26(20)	0.78(5)	0.94(11)	0.99(3)	1.45(4)	0.18(8)	1.11(8)	0.31(6)	0.73(8)	0.59(7)	0.48(30)	0.72(6)	-	-
x-28	0.05(5)	0.05(20)	0.08(5)	0.48(11)	0.22(3)	0.08(4)	0.03(8)	0.36(8)	0.11(6)	0.15(8)	0.06(7)	0.07(30)	0.26(6)	-	-
x-29	0.14(5)	0.10(20)	0.64(5)	0.42(11)	1.33(3)	0.17(4)	0.19(8)	0.30(8)	0.72(6)	0.24(8)	-	0.38(30)	0.65(6)	-	-
x-30	0.09(5)	0.10(20)	0.69(5)	0.53(11)	0.35(3)	0.27(4)	0.05(8)	0.36(8)	0.24(6)	0.22(8)	-	-	-	-	-
x-31	0.08(5)	0.07(20)	0.14(5)	2.94(11)	0.36(3)	0.83(4)	0.06(8)	0.35(8)	0.27(6)	0.56(8)	0.30(7)	0.06(30)	0.33(6)	0.14(6)	0.04(6)
x-32	0.22(5)	0.11(20)	0.17(5)	0.68(11)	0.54(3)	0.09(4)	0.09(8)	0.46(8)	0.18(6)	-	-	-	-	-	-
x-33	0.07(5)	0.11(20)	0.09(5)	0.27(11)	0.28(3)	0.06(4)	0.04(8)	0.39(8)	0.12(6)	0.11(8)	0.11(7)	0.05(30)	0.19(6)	0.011(6)	0.011(6)
x-34	0.53(5)	0.27(20)	0.88(5)	1.05(11)	0.63(3)	1.18(4)	0.19(8)	1.34(8)	0.66(6)	-	-	-	-	-	-
x-35	0.43(5)	0.20(20)	0.21(5)	0.44(11)	0.01(3)	0.44(4)	0.26(8)	0.82(8)	0.56(6)	-	0.05(7)	-	-	0.03(6)	-
x-36	0.33(5)	0.12(20)	0.29(5)	0.81(11)	0.08(3)	0.46(4)	0.14(8)	1.27(8)	0.09(6)	-	0.27(7)	-	--	0.03(6)	-
x-37	0.10(5)	0.14(20)	0.11(5)	0.52(11)	0.10(3)	0.19(4)	0.06(8)	0.51(8)	0.23(6)	0.80(8)	0.06(7)	0.14(30)	0.15(6)	0.02(6)	0.03(6)
x-38	0.07(5)	0.14(20)	0.07(5)	0.05(11)	0.12(3)	0.11(4)	0.04(8)	0.43(8)	0.16(6)	0.14(8)	0.05(7)	0.05(30)	0.12(6)	0.02(6)	0.03(6)
x-39	0.22(5)	0.14(20)	0.56(5)	5.13(11)	0.23(3)	0.12(4)	0.25(8)	0.34(8)	0.93(6)	-	-	-	-	-	-
x-40	0.14(5)	0.17(20)	0.11(5)	0.11(11)	0.12(3)	0.66(4)	0.06(8)	1.17(8)	0.25(6)	0.37(8)	0.04(7)	0.09(30)	0.19(6)	0.03(6)	0.04(6)
x-41	0.16(5)	0.17(20)	0.27(5)	0.21(11)	0.25(3)	0.30(4)	0.09(8)	0.50(8)	0.25(6)	0.26(8)	0.17(7)	0.16(30)	0.24(6)	0.10(6)	0.37(6)
x-42	0.53(5)	0.21(20)	0.64(5)	0.31(11)	0.43(3)	0.37(4)	0.22(8)	0.73(8)	0.35(6)	-	0.49(7)	-	-	0.25(6)	-
x-43	0.11(5)	0.09(20)	0.24(5)	3.42(11)	0.14(3)	0.22(4)	0.05(8)	0.63(8)	0.32(6)	-	-	-	-	0.17(6)	-
x-44	0.07(5)	0.07(20)	0.09(5)	0.48(11)	0.19(3)	0.14(4)	0.04(8)	0.42(8)	0.06(6)	-	0.06(7)	-	-	0.03(6)	-
x-45	0.38(5)	0.45(20)	0.42(5)	0.15(11)	0.20(3)	0.38(4)	0.28(8)	1.25(8)	0.16(6)	1.74(8)	0.27(7)	-	0.32(6)	0.21(6)	-
x-46	0.18(5)	0.13(20)	0.39(5)	0.49(11)	0.20(3)	0.44(4)	0.12(8)	0.43(8)	0.14(6)	0.82(8)	0.44(7)	0.20(30)	0.28(6)	0.04(6)	0.21(6)
x-47	0.14(5)	0.13(20)	0.05(5)	0.57(11)	0.03(3)	0.29(4)	0.12(8)	1.13(3)	0.07(6)	0.43(8)	0.02(7)	0.06(30)	0.18(6)	0.01(6)	0.02(6)
x-48	0.26(5)	0.15(20)	0.51(5)	0.67(11)	0.30(3)	0.96(4)	0.22(8)	0.54(8)	0.14(6)	0.97(8)	0.09(7)	0.27(30)	0.28(6)	0.23(6)	-
x-49	0.26(5)	0.21(20)	0.38(5)	0.06(11)	0.72(3)	0.78(4)	0.12(8)	0.88(8)	0.18(6)	0.31(8)	-	0.26(30)	0.16(6)	-	-
x-50	0.67(5)	0.68(20)	0.67(5)	0.15(11)	1.35(3)	1.77(4)	0.32(8)	0.99(8)	0.25(6)	0.38(8)	-	0.5(30)	0.42(6)	-	-
x-51	0.17(5)	0.27(20)	0.46(5)	0.99(11)	0.78(3)	0.13(4)	0.24(8)	0.45(8)	0.24(6)	0.37(8)	-	0.22(30)	0.53(6)	-	-
x-52	0.12(5)	0.30(20)	0.23(5)	0.27(11)	0.31(3)	0.20(4)	0.07(8)	0.52(8)	0.17(6)	0.08(8)	-	0.20(30)	0.22(6)	-	-
x-53	0.27(5)	0.60(20)	0.72(5)	0.64(11)	0.60(3)	0.89(4)	0.13(8)	1.05(8)	0.31(6)	0.38(8)	-	0.81(30)	0.55(6)	-	-
x-54	0.16(5)	0.29(20)	0.23(5)	0.23(11)	0.32(3)	0.10(4)	0.10(8)	0.61(8)	0.25(6)	0.12(8)	-	0.16(30)	0.49(6)	-	-
x-55	0.12(5)	0.24(20)	0.56(5)	1.72(11)	0.52(3)	1.19(4)	0.16(8)	0.27(8)	0.43(6)	0.43(8)	0.25(7)	0.14(30)	0.96(6)	-	-
x-56	0.13(5)	0.25(20)	0.30(5)	0.43(11)	0.36(3)	0.22(4)	0.07(8)	0.42(8)	0.33(6)	0.26(8)	-	0.22(30)	0.32(6)	-	-
x-57	0.15(5)	0.26(20)	0.19(5)	0.29(11)	0.36(3)	0.16(4)	0.10(8)	0.60(8)	0.17(6)	0.16(8)	-	0.16(30)	0.29(6)	-	-
x-58	0.06(5)	0.04(20)	0.40(5)	0.60(11)	0.44(3)	0.07(4)	0.08(8)	0.26(8)	0.33(6)	0.23(8)	-	0.08(30)	0.59(6)	-	-
x-59	0.07(5)	0.15(20)	0.16(5)	1.10(11)	0.57(3)	0.21(4)	0.04(8)	0.50(8)	0.77(6)	0.31(8)	0.16(7)	0.06(30)	0.37(6)	-	0.16(6)
x-60	0.18(5)	0.34(20)	0.17(5)	0.05(11)	0.08(3)	0.29(4)	0.09(8)	1.38(8)	0.08(6)	0.21(8)	-	0.17(30)	0.11(6)	-	-
x-61	0.11(5)	0.20(20)	0.26(5)	0.35(11)	0.83(3)	0.10(4)	0.11(8)	0.42(8)	0.41(6)	0.24(8)	-	0.14(30)	0.46(6)	-	-
x-62	0.05(5)	0.16(20)	0.08(5)	0.81(11)	0.17(3)	0.08(4)	0.04(8)	0.14(8)	0.20(6)	0.24(8)	-	0.04(30)	0.33(6)	-	0.09(6)

x-63	0.17(5)	0.68(20)	0.17(5)	0.03(11)	0.13(3)	0.55(4)	0.09(8)	1.93(8)	0.08(6)	0.08(8)	-	0.12(30)	0.99(6)	-	-
x-64	0.25(5)	0.34(20)	0.57(5)	0.59(11)	0.72(3)	0.37(4)	0.22(8)	0.62(8)	0.19(6)	0.43(8)	-	0.45(30)	0.29(6)	-	-
x-65	0.05(5)	0.15(20)	0.12(5)	0.04(11)	0.10(3)	0.08(4)	0.03(8)	0.25(8)	0.04(6)	0.15(8)	0.09(7)	0.06(30)	0.16(6)	-	-
x-66	0.18(5)	0.20(20)	0.23(5)	0.17(11)	0.26(3)	0.27(4)	0.09(8)	0.89(8)	0.10(6)	0.25(8)	0.13(7)	0.32(30)	0.44(6)	0.09(6)	-
x-67	0.31(5)	0.43(20)	0.25(5)	0.19(11)	0.53(3)	0.19(4)	0.12(8)	0.78(8)	0.25(6)	0.07(8)	0.52(7)	0.10(30)	0.49(6)	0.23(6)	-
x-68	0.43(5)	0.55(20)	0.84(5)	0.61(11)	0.50(3)	1.06(4)	0.23(8)	1.29(8)	0.54(6)	0.39(8)	0.61(7)	0.66(30)	0.79(6)	-	-
x-69	0.04(5)	0.20(20)	0.05(5)	0.04(11)	0.09(3)	0.10(4)	0.01(8)	0.65(8)	0.02(6)	0.07(8)	0.02(7)	0.20(30)	0.12(6)	-	-
x-70	0.28(5)	0.30(20)	0.62(5)	0.46(11)	0.66(3)	0.50(4)	0.16(8)	0.58(8)	0.19(6)	0.32(8)	0.43(7)	0.28(30)	0.64(6)	-	-
x-71	0.29(5)	0.62(20)	0.35(5)	0.04(11)	0.31(3)	0.34(4)	0.11(8)	2.95(8)	0.12(6)	0.21(8)	0.19(7)	0.31(30)	-	0.16(6)	-
x-72	0.13(5)	0.25(20)	0.08(5)	0.64(11)	0.13(3)	0.50(4)	0.08(8)	0.68(8)	0.12(6)	0.56(8)	0.09(7)	0.15(30)	0.42(6)	0.05(6)	0.07(6)
x-73	0.93(5)	1.04(20)	1.68(5)	0.76(11)	3.00(3)	0.66(4)	0.64(8)	1.10(8)	1.11(6)	0.57(8)	-	0.89(30)	1.96(6)	-	-
x-74	0.09(5)	0.17(20)	0.10(5)	0.36(11)	0.07(3)	0.14(4)	0.05(8)	0.88(8)	0.09(6)	0.38(8)	0.08(7)	0.18(30)	0.23(6)	0.03(6)	0.04(6)
x-75	0.05(5)	0.19(20)	0.05(5)	0.13(11)	0.10(3)	0.05(4)	0.02(8)	1.40(8)	0.12(6)	0.04(8)	0.05(7)	0.06(30)	0.19(6)	-	-
x-76	0.05(5)	0.14(20)	0.06(5)	0.23(11)	0.06(3)	0.04(4)	0.03(8)	0.54(8)	0.06(6)	-	0.03(7)	-	-	0.02(6)	-
x-77	0.09(5)	0.56(20)	0.08(5)	0.61(11)	0.27(3)	0.07(4)	0.04(8)	0.32(8)	0.28(6)	0.17(8)	0.08(7)	0.06(30)	0.14(6)	0.08(6)	-
x-78	0.12(5)	0.28(20)	0.52(5)	1.63(11)	1.42(3)	0.10(4)	0.19(8)	0.31(8)	0.72(6)	0.63(8)	-	0.15(30)	-	-	-
x-79	0.26(5)	1.40(20)	0.25(5)	1.19(11)	0.44(3)	0.46(4)	0.10(8)	0.52(8)	1.57(6)	0.68(8)	0.24(7)	0.05(30)	0.55(6)	0.25(6)	-
x-80	0.06(5)	0.25(20)	0.04(5)	1.18(11)	0.19(3)	0.16(4)	0.04(8)	0.41(8)	0.11(6)	0.32(8)	0.03(7)	0.05(30)	0.14(6)	0.02(6)	-
x-81	0.14(5)	0.45(20)	0.15(5)	0.16(11)	0.35(3)	0.29(4)	0.07(8)	0.41(8)	0.24(6)	0.37(8)	0.05(7)	0.07(30)	0.45(6)	0.10(6)	-
x-82	0.11(5)	0.38(20)	0.13(5)	0.19(11)	0.12(3)	0.45(4)	0.06(8)	0.48(8)	0.14(6)	0.35(8)	0.11(7)	0.09(30)	0.21(6)	0.04(6)	0.04(6)
x-83	0.10(5)	0.28(20)	0.14(5)	0.91(11)	0.31(3)	0.15(4)	0.05(8)	0.34(8)	0.09(6)	0.26(8)	0.14(7)	0.06(30)	0.20(6)	0.09(6)	0.07(6)
x-84	0.14(5)	0.46(20)	1.43(5)	0.98(11)	0.47(3)	0.79(4)	0.10(8)	1.16(8)	0.25(6)	0.67(8)	1.36(7)	0.41(30)	1.04(6)	0.75(6)	-
x-85	0.15(5)	0.85(20)	0.22(5)	0.03(11)	0.51(3)	0.22(4)	0.07(8)	0.97(8)	0.11(6)	0.26(8)	-	0.10(30)	0.11(6)	-	-
x-86	0.40(5)	1.32(20)	0.66(5)	6.23(11)	2.28(3)	0.44(4)	0.41(8)	0.60(8)	2.97(6)	-	-	0.47(30)	-	-	-
x-87	0.07(5)	0.23(20)	0.12(5)	0.33(11)	0.16(3)	0.05(4)	0.04(8)	0.48(8)	0.11(6)	0.09(8)	0.13(7)	0.08(30)	0.35(6)	0.09(6)	-
x-88	0.13(5)	0.37(20)	0.34(5)	0.52(11)	0.28(3)	0.24(4)	0.08(8)	0.48(8)	0.32(6)	0.33(8)	0.10(7)	0.24(30)	0.72(6)	-	-
x-89	0.09(5)	0.59(20)	0.20(5)	1.25(11)	0.52(3)	0.18(4)	0.04(8)	0.31(8)	0.23(6)	0.31(8)	0.07(7)	0.11(30)	0.39(6)	-	-
x-90	0.11(5)	0.58(20)	0.13(5)	0.37(11)	0.29(3)	0.18(4)	0.06(8)	0.32(8)	0.08(6)	0.16(8)	0.04(7)	0.10(30)	0.21(6)	-	-
x-91	0.61(5)	1.64(20)	0.66(5)	0.91(11)	0.94(3)	0.78(4)	0.34(8)	0.76(8)	0.69(6)	0.16(8)	0.19(7)	0.60(30)	-	-	-
x-92	0.09(5)	0.50(20)	0.10(5)	2.27(11)	0.47(3)	0.19(4)	0.05(8)	0.22(8)	0.13(6)	0.45(8)	0.10(7)	0.04(30)	0.22(6)	0.10(6)	0.08(6)
x-93	0.20(5)	0.48(20)	0.19(5)	0.14(11)	0.28(3)	0.21(4)	0.08(8)	0.72(8)	0.10(6)	0.17(8)	0.04(7)	0.10(30)	-	0.08(6)	-
x-94	0.09(5)	0.56(20)	0.07(5)	0.15(11)	0.33(3)	0.18(4)	0.04(8)	0.45(8)	0.05(6)	0.15(8)	0.02(7)	0.04(30)	0.10(6)	-	-
x-95	0.24(5)	0.71(20)	0.16(5)	0.24(11)	0.67(3)	1.26(4)	0.10(8)	0.58(8)	0.24(6)	0.15(8)	0.03(7)	0.05(30)	0.14(6)	-	-

## G. Radionuclides concentrations in mosses

The concentrations of  $^7\text{Be}$ ,  $^{137}\text{Cs}$ ,  $^{40}\text{K}$ ,  $^{210}\text{Pb}_{\text{uns}}$ ,  $^{210}\text{Pb}_{\text{tot}}$ ,  $^{232}\text{Th}$ ,  $^{226}\text{Ra}$  and their uncertainties are presented in Table G1. All the activities and their uncertainties are given in  $\text{Bq kg}^{-1}$ .

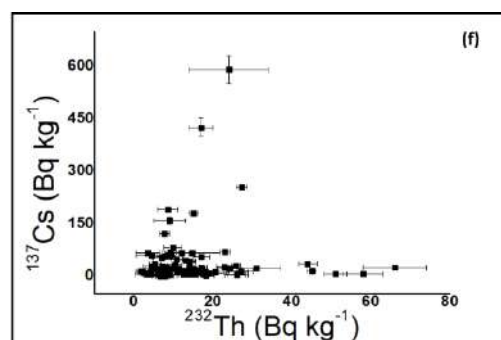
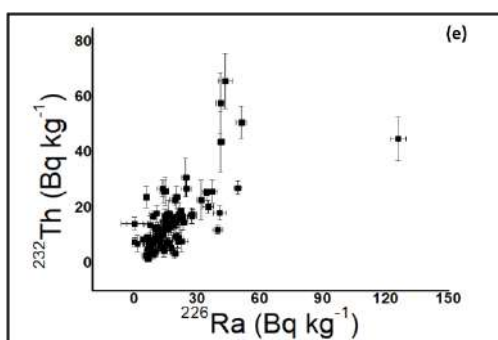
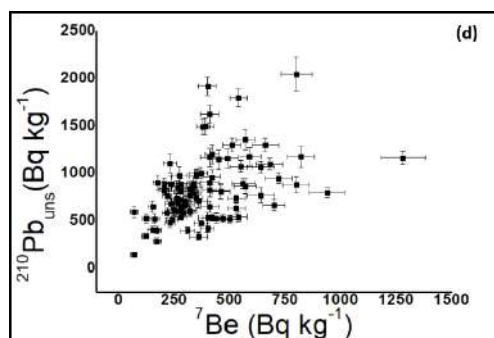
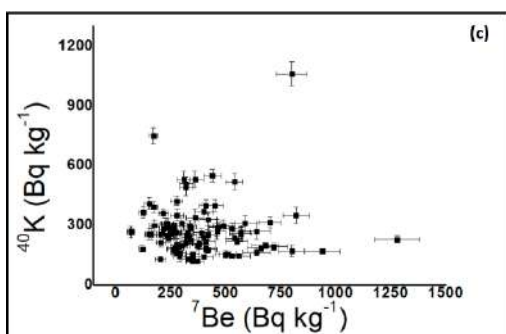
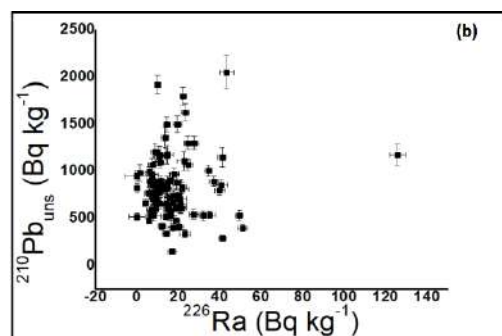
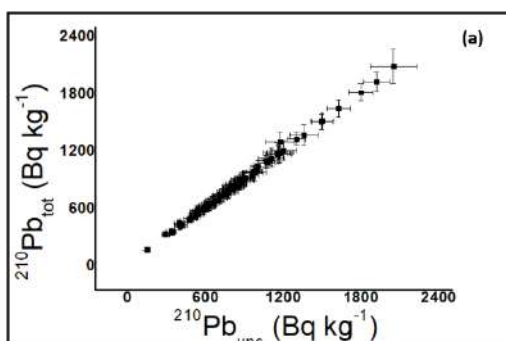
**Table G1.** The activities of the radionuclides  $^7\text{Be}$ ,  $^{137}\text{Cs}$ ,  $^{40}\text{K}$ ,  $^{210}\text{Pb}_{\text{uns}}$ ,  $^{232}\text{Th}$ ,  $^{226}\text{Ra}$  with their uncertainties given in  $\text{Bq kg}^{-1}$ .

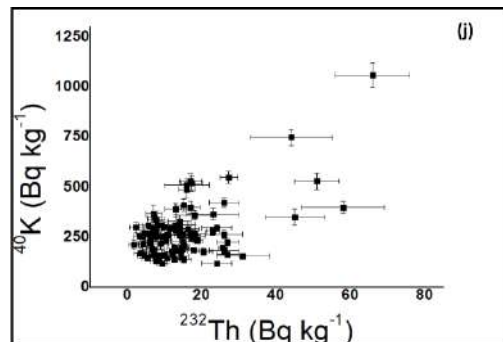
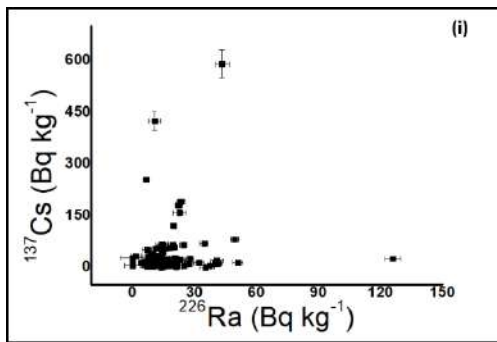
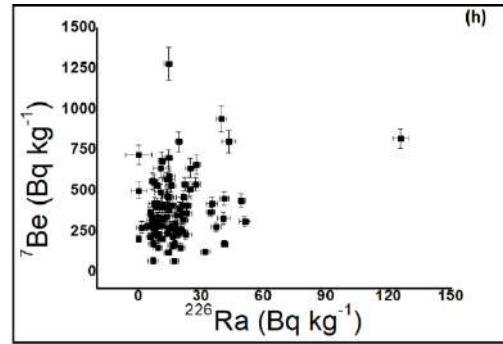
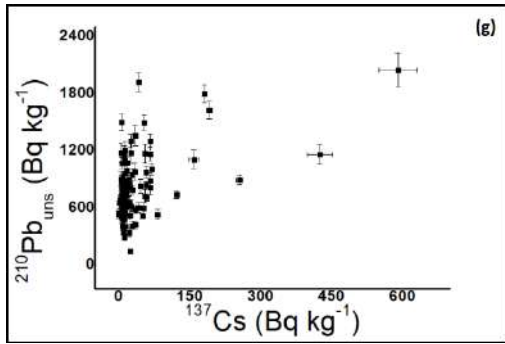
samp les	$^7\text{Be}$ ( $\text{Bq kg}^{-1}$ )	$^{137}\text{Cs}$ ( $\text{Bq kg}^{-1}$ )	$^{210}\text{Pb}_{\text{uns}}$ ( $\text{Bq kg}^{-1}$ )	$^{210}\text{Pb}_{\text{tot}}$ ( $\text{Bq kg}^{-1}$ )	$^{232}\text{Th}$ ( $\text{Bq kg}^{-1}$ )	$^{226}\text{Ra}$ ( $\text{Bq kg}^{-1}$ )	$^{40}\text{K}$ ( $\text{Bq kg}^{-1}$ )
x-01	173±18	7.6±1.3	403±40	420±40	13.0±3.0	17.36±2.40	391±27
x-02	550±50	17.6±1.4	1072±60	1080±60	5.9±1.2	7.23±1.77	221±17
x-03	410±40	1.8±1.1	649±60	670±60	8.9±2.0	21.00±2.83	220±30
x-04	330±40	20.3±2.0	856±60	900±60	18.2±2.6	40.71±3.12	255±22
x-05	300±40	5.7±1.5	673±70	690±70	5.6±2.5	17.50±2.83	310±40
x-06	500±50	5.6±1.6	520±40	520±40	14.4±2.2	0	156±18
x-07	640±60	15.1±2.2	770±80	780±80	18.0±3.0	0	270±40
x-08	640±60	6.0±1.2	1069±60	1100±60	27.0±3.0	24.66±2.38	166±17
x-09	153±19	13.8±1.4	651±60	660±60	3.3±1.5	9.15±1.98	256±28
x-10	206±22	11.1±1.4	840±70	850±70	4.2±1.4	10.03±1.96	215±24
x-11	176±20	3.9±1.0	903±80	910±80	2.3±1.7	6.86±2.09	300±28
x-12	264±25	5.4±1.1	853±70	860±70	7.1±1.8	7.37±1.97	262±23
x-13	420±30	13.1±1.5	1201±100	1210±100	4.2±1.3	8.74±2.05	252±24
x-14	319±28	17.3±1.7	774±70	780±70	1.8±1.3	6.22±2.01	212±24
x-15	236±26	20.0±1.8	891±80	900±80	7.6±1.6	8.31±2.05	251±26
x-16	218±21	6.3±1.0	765±60	770±60	0	5.65±2.01	280±25
x-17	300±27	13.1±1.5	702±60	710±60	6.6±1.5	7.56±2.01	196±22
x-18	322±24	40.9±1.7	600±50	610±50	17.2±1.5	9.08±1.35	242±15
x-19	420±40	12.9±1.6	963±80	970±80	14.0±3.0	0	330±30
x-20	570±40	34.7±2.6	1356±110	1370±110	6.1±2.3	13.55±2.05	266±24
x-21	172±18	12.2±1.2	289±30	330±30	44.0±11.0	41.12±1.71	750±40
x-22	217±21	6.4±1.0	583±50	600±50	18.0±5.0	16.37±1.39	361±24
x-23	450±40	11.7±1.4	1149±100	1190±100	58.0±11.0	41.09±2.18	400±30
x-24	320±30	22.9±2.0	838±80	860±80	16.0±6.0	21.44±2.40	510±30
x-25	510±40	66.3±2.3	1302±70	1330±70	31.0±7.0	24.37±1.72	157±12
x-26	390±40	5.2±1.1	1499±90	1520±90	14.8±2.1	19.41±2.06	263±19
x-27	590±50	4.2±1.2	1176±100	1190±100	13.0±5.0	14.50±2.83	310±40
x-28	236±27	3.2±0.9	681±60	690±60	9.0±3.0	9.35±2.18	308±26
x-29	278±27	4.6±1.0	893±50	930±50	26.0±4.0	37.08±2.40	423±23
x-30	162±22	24.2±2.1	524±50	540±50	7.4±1.4	15.92±2.05	255±28
x-31	490±50	425±27	1160±100	1170±100	10.0±3.0	10.50±2.83	299±28
x-32	360±40	22.1±2.3	337±40	360±40	17.0±3.0	23.00±2.57	530±40
x-33	700±50	2.8±0.8	666±60	680±60	14.0±4.0	14.28±2.01	316±27
x-34	279±25	8.8±0.7	543±30	550±30	6.9±1.1	6.54±0.91	166±10
x-35	410±40	191±6.0	1626±90	1650±90	14.7±2.5	23.36±2.01	188±17
x-36	330±30	18.3±1.5	808±50	820±40	8.6±1.3	12.00±1.78	131±13
x-37	280±25	13.1±1.0	664±40	670±60	8.6±0.9	3.91±1.01	160±10
x-38	340±40	23.6±2.4	856±60	870±40	27.0±3.0	13.53±2.57	226±20
x-39	266±26	59.3±2.1	710±40	730±40	24.0±4.0	20.20±1.66	296±17
x-40	290±30	32.9±2.3	583±40	590±40	4.5±1.8	7.23±2.44	162±19
x-41	241±26	49.5±2.2	515±30	530±30	10.3±1.5	13.70±2.24	235±19
x-42	327±27	57.8±1.7	837±40	850±40	10.8±0.9	12.18±1.20	262±13

x-43	204±19	5.6±0.6	898±50	910±50	9.0±1.5	11.31±1.03	254±14
x-44	350±30	57.9±2.5	971±60	990±60	15.2±2.1	18.03±2.18	140±16
x-45	230±30	159±10	1107±100	1130±100	8.0±4.0	22.56±3.12	310±30
x-46	410±40	55.0±4.0	1169±100	1180±100	9.0±3.0	11.00±2.4	220±30
x-47	280±30	55.0±4.0	725±70	740±70	7.3±2.0	15.64±2.40	350±30
x-48	69±14	24.6±1.5	147±19	169±19	17.1±1.6	16.97±2.12	270±19
x-49	410±30	45.0±3.0	826±70	840±70	17.0±2.7	14.58±1.48	400±30
x-50	340±30	29.6±1.3	790±40	800±40	13.0±1.2	9.62±1.27	288±17
x-51	370±30	70.2±2.3	1006±60	1040±60	25.7±1.2	34.50±2.12	197±13
x-52	124±18	13.4±1.5	528±50	560±50	23.0±7.0	32.00±2.12	365±27
x-53	231±23	6.1±1.0	481±50	500±50	14.0±3.0	18.63±2.01	294±28
x-54	380±30	53.4±2.1	1495±80	1510±80	15.3±1.4	14.34±1.66	207±16
x-55	280±30	4.9±1.4	811±70	820±70	0	9.00±2.83	205±29
x-56	120±16	9.0±1.0	342±26	357±26	26.0±4.0	14.05±1.83	183±14
x-57	540±40	181±5.0	1798±90	1820±90	18.9±1.2	22.13±1.62	235±13
x-58	153±22	28.2±2.5	410±40	430±40	15.1±2.3	20.08±2.40	410±30
x-59	460±40	67.0±5.0	816±80	830±80	4.5±2.1	14.00±2.83	270±40
x-60	350±30	17.0±1.1	994±50	1000±50	9.3±1.2	6.02±1.32	120±11
x-61	337±29	11.4±1.4	892±80	900±80	7.0±2.1	8.72±1.54	299±26
x-62	720±60	28.4±1.9	950±59	950±60	14.4±2.2	0	194±16
x-63	400±40	5.7±1.5	532±59	540±60	7.1±2.2	0	370±40
x-64	272±25	15.7±1.4	605±60	620±60	26.0±5.0	14.53±1.73	265±23
x-65	203±22	10.3±1.2	820±50	820±50	7.7±1.5	0	131±13
x-66	320±30	5.0±1.0	610±60	630±60	15.9±2.3	21.20±2.40	490±40
x-67	680±60	12.3±1.5	1099±60	1110±60	12.5±1.7	11.02±1.87	198±15
x-68	540±40	13.0±1.6	543±50	570±50	17.2±2.9	27.41±2.29	520±40
x-69	420±40	0	537±40	580±40	20.5±2.4	35.00±2.57	179±18
x-70	360±40	5.2±1.7	710±70	730±70	7.8±2.3	20.61±3.12	340±40
x-71	400±30	34.5±2.6	418±40	430±40	6.3±1.5	11.95±1.80	238±22
x-72	560±50	255±7.0	894±50	900±50	5.3±1.4	6.48±1.42	148±12
x-73	440±40	82.0±5.0	530±50	580±50	27.3±2.3	49.40±1.96	550±30
x-74	350±30	122±3.0	738±40	760±40	9.8±1.3	19.81±1.39	159±10
x-75	530±40	6.5±1.1	633±60	650±60	7.7±1.7	15.32±2.40	283±28
x-76	660±60	25.5±1.4	1300±70	1330±70	17.7±1.6	27.68±1.87	185±14
x-77	530±40	15.3±1.0	740±40	750±40	8.2±1.0	8.98±1.05	150±10
x-78	820±60	25.3±2.3	1175±110	1300±110	45.0±8.0	125.77±3.84	350±40
x-79	800±70	590±40	2049±80	2090±180	66±10	43.23±3.33	1060±60
x-80	370±30	11.0±1.0	476±28	483±28	24.0±4.0	5.71±1.12	120±10
x-81	460±40	21.4±2.3	809±80	830±80	16.2±2.9	21.50±3.54	290±40
x-82	1280±100	66.7±2.7	1166±70	1180±70	15.0±3.0	14.27±1.87	231±17
x-83	800±60	66.0±4.0	881±80	900±80	3.5±1.6	19.18±1.87	171±27
x-84	940±80	11.7±1.2	796±50	840±50	12.2±1.5	39.8±2.40	169±13
x-85	410±40	6.8±1.6	904±80	920±80	12.1±2.9	16.00±3.54	180±40
x-86	310±30	13.9±1.6	398±40	450±40	51.0±6.0	50.88±2.40	530±40
x-87	400±40	41.9±1.9	1920±100	1930±100	12.6±1.4	9.97±1.49	141±12
x-88	570±50	10.9±1.8	867±80	880±80	14.0±3.0	14.49±3.12	260±40
x-89	262±28	5.2±1.1	741±50	760±50	13.7±2.4	17.40±2.40	183±15
x-90	250±30	26.1±2.4	619±60	640±60	17.7±2.0	21.00±2.83	260±30
x-91	250±26	13.4±1.3	609±40	630±40	22.9±1.7	19.11±2.12	281±20
x-92	289±28	23.1±2.1	659±60	670±60	10.7±2.1	11.00±2.12	146±29
x-93	470±40	0	526±40	540±40	11.4±2.2	13.80±2.40	293±23
x-94	70±17	52.4±3.8	594±58	602±58	6.7±2.2	6.81±2.30	266±29
x-95	274±35	33.3±4.5	981±90	983±90	7.0±3.0	0	187±39

## H. Relationship between the radionuclides

In Figures H(a)-(j) the correlations between the radionuclides ( $^7\text{Be}$ ,  $^{137}\text{Cs}$ ,  $^{210}\text{Pb}_{\text{uns}}$ ,  $^{210}\text{Pb}_{\text{tot}}$ ,  $^{40}\text{K}$ ,  $^{226}\text{Ra}$ ,  $^{232}\text{Th}$ ) are presented. There is a strong correlation between  $^{210}\text{Pb}_{\text{uns}}$  and  $^{210}\text{Pb}_{\text{tot}}$ , which shows that the majority of  $^{210}\text{Pb}$  that was detected in mosses comes from the decay of  $^{222}\text{Rn}$  in the atmosphere. The rest nuclides do not present a linear correlation either due to the fact that they are accumulated in mosses through different processes (e.g  $^{40}\text{K}$  and  $^7\text{Be}$ ) or other parameters may influence their deposition.

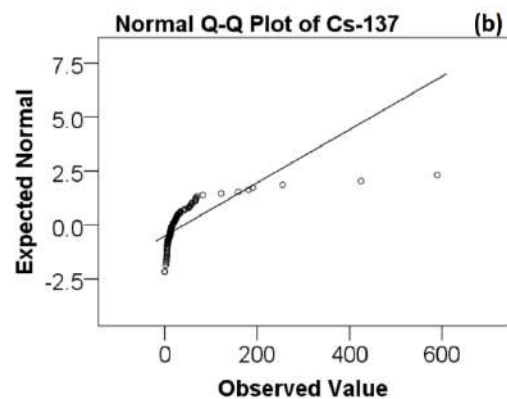
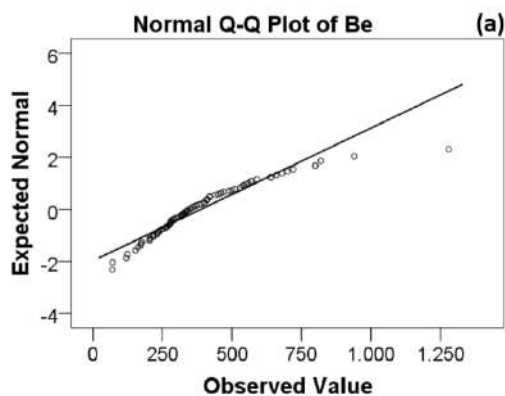


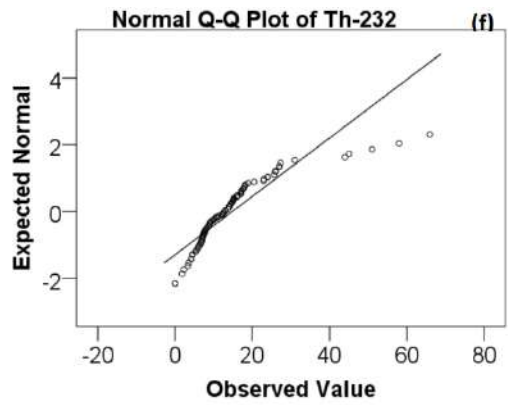
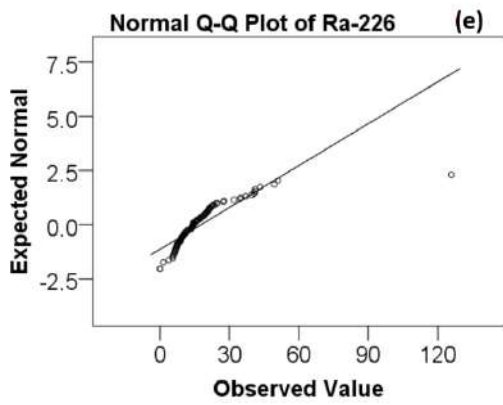
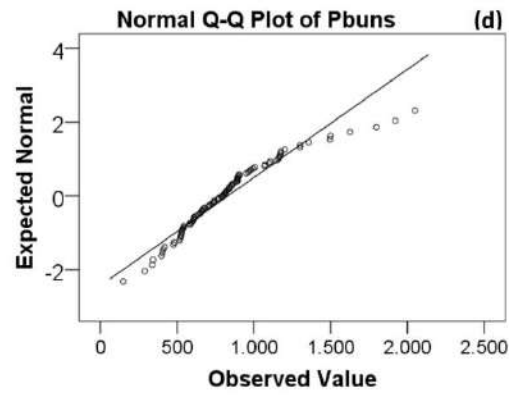
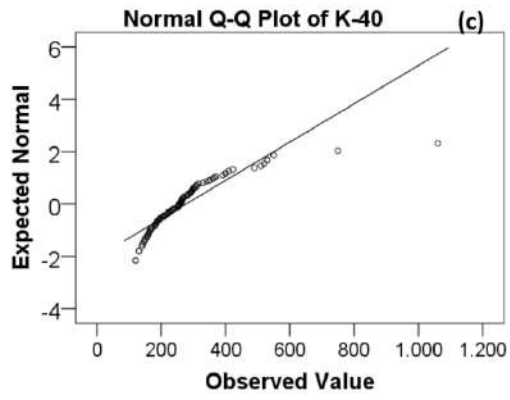


Figures H (a)-(j). The correlation diagrams of the measured radionuclides in mosses.

## I. Statistical analysis: Q-Q plots of radionuclides

After a short statistical analysis with SPSS 23 software, the Q-Q plots of the radionuclides are presented. The non-normality of their distribution, with the  $^{210}\text{Pb}_{\text{uns}}$  exception is revealed.





**Figures I (a)-(f).** The Q-Q plots revealing the non-normality of the distribution of the radionuclides in mosses.

## J. Radionuclides concentrations in mosses

The concentrations of  $^{137}\text{Cs}$ ,  $^{40}\text{K}$  and  $^{210}\text{Pb}$  among with their uncertainties are presented in **Table J1**. All the activities and the uncertainties are given in  $\text{Bq kg}^{-1}$ .

**Table J1.** The activities of the radionuclides  $^{137}\text{Cs}$ ,  $^{40}\text{K}$  and  $^{210}\text{Pb}$  and their uncertainties are presented and given in  $\text{Bq kg}^{-1}$ .

samples	$^{137}\text{Cs}$ ( $\text{Bq kg}^{-1}$ )	$^{210}\text{Pb}$ ( $\text{Bq kg}^{-1}$ )	$^{40}\text{K}$ ( $\text{Bq kg}^{-1}$ )
x-01	177.10±4.53	93.79±4.55	552.55±21.66
x-02	7.45±0.25	43.63±1.97	449.09±17.31
x-03	3.85±0.21	25.79±1.59	253.75±10.35
x-04	3.57±0.19	22.57±1.38	403.46±15.92
x-05	4.32±0.15	35.83±1.89	396.94±15.14
x-06	0.34±0.26	28.86±5.96	408.61±16.27
x-07	17.62±0.57	99.98±5.09	561.38±21.98
x-08	110.80±2.88	213.64±8.94	553.74±21.73
x-09	84.89±2.25	225.64±9.43	433.42±17.40
x-10	10.93±0.40	77.72±3.76	273.19±11.31
x-11	4.28±0.23	27.47±1.76	142.87±6.33
x-12	14.58±0.48	187.97±7.98	862.58±33.17
x-13	107.73±2.43	242.89±10.29	1000.8±38.56
x-14	22.20±0.62	38.79±2.08	139.7±5.83
x-15	16.94±0.54	64.95±4.04	604.68±23.56
x-16	55.68±1.48	92.67±4.05	68.69±3.59
x-17	101.21±2.64	158.49±6.08	224.63±9.36
x-18	27.87±0.81	55.81±3.41	566.83±22.20
x-19	14.41±0.45	97.73±4.14	374.73±14.86
x-20	18.22±0.59	182.64±7.58	624.40±24.50
x-21	2.35±0.22	61.98±3.18	853.46±33.01
x-22	5.26±0.26	50.78±2.68	545.74±21.36
x-23	86.10±2.26	330.12±13.6	545.24±21.27
x-24	7.39±0.31	71.28±3.58	476.13±18.75
x-25	21.97±0.65	53.19±2.73	486.82±19.14
x-26	5.15±0.30	77.95±3.96	916.08±35.36
x-27	5.93±0.26	54.42±2.54	514.39±20.10
x-28	1.92±0.16	70.12±3.54	456.33±17.67
x-29	3.12±0.24	126.86±5.46	936.83±36.09
x-30	308.05±6.36	206.39±8.8	801.89±29.12
x-31	0.80±0.31	86.44±6.55	756.24±27.35
x-32	76.58±1.80	160.89±9.99	602.23±22.80
x-33	18.44±0.58	81.00±23.00	482.04±18.28
x-34	3.52±0.20	64.00±3.58	420.55±15.63
x-35	218.37±4.62	164.87±7.12	290.51±11.83
x-36	35.62±1.05	79.33±3.64	134.89±7.28
x-37	34.26±1.06	49.87±3.44	468.38±19.29
x-38	14.8±0.48	41.64±2.49	417.96±16.03
x-39	39.14±1.00	109.13±5.66	911.17±32.93
x-40	149.2±3.34	75.75±3.97	148.09±7.78
x-41	18.61±1.00	94.53±4.89	568.25±21.05
x-42	5.20±0.26	63.22±3.30	468.16±17.50
x-43	17.57±0.54	53.48±2.93	578.11±22.59

x-44	74.70±2.00	175.17±7.59	473.57±18.88
x-45	2568.8±64.5	1380.87±55.45	240.36±11.72
x-46	267.39±6.79	261.70±10.93	423.52±16.89
x-47	59.52±1.59	55.94±2.85	154.55±6.73
x-48	512.07±12.87	170.36±8.08	436.86±16.93
x-49	78.74±2.01	58.23±2.76	495.03±18.87
x-50	229.70±5.88	198.42±8.24	343.17±14.09
x-51	9.19±0.39	189.99±8.26	831.30±32.01
x-52	13.78±0.45	94.03±4.35	564.65±21.86
x-53	29.49±0.86	80.47±4.17	529.65±20.73
x-54	27.33±0.81	94.42±4.22	475.84±18.80
x-55	17.12±0.57	89.79±4.54	1123.77±43.16
x-56	38.07±1.02	178.66±7.34	937.31±35.62
x-57	51.45±1.41	117.57±5.65	584.30±22.94
x-58	7.12±0.25	55.00±2.60	890.64±33.86
x-59	6.84±0.25	47.52±2.48	360.14±14.01
x-60	2.13±0.11	11.46±1.00	73.80±3.52
x-61	14.29±0.46	73.83±3.64	731.98±28.25
x-62	6.47±0.29	48.63±2.70	1010.23±38.73
x-63	11.86±0.39	42.50±2.00	141.48±6.18
x-64	8.82±0.31	100.09±4.51	729.79±27.88
x-65	0.95±0.20	42.65±2.29	602.26±23.54
x-66	4.01±0.22	57.26±2.78	338.51±13.62
x-67	29.23±0.85	297.31±12.41	413.91±16.57
x-68	21.03±0.58	48.16±2.29	364.73±14.12
x-69	1.40±0.12	34.67±1.72	133.56±6.01
x-70	8.75±0.40	126.3±5.00	763.93±29.75
x-71	7.12±0.25	28.38±5.6	52.79±2.61
x-72	108.35±2.83	173.41±7.66	387.69±15.64
x-73	13.34±0.44	89.51±4.09	556.76±21.65
x-74	69.99±1.86	103.76±4.76	216.54±9.11
x-75	5.07±0.23	20.00±1.41	247.28±10.15
x-76	11.18±0.41	112.34±4.87	1148.30±43.85
x-77	36.05±1.00	89.90±3.87	537.73±20.75
x-78	26.78±0.79	236.66±10.0	1076.20±41.00
x-79	6.00±0.34	74.81±3.54	843.43±32.63
x-80	1.12±0.19	30.34±2.31	446.23±17.86
x-81	86.33±2.25	125.85±5.52	458.68±17.99
x-82	20.81±0.56	69.78±3.60	353.43±13.59
x-83	11.31±0.36	97.25±4.97	269.33±10.71
x-84	25.84±0.75	77.28±3.83	481.08±18.94
x-85	6.52±0.25	44.78±2.16	167.35±6.96
x-86	2.77±0.21	92.45±5.19	772.07±29.5
x-87	1.38±0.17	122.00±5.59	479.23±18.7
x-88	80.07±2.08	74.60±3.77	546.71±21.15
x-89	48.01±1.26	210.71±8.98	661.18±25.28
x-90	46.27±1.23	84.59±5.28	615.08±23.68
x-91	21.56±0.64	40.25±2.27	547.21±21.41
x-92	5.62±0.28	67.43±3.36	734.91±28.47
x-93	0.84±0.13	35.75±1.68	445.80±17.56
x-94	101.89±2.70	565.34±21.45	383.36±15.74
x-95	203.86±5.25	694.44±26.55	410.13±16.72

## K. Transfer of resuspended soil to mosses for Radionuclides

The transfer of resuspended soil to mosses of  $^{137}\text{Cs}$ ,  $^{40}\text{K}$  and  $^{210}\text{Pb}$  radionuclides are presented in **Table K1**.

**Table K1.** The transfer of resuspended soil to mosses for the radionuclides  $^{137}\text{Cs}$ ,  $^{40}\text{K}$  and  $^{210}\text{Pb}$ .

site	Pb-210	K-40	Cs-137
x-01	4.29±0.47	0.71±0.05	0.04±0.01
x-02	24.57±1.77	0.49±0.04	2.36±0.2
x-03	25.16±2.79	0.87±0.12	0.47±0.29
x-04	37.93±3.52	0.63±0.06	5.69±0.64
x-05	18.77±2.19	0.78±0.11	1.32±0.35
x-06	18.02±3.97	0.38±0.05	16.47±13.45
x-07	7.70±0.89	0.48±0.07	0.86±0.13
x-08	5.00±0.35	0.3±0.03	0.05±0.01
x-09	2.88±0.29	0.59±0.07	0.16±0.02
x-10	10.81±1.04	0.79±0.09	1.02±0.13
x-11	32.88±3.59	2.1±0.22	0.91±0.24
x-12	4.54±0.42	0.3±0.03	0.37±0.08
x-13	4.95±0.46	0.25±0.03	0.12±0.01
x-14	19.95±2.1	1.52±0.18	0.78±0.08
x-15	13.73±1.5	0.42±0.05	1.18±0.11
x-16	8.25±0.74	4.08±0.42	0.11±0.02
x-17	4.43±0.41	0.87±0.10	0.13±0.02
x-18	10.76±1.11	0.43±0.03	1.47±0.07
x-19	9.85±0.92	0.88±0.09	0.9±0.11
x-20	7.43±0.67	0.43±0.04	1.9±0.16
x-21	4.66±0.54	0.88±0.06	5.19±0.7
x-22	11.48±1.16	0.66±0.05	1.22±0.2
x-23	3.48±0.33	0.73±0.06	0.14±0.02
x-24	11.76±1.27	1.07±0.08	3.1±0.30
x-25	24.48±1.82	0.32±0.03	3.02±0.14
x-26	19.23±1.51	0.29±0.02	1.01±0.22
x-27	21.6±2.10	0.61±0.08	0.71±0.20
x-28	9.71±0.98	0.67±0.06	1.67±0.49
x-29	7.04±0.50	0.45±0.03	1.47±0.34
x-30	2.54±0.26	0.32±0.04	0.08±0.01
x-31	13.41±1.54	0.4±0.04	531.25±209
x-32	2.10±0.28	0.88±0.07	0.29±0.03
x-33	8.22±2.45	0.66±0.06	0.15±0.04
x-34	8.49±0.67	0.39±0.03	2.5±0.24
x-35	9.86±0.69	0.65±0.01	0.87±0.03
x-36	10.18±0.78	0.97±0.11	0.51±0.04
x-37	13.32±1.22	0.34±0.03	0.38±0.03
x-38	20.56±1.89	0.54±0.05	1.59±0.17
x-39	6.50±0.50	0.32±0.02	1.52±0.07
x-40	7.69±0.66	1.1±0.14	0.22±0.02
x-41	5.45±0.42	0.41±0.04	2.66±0.19
x-42	13.24±0.94	0.56±0.03	11.12±0.64
x-43	16.79±1.31	0.44±0.03	0.32±0.04
x-44	5.55±0.42	0.30±0.04	0.78±0.04

x-45	0.80±0.08	1.29±0.14	0.06±0.004
x-46	4.47±0.43	0.52±0.07	0.21±0.02
x-47	12.95±1.41	2.26±0.22	0.92±0.07
x-48	0.87±0.12	0.62±0.05	0.048±0.003
x-49	14.19±1.38	0.81±0.07	0.57±0.04
x-50	3.98±0.26	0.84±0.06	0.13±0.01
x-51	5.29±0.39	0.24±0.02	7.64±0.41
x-52	5.62±0.59	0.65±0.05	0.97±0.11
x-53	5.98±0.69	0.56±0.06	0.21±0.03
x-54	15.84±1.10	0.44±0.04	1.95±0.10
x-55	9.03±0.90	0.18±0.03	0.29±0.08
x-56	1.92±0.16	0.2±0.02	0.24±0.03
x-57	15.29±1.06	0.4±0.03	3.52±0.14
x-58	7.44±0.81	0.46±0.04	3.96±0.38
x-59	17.17±1.91	0.75±0.11	9.8±0.81
x-60	86.73±8.73	1.63±0.17	7.98±0.66
x-61	12.08±1.24	0.41±0.04	0.80±0.10
x-62	19.54±1.63	0.19±0.02	4.39±0.35
x-63	12.52±1.53	2.62±0.30	0.48±0.13
x-64	6.05±0.66	0.36±0.03	1.78±0.17
x-65	19.23±1.56	0.22±0.02	10.84±2.61
x-66	10.64±1.17	1.45±0.13	1.25±0.26
x-67	3.7±0.25	0.48±0.04	0.42±0.05
x-68	11.27±1.17	1.43±0.12	0.62±0.08
x-69	15.49±1.38	1.34±0.15	0
x-70	5.62±0.61	0.45±0.06	0.59±0.20
x-71	14.73±1.62	4.51±0.47	4.85±0.40
x-72	5.15±0.37	0.38±0.03	2.35±0.09
x-73	5.93±0.62	0.99±0.07	6.15±0.43
x-74	7.11±0.50	0.73±0.06	1.74±0.06
x-75	31.65±3.73	1.14±0.12	1.28±0.22
x-76	11.57±0.80	0.16±0.01	2.28±0.15
x-77	8.23±0.57	0.28±0.02	0.42±0.03
x-78	4.96±0.51	0.33±0.04	0.94±0.09
x-79	27.38±2.73	1.26±0.09	98.33±8.69
x-80	15.7±1.51	0.27±0.02	9.82±1.89
x-81	6.42±0.69	0.63±0.09	0.25±0.03
x-82	16.7±1.32	0.65±0.05	3.21±0.16
x-83	9.06±0.94	0.63±0.10	5.84±0.40
x-84	10.3±0.82	0.35±0.03	0.45±0.05
x-85	20.19±2.03	1.08±0.24	1.04±0.25
x-86	4.31±0.49	0.69±0.06	5.02±0.69
x-87	15.74±1.10	0.29±0.03	30.36±3.99
x-88	11.62±1.22	0.48±0.08	0.14±0.02
x-89	3.51±0.28	0.28±0.03	0.11±0.02
x-90	7.32±0.84	0.42±0.05	0.56±0.05
x-91	15.14±1.31	0.51±0.04	0.62±0.06
x-92	9.77±1.01	0.2±0.04	4.11±0.43
x-93	14.7±1.31	0.66±0.06	0
x-94	1.05±0.11	0.69±0.08	0.51±0.04
x-95	1.41±0.14	0.46±0.10	0.16±0.02

## L. The coordinates

In the below Table L1, the coordinates of the sampling sites are presented.

**Table L1.** The longitude and latitude of the sampling sites.

site	Longitude	Latitude
x-01	2.310.825	4.059.600
x-02	2.316.655	4.081.600
x-03	2.335.061	4.082.825
x-04	2.358.183	4.075.877
x-05	2.362.119	4.065.675
x-06	2.328.669	4.055.250
x-07	2.310.222	4.044.505
x-08	2.291.694	4.073.802
x-09	2.614.730	4.164.555
x-10	2.619.277	4.151.027
x-11	2.621.722	4.140.208
x-12	2.606.438	4.127.105
x-13	2.592.147	4.113.591
x-14	2.570.847	4.126.138
x-15	2.559.666	4.122.291
x-16	2.553.361	4.094.472
x-17	2.575.230	4.097.644
x-18	2.626.119	4.113.669
x-19	2.563.766	4.116.686
x-20	2.542.833	4.120.208
x-21	2.535.111	4.116.333
x-22	2.516.566	4.112.458
x-23	2.490.438	4.114.702
x-24	2.484.444	4.119.666
x-25	2.499.594	4.134.922
x-26	2.486.547	4.136.055
x-27	2.500.000	4.126.922
x-28	2.487.238	4.125.755
x-29	2.465.947	4.127.258
x-30	2.129.617	4.059.225
x-31	2.130.277	4.085.355
x-32	2.168.436	4.087.769
x-33	2.148.111	4.060.641
x-34	2.151.055	4.043.986
x-35	2.096.583	4.028.658
x-36	2.101.763	4.009.650
x-37	2.120.950	4.003.555
x-38	2.161.830	4.004.338
x-39	2.194.175	4.006.255
x-40	2.188.608	4.033.011
x-41	2.124.102	4.025.883
x-42	2.123.658	4.013.066
x-43	2.258.944	3.996.597
x-44	2.250.147	4.003.041
x-45	2.242.922	4.009.566
x-46	2.231.541	4.021.161

---

x-47	2.226.580	4.030.719
x-48	2.222.972	4.019.850
x-49	2.240.222	4.041.991
x-50	2.393.477	4.108.775
x-51	2.413.505	4.142.641
x-52	2.419.625	4.149.288
x-53	2.423.755	4.150.244
x-54	2.431.430	4.149.627
x-55	2.428.638	4.142.861
x-56	2.422.225	4.129.983
x-57	2.369.563	4.126.366
x-58	2.383.763	4.140.516
x-59	2.391.225	4.138.700
x-60	2.392.327	4.129.247
x-61	2.446.694	4.131.527
x-62	2.433.847	4.119.877
x-63	2.358.500	4.110.866
x-64	2.357.486	4.120.555
x-65	2.338.883	4.138.611
x-66	2.328.900	4.129.252
x-67	2.303.658	4.129.386
x-68	2.289.775	4.130.194
x-69	2.316.530	4.117.791
x-70	2.355.961	4.110.722
x-71	2.204.430	4.061.091
x-72	2.205.097	4.055.625
x-73	2.211.438	4.040.019
x-74	2.225.758	4.046.538
x-75	2.307.566	4.093.213
x-76	2.313.183	4.099.077
x-77	2.294.852	4.112.022
x-78	2.247.744	4.106.944
x-79	2.240.083	4.091.344
x-80	2.228.691	4.108.097
x-81	2.191.552	4.095.461
x-82	2.195.319	4.084.369
x-83	2.191.222	4.075.027
x-84	2.215.472	4.090.155
x-85	2.463.075	4.102.797
x-86	2.357.563	4.048.275
x-87	2.369.697	4.055.008
x-88	2.365.577	4.045.866
x-89	2.362.366	4.028.297
x-90	2.380.147	4.010.558
x-91	2.354.858	3.997.277
x-92	2.333.055	4.045.055
x-93	2.342.097	4.002.150
x-94	2.444.683	4.108.600
x-95	2.421.138	4.092.111

---